VOLUME 120 NUMBER 2

THE ASTROPHYSICAL JOURNAL

AN INTERNATIONAL REVIEW OF SPECTROSCOPY AND ASTRONOMICAL PHYSICS

SEPTEMBER 1954

SIX-COLOR PHOTOMETRY OF STARS. VIII. THE PULSATING STAR β CEPHEI *Joel Stebbins and Gerald E. Kron* 189
THREE-COLOR OBSERVATIONS OF 108 STARS INTENDED FOR USE AS PHOTOMETRIC STANDARDS *H. L. Johnson and D. L. Harris III* 196
PHOTOMETRIC STUDIES OF ASTEROIDS. I *Ingrid Groeneveld and Gerard P. Kuiper* 200
SOLAR LIMB DARKENING IN THE REGION λλ 7793–24388 *A. Keith Pierce* 221
PHOTOELECTRIC OBSERVATIONS OF THE PROFILE OF H_α IN THE SUN'S SPECTRUM *A. Keith Pierce* 233
SOME CHARACTERISTICS OF SOLAR FLARES *Constance S. Warwick* 237
CORRELATION ANALYSES OF TURBULENT VELOCITIES AND BRIGHTNESS OF THE PHOTOSPHERIC GRANULATION *F. E. Stuart and J. H. Rush* 245
A STATISTICAL INVESTIGATION OF SUNSPOT OBSERVATIONS WITH SPECIAL REFERENCE TO H. ALFVÉN'S SUNSPOT MODEL *P. Whittle* 251
THE STRUCTURE OF THE OWL NEBULA *R. Minkowski and L. H. Aller* 261
WOLF-RAYET AND OTHER SPECTRA OF EARLY TYPE IN THE 1μ REGION *Freeman D. Miller* 265
THE SPECTRUM OF BETA LYRAE *Erika Böhm-Vitense* 271
ROTATION OF THE PRIMARY OF BETA LYRAE *Richard I. Mitchell* 274
PHOTOELECTRIC AND SPECTROSCOPIC OBSERVATIONS OF UX URSAE MAJORIS *Merle F. Walker and George H. Herbig* 278
A DETERMINATION OF LOWER LIMITS TO THE ABUNDANCE RATIO OF CARBON 12 TO CARBON 13 IN THE ATMOSPHERES OF G8–K5 GIANT STARS *John D. Schopp* 305
RED SHIFT IN THE SPECTRUM OF 40 ERIDANI B *Daniel M. Popper* 316
VISUAL BINARIES FOR THE MASS-LUMINOSITY RELATION *K. Aa. Strand and R. G. Hall* 322
GALACTIC CLUSTERS AND STELLAR EVOLUTION *Harold L. Johnson* 325
EVOLUTION OF MASSIVE STARS *R. J. Tayler* 332
THE STRUCTURE OF STARS WITH NEGLIGIBLE CONTENT OF HEAVY ELEMENTS *Anders Reiz* 342
APSIDAL MOTION AND RADIUS OF GYRATION OF SOLAR MODELS *I. Epstein and L. Motz* 353
ON THE GRAVITATIONAL STABILITY IN A ROTATING ISOTHERMAL MEDIUM *Walter Fricke* 356
THE EXCITATION OF HYDROGEN IN AURORAE *Joseph W. Chamberlain* 360

NOTES

POLARIZATION OF THE CLUSTER M29 *W. A. Hiltner* 367
GALACTIC ABSORPTION OF RADIO WAVES *John P. Hagen and Edward F. McClain* 368
THE LOCATION OF CEPHEIDS WITH RESPECT TO THE SPIRAL ARMS IN THE ANTICENTER REGION OF THE MILKY WAY *Ingrid Torgård* 370

ABSTRACTS OF ASTROPHYSICAL JOURNAL: SUPPLEMENT SERIES

ON NUCLEAR REACTIONS OCCURRING IN VERY HOT STARS. I. THE SYNTHESIS OF ELEMENTS FROM CARBON TO NICKEL *F. Hoyle* 373
ON THE DISSIPATION OF GAS AND VOLATILIZED ELEMENTS FROM PROTOPLANETS *Harold C. Urey* 373
CATALOGUE AND BIBLIOGRAPHY OF EMISSION-LINE STARS OF TYPES LATER THAN B *William P. Bidelman* 375

THE UNIVERSITY OF CHICAGO PRESS
CHICAGO, ILLINOIS, U.S.A.

September 1954 Vol. 120, No. 2

THE ASTROPHYSICAL JOURNAL

AN INTERNATIONAL REVIEW OF SPECTROSCOPY AND ASTRONOMICAL PHYSICS

Founded in 1895 by George E. Hale and James E. Keeler

Published in Collaboration with the American Astronomical Society

S. CHANDRASEKHAR
Managing Editor

GERARD P. KUIPER
Associate Editor

Yerkes Observatory of the University of Chicago

EDITORIAL BOARD

MARTIN SCHWARZSCHILD, JR. (1954-58)
Princeton University Observatory

O. HERZBERG (1952-56)
National Research Council, Ottawa

H. W. BABCOCK (1951-57)
Mount Wilson Observatory of the Carnegie Institution of Washington

FRED L. WHIPPLE (1952-56)
Harvard College Observatory

C. D. SHANE (1952-55)
Lick Observatory, University of California

The Astrophysical Journal is published bimonthly by the University of Chicago at the University of Chicago Press, 5750 Ellis Avenue, Chicago 37, Illinois, during January, March, May, July, September, and November. ¶Two volumes are published per year, one beginning with the January issue and the other beginning with the July issue. The subscription price is $6.00 per volume or $12.00 per year; the price of single copies is $3.00. (Orders for service of less than a volume will be charged at the single copy rate.) ¶Postage is prepaid by the publishers on all orders from the United States and its possessions. No extra charge is made for postage to countries in the Pan American Postal Union. ¶Postage is charged extra as follows: for Canada, 20 cents per volume, 40 cents per year (total $6.20 per volume, $12.40 per year); on single copies 5 cents (total $3.05); for all other countries in the Postal Union, 40 cents per volume, 75 cents per year (total $6.40 per volume, $12.75 per year), on single copies 10 cents (total $3.10). ¶Subscriptions are payable in advance. Please make all remittances payable to The University of Chicago Press, in United States currency or its equivalent by postal or express money orders or bank drafts.

The following is an authorized agent:

For the British Commonwealth, except North America and Australasia: The Cambridge University Press, Bentley House, 200 Euston Road, London, N.W. 1, England. Prices of yearly subscriptions and of single copies may be had on application.

Claims for missing numbers should be made within the month following the regular month of publication. The publishers expect to supply missing numbers free only when losses have been sustained in transit, and when the reserve stock will permit.

Business correspondence should be addressed to The University of Chicago Press, Chicago 37, Illinois.

Communications for the editors and manuscripts should be addressed to: S. Chandrasekhar, Editor of THE ASTROPHYSICAL JOURNAL, Yerkes Observatory, Williams Bay, Wisconsin.

Line drawings and photographs should be made by the author, and all marginal notes such as co-ordinates, wave lengths, etc., should be included in the cuts. It will not be possible to set up such material in type.

One copy of the corrected galley proof should be returned as soon as possible to the editor, Yerkes Observatory, Williams Bay, Wisconsin. Authors should take notice that the manuscript will not be sent to them with the proof.

The cable address is "Observatory, Williamsbay, Wisconsin."

The articles in this journal are indexed in the *International Index to Periodicals*, New York, N.Y.

Applications for permission to quote from this journal should be addressed to The University of Chicago Press, and will be freely granted.

Microfilms of complete journal volumes are available to regular subscribers only and may be obtained at the end of the year. Orders and inquiries should be addressed to University Microfilms, 313 North First Street, Ann Arbor, Michigan.

Notice to subscribers: If you change your address, please notify us and your local postmaster immediately.

Entered as second-class matter, July 21, 1930, at the Post-Office at Chicago, Ill., under the Act of March 3, 1879.

Acceptance for mailing at special rate of postage provided for in United States Postal Act of October 3, 1917, Section 1103, amended February 28, 1925.

Copyright 1954 by the University of Chicago.

[PRINTED IN U.S.A.]

THE ASTROPHYSICAL JOURNAL

AN INTERNATIONAL REVIEW OF SPECTROSCOPY AND ASTRONOMICAL PHYSICS

VOLUME 120 SEPTEMBER 1954 NUMBER 2

SIX-COLOR PHOTOMETRY OF STARS. VIII. THE PULSATING STAR β CEPHEI*

JOEL STEBBINS AND GERALD E. KRON
Lick Observatory, University of California

Received May 5, 1954

ABSTRACT†

The light-curves of β Cephei in six colors show the same retardation of phase in the longer wave lengths as do the curves of the regular Cepheid variables. When the variation in area, due to the pulsating radius, is taken out of the final light-curves, the resulting radiation-curves for the different colors agree in phase. Because of the small amplitudes, 0.05 and 0.01 mag. in the ultraviolet and infrared, respectively, the solution for the radius of the star from a combination of the light- and velocity-curves would be indeterminate, except for the condition that the ratio of the amplitudes in short and long wave lengths should agree with the calculated ratio for small variations in the temperature of a B1 star at 23,000°. When the photometric and spectroscopic data for β Cephei are analyzed on this basis, the radius of the star comes out as $R = 9.0\ R_\odot$, and the absolute magnitude $M_{pv} = -4.2$. Although these values could be improved by simultaneous photometric and spectroscopic measures over the same cycles, the variations of this star are satisfactorily explained on the pulsation theory.

The star β Cephei should perhaps be called, as Struve and Swings (1941) have suggested, the prototype of the class of variables in light and velocity that have become known as the β Canis Majoris stars. They are characterized by early B-type spectra and by small and continuous variations in light and velocity in periods of the order of 4 or 5 hours. The 4.6-hour velocity variation of β Cephei was established at the Yerkes Observatory by Frost (1906) and has since been the subject of various exhaustive spectroscopic investigations that have been summarized in the latest work by Struve, McNamara, Kung, and Beymer (1953). Beta Cephei was also the first star to be tested by P. Guthnick with his new photoelectric photometer, and he established a light-range of 0.05 mag. or more in the spectroscopic period of 0.1905 day. This discovery was followed up by Guthnick and Prager (1914), and the star has also been observed photometrically by others, including Miss Cummings (1923), who used β Cephei to demonstrate the possibilities of a new photoelectric photometer at the Lick Observatory.

All observers have agreed that the variations of this star are slightly irregular both in light and in velocity. The amplitudes, even during successive cycles, are often not the same; and, while the period of 0.1905 day seems to be changing only slowly over the

* *Contributions from the Lick Observatory*, Ser. II, No. 53.

† This work was supported by the Office of Naval Research under a contract with the University of California.

years, the sudden jumps in the variation preclude exact prediction of the phase at any time. Struve and his collaborators have not found a beat period between two nearly equal short periods, such as exists in other stars of this class. Because of their short periods, early spectral types, high luminosities, and nonconformity with the period-luminosity relation, these stars have not been considered to be closely related either to the cluster-type or to the classical Cepheid variables; and it has been assumed that the fundamental conditions in the β Canis Majoris type could be quite different from those in the other continuous variables.

In our list of stars measured for six colors, β Canis Majoris and β Cephei stand at the top as the bluest of the B1 stars, though this rank probably is caused by the other B1 stars being more or less space-reddened, most of them having been chosen because of that fact. After β Cephei had been measured only twice, we noted that no test had been made for possible change of color in the 4.6-hour period. Also we stated (Stebbins and Whitford 1945) that the similar star, 12 Lacertae, which follows β Cephei in the B1 list, showed no detectable change of color in the light-period. This last statement is inaccurate and obviously must be wrong. A re-examination of the original records shows that 12 Lacertae was compared with near-by 10 Lacertae three times within 4 hours on one night and that the range in magnitude was 0.083 in the violet, 0.060 in the infrared, and hence 0.023 in $V - I$. When reduced to the International scale by the factor $\frac{1}{3}$, this variation in color index becomes less than 0.01 mag., and the announced lack of change was only a slight understatement. Since it is difficult to conceive of a star undergoing a pulsation of size with no accompanying variation in surface brightness, we may assume that β Cephei and all others of the class will show variations in color when properly tested.

With these ideas in mind, we made complete runs on β Cephei in six colors on each of the nights of August 19 and 20, 1952. The comparison star was α Cephei, spectrum A7 and visual magnitude 2.60, or about 0.7 mag. brighter than β. While α is not so near β in either color or magnitude as we should like, we can reasonably count on α's being constant over a few hours; and, though α is 8° south of β, the differential atmospheric extinction is small up to several hours from the meridian. The observations are given in Table 1; the first column gives the heliocentric Julian date; the second column the phase, computed from the elements,

$$\text{Max.} = \text{JD } 2434344.866 + 0^{d}1904885E\,. \tag{1}$$

The epoch is taken from the approximate maximum on August 19; the present period is derived from Struve *et al.* (1953), though any rough period will suffice for two successive nights. Under the colors and at the appropriate phase, each difference of magnitude, the mean of two sets, is referred to the median magnitude of that color for the night. Thus, for the first number under U, the $+0.002$ added to the median -1.930 at the bottom gives -1.928, the amount that β was measured brighter than α Cephei, with α taken uniformly with the sensitivity reduced by 1.0 mag. The individual observations are given just as they were measured, but the minima and maxima for each color and date have been smoothed by one or two thousandths rather than simply being the highest and lowest observed values for the extremes. The first two measures in the infrared on the second night should be rejected; they were made in a different sequence of the colors, in an effort to eliminate a fatigue effect on the small deflections in the infrared; but it was soon seen that this change was a mistake, and the regular sequence was resumed. Everything must be just right to get a reliable light-curve with an amplitude of 0.01 mag. The amplitudes, summarized at the bottom of the table, run smoothly enough on the first night, but not so well on the second, where a judicious doctoring of, say, 0.005 mag. here and there would make them better. It is quite evident, however, that the variations decrease from short to long wave lengths and that the amplitudes averaged less on the second night than on the first.

The observations of Table 1 are shown in the light-curves of Figure 1. Except for the

rejected measures in the infrared on the second night, the only bad discordances are at phase $0^{p}18$ on that night, where the points for every color are down by about 0.01 mag. Such unrepeated jumps in the variation have been found by other observers, but it is difficult to see how a sudden fading of the star could be the same at all wave lengths. The smooth run of the deflections on the comparison star apparently rules out the possibility of a variable atmospheric extinction or a change in the photometer. Also the readings show no evidence of an accidental cutoff by the edge of the dome opening. From the past history of β Cephei, we were perhaps lucky to get the curves as smooth as they are.

TABLE 1

SIX-COLOR OBSERVATIONS OF β CEPHEI

JD 2430000+	Phase	*U* 3530 A	*V* 4220 A	*B* 4880 A	*G* 5700 A	*R* 7190 A	*I* 10,300 A
4244.730	$0^{p}286$	+0.002	−0.003	−0.001	−0.011	−0.001	−0.006
.768	.486	+ .030	+ .021	+ .013	+ .010	+ .008	+ .002
.784	.570	+ .028	+ .019	+ .019	+ .015	+ .012	+ .004
.803	.669	+ .018	+ .011	+ .013	+ .011	+ .013	+ .006
.823	.774	.000	+ .001	+ .001	+ .009	+ .012	+ .006
.844	.885	− .021	− .014	− .011	− .007	− .004	− .004
.866	.000	− .031	− .020	− .015	− .011	− .010	− .005
.892	.136	− .025	− .017	− .018	− .015	− .012	− .005
.912	0.241	+0.006	+0.009	−0.002	−0.013	−0.004	+0.002
	Min.	+0.029	+0.020	+0.017	+0.013	+0.012	+0.006
	Max.	−0.028	− .019	− .017	− .013	− .011	− .005
	Med.	−1.930	−0.835	−0.427	−0.225	+0.096	+0.500
4245.686	0.305	+0.007	+0.006	−0.001	0.000	−0.004	(−0.016)*
.706	.410	+ .020	+ .012	+ .012	+ .009	+ .002	(− .013)*
.725	.509	+ .021	+ .010	+ .011	+ .010	+ .013	+ .005
.746	.620	+ .022	+ .016	+ .010	+ .007	+ .008	+ .005
.768	.735	+ .009	+ .008	+ .012	+ .012	+ .012	+ .004
.788	.840	− .005	− .006	− .001	+ .002	.000	+ .003
.812	.966	− .019	− .010	− .010	− .007	− .011	− .005
.832	.071	− .022	− .017	− .011	− .014	− .012	− .006
.853	.181	− .011	− .010	.000	− .002	− .001	+ .004
.879	.318	− .003	− .003	− .003	− .005	− .007	− .003
.900	0.428	+0.009	+0.004	+0.006	+0.009	−0.001	−0.005
	Min.	+0.021	+0.013	+0.011	+0.011	+0.011	+0.005
	Max.	−0.021	− .014	− .011	− .011	− .012	− .005
	Med.	−1.927	−0.834	−0.431	−0.234	+0.096	+0.501
Aug. 19	Amp.	0.057	0.039	0.034	0.026	0.023	0.011
Aug. 20	Amp.	.042	.027	.022	.022	.023	.010
	Ratio	0.74	0.69	0.65	0.85	1.00	0.91

* Infrared defective.

The changing six colors of β Cephei are determined differentially from those of α Cephei, which, in turn, were referred to polar standards several times during 1952. In a pulsating star the extremes of color index do not necessarily coincide with the maximum and minimum of light at one selected wave length; so we proceed to find the variations without restriction by the phase. In Table 2 the results are summarized after taking the means of the two nights and reducing everything to the standard system of six colors. The thousandths of a magnitude are significant only for the differential change; the range of 0.025 mag. in $V - I$ corresponds to about 0.008 mag. on the international scale. Both β and α Cephei were measured independently in other years, without regard to the phase

of β; and for β we simply round off the mean of all, as in the table. As already mentioned, the over-all $V - I = -2.50$ for β Cephei and -2.55 for β Canis Majoris, which undoubtedly also varies in color, make them the bluest B1 stars we have measured. The lower value of $V - I = -2.29$ for 12 Lacertae is probably caused by space reddening.

As in the cases of δ Cephei and η Aquilae (Stebbins 1953), the light-curves in Figure 1 show the retardation of phase for longer wave lengths. These differences of phase can be removed, as before, by taking out of the light-curves the variations caused by the pulsa-

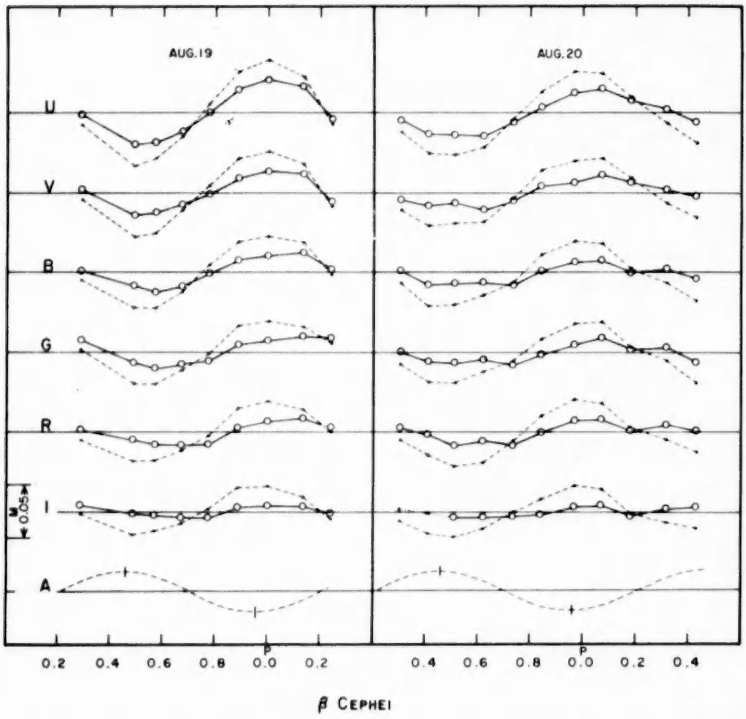

FIG. 1.—Light-curves of β Cephei. The combination of the area-curve A with the respective radiation-curves gives the resulting continuous light-curves.

tion in size. The velocities measured by Struve *et al.* (1953) can be represented nearly enough by sine curves; hence, by interpolating between August 14 and 23, we find a maximum velocity at JD 2434245.001. Then from elements (1) the light-phase of maximum velocity is $0^{d}135 = 0^{p}71$, and of minimum velocity $0^{p}21$. The average K of the velocity variation in 1952 was about 13.2 km/sec; we increase this by the factor $\frac{24}{16}$ to allow for integration over a hemisphere with no darkening at the limb. Then the variation of the pulsating radius r may be represented by

$$\frac{dr}{dt} = k \cos \theta , \qquad (2)$$

where $k = 20$ km/sec, $\theta = 2\pi\,(p - 0^{p}21)$, and the phase p is in fractions of the period.

Let R be the mean radius in regard to the time, P the period in seconds, and t the time counted from phase $0^{p}21$; then for maximum r at phase $0^{p}46$ we have

$$r_{max} - R = a = \int_0^{P/4} \frac{dr}{dt}\,dt = \frac{kP}{2\pi}\int_0^{\pi/2} \cos\theta\; d\theta = \frac{kP}{2\pi}, \tag{3}$$

from which

$$a = 5.24 \times 10^{4}\ \text{km} = 0.075 R_{\odot}\,. \tag{4}$$

We have now to determine the amplitude of the variations in area, expressed in magnitude. The changes of this star are too small for selection of pairs of phases on the increasing and decreasing branches of the light-curves, where the colors are the same but the

TABLE 2

SIX-COLOR RANGES OF β CEPHEI

	Phase	U	V	B	G	R	I	$V-I$	No. Nights
Min	$0^{p}54$	−2.098	−1.145	−0.548	−0.065	+0.612	+1.330	−2.475	2
Max	0.07	−2.122	−1.152	−0.550	−0.065	+0.615	+1.348	−2.500	2
Diff.	0.53	−0.024	−0.007	−0.002	0.000	+0.003	+0.018	−0.025	2
1942, 1949	.....	−2.12	−1.16	−0.54	−0.07	+0.61	+1.36	−2.52	3
All	.....	−2.12	−1.15	−0.54	−0.07	+0.61	+1.35	−2.50	5
α Ceph.	.....	−0.49	−0.61	−0.29	−0.04	+0.33	+0.62	−1.23	6

total magnitudes different, as is possible for δ Cephei and other stars of larger range than β Cephei. We can get at the problem in another way by writing, for the magnitude variation due to the pulsating radius,

$$A = \Delta m \sin\theta = 5 \log\left(\frac{R+a}{R}\right)\sin\theta\,. \tag{5}$$

Hence, with sufficient approximation,

$$\Delta m = 5 \log\left(1 + \frac{a}{R}\right) = 5 \times 0.434\,\frac{a}{R}, \tag{6}$$

and, for the mean radius,

$$R = 2.17\,\frac{a}{\Delta m}\,. \tag{7}$$

If we take out the variation in area with amplitude $2\Delta m$ from each of the six light-curves, the remaining radiation-curves should agree in phase with one another. At first, we deduced by trial that the value $2\Delta m = 0.016$ would bring about this agreement, but further consideration shows that this reasoning was insufficient. Not only should the pure radiation-curves agree in phase, but the relative amplitudes in short and long wave lengths should agree with the relative amplitudes computed for the small energy variations of an approximate black body at the temperature of a B1 star. To smooth the data, we combine the curves on the two nights and compare the violet amplitude with the mean of the red and infrared amplitudes. The ultraviolet-curve is not used because of possible complication by the Balmer absorption.

In Table 3 are the amplitudes of the radiation-curves obtained by taking out successively different arbitrary amounts of area variation from the original light-curves. For comparison, the first line of the table gives the results with the assumption of no area

variation, while the last line gives the computed ratio of amplitudes, $V/RI = 1.36$, taken at 23,000° for the proper wave lengths from our tables of black-body radiation. Any one of the assumed area variations will bring the resulting radiation-curves nearly enough into the same phase; but, by inspection of Table 3, we see that the black-body value of $V/RI = 1.36$ corresponds to $2\Delta m = 0.036$. This value is not very sensitive to variations in the assumed temperature; at 23,000° a variation of 1000° in T would change the computed 1.36 by about 1.5 units in the last place.

It must be noted that although the assumption of variation like a black body may hold for an early-type star like β Cephei with its simple spectrum, the condition does not hold at all for variables of F and G type like δ Cephei and η Aquilae, where there are great changes in the spectral lines between maximum and minimum (Stebbins 1953). For δ Cephei we find for the ratio of amplitudes of the radiation-curves V/I, observed 3.2, computed 2.2; and for η Aquilae, observed 3.1, computed 2.3. The computed amplitudes are based upon the maximum and minimum color temperatures derived for each star.

The results of the present analysis are shown in Figure 1. At the bottom for each date is the area-curve drawn in proper phase with the amplitude $2\Delta m = 0.036$. For each color

TABLE 3

AMPLITUDES OF RADIATION-CURVES

$2\Delta m$	V	RI	V/RI
0.000	0.033	0.017	1.94
.016	.050	.031	1.61
.032	.064	.046	1.39
.040	.072	.054	1.33
0.048	0.079	0.062	1.27
Black body, 23,000°			1.36

the combination of the derived radiation-curve with the common area-curve gives the final light-curve. Thus we see, especially in the red- and infrared-curves, that the final variation is the resultant of two larger variations, nearly but not quite opposite in phase. It is scarcely possible to determine objectively the maxima of the radiation-curves from the data at hand or to say whether the agreement in phase for the different colors could be improved. This agreement is at least better than in the original light-curves. By taking an average of all curves on both nights, we find that the radiation maximum comes close to the epoch first chosen for the maxima of the original light-curves in the short wave lengths. Since the area minimum comes at light-phase $09^{p}6$, the star is smallest at $0^{p}04$ before radiation maximum, compared with $0^{p}08$–$0^{p}12$ for this difference in several classical Cepheid variables.

We now substitute $a = 0.075R_{\odot}$ and $\Delta m = 0.018$ in equation (7), and get, for the radius,

$$R = 9.0R_{\odot} . \tag{8}$$

This value is affected by any approximation in equation (3). We find by integrating the mean velocity-curve for two nights that the differences between the area-curve and a sine-curve do not exceed 0.002 mag. Therefore, varying Δm by this amount in equation (7) would change R by 2 parts in 18 or by $1.0R_{\odot}$. But there are worse uncertainties. By adopting a constant area-curve for all cycles, we throw all the irregularities of the light-curves into the radiation-curves. Thus, if we take the amplitudes of the light-curves for the two nights separately instead of their mean, we find, following the procedure used in

Table 3, that $2\Delta m = 0.050$ and 0.022, and $R = 6.5$ and $14.8R_\odot$, respectively. Obviously, consistent results cannot be obtained unless both light- and velocity-curves are derived for the same cycle, and even then the outcome is doubtful because of the irregularities. During the season of 1952 Struve *et al.* (1953) found the velocity range $2K$ to vary from 18 to 32 km/sec.

Nevertheless we compute the absolute magnitude of β Cephei from the data at hand. Referring the quantities to the sun, we have the relation

$$M_{pv} = M_\odot - 5 \log R + j \ , \tag{9}$$

where j is the surface brightness expressed in magnitudes. Following Kuiper (1938), we adopt $M_\odot = +4.73$ and effective temperature $T = 5700°$ for the sun and $T = 23{,}000°$ for β Cephei with spectrum B1. Then with these temperatures and $\lambda = 5400$ A in our tables of black-body radiation, computed with Planck's formula, we find $j = -4.21$. This value can be checked by the formula in Russell, Dugan, and Stewart (1927), given with revised constants by Goldberg and Aller (1943) for high temperatures as

$$M_{pv} = -0.66 - 5 \log R + \frac{28{,}400}{T} . \tag{10}$$

If in this equation we put $R = 1$ and $T = 23{,}000°$, then $M_{pv} = +0.57$. Hence $j = +0.57 - 4.73 = -4.16$. The difference from the preceding $j = -4.21$ is due to slightly different adopted values of the radiation constant c_2 and of the photovisual wave length. We substitute $R = 9.0$ and $j = -4.2$ in equation (9) and get, for β Cephei,

$$M_{pv} = -4.2 \ .$$

The close agreement with $M_v = -4.1$ for stars of their class B2 III by Keenan and Morgan (1951)[1] must be accidental, but the present solution, even from light-curves of such small amplitudes, leads to a credible result.

We note that by his method, based upon the strength of the $H\gamma$ line, Petrie (1952) has found $M_{pv} = -2.5$ for β Cephei, or fainter by 1.7 mag. than our result. It does not seem possible to reduce our radius to less than $\frac{1}{2}$ to account for the discordance.

The variations of β Cephei, without a beat period, seem to be simpler than those of some other stars of this class studied by Struve (1952) and his group. By the use of a long base line for the colors and the application of the principle that small variations in the surface brightness should agree with those of a black body, it has been possible in the present study to derive values for the radius and absolute magnitude that are not at variance with accepted ideas on these stars.

REFERENCES

Cummings, Edith E. 1923, *Lick Obs. Bull.*, **11**, 115 (No. 349).
Frost, E. B. 1906, *Ap. J.*, **24**, 259.
Goldberg, L., and Aller, L. H. 1943, *Atoms, Stars, and Nebulae* (Philadelphia: Blakiston Co.), pp. 296–297.
Guthnick, P., and Prager, R. 1914, *Pub. Berlin-Babelsberg*, **1**, 23.
Keenan, P. C., and Morgan, W. W. 1951, *Astrophysics*, ed. J. A. Hynek (New York: McGraw-Hill Book Co.), pp. 16 and 23.
Kuiper, G. P. 1938, *Ap. J.*, **88**, 429.
Petrie, R. M. 1952, *Pub. Dom. Ap. Obs., Victoria*, **9**, 251.
Russell, H. N.; Dugan, R. S.; and Stewart, J. Q. 1927, *Astronomy* (New York: Ginn & Co.), **2**, 732–733.
Stebbins, J. 1953, *Pub. A.S.P.*, **65**, 118.
Stebbins, J., and Whitford, A. E. 1945, *Ap. J.*, **102**, 283.
Struve, O. 1952, *Ann. d'ap.*, **15**, 157.
Struve, O.; McNamara, D. H.; Kung, S. M.; and Beymer, C. 1953, *Ap. J.*, **118**, 39.
Struve, O., and Swings, P. 1941, *Ap. J.*, **94**, 105.

[1] At our request Dr. J. A. Pearce has re-examined spectrograms of β Cephei, and he places this star definitely at B1 on the Victoria system. A change from B1 to B2 would cause a difference of only 0.2 mag. in the computed absolute magnitude.

THREE-COLOR OBSERVATIONS OF 108 STARS INTENDED FOR USE AS PHOTOMETRIC STANDARDS

H. L. JOHNSON
Lowell Observatory

AND

D. L. HARRIS III
Yerkes and McDonald Observatories
Received March 12, 1954

ABSTRACT

Three-color observations on the (*U*, *B*, *V*) system have been made for 108 stars, including the 10 primary standards. These observations, which are of relatively high weight, are intended, along with the three standard regions—Praesepe, the Pleiades, and IC 4665—for use as standards for the three-color photometric system.

In this paper are presented magnitudes and colors on the (*U*, *B*, *V*) system (Johnson and Morgan 1953) for a total of 108 stars which are intended for use as standards of the system. The measures have been made over the time interval from 1950 to 1954, both at the McDonald Observatory and at the Lowell Observatory. With the exception of the ten primary standards, the average number of nights on which the stars were observed is 7.3. As many as possible of the primary standards were observed on each night. In addition to these stars, there are three standard regions—the Pleiades (Johnson and Morgan 1953), Praesepe (Johnson 1952), and IC 4665 (Johnson 1954). These stars and standard regions could be considered as defining the photometric system.

The 108 stars are listed in Table 1, where the first column givest the HD numbers of the stars; the second, the names or BD numbers; the third, fourth, and fifth, the measured magnitudes and colors; the sixth, the number of nights on which the stars were observed; and the last column the spectal type by W. W. Morgan on the MK system.

The values given for the ten primary standards (the last ten stars in Table 1) are slightly different from those originally given (Johnson and Morgan 1953). Additional observations that have been made since 1951 have been used to make these small changes, but it is not known whether these changes are due to variability of the stars. When transformations to the system are made, it is best not to use the primary standards alone but, instead, to use at least 20 stars of all types selected from Table 1 or the standard regions. In this way the effects of small variations in the standard stars can be reduced. In general, unless one is working in a very small regior of the sky, it is better to use standards scattered over a considerable area of the sky; such a procedure will help to minimize systematic regional errors that might appear in the transformations.

If stars of a particular type not available in Table 1 are required, it may be possible to select suitable stars from Johnson and Morgan (1953, Table 3). One must keep in mind, however, that these latter observations are of lower weight than those given in Table 1.

TABLE 1—THE PHOTOMETRIC STANDARDS

HD	Name	V	$B-V$	$U-B$	n	Sp.
886	γ Peg	2.83	−0.23	−0.87	6	B2 IV
1280	θ And	4.61	+0.06	+0.04	6	A2 V
4727	ν And	4.53	−0.15	−0.58	5	B5 V
6961	θ Cas	4.33	+0.17	+0.11	5	A7 V
8538	δ Cas	2.68	+0.13	+0.12	5	A5 V
9270	η Psc	3.62	+0.97	+0.76	5	G8 III
10476	107 Psc	5.23	+0.83	+0.50	5	K1 V
10700	τ Cet	3.50	+0.72	+0.20	5	G8 Vp
11636	β Ari	2.65	+0.13	+0.10	5	A5 V
.....	−18°359	10.18	+1.53	+1.16	3	.....
.....	+2°348	10.03	+1.44	+1.08	3	.....
15318	ξ^2 Cet	4.28	−0.06	−0.13	5	B9 III
16160	HR 753 A	5.82	+0.97	+0.79	11	.....
.....	HR 753 B	11.65	+1.61	+1.12	3	.....
20630*	κ Cet	4.82	+0.68	+0.18	7	G5 V
21120	o Tau	3.59	+0.89	+0.62	5	G8 III
21447	HR 1046	5.08	+0.05	+0.03	5	A1 V
22049	ϵ Eri	3.73	+0.89	+0.57	6	K2 V
27371*	γ Tau	3.65:	+0.99	+0.82	6	K0 III
27697*	δ Tau	3.76:	+0.98	+0.82	6	K0 III
28305	ϵ Tau	3.54	+1.02	+0.88	6	K0 III
30652	π^3 Ori	3.19	+0.45	−0.01	11	F8 V
30836	π^4 Ori	3.69	−0.17	−0.80	9	B2 III
32630	η Aur	3.17	−0.18	−0.67	6	B3 V
33111	β Eri	2.80	+0.13	+0.10	8	A3 III
35299	.....	5.70	−0.22	−0.87	15	B5 V
35468	γ Ori	1.64	−0.23	−0.87	5	B2 III
35497	β Tau	1.65	−0.13	−0.49	5	B7 III
36395	−3°1123	7.97	+1.47	+1.21	17	M1 V
36512	υ Ori	4.63	−0.26	−1.07	11	B0 V
36591	.....	5.35	−0.20	−0.94	9	B1 V
37043	ι Ori	2.77	−0.25	−1.08	5	O9 III
37128	ϵ Ori	1.70	−0.19	−1.04	6	B0 Ia
38678	ζ Lep	3.55	+0.10	+0.06	5	.....
38899	134 Tau	4.90	−0.07	−0.18	5	B9 IV
.....	+17°1320	9.63	+1.50	+1.18	4	.....
47105	γ Gem	1.93	0.00	+0.03	5	A0 IV
.....	+5°1668	9.82	+1.56	+1.12	3	.....
56537	λ Gem	3.58	+0.11	+0.10	6	A3 V
58946	ρ Gem	4.16	+0.32	−0.03	6	F0 V
62345	κ Gem	3.57	+0.93	+0.68	5	G8 III
71155	HR 3314	3.90	−0.02	−0.02	5	A0 V
76644	ι U Ma	3.14	+0.18	+0.07	6	A7 V
79469	θ Hya	3.88	−0.06	−0.13	6	A0 p
.....	−12°2918	10.06	+1.53	+1.15	2	.....
82885	11 LMi	5.41	+0.77	+0.45	14	G8 IV–V
87696	21 LMi	4.48	+0.18	+0.08	7	A7 V
87901	α Leo	1.36	−0.11	−0.36	7	B8 V
89021	λ U Ma	3.45	+0.03	+0.06	6	A2 IV
.....	+1°2447	9.63	+1.52	+1.19	3	.....
91316	ρ Leo	3.85	−0.14	−0.95	6	B1 Ib
100600	90 Leo AB	5.95	−0.16	−0.64	23	.....
102647	β Leo	2.14	+0.09	+0.07	8	A3 V
102870	β Vir	3.61	+0.55	+0.10	9	F8 V
103095	HR 4550	6.45	+0.75	+0.17	25	G8 Vp

* The stars indicated by asterisks:

20630 κ Cet has been found to be variable in magnitude by Kron, White, and Gascoigne (1953). Our data, however, do not definitely show this variation.

27371, 27697 These two Hyades giants appear to be variable in magnitude with an amplitude of about 0.1 mag. The third Hyades giant in the table, ϵ Tau, does not show this variation.

116658 Eclipsing variable.

+4°3561 Barnard's proper-motion star.

TABLE 1—*Continued*

HD	Name	V	$B-V$	$U-B$	n	Sp.
103287	γ U Ma	2.44	0.00	+0.01	6	A0 V
106591	δ U Ma	3.31	+0.08	+0.07	9	A3 V
106625	γ Crv	2.60	−0.11	−0.35	5	B8 III
.....	+0°2989	8.49	+1.41	+1.26	3	M0.5 V
113139	78 U Ma	4.93	+0.36	+0.01	16	F2 V
114710	β Com	4.28	+0.57	+0.07	11	G0 V
115617	61 Vir	4.75	+0.71	+0.25	5	G5 V
116658*	α Vir	0.96	−0.23	−0.94	7	B1 V
116842	80 U Ma	4.01	+0.16	+0.08	15	A5 V
117176	70 Vir	4.98	+0.71	+0.26	8	G5 V
121370	η Boo	2.69	+0.58	+0.19	8	G0 IV
130109	109 Vir	3.74	0.00	−0.03	7	A0 V
130819	α^1 Lib	5.16	+0.41	−0.04	7	.....
130841	α^2 Lib	2.75	+0.15	+0.08	8	.....
.....	−7°4003	10.56	+1.61	+1.20	6	.....
141003	β Ser A	3.67	+0.06	+0.07	8	A2 IV
141004	λ Ser	4.43	+0.60	+0.10	7	G0 V
142860	γ Ser	3.85	+0.48	−0.03	6	F6 V
.....	−12°4523	10.13	+1.60	+1.18	5	.....
149757	ζ Oph	2.56	+0.02	−0.86	10	O9.5 V
154363	−4°4225	7.73	+1.16	+1.05	5	K5 V
.....	−4°4226	10.07	+1.43	+1.09	5	M3.5 V
157881	+2°3312	7.54	+1.36	+1.26	5	K7 V
159561	α Oph	2.08	+0.15	+0.10	11	A5 III
161096	β Oph	2.77	+1.16	+1.24	10	K2 III
161868	γ Oph	3.75	+0.04	+0.04	9	A0 V
..... *	+4°3561	9.54	+1.74	+1.29	9	M5 V
.....	−3°4233	9.38	+1.52	+1.21	5	.....
172167	α Lyr	+.04	0.00	−0.01	10	A0 V
176437	γ Lyr	3.25	−0.05	−0.09	10	B9 III
177724	ζ Aql	2.99	0.00	−0.01	6	.....
.....	+4°4048	9.13	+1.49	+1.16	6	M3.5 V
184279	+3°4065	6.82	+0.02	−0.83	5	.....
184915	κ Aql	4.96	−0.01	−0.87	6	B0.5 III
187642	α Aql	0.77	+0.22	+0.08	14	A7 IV, V
188512	β Aql	3.71	+0.86	+0.48	16	G8 IV
196867	α Del	3.77	−0.06	−0.22	6	B9 V
198001	ϵ Aqr	3.77	+0.01	+0.04	5	A1 V
.....	−15°6290	10.17	+1.60	+1.15	4	.....
216494	74 Aqr	5.81	−0.08	−0.32	6	.....
218045	α Peg	2.49	−0.05	−0.06	7	B9 V
222368	ϵ Psc	4.13	+0.51	0.00	8	F7 V
.....	+1°4774	8.98	+1.48	+1.09	5	M2 V
	The Ten Primary Standards					
12929	α Ari	2.00	+1.151	+1.12	std	K2 III
18331	HR 875	5.17	+0.084	+0.05	std	A1 V
69267	β Cnc	3.52	+1.480	+1.78	std	K4 III
74280	η Hya	4.30	−0.195	−0.74	std	B3 V
135742	β Lib	2.61	−0.108	−0.37	std	B8 V
140573	α Ser	2.65	+1.168	+1.24	std	K2 III
143107	ϵ CrB	4.15	+1.230	+1.28	std	K3 III
147394	τ Her	3.89	−0.152	−0.56	std	B5 IV
214680	10 Lac	4.88	−0.203	−1.04	std	O9 V
219134	HR 8832	5.57	+1.010	+0.89	std	K3 V

The estimated probable errors of the observations given in Table 1 are listed in Table 2, which is self-explanatory.

These observations have been compared with the red and infrared observations of Kron, White, and Gascoigne (1953), with results not significantly different from those given by them. The numbers of stars in the comparisons are now greater, but the scatter

TABLE 2

ESTIMATED PROBABLE ERRORS OF THE OBSERVATIONS

No. of Observations	Probable Errors (Mag.) of		
	V	$B-V$	$U-B$
2	±0.020	±0.010	±0.020
3	± .016	± .008	± .016
4	± .014	± .007	± .014
5 or more	±0.012	±0.006	±0.012

and general trends of the diagrams are not changed. The reader is referred to Figures 1 and 2 of Kron *et al.* (1953).

REFERENCES

Johnson, H. L. *Ap. J.*, **116**, 640, 1952.
———. *Ap. J.*, **119**, 181, 1954.
Johnson, H. L., and Morgan, W. W. *Ap. J.*, **117**, 313, 1953.
Kron, G. E.; White, H. S.; and Gascoigne, S. C. B. *Ap. J.*, **118**, 502, 1953.

PHOTOMETRIC STUDIES OF ASTEROIDS. I*

INGRID GROENEVELD AND GERARD P. KUIPER
Yerkes and McDonald Observatories
Received April 2, 1954

ABSTRACT

This paper is the first of a series describing a systematic photometric study of the asteroids. Fourteen light-curves based on 27 nights, are communicated here, and four color-curves. The principal data are summarized in Table 1 and the diagrams. The rotation of Eunomia is discussed in Section IV and found to be retrograde.

I. PLAN OF INVESTIGATION

A systematic photometric study of the asteroids was organized and initiated at the McDonald Observatory by Mr. Kuiper in 1949. It consisted of two parts: (A) A systematic survey with a 10-inch, $f/7$ telescope, which was to cover all asteroids down to about 16.5 mag. photographic. The purpose of this photometry was to obtain approximate magnitudes on the international photographic scale and to reach a known degree of completeness, so that the statistics of the asteroids down to $m = 16$ could be placed on a reliable basis. (B) Detailed photometry of all asteroids brighter than about 10 and of selected fainter ones; the purpose of this work was to obtain periods of rotation; the characteristics of the light-curves; the colors and possible color variations; and, by continued observation over a number of years, some information on the shapes of these bodies and on the orientations of their rotational axes in space. The present report, the first of a series, is concerned largely with results obtained under program B. It seems useful, however, to make at this time a brief statement about the status of program A.

Program A was carried out with the 10-inch Ross-Fecker telescope belonging to the Cook Observatory of the University of Pennsylvania, which, through the gracious cooperation of Dr. Olivier and the officers of the University of Pennsylvania, was acquired on a loan basis for a period of 5 years. Later the period of the loan was extended. It was shipped to the McDonald Observatory during the summer of 1949 and, after the necessary overhaul and repairs, was put into operation in a new housing in June, 1950. The observations for the regular asteroid program started in August, 1950, and were completed May 26, 1952. The program of observations consisted of the photography during each dark-of-the-moon period of an area of $40° \times 40°$, centered on the opposition point of the sun at the time of new moon. This program was continued without interruption for 23 lunations, so that a belt 40° wide, centered on the ecliptic, was covered in nearly two complete annual cycles. Since the synodic period of an asteroid situated at 2.8 astronomical units is 15 months, ample overlap was provided in this manner. Essentially all asteroids brighter than 16 and with a ≥ 1.7 will have been included; only occasional objects with high inclinations will have been missed. The plates are all 8×10 inches in size, exposed for 10 minutes each, taken in pairs separated by about 1 hour. This caused the asteroid images to appear essentially stellar and to move from 2 to 6 image diameters between the two plates. Usually 48 plate pairs were needed to cover the monthly area of $40° \times 40°$. Consecutive monthly centers were about 30° apart, so that a safe margin of overlap was provided each month. In all, over 2400 program plates were taken, including Selected Areas, one for each night. The observations were made almost entirely by two night assistants, first, Mr. W. Braun and, later, Mr. H. Rubingh, who carried out their assignments with great devotion and care.

The reduction of the plates consists of four stages: (1) the blinking of all the plate

* *Contributions from the McDonald Observatory, University of Texas*, No. 239.

pairs, in order that an entirely independent survey of the asteroid belt becomes available down to $m = 16$ or 16.5; (2) the measurement of the positions and daily motions of the asteroids found; (3) the identification of the known objects and the re-examination of the plates for known objects missed; and (4) the measurement of the magnitudes of known and new asteroids.

At this time of writing, over 500 pairs have been blinked, about 45 per cent of the total, while the measurements have nearly kept pace with the blinking. The reduction work was started by Messrs. A. Fujita and J. Kent and is currently continued by Miss I. Groeneveld, and Messrs. G. Van Biesbroeck, A. Gehrels, and C. J. Van Houten, ably assisted by Mrs. H. E. Thorson. The results are being prepared for publication in consultation with the Minor Planet Center at Cincinnati.

Program B became practicable after the introduction of the new photoelectric techniques with the 1P21 photomultiplier tubes. Nearly all observations were made with the 82-inch telescope. They were begun in 1949 by Messrs. Kuiper and Shatzel and have been continued at regular intervals since. It was clear that the most efficient observing procedure would be to make long continuous runs on first-class nights, of preferably 8 hours or more, so as to simplify the problem of finding the period and the shape of the light-curve. Often two or three consecutive nights were used to cover one object.

Mr. Shatzel is publishing the result of 44 Nysa in a separate paper, while some other 1949 observations are given below. The work was continued in 1950 and 1952 by Messrs. Harris and Kuiper; most of these results are incorporated in this paper. Early in 1953 Messrs. Ahmad and Harris obtained extensive observations on asteroids 1, 8, and 22, which were reduced by Mr. Ahmad and will be published by him. Later in 1953 the present authors observed Nos. 8, 15, 17, 39, and 511; most of that material is included here. The reductions of the observations here discussed were made by Miss Groeneveld and Messrs. Ahmad and Harris. Mr. Harris' contributions to this program have been so extensive that he may in several ways be regarded as a co-author of this paper. Some of the comparison stars used in this paper were kindly measured by Mr. Hiltner, who has also advised us on procedures of measurement and reduction. Additional measures, made in December, 1953—January, 1954, are now being prepared for publication. A preliminary report on some of the material included in this paper was presented by Kuiper and Ahmad (1953) at the December, 1952, meeting of the A.A.S.

II. THE PHOTOELECTRIC OBSERVATIONS

All observations were made with the 82-inch telescope. The photometers and amplifiers used were constructed by Messrs. Hiltner and Johnson, to whom the authors are greatly indebted. The blue filter used in 1949 and 1950 had a somewhat wider transmission band than that used thereafter, which is the standard combination introduced by Johnson and Morgan (1951); furthermore, since 1953, ultraviolet observations have been added. The 1949–1950 colors are therefore not on the "standard" system, defined later, but can be used to check for the presence of color variations.

The magnitude system adopted is that defined by Johnson and Morgan (1953). The standard stars were all taken from that paper. The normal procedure was to observe, first, a pair of standard stars of very different color, then the asteroid and its comparison star, in turn, throughout the entire run; and, finally, another pair of standard stars. The standards were observed in three colors, B, V, and UV, but the comparisons between the asteroid and the comparison star were mostly made in yellow light, with only occasional measures made at the two other wave lengths. In several of the 1950 runs all comparisons were made in both yellow and blue. Since, however, it was found that the asteroids do not change their colors appreciably in the course of their light-variation, this procedure was abandoned, and blue comparisons were made thereafter only for color measurements two or three times per night. All photometer readings were made in duplicate, separated by a sky reading in the same color.

The data were recorded on a Brown potentiometer, with individual readings lasting about 40 seconds. The comparison stars were selected for their proximity to the asteroid, usually within $\frac{1}{4}°$, and for their similarity in color and magnitude. Comparison stars used for the same asteroid on different nights were intercompared afterward.

The coefficient of extinction was occasionally determined from the observations of the standards and the comparison star; usually, a mean extinction coefficient was used to correct for the differential effects between the standards and the comparison star. Differential extinction between the comparison star and the asteroid was allowed for when necessary, but was always very small. The differential extinction effects caused by the small differences in color were negligible for the yellow measures used in the light-curves. The only remaining correction to the standard system is that introduced by the use of different multiplier tubes at different times, which may cause slight shifts in effective wave length even if used in combination with the standard filters. This correction is in the nature of a color term and has been evaluated and applied.

III. THE LIGHT-CURVES

The light-curves derived as described earlier are reproduced in the figures. These are arranged according to a uniform procedure: the number of the asteroid, the date of observation, and the U.T. are given, as well as the magnitude of the asteroid at maximum light expressed in the standard system. In a few cases the magnitude of the maximum is missing because no suitable standards had been measured. Individual pairs of measures are plotted as points; open circles represent uncertain values, unless a different explanation is given in the legend. Supplementary data, among which are the geocentric coordinates of the asteroid at the time of observation, are given in Table 1. These coordinates determine the *aspect* of the object and are needed when different light-curves of the same asteroid are compared. The U.T. values given are as observed, uncorrected for light-time.

The principal derived quantities are collected in Table 1. The columns contain, respectively, the number of the asteroid, the date of observation, the observers, the visual magnitude of the maximum, $B-V$ and $U-B$, all three in the standard system; the amplitude in visual light, the period and its estimated uncertainty, the mean magnitude derived from the entire light-curve; the resulting quantities m_0 and g used in ephemerides; the phase coefficient; the interval covered by the observations, in hours; the R.A. and Dec. of the asteroid at the time of observation (aspect); and the figure number showing the observations. For two cases the phase coefficients were computed from our own data, as mentioned in the discussion of the light-curves. For five others Müller's (1897) phase coefficients were used; they are designated by M. For 97 and 511 the adopted values are somewhat arbitrary. Improved phase coefficients will lead to more accurate values of m_0 and g. Dr. W. Strobel, of the Rechen Institut at Heidelberg, kindly supplied us with the heliocentric and geocentric distances of the majority of the asteroids observed here, while Dr. D. L. Harris kindly computed the remainder.

Vesta (No. 4).—Reference is made to a previous publication by Stephenson (1951), based on a one-night run with the 82-inch telescope by Johnson and plotted in our Figure 1 and six nights with the Yerkes Observatory 12-inch telescope. The period derived was 5^h20^m, but the possibility of the double period (10^h41^m) was left open. Stephenson also listed previously announced periods and color changes. Mr. Harris secured a 10-hour run with the 82-inch telescope, which is shown in Figure 2. This long run shows two very similar cycles and would suggest that the shorter period is correct. However, additional observations from different aspects are needed before this can be considered established. For comparison, the earlier 82-inch observations in Figure 1 are shown with the short period; the original observations are plotted as dots and have been replotted one period earlier or later as triangles, so as to bring out the shape of the light-curve. It appeared necessary to add a vertical displacement of 0.013 mag. per cycle, which is in approxi-

TABLE 1

SUMMARY OF PHOTOMETRIC RESULTS

No.	Day	Month & Year	Obs.	V of Zero	$V-B$	$U-B$	Amp.	Period	Mean V of One Period	m_0	g	Phase Coeff.	Interval Observed (Hours)	R.A.	Dec.	Fig.
4.....	22	Dec., 1950	J	7.30	.....	.....	0.13	5^h20^m5	7.36	6.12	3.58	0.022M	6.0	2^h26^m	+ 6°.5	1
	7	Mar., 1952	H	6.10	0.78	0.45	.12	(see text)	6.15	6.04	3.50	.022M	10.1	10 44	+19°.0	2
7.....	12	Aug., 1950	K, H										2.2			
	13	Aug., 1950	K, H										3.7			
	14	Aug., 1950	K, H	*	.....	.....	.29	7 07.5±2	*	*	*	.019M	2.4	18 06	−19°.5	3
	16	Aug., 1950	K, H										1.7			
	28	Jan., 1952	K, H	8.11	.84	.41	.22	7 03 ±2	8.22	8.67	6.08	.019M	7.9	7 54	+13°.9	4
9.....	2	Nov., 1949	K, S	8.27	.....	.....	.11	5 03 ±2	8.34	6.31	8.91	.041M	6.6	2 41	+10°.5	5
15.....	11	Aug., 1950	K, H	*	.....	.....	.43	6 05	*	*	*	.042	4.6	19 18	−20°.3	6 (8)
	15	Aug., 1950	K, H										3.6	19 16	−20°.2	7 (8)
	25	Jan., 1952	K, H	8.62	.82	.44	.48	6 05	8.86	8.63	5.44	(.042)	6.0	5 58	+26°.0	9
	7	Apr., 1953	G, K	9.66	.812	.41	.42	.....	9.83†	8.66†	5.46†	(.042)	4.2	12 03	−18°.6	10
17.....	28	Mar., 1953	G, K	10.82	.865	.....	.....	.....	.....	.....	.....	.....	2.3	11 46	+ 9°.7	14
	31	Mar., 1953	G, K	10.871	.843	.....	.32						6.5	11 45	+10°.1	11 (13)
	2	Apr., 1953	G, K	10.912	.822	.414	.32	12 16.5	11.02†	10.87†	8.07†	.040	8.0	11 42	+10°.3	12 (13)
	19	Apr., 1953	G, K	11.188	.859	.460	.36						4.7	11 33	+11°.3	15
25.....	5	Aug., 1950	K, H										3.2			
	6	Aug., 1950	K, H	9.93‡	.....	.....	.18	9 56.7	10.02:	10.90:	8.27:	.025M	5.1	19 11	+22°.3	16
	7	Aug., 1950	K, H										0.9			
	10	Aug., 1950	K, H										4.7			
39.....	29	Jan., 1952	K, H	10.17	.89	.52	.18	5 11	10.28	9.83	6.38	.022M	6.5	6 26	+11°.6	17
	4	Apr., 1953	G, K		.86	.....	.....	.....	.....	.....	.....	.....	(5.7)	12 15	+ 6°.2	.....
	10	Apr., 1953	G, K	10.53	.88	.49	.22	5 09.5±1	10.65	9.87	6.42	.022M	5.7	12 11	+ 6°.8	18
97.....	4	Nov., 1949	K, S	*	.....	.....	.....	.....	.....	.....	.....	(.040)	4.0	1 09	− 8°.8	19
	5	Nov., 1949	K, S	*	.....	.....	.....	.....	.....	.....	.....	.....	3.8	1 08	− 8°.8	
511.....	26	Jan., 1952	K, H	9.95	.71	0.34	.06	5 07 ±5	9.98	10.62	6.40	(.030)	7.3	7 36	+25°.0	20
	8	Apr., 1953	G, K	11.309	0.724	.....	0.25	5 13 ±4	11.44	10.87	6.65	(0.030)	5.9	13 47	+12°.7	21

* Data incomplete; to be published later. † Half-period used only. ‡ Without color reduction.

mate agreement with the shift expected from the motion of the asteroid. The change in the light-curve between Figures 1 and 2 is apparent. If the short period is confirmed in future observations, Vesta will be the only object so far observed showing one maximum and one minimum during a cycle; this circumstance would lead one to look on the 5-hour period with suspicion.

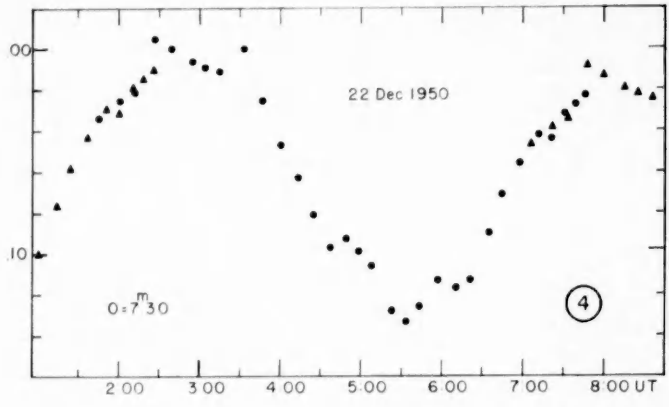

FIG. 1.—Light-curve of 4 Vesta. Triangles are observations replotted one cycle earlier or later and moved vertically 0.013 mag.

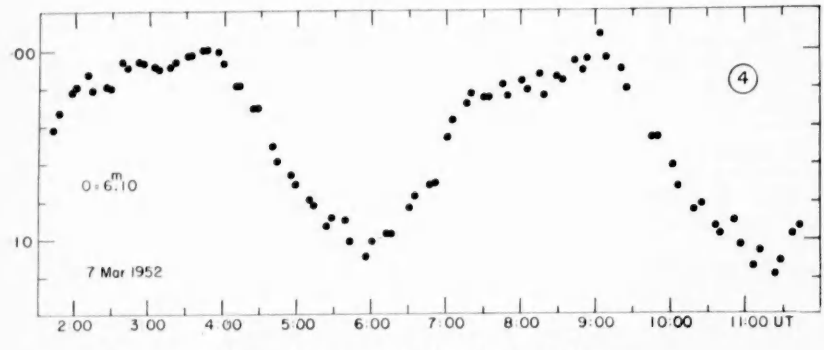

FIG. 2.—Light-curve of 4 Vesta. Single night's run

The phase angles of the 1950 and 1952 observations are 18°.0 and 4°.3, respectively. The g values may be brought into coincidence, at 3.48, by using the coefficient 0.028 mag/degree.

Reference is made to an important series of 138 photoelectric measures of Vesta published by Giclas (Slipher *et al.* 1951), covering the period of October 8, 1950, to March 6, 1951. The measures were made in both blue and yellow light and lead to phase coefficients of 0.035 and 0.033 mag/degree, respectively. Actually, some small deviation from a linear relationship between magnitude and phase angle was found. Giclas derived the period

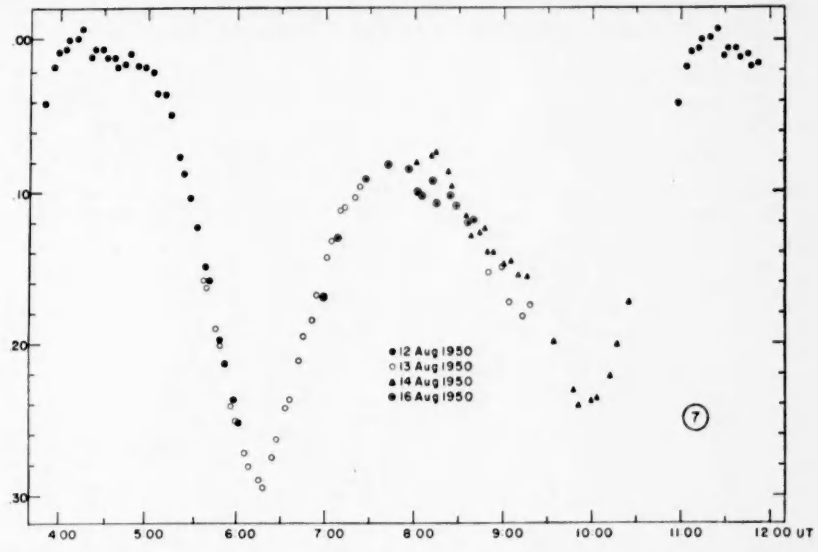

FIG. 3.—Light-curve of 7 Iris. Times refer to August 12 observations; magnitudes all reduced to August 12 (see text). Observations 11^h–12^h are replotted from earlier cycle to complete light-curve.

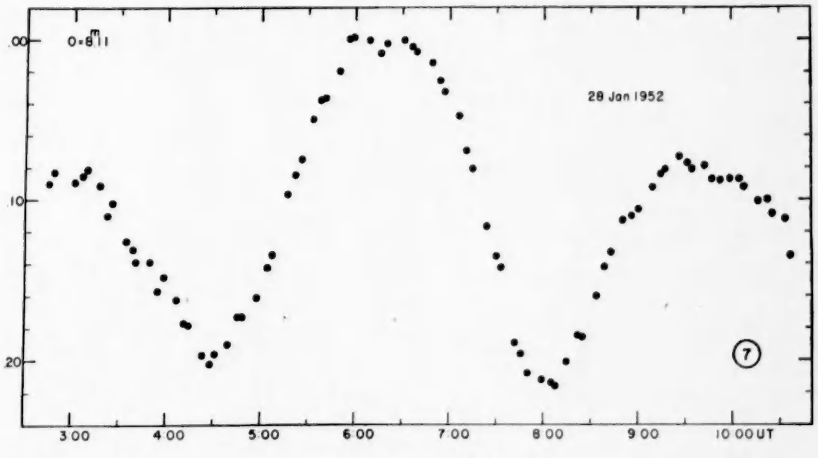

FIG. 4.—Light-curve of 7 Iris

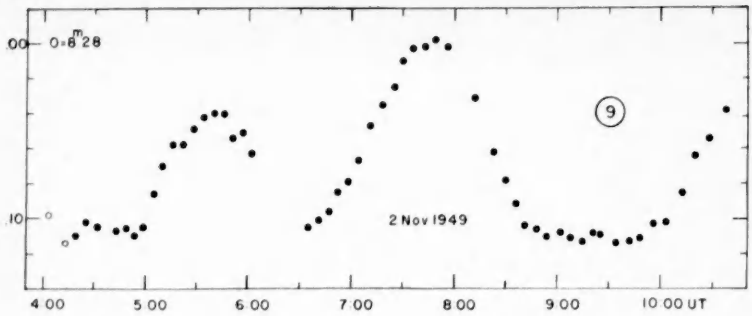

FIG. 5.—Light-curve of 9 Metis. The zero point is 8.27 (corrected)

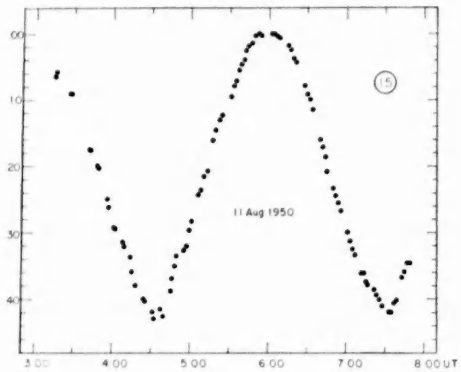

FIG. 6.—Observations of 15 Eunomia

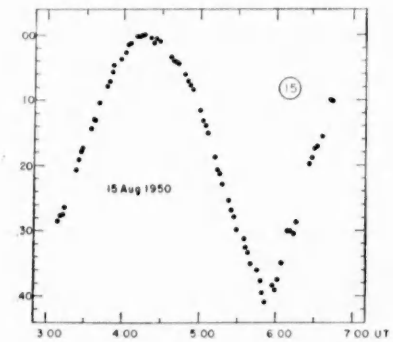

FIG. 7.—Observations of 15 Eunomia

$5^h20^m5653 = 0.222615$ days, in full accord with that found by Stephenson from observations during the same opposition. The light-curves found were also quite similar.

Iris (7).—Observations were made at two epochs; they are shown in Figures 3 and 4. Figure 3 is based on measures taken on four nights, all reduced to August 12, 1950. Allowance was made for the changes in distance of the asteroid to the sun and to the earth (corrections −0.006, −0.013, and −0.027 mag.) and for changes in phase angle by using Müller's phase coefficient of 0.019 mag/degree (corrections −0.006, −0.011, and −0.022 mag.).

Comparison of the two light-curves shows a considerable change in amplitude but a general resemblance in shape. The high minimum occurs in both cases before the high maximum. The periods derived from the two curves are mutually just consistent, as is

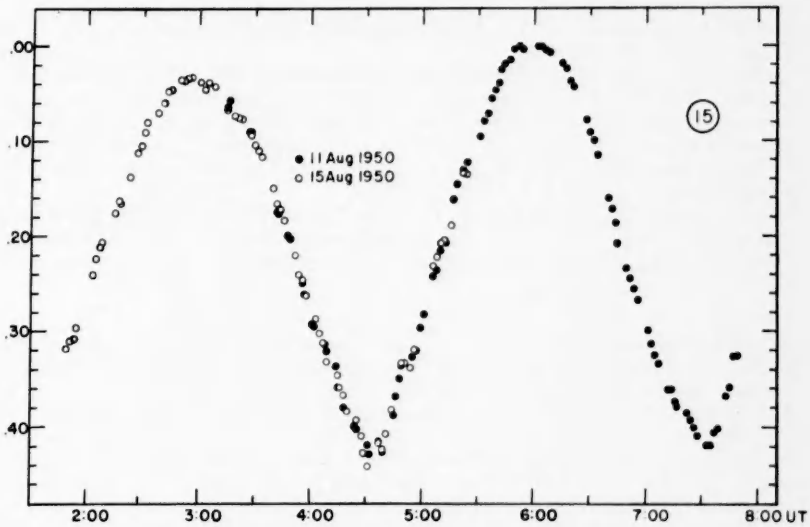

FIG. 8.—Curves 6 and 7 combined, reduced to August 11 (see text)

seen from the data in Table 1. The number of cycles between the two sets of data is still uncertain.

Metis (9).—The observations (Fig. 5) are exceptionally accordant. A second series was obtained in January, 1954, which is published in Paper II.

Eunomia (15).—Figures 6 and 7 show the observations of the separate nights, and Figure 8 the combined result of the 1950 observations. The August 15 measures were reduced to August 11 by allowing for the change in the distances (0.007 mag.) and in phase. The phase angle changed 1°.6, and the two light-curves indicate a shift of 0.068 mag. due to phase, corresponding to a phase coefficient of 0.042 mag/degree. This is slightly higher than Müller's value of 0.028 mag.

The 1952 observations (Fig. 9) show a somewhat increased amplitude, but an otherwise very similar light-curve, with two unequal maxima and a small difference between the minima; the deepest minimum precedes the highest maximum. The periods derived are the same. The 1953 observations (Fig. 10) show one of the maxima flanked by the two minima. The period may now be determined more accurately by comparing the three

sets of data. This is done in Section IV. It indicates that the maximum in Figure 10 is a primary maximum.

Thetis (*17*).—This object was observed on four nights, in March and April, 1953. The long runs of March 31 (Fig. 11) and April 2 (Fig. 12) appeared to define a very similar light-curve and could accordingly be combined (Fig. 13). The reduction of March 31 to April 2 appeared to be +0.042 mag. This is interpreted as due to a distance correction of +0.002 mag. and a phase correction of +0.040 mag., caused by an increase in phase of 0°.9 (from 8° to 9°). This indicates a phase coefficient of the order of 0.04 mag/degree. The amplitude of the light-curve of April 19 (Fig. 15) was distinctly different, and even the shorter run on March 28 (Fig. 14) showed a somewhat different slope. The period, 12^h16^m5, is the longest among the asteroids here included.

Phocaea (*25*).—The period of this curious light-curve (Fig. 16) is nearly 10 hours. The measures, obtained during four nights, are reduced to August 5.25 by correcting for the varying distances but not for changes in phase, which were very small (from 24°.78 to 25°.15 during the 5-day interval).

Laetitia (*39*).—Light-curves for two nights are reproduced here as Figures 17 and 18. The curves are similar and define precisely the same period; but the amplitudes are 0.17 and 0.18 mag. on Figure 17, and 0.21 and 0.22 mag. on Figure 18. The secondary maximum is quite low in Figure 17. Observations on a third night (April 4, 1953) were disturbed by clouds and cannot be used except for a check on the period. A secondary maximum occurred on 7^h0^m U.T., April 4, 1953.

Because the epoch of the April 4 observation may be uncertain by possibly as much as 5 minutes, the number of cycles between the 1952 and the 1953 observations cannot yet be determined with certainty. The combined 1953 observations make the period

$$P = 5^h10^m75 \pm 0^m2 = 0.21580 \pm 0.00014 \text{ days}.$$

If Müller's phase coefficient 0.022 mag/degree is used, the g values become 6.38 and 6.42 mag. Coincidence would be obtained by using 0.013/degree; but since the aspect has changed by nearly 90°, such precise coincidence is not required.

Klotho (*97*).—Two runs, on consecutive nights, of about 4 hours each, are shown in Figure 19. The second night was reduced to the first by a shift of −0.020 mag., based on the correction for the distances (0.004 mag.) and phase, with an assumed phase coefficient of 0.040 mag/degree. The total range shown is 0.07 mag., but the period is still unknown and the light-curve incomplete.

Davida (*511*).—The two light-curves (Figs. 20 and 21) look very different, but define the same period of approximately 5^h10^m. The scatter near the minima on Figure 21 is somewhat surprising. The g values differ by about 0.25 mag., suggesting that the average area visable in Figure 20 was larger than that in Figure 21. The aspects differed about 90°. To attribute the difference to phase effects would lead to wholly spurious results; the phase angles are 3° and 6°. This points up a general difficulty: that determinations of the phase coefficient may contain an effect of *area change*, resulting from a change in aspect.

The reductions for light-time have not been made in the abscissae used in the light-curves. They are listed separately in Table 2, which also gives the phase angles corresponding to the light-curves.

IV. PERIOD, AXIS OF ROTATION, AND SHAPE

The observed period of an asteroid during a limited interval of time (say, a week or two) will not, in general, be the true period of rotation but the instantaneous synodic period. If it be assumed that the true period is constant and that the axis of rotation is fixed in space (a dangerous assumption that will need verification for each object), a simple relation exists between the true period and the synodic period.

Consider a nonrotating co-ordinate system, centered on and moving with the asteroid;

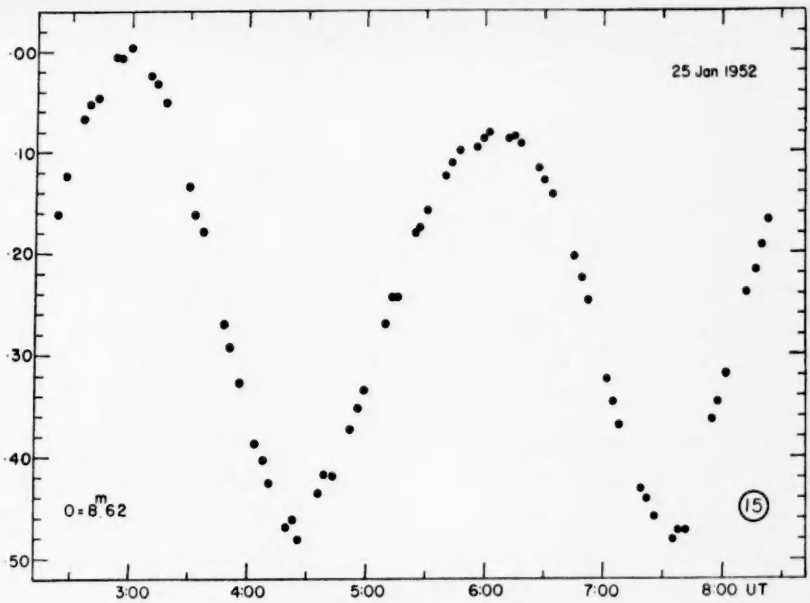

FIG. 9.—Light-curve of 15 Eunomia

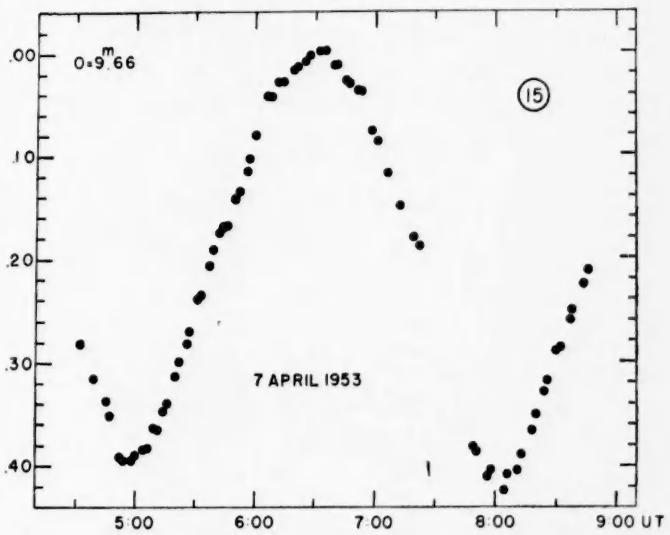

FIG. 10.—Observations of 15 Eunomia

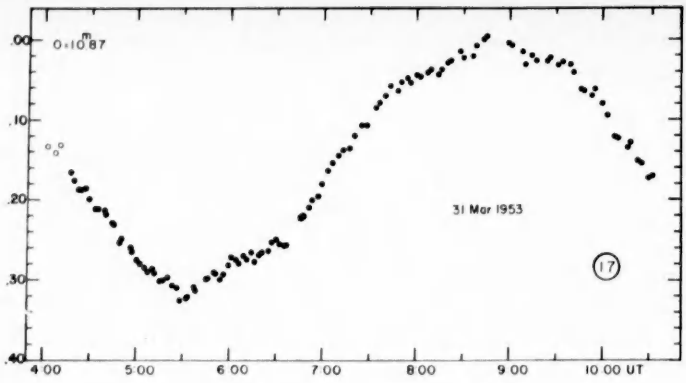

FIG. 11.— Observations of 17 Thetis

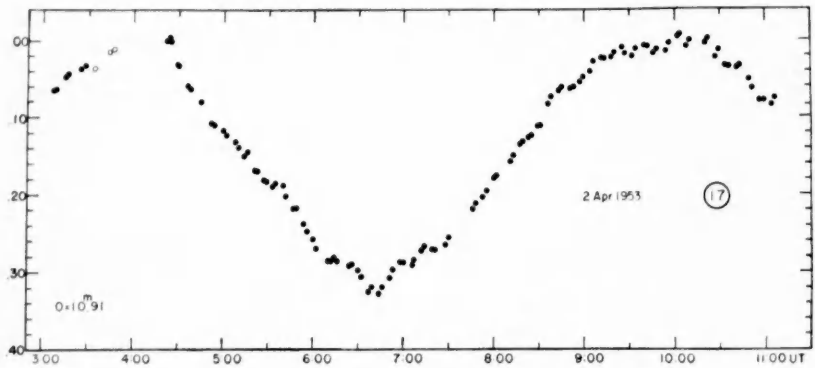

FIG. 12.— Observations of 17 Thetis

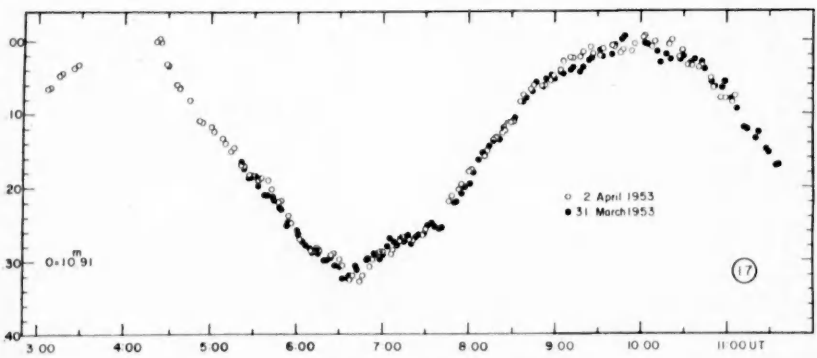

FIG. 13.—Combination of curves 12 and 13, reduced to April 2, 1953

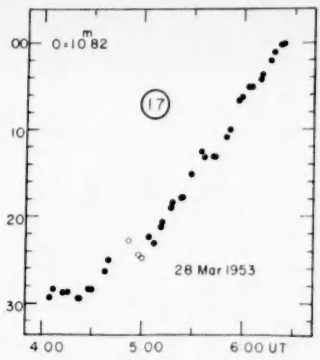

FIG. 14.—Observations of 17 Thetis

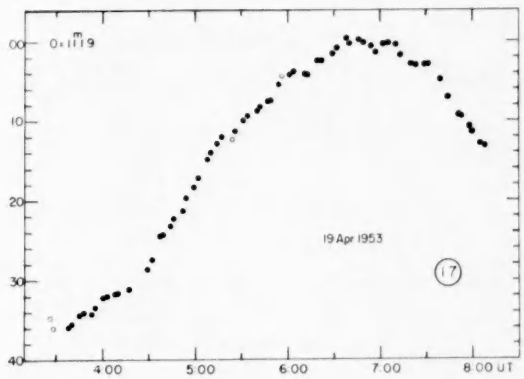

FIG. 15.—Observations of 17 Thetis

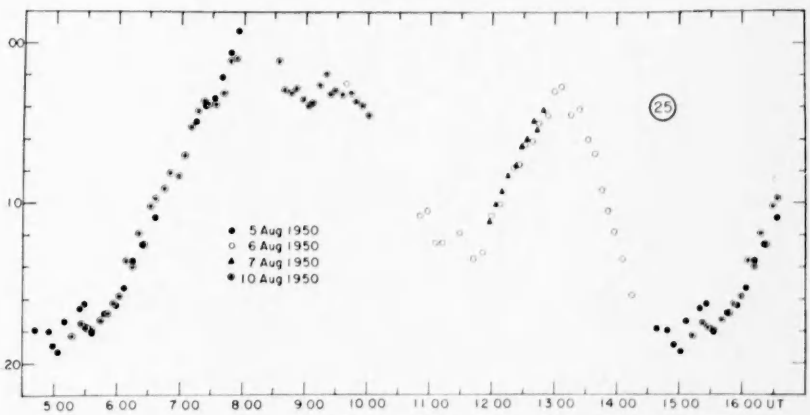

FIG. 16.—Light-curve of 25 Phocaea, reduced to August 5, 1950 (see text). Observations beyond 14^h30^m replotted to define light-curve.

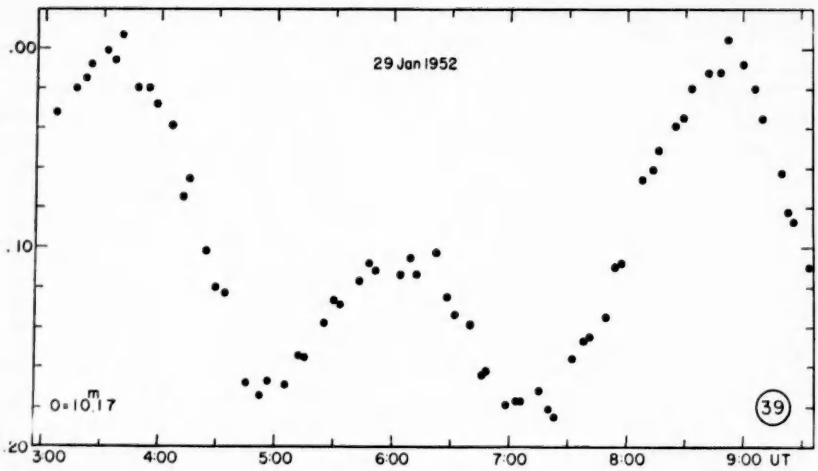

FIG. 17.—Light-curve of 39 Laetitia

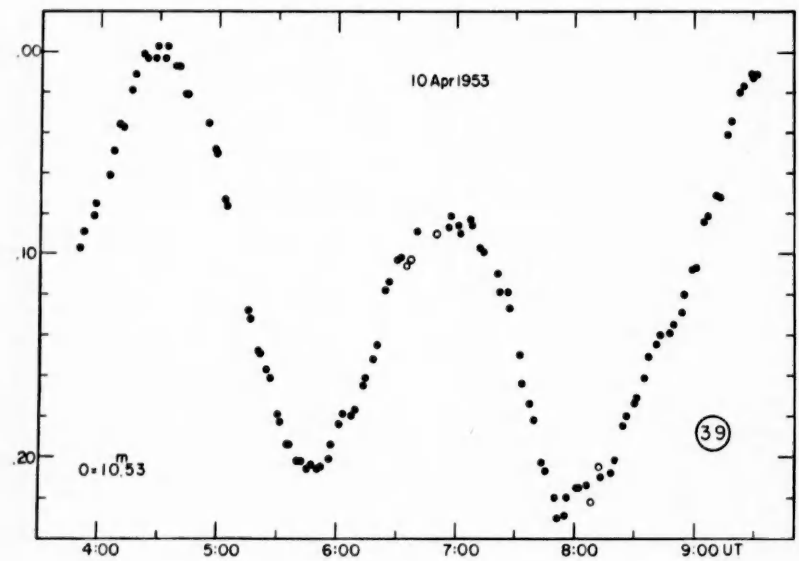

FIG. 18.—Light-curve of 39 Laetitia

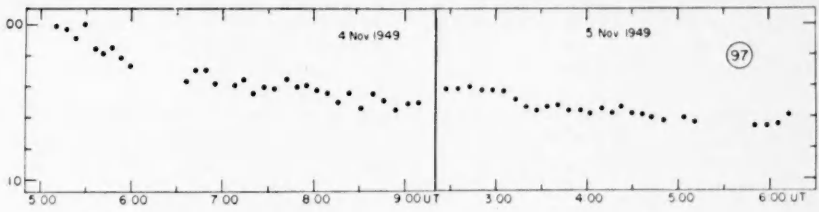

FIG. 19.—Observations of 97 Klotho

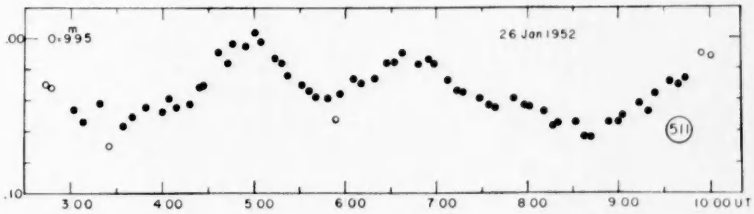

FIG. 20.—Light-curve of 511 Davida

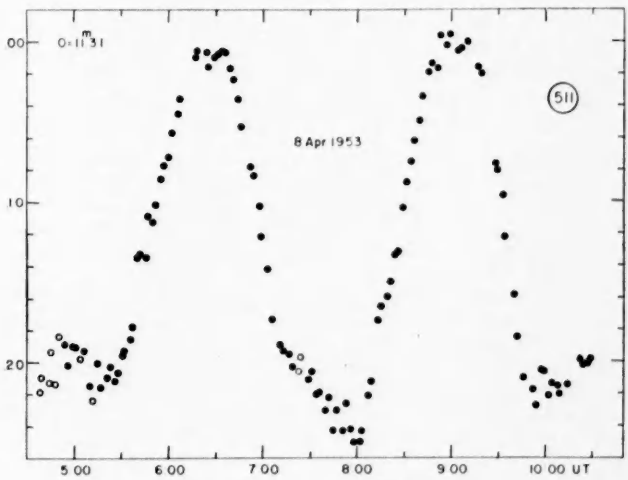

FIG. 21.—Light-curve of 511 Davida

and let the instantaneous position of the earth be on the positive y-axis (see Fig. 22). Further, let the xy-plane be so chosen that it contains the velocity vector of the earth, taken relative to the asteroid, with the negative x-direction parallel to the velocity vector. Now let the obliquity of the instantaneous rotational axis of the asteroid be θ (the angle with the z-axis), and let the azimuth of the axis from the xz-plane be $-\phi$. Assume that the asteroid, as seen from a distant stationary point in the plane of its equator, shows two light maxima and two minima, somewhat like a rotating book or box having its axis in the principal plane of symmetry. One can then derive the phase relations observed from a moving earth by watching the sweep of the normal to the broad face of the object.

TABLE 2

LIGHT-TIMES AND PHASE ANGLES

No.	Date	Light-Time (Minutes)	ϕ
4	22 Dec. 1950	−15.4	18°0
	7 Mar. 1952	−11.4	4.3
7	14 Aug. 1950	−14.2	17.8
	28 Jan. 1952	− 9.8	5.1
9	2 Nov. 1949	− 9.4	2.7
15	13 Aug. 1950	−13.6	12.0
	25 Jan. 1952	−12.8	13.3
	7 Apr. 1953	−17.8	6.0
17	28 Mar. 1953	−11.7	6.8
	31 Mar. 1953	−11.7	8.1
	2 Apr. 1953	−11.8	8.9
	19 Apr. 1953	−12.4	16.0
25	7 Aug. 1950	− 7.8	24.9
39	29 Jan. 1952	−16.0	11.2
	10 Apr. 1953	−17.7	6.8
97	4 Nov. 1949	− 9.8	14.6
511	26 Jan. 1952	−14.6	5.0
	8 Apr. 1953	−20.3	6.6

The normal will sweep out the equator and have an inclination on the xy-plane of θ and the ascending node, N, at $90-\phi$. The earth will see maximum light when the normal reaches the point on the sphere closest to the y-axis. Let this point be designated by E. Then the great-circle arc $\overline{NE}$ (and hence the fraction of the period after the nodal passage) may be found from the spherical triangle NEY, in which Y is the point on the unit sphere defined by the positive y-axis. Now $\overline{EY} = \theta$, $NEY = 90°$, and $\overline{NY} = \phi$. Accordingly, from spherical trigonometry,

$$\tan \overline{NE} = \cos \theta \tan \phi \,. \tag{1}$$

We are not interested in equation (1) itself but in how the epoch of maximum light will be delayed if the earth now moves by a known amount, reflected by an equal geocentric motion of the asteroid between the stars. Or we must find the change δE in $\overline{NE}$ as ϕ

changes by $\delta\phi$, owing to the motion of the earth. Differentiating equation (1), we find, after some reduction,

$$\delta E = \frac{\cos\ \theta}{\cos^2\ \phi + \sin^2\ \phi\ \cos^2\ \theta}\ \delta\phi\ . \qquad (2)$$

This equation gives the correction to the epoch of maximum for a given geocentric displacement $\delta\phi$ of the asteroid between the stars. More general formulae have been derived by Stobbe (1940), Huruhata (1940), and others in connection with the study of Eros; but the simple relation (2) shows the essentials of the problem.

Application of equation (2) to a determination of the orientation of the rotational axis, θ and ϕ, is straightforward, although the accuracy is quite limited, as will be seen. In the first place, θ and ϕ refer to the instantaneous co-ordinate system defined above. Since the true period will not, in general, be known, one may combine two series of observations, one before and one after the stationary point, so that the co-ordinates for the

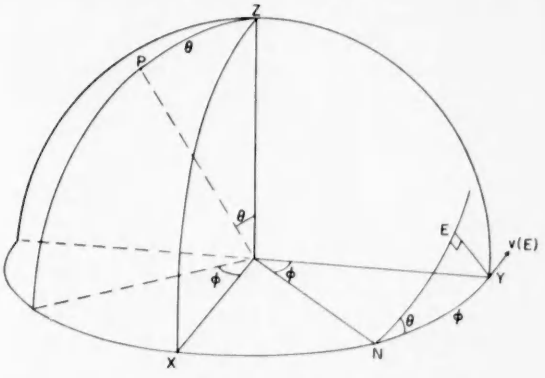

FIG. 22.—Co-ordinate system defining symbols used

two runs will be essentially the same. Since the values of $\delta\phi$ are known and since the sign reverses while θ and ϕ are constant (by assumption), the true period is found by imposing the condition that δE is proportional to $\delta\phi$; at the same time, one determination of the coefficient of $\delta\phi$ is made. A similar set of data taken at a different opposition, with the asteroid about 90° displaced, completes the determination of the orientation of the axis in space.

While the method described is correct in principle (provided that the axis keeps its orientation during the required 20 months or so), it is not very accurate. The epochs of maximum may, under favorable conditions, be determined with a precision of about 1 minute, so that an interval bounded by two such epochs is determined to ± 0.001 day. If, during each opposition, one establishes three epochs, one at the stationary point, one 2–3 months earlier, when the asteroid was, say, 10° from the stationary point, and one some 2 months *after* the stationary point, when the asteroid had returned to its first position, then $\delta\phi$ is of the order of 10° and δE also. Hence δE is about $\frac{1}{36}$ of the period, or about 0.007 days. The trigonometric coefficient in equation (2) is then known with an accuracy of some 14 per cent, which is hardly good enough.

Optimum conditions for the use of equation (2) are obtained by the use of the stationary points only. The average synodic period of rotation is then found from comparison of the epochs of one opposition with those of the next, while the two stationary points

provide the maximum possible value of $\delta\phi$, covering the entire interval of retrograde motion. For an asteroid moving in the ecliptic with a circular orbit and $a = 2.8$ a.u., the stationary points are 13°.40 apart. The trigonometric coefficient in equation (2) may therefore be determined with the precision of about 10 per cent. The method requires the derivation of accurate times of maximum at *four epochs* instead of six, covering a total interval of about 18–20 months.

A second method for the determination of the orientation of the axis depends on the *shape* of the light-curve and its time variations. The method has been used successfully for Eros (Watson 1937; Huruhata 1940; Stobbe 1940; Beyer 1953). In this case the amplitude varies between about 1.5 and 0.0 mag., and a good determination of the orientation may be made. The rotation of Eros is found to be direct and the position of the pole variable, though there is disagreement on the amount of variation.

In the case of 15 Eunomia, however, the amplitude of the light-curve does not vary greatly at the epochs observed. One may provisionally conclude that the axis of rotation is roughly at right angles to the ecliptic and attempt to establish the *sense of rotation* from the epochs. One thus assumes $\theta = 0°$ in equation (2), so that $\delta E = \delta\phi$. Unless one can make use of the occasional retrograde motion of the asteroid, one would find only the synodic period and could not determine the sense of the rotation. However, the four epochs covered by our observations appear to be sufficiently irregular for this purpose. The light-curves define the epochs, uncorrected for light-time, given in the accompanying tabulation; dates are JD − 2430000. From these data the mean intervals between the four

3504.690	I Min.	4036.625	I Max.
.750	I Max.	.683	II Min.
.814	II Min.	.753	II Max.
		.815	I Min.
3508.678	II Max.		
.746	I Min.	4474.706	I Min.
		.772	I Max.
		.835	II Min.

cardinal points on the light-curve may be found, and thereafter they can be combined into four main epochs of primary maximum. These are given in Table 3. The third column gives the Julian day corrected for light-time.

TABLE 3

EPOCHS OF PRIMARY MAXIMUM, 15 EUNOMIA

No.	JD	JD(c)	R.A.	Dec.	λ	β
1	3504.751	3504.742	19^{h}18^m	−20°.3	288°	+ 2°
2	3508.804	3508.795	19 16	−2°.2	287.5	+ 2
3	4036.623	4036.614	5 58	+20.5	89.5	− 3
4	4474.771	4474.759	12 02	−18.6	186	−17

A further correction needs to be made when the phase angle exceeds 10° or 15°, as was shown by Huruhata (1940); it arises from the illumination of the asteroid depending on the phase angle and the resulting shift in the epochs of maximum and minimum light. It is readily shown that for small values of ϕ the displacement varies as ϕ^2; the effects on our observations of 15 Eunomia may be neglected.

The uncertainty of the four epochs is estimated to be between ±0.001 and 0.002 day; we adopt ±0.0015 day. Table 1 gives $P = 6^h05^m \pm 1 = 0.2535 \pm 0.0007$ day. Hence

$16P = 4.056 \pm 0.011$ days, while the interval (2–1) in Table 3 gives 4.053 ± 0.002 days. Since $\lambda_1 \cong \lambda_2$, the true period is $(4.053 \pm 0.002)/16 = 0.25331 \pm 0.00013$ day.

The light-curves of (15) suggest that the axis of rotation is oriented roughly at right angles to the ecliptic. We must then be able to represent the epochs either by direct or retrograde rotation.

	λ
JD 3506.768	288°
4036.614	89.5
4474.759	186

Now $\Delta_1\lambda = 161.5° = 0.114$ day; $\Delta_2\lambda = 96.5° = 0.068$ day.

With direct rotation $n_1P = 529.844 - 0.114 = 529.730$ days
and $n_2P = 438.145 - 0.068 = 438.077$ days.
With retrograde rotation $n_1P = 529.844 + 0.114 = 529.958$ days
and $n_2P = 438.145 + 0.068 = 438.213$ days.

With $n_1 = 2091$ and $n_2 = 1729$, P is found to be 0.2533381 and 0.2533702 day for direct rotation; and 0.2534472 and 0.2534488 day for retrograde. The discrepancy in P for direct rotation can be reduced by using $n_1 = 2092$ and $n_2 = 1730$; then P is found to be 0.2532170 and 0.2532237 day.

All these six periods are compatible with the true period derived earlier from the 4-day interval, while no others would be. The long intervals give $\Delta P = 0.0000067$ for direct and 0.0000016 for retrograde rotation. The uncertainty of each interval being ± 0.002 day, the two P values are uncertain by ± 0.0000010 and ± 0.0000012 day, respectively; their difference by ± 0.0000016 day. Therefore, *retrograde rotation* is compatible with the data, but direct rotation is not. Clearly, some extra uncertainty may be introduced in ΔP by the assumptions made above concerning the position of the rotational axis.

The *shape* of an asteroid is, strictly speaking, undeterminable from its light-curve, as Russell (1906) has shown, because the light-curve depends at the same time on the spottiness of the surface. It may turn out, however, that in most cases the average brightness over a hemisphere does not vary considerably, so that the light-variations would be due primarily to variations in the visible area—at least, when observations are made close to opposition so that shadows have no effect. There is some reason to anticipate this situation: from preliminary results on asteroid diameters, obtained with the disk meter on the 82-inch telescope, it appears that the asteroid albedos are quite similar, with, so far, only one definite exception, Vesta, which is brighter. Some of the tests proposed by Russell will disclose for which objects the hypothesis of constant surface brightness is valid. In those cases at least a simplified model may be found which, for objects brighter than the ninth magnitude, can be tested visually with the largest telescopes. The case of Eros, seen elongated by Van den Bos and Finsen in 1931, is a case in point.

The results of this section may be summarized as follows: For an asteroid with light-curve like 15 Eunomia, which shows little change in amplitude with aspect, the most efficient observational procedure is to measure accurate epochs during the two stationary points of each opposition. The combination of the results of two or more oppositions will then disclose whether the rotation of the asteroid is direct or retrograde. If the epochs have great accuracy, ± 0.001 day or better, the trigonometric factor in equation (2) may be determined for each opposition, and a rough determination of the orientation of the axis may be made. If the light-curve shows large amplitude variations with aspect, utilization of these data will greatly increase the precision of the axis position.

V. ASTEROID COLORS

Color measurements of the asteroids observed were usually made at the beginning and the end of each nightly run. In a few cases the color measurements were made con-

tinuously through the entire run. The latter results are shown in Figure 23. Comments on the three asteroids included follow.

Vesta (4).—The apparent color variations are not more than 0.015 mag. If the 5-hour period is correct, a slight systematic error (about 0.005 mag.) appears to be present, causing the second cycle to be slightly bluer than the first. On the double period this difficulty disappears. If we consider only the most accurate part of the curve (smallest

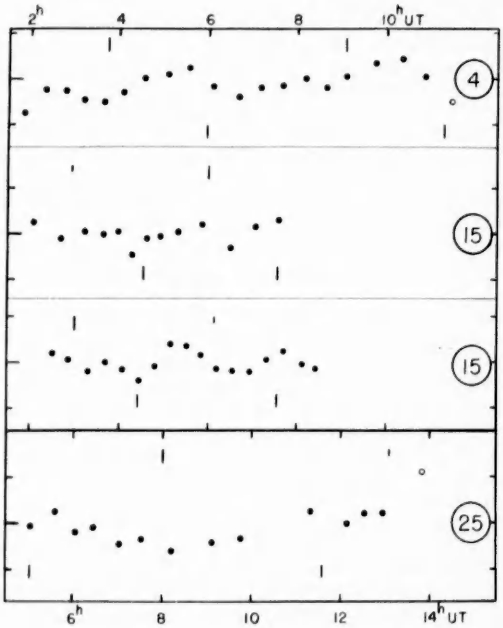

FIG. 23.—Color index ($B-V$) of three asteroids versus time (or phase). Vertical divisions are 0.02 mag. apart, with red toward bottom. Dots are averages of four measures, consecutive in phase, for 4 Vesta; six and four for 15 Eunomia; and seven for 25 Phocaea. The abscissae corresponding to the maxima are marked with short lines *above* the color curves; the minima *below*. For 15 and 25, slightly less than one cycle each is given, while two maxima and two minima occur in each cycle; the primary maximum is marked with a longer index line. The dates are, respectively, March 7, 1953; August 11, 15, 1950; January 25, 1952; August 5, 6, 7, 10, 1950. The light-curves corresponding to the color-curves are found in Figures 2, 8, 9, and 16.

zenith distances), namely, from maximum to maximum, we find 11 points which deviate, on the average, ± 0.003 mag. from the mean and which show a systematic variation of no greater than 0.010 mag.

Eunomia (15).—The first curve shows no distinct variation; the color index appears constant to within 0.01 mag.; the average residual with respect to the mean is 0.003 mag. The second curve indicates a minor variation of 0.01 mag. total amplitude; but if the color index is assumed to be constant, the mean residual is also 0.003 mag., so that we may suppose that no variation is established.

Phocaea (*25*).—If one ignores the uncertain point near 14 hours (obtained at $2\frac{1}{2}$ air masses), a wave of 0.01 mag. total amplitude seems indicated. However, if one assumes a constant color index, the mean residual is 0.005 mag.

The color variations of these three objects are remarkably small and suggest that color measurements cannot, in general, be used to determine the period of rotation or even remove ambiguities (single or double period).

Since the color variations of the asteroids appear to be small, representative color indices may be determined from occasional measures. The values so far derived are listed in Table 1. The $B-V$ colors of Nos. 7, 17, and 39 are very similar to those of Mercury and the moon; but Nos. 15, 4, and 511 are somewhat bluer by increasing amounts. These small differences are of distinct physical interest. The ultraviolet colors show similar differences.

VI. CONCLUDING REMARKS

Examination of the photometric results included in this paper shows that a greatly increased body of data will be needed before an adequate picture of the rotation and the shapes of asteroids can be constructed. The present program calls for the repeated observation of all asteroids reaching tenth magnitude at opposition, plus one or two dozen fainter objects. It has been shown that a single asteroid must be observed on at least four epochs during two oppositions, preferably near the stationary points, before something definite can be said about the axis of rotation and the shape of the body; but because of the uncertainty of the assumption of a constant orientation of the axis, observations at additional oppositions are necessary as checks. The period of rotation can usually be found during one long night or otherwise on two or three consecutive nights. Long, continuous runs on excellent nights are by far the most productive; because of the declination of the opposition point, winter nights are far more suitable than summer nights. From inspection of the light-curves it is clear also that, in general, visual or photographic observations would have been insufficiently accurate to allow a determination of the period. Comparison of our results with occasional earlier data obtained photographically confirms this conclusion. Even photoelectric work requires really good nights for successful observation.

All asteroids observed so far, with the possible exception of Vesta, show two maxima and two minima during one cycle. This is in accord with expectation if one is dealing with irregularly shaped bodies having a fairly uniform reflectivity over the surface, since the projected area will show two maxima and two minima during one cycle. On the other hand, a distribution of spots could give one maximum and one minimum per cycle. It is too early to make conclusions about the line of demarcation between *fragments*, resulting from violent collisions in the asteroid ring (such as leading to the Hirayama families; cf. Brouwer 1951); and *original condensations*, which would be roughly spherical, though they may have experienced minor collisions. The very frequent collisions expected in the asteroid ring (Kuiper 1953) may well have led to a roughly *random* distribution of axial orientations, i.e., to a roughly equal number of direct and retrograde rotations, with all possible obliquities. At the same time, all sorts of angles between the instantaneous axis of rotation and the axes of the inertia ellipsoid must have resulted. Unless dissipative forces are present, similar to those which damp the terrestrial latitude variation (Jeffreys 1952), the orientations of the rotational axes must be variable in periods of hours or days instead of years, while the absence of such rapid variations would prove the presence of dissipative forces in the asteroid interiors. This whole subject is full of promise for a deeper understanding of the origin and the physical properties of asteroids, which will repay the very large amount of painstaking photometric work that will be required in the solution.

Our indebtedness to Dr. Olivier and the University of Pennsylvania has already been recorded. The Research Corporation of America supported the transportation of the Cook Observatory telescope and its new housing to the McDonald Observatory. The research programs A and B were partly supported by the Office of Naval Research for three years, beginning July, 1950, under Contracts N9 onr-87100 and Nonr-443(00), while currently this work is partly supported by the National Science Foundation. Without this generous aid, the work could not have been undertaken.

REFERENCES

Beyer, M. 1953, *A.N.*, **281,** 121.
Brouwer, D. 1951, *A.J.*, **56,** 9.
Huruhata, H. 1940, *Harvard Obs. Circ.*, No. 442.
Jeffreys, H. 1952, *The Earth* (3d ed.; Cambridge: At the University Press), p. 210.
Johnson, H. L., and Morgan, W. W. 1951, *Ap. J.*, **114,** 522.
———. 1953, *ibid.*, **117,** 313.
Kuiper, G. P. 1953, *Proc. Nat. Acad. Sci.*, **39,** 1170.
Kuiper, G. P., and Ahmad, I. I. 1953, *Sky and Telescope*, **12,** 129.
Müller, G. 1897, *Die Photometrie der Gestirne* (Leipzig: Engelmann), p. 378.
Russell, H. N. 1906, *Ap. J.*, **24,** 1.
Slipher, E. C., *et al.* 1951, *The Project for the Study of Planetary Atmospheres* (Report No. 9).
Stephenson, B. C. 1951, *Ap. J.*, **114,** 500.
Stobbe, J. 1940, *A.N.*, **270,** 1, and references given there.
Watson, F. 1937, *Harvard Obs. Circ.*, No. 419.

SOLAR LIMB DARKENING IN THE REGION λλ 7793–24388*

A. KEITH PIERCE
McMath-Hulbert Observatory, University of Michigan, Pontiac, Michigan
Received March 12, 1954

ABSTRACT

Observed values of limb darkening determined with a *PbS* cell and the Snow telescope of the Mount Wilson Observatory are given for the near infrared. The method of correcting the observed curves for seeing, scattered light, and time constant is given in detail. The observed brightness distribution extends from $\cos\theta = 1.00$ to $\cos\theta = 0.10$, and covers the interval λλ 7793–24388 with values at 26 different wave lengths.

INTRODUCTION

The elementary theory of limb darkening, which closely fits the observed darkening, predicts that the distribution of intensity over the solar disk can be represented by the sum of two quantities, namely, half of an ellipse and a rectangle. The ellipse represents the variation of intensity over the disk, and the rectangle the finite boundary intensity. It is the steep intensity gradient at the limb that makes difficult the accurate determination of the limb darkening; for here the distribution is greatly modified by the effects of seeing, scattered light, and finite size of the scanning aperture. In addition, we also have the positional problem of determining the sun's limb and points within the solar disk.

Minnaert, van den Hoven van Genderen, and van Diggelen (1949) have given a method for evaluating the influence of seeing that blurs the limb-darkening-curves. Their procedure is based on a formula of Wanders (1934), who assumes that the seeing blurs the image of a point source according to a normalized two-dimensional Gaussian distribution with seeing constant a,

$$j = \frac{a}{\pi}\, e^{-a(\xi^2+\eta^2)}. \tag{1}$$

They next approximate the true limb-darkening distribution by the formula

$$i(r) = A + B\sqrt{r}\,, \tag{2}$$

in which A and B are constants determined from the observed limb darkening and r is the distance from the limb in units of the sun's radius. Equation (1) is applied to the points at the limb of the sun, considered as a straight edge. Integrating over η, they derive the expression

$$i(r) = \frac{A}{\sqrt{\pi}} \int_{-r\sqrt{a}}^{\infty} e^{-z^2} dz + \frac{B}{a^{1/4}\sqrt{\pi}} \int_0^{\infty} \sqrt{w}\, e^{-(r\sqrt{a}-w)^2} dw. \tag{3}$$

Equation (3) represents a family of S-shaped curves parametric in the seeing constant a. By fitting the observed contour of the solar limb to this family of curves, a value of a can be determined. Next the observed curve is represented as the sum of the theoretical curve (eq. [3]) and a correction-curve. Finally, the true profile at the limb is obtained through the procedure of sharpening the correction-curve by an iterative process and adding the result to $i(r)$ of formula (2). The use of the first term of equation (3) will be found in a later section.

Scattered light from instrument or sky is generally small. In the past the scattered light has been disregarded, or an average value of its intensity has been subtracted from

* Supported in part by Contract N60nr-232-V with the Office of Naval Research.

the limb-darkening-curves. Because the effects of scattering have been large in the author's observations, it has been necessary to make a more detailed study and correction for this error.

In the past the positional problem, that of relating intensity to points on the sun's disk, has been solved in two ways: (1) by the timing method; (2) by the measurement of position on photographic plates. Almost universally, the timing method, utilizing the diurnal motion, has been used. The advantage of stopping the telescope and allowing the sun to drift over the receiver was first noted by Abbot (1908). By this procedure, each point of the sun is observed through identical optical paths of the instrument and through identical atmospheric air masses. Abbot's method of obtaining 2-minute drift-curves was used. In addition, the writer obtained expanded runs near the limb by changing the rate of the coelostat drive.

The present observations cover the near infrared region in greater detail than previous observations (Abbot 1913, 1922; Peyturaux 1952; Pierce, McMath, Goldberg, and Mohler 1950). They were made on selected days of good seeing in the months of May and June, 1952, with the Snow telescope of Mount Wilson Observatory. The wave lengths were selected arbitrarily from regions of the spectrum free of absorption lines.

PROCEDURE OF OBSERVATION

The Snow horizontal telescope projects an achromatic image of the sun 18 cm in diameter on the first slit of a monochromator which acts as a filter before a grating spectrometer. For the present set of observations, the receiver was a cooled Cashman *PbS* cell. The modulated output of the cell was amplified by an a.c. amplifier, rectified, smoothed by an R.C. circuit, and recorded by a Leeds and Northrup Speedomax recorder. The deviation of the Wilson amplifier from linearity (Mohler, Pierce, Goldberg, and McMath 1950) was corrected in part by moving the zero point up and away from the toe of the curve. The remaining nonlinearity of about 1 per cent was evaluated on each day of observation by means of a series of rotating sectors.

A slit length of 10 mm and widths of from 0.1 to 0.25 mm were employed. The sagitta of the sun's limb, with this slit as a chord, corresponds to 0.15 per cent of the solar radius, while the widths correspond to 0.11 and 0.28 per cent of the radius. The second slit was opened until a relatively smooth trace was obtained. Wave-length intervals from 0.2 to 2.5 A were used.

In the early morning, 1–2 hours after sunrise, when the best seeing occurred, large-scale runs of the region near the limb were made, using the "off-rate" coelostat drive. Figure 1, *a*, illustrates the type of trace obtained on a day of excellent seeing. The double humps to the left are two fast runs across the central region of the sun's disk obtained by actuating the east-west slow-motion drive. The center was traced twice to improve the accuracy of the measured central deflection.

In the late morning the coelostat drive was stopped, and five 2-minute drift-curves were made across the complete diameter at each wave length (see Fig. 1, *b*). These runs extended from a point 1 solar radius away from the limb to a similar point on the opposite side. The scale of the original recording was 352 mm for the solar diameter.

On occasion, astigmatic differences as large as 20 cm were observed in the sun's image formed from the two plane mirrors of the coelostat system and the 24-inch concave, which are of glass coated with aluminum. In practice, these differences cause no great difficulty if the proper astigmatic focus can be selected so that the slit is parallel to the line of astigmatism. However, the slit of the spectrometer was fixed in a vertical plane, and the relative position of the coelostat and second flat were selected to drift the image horizontally; this arrangement used up all the degrees of freedom of the system, making it necessary to rotate the plane of astigmatism by other means. The various mirrors were rotated in their cells, but this proved to be only a temporary curve. It was found that if the mirrors were fully and equally illuminated or, in the case of the early morning runs,

if the elliptical beam from the coelostat to the first flat was rotated to the vertical plane or reduced to a circle by a suitably shaped and oriented paper diaphragm placed over the coelostat mirror, then the astigmatism could be reduced and rotated into proper orientation.

MEASUREMENT OF THE TRACINGS

A special machine was constructed for the measurement of the runs. Its basic structure consists of a drum 10.65 inches in diameter, around which the tracing is wrapped. A

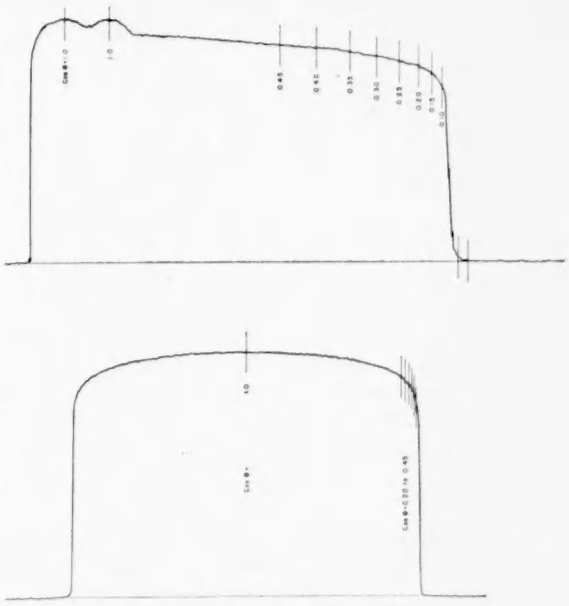

FIG. 1.—*Top*, Profile of the solar limb (λ 23,595 A) with a rapid traverse across the sun's center, the latter repeated twice. Points of measurements are indicated by vertical lines and the associated values of cos θ are given. *Bottom*, Limb-darkening-curve (λ 23,595 A) obtained by stopping the coelostat drive. A few of the measurement points are indicated.

millimeter screw drives a nut and microscope carriage parallel to the drum axis. One drum end is fitted with a large worm wheel, one turn of the worm corresponding to 2 mm on the paper. The other end of the drum is fitted with a millimeter scale around its periphery. A split nut and worm disengaging mechanism permits one to set quickly on any point within the 250 × 750-mm range of the engine.

From the measured length of a 2-minute limb-darkening-curve, the setting points corresponding to cos θ = 1.0, 0.9992, 0.95, 0.90, . . . , 0.20 were computed for both limbs and were set in the measuring machine with an accuracy of about 0.02 mm. The height of the curve was next read with an error of less than 0.05 mm. With the inclusion of points within and off the disk, 61 points were measured for each tracing. The center point, cos θ = 1.0, received one measure; all others, 2 measures, one for each limb.

CORRECTION FOR RECEIVER TIME CONSTANT

The observed limb-darkening-curves show a well-marked asymmetry due to the time constant of the smoothing circuits and the Speedomax recorder. At 2 per cent of the radius from the limb ($\cos\theta = 0.2$), the ascending limb is about 2 per cent lower than the descending limb. This difference decreases rapidly toward the center of the sun's disk. For example, at 4.6 per cent from the limb ($\cos\theta = 0.3$), the difference has decreased to 1 per cent.

A general method for correcting the drift-curves for time delay has been given in an earlier paper (Pierce *et al.* 1950). By use of the superposition theorem, the observed recorder deflection $\delta(t)$ can be related to the time rate of change of the incident radiation

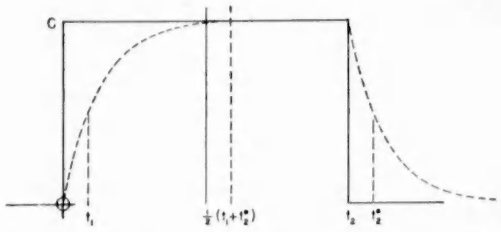

FIG. 2.—The effect of an exponential time delay in recording a rectangular light-pulse

$I'(\lambda)$. If $K(t)$ represents the deflection of the recorder in response to a unit step in intensity I, and if $I(0)$ is a finite step in intensity at the origin of time, then one form of the superposition theorem is

$$\delta(t) = I(0)\,K(t) + \int_0^t K(t-\lambda)\,I'(\lambda)\,d\lambda\,. \tag{4}$$

If equation (4) is applied to a simplified solar intensity distribution corresponding to a rectangular light-pulse, as illustrated by Figure 2, the deflection for the rise is

$$\delta(t) = c\,(1 - e^{-ft})\,, \tag{5}$$

where c is the height of the step, and we assume that the recorder responds exponentially with a time constant $1/f$. In like manner, the resulting deflection for the fall is

$$\delta(t^*) = c\,(1 - e^{-ft_2})\,e^{-ft^*}\,, \tag{6}$$

where t^* is referred to an origin of time beginning at t_2. Equations (5) and (6) are represented by the dashed lines of Figure 2. If the limb points are considered to be at $c/2$ of the time-delay-curve, then the center point is at

$$\tfrac{1}{2}t_2 + f^{-1}\ln 2\,c\,. \tag{7}$$

It is apparent from the figure that the least error in representing the rectangular pulse occurs for the last half of the curve, except at the extreme limb within a distance of about the time constant from the edge.

A more accurate representation of the limb-darkening-curves can be made by the proper selection of a rectangular light-pulse, together with an exponential variation. The boundary intensity jump is denoted by c, and the limb-darkening variation by a single

exponential with parameters g and h (see Fig. 3). For this simplified case the quantities entering equation (4) are the intensity distribution,

$$I(\lambda) = c + g(1 - e^{-h\lambda}), \tag{8}$$

and the recorder response to a unit step function,

$$K(t) = 1 - e^{-ft}. \tag{9}$$

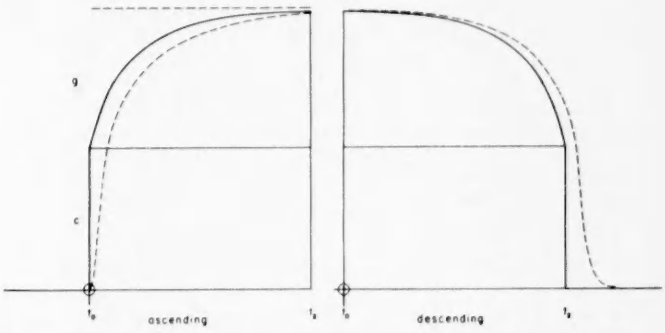

FIG. 3.—The effect of an exponential time delay in recording a finite step c with superimposed exponential variation. The ascending and decending limbs are treated separately, for convenience of mathematical notation in the text.

The solution of equation (4) for the ascending limb is

$$\delta_a(t) = c(1 - e^{-ft}) + g(1 - e^{-ht}) + \frac{g}{n-1} e^{-nht}[1 - e^{(n-1)ht}], \tag{10}$$

in which we have let $f = nh$. The first term is identical with equation (5). In the second term we have reproduced the original exponential variation, and the third term is a rapidly decreasing correction. For the descending limb, the solution is

$$\delta_d(t) = c(1 - e^{-2ft_2}) e^{-ft'} + g[1 - e^{-h(t_2 - t)}] + \frac{g}{n+1} e^{-ht_2} e^{-nht}[1 - e^{-(n+1)ht}], \tag{11}$$

where, for simplicity of notation, the first term refers to an origin of time at the true limb and the second two terms refer to a time origin at a point bisecting the true limb-darkening-curve. Again we have reproduced the original exponential variation which represents the limb darkening, with a third term as a correction.

In practice the observed limb-darkening-curves were very well fitted by a finite step and the sum of three exponentials, the time delay by two exponentials. With these additions the extended forms of equations (10) and (11) have been used to calculate time-delay drift-curves. A comparison between computed and observed curves showed that the fit was best on the descending limb. The greatest difference occurred near the ascending limb and was principally due to the finite boundary intensity c. On the basis of these trials, the following procedure was used: In the interval $\cos\theta = 1.0$–0.35, the observed ascending and descending limbs were averaged together. In the interval $\cos\theta = 0.34$–

0.20 the theoretical correction based on the observed time constant was applied to the ascending limb, and then it was averaged with the descending limb.

CORRECTION FOR SCATTERED LIGHT

The observed aureole around the sun, outside the bounds of the seeing tremor disk, was principally due to scattering by dust, scratches, and defects on the imaging mirrors. Atmospheric haze also contributed an appreciable amount of stray light, since the observations were made in the early morning when the sun was at a low altitude. Van de Hulst (1949) suggests that the intensity distribution appropriate for the region $0.°5 < r < 5°$ can be expressed by a formula of the form

$$B(r) = A r^{-q}, \tag{12}$$

in which the value of q varies between 1.8 and 1.2. The functional form is in agreement with the experimental work of Zanstra (1943), who finds, however, $q = 2.28$. Redman's observations (1938) for stars are represented by $q = 1.70$ for $r > 0.'5$. In view of the many uncertainties, it was thought that sufficient accuracy would be obtained if formula (12) was adopted with $q = 2.0$ and with a minimum value of $r > 0.'5$. In the interval $r = 0.'0$–$0.'5$, the value of $B(r)$ was assumed to be a constant.

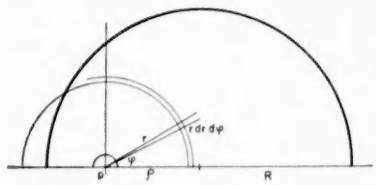

FIG. 4.—Geometry of the scattering computed for point p

In Figure 4 the sun's disk is of radius $R = 15'$ and for the moment is considered to be of uniform brightness. The point p at which scattering is to be computed is at a distance ρ from the sun's center. The intensity at p is

$$s(\rho) = 2\int_{1/2}^{R+\rho}\int_{0}^{\phi/2} \frac{B r\, dr\, d\phi}{r^2} + m \tag{13}$$

or

$$s(\rho) = 2\pi\int_{1/2}^{R+\rho} \frac{B}{r}\cos^{-1}\left(\frac{R^2-\rho^2-r^2}{2r\rho}\right) dr + m, \tag{14}$$

where m is the correction for $r < 0.'5$. Part of the integration can be performed. The result is

$$s(\rho) = 2.3026\pi B \log\frac{R-\rho}{\frac{1}{2}} + \int_{R-\rho}^{R+\rho} \frac{B}{r}\cos^{-1}\left(\frac{R^2-\rho^2-r^2}{2r\rho}\right) dr + \frac{B\pi}{2}. \tag{15}$$

This expression has been evaluated by numerical integration, and the result is given in Table 1. The scattering intensity reduced to unity at the sun's center is tabulated in the second column for a series of points p given in the first column.

The theoretical scattering correction for each limb-darkening-curve can be determined by representing the limb darkening as the sun of a series of uniform disks of different radii and by applying the results given in Table 1 to each subdivision. The computed curves are fitted to the observed scattering beyond the limb; hence the magnitude

of the corrections for points within the limb can be determined. It was found that the scattering correction $s(\rho)$ was closely a reflection of the limb-darkening-curves, i.e., one obtains nearly straight lines on an $s(\rho)$ versus cos θ scale. It remains to indicate how the magnitude of $s(\rho)$ was determined.

TABLE 1

SCATTERED LIGHT FROM A HOMOGENEOUS DISK OF DIAMETER 15′

Min. of Arc	$s(\rho)$	Min. of Arc	$s(\rho)$	Min. of Arc	$s(\rho)$	Min. of Arc	$s(\rho)$
0	1.000	10	0.925	20	0.104	34	0.028
2	.998	12	.869	22	.080	38	.022
4	.990	14	.738	24	.064	42	0.017
6	.978	16	.270	26	.052		
8	0.959	18	0.155	30	0.037		

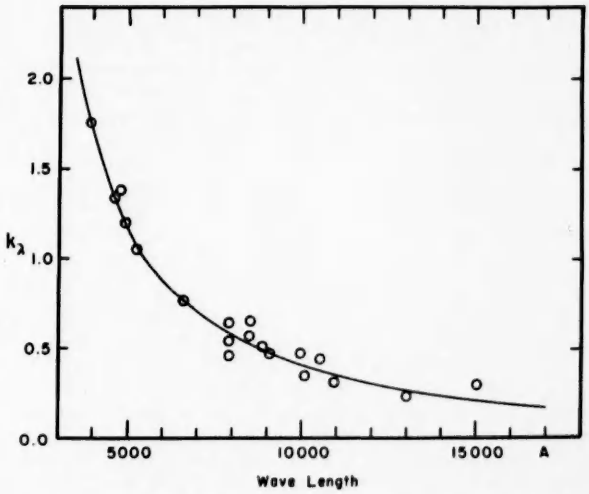

FIG. 5.—The observed scattering coefficient k_λ expressed in percentage of the intensity at the sun's center.

Empirically, it was found that the scattered light observed beyond the sun's limb was well represented by an expression of the form

$$s(d) = k_\lambda \log \frac{45'}{d} \qquad (d > 0'.3) , \tag{16}$$

where d is the distance from the sun's limb in minutes of arc ($d = \rho - 15'$). This equation predicts zero scattering at a distance of 45′ from the limb, which, in fact, is not true. But, observationally, the values of $s(d)$ were zero and lost in the noise of the tracing at a distance of 25′–30′. Figure 5 gives the observed values of k_λ derived from observations beyond the sun's limb. The fit between theory and observation was made at $d = 1'.5$; thus the values of $s(\rho)$ were known.

The method used for correcting the limb-darkening-curves is as follows: The true intensity at ρ is denoted as $I(\rho)$, to which is added the scattered light in amount $s(\rho)$. When these quantities are expressed in terms of the central intensity $1.0 + s(0)$, the observed intensity $I'(\rho)$ is found to be

$$I'(\rho) = \frac{s(\rho) + I(\rho)}{1 + s(0)}, \tag{17}$$

from which $I(\rho)$ can be found. For the shortest wave length (λ 7793) the maximum correction, which occurs for points near the limb, was 1.0 per cent.

CORRECTION FOR SEEING

Seeing distorts the true intensity profile of the sun's limb. The first term of equation (3) shows that, for a homogeneous disk, the intensity discontinuity at the edge becomes a symmetrical S-shaped curve, through the blurring effect of seeing. That is, point for point, within and off the disk, the loss and gain are the same. The second term of equation (3) takes into account the effects caused by the variation in intensity over the sun's disk. However, in the infrared this variation is small. Hence the second term of equation (3) has been neglected in the reduction of extreme limb observations. The maximum error introduced by using only the first term amounts to 0.3 per cent. Another argument for this procedure is that each point was observed at a different time, and, because seeing changes so rapidly, no detailed correction for its effect is possible unless a great number of runs are obtained and averaged.

The average value of the seeing parameter $\sqrt{a}$ was 260. Hence, at a distance of $1/260$ of the solar radius from the limb (3".7) the intensity fell to the value $1/e$. At $\cos\theta = 0.10$, the intensity was increased by 2.01 per cent when $\sqrt{a} = 260$. For $\cos\theta = 0.125$, the correction was 0.74 per cent, and for $\cos\theta = 0.15$, 0.35 per cent; for all others, zero.

RESULTS

The observed limb-darkening-curves corrected in the manner described previously are presented in Table 2. The first column gives values of $\cos\theta$. The succeeding columns give the intensity expressed in percentage of the intensity at the center of the sun's disk for wave lengths listed at the head of each pair of columns. The columns headed by the weight values list intensities determined from the 2-minute complete disk runs, while the adjacent columns on the right refer to measures made only near the limb.

Values of $I_\lambda(\theta)/I_\lambda(0)$ as a function of wave length are shown in Figure 6. This plots the complete runs by circles of different sizes, the largest having the greatest weight; dots for $\cos\theta = 0.15$ are values obtained from the limb traces. Curves similar to Figure 6 have been published by Peyturaux (1953) and Neven and de Jager (1951). The same features evident in our figure appear, but the details are somewhat concealed by the scatter of points in their curves.

The 2-minute runs form a more or less homogeneous set to which weights have been assigned. For each tracing a weight from 1 to 4 was applied, depending on the noise and smoothness of the trace, the latter being determined by sky transparency and by facular areas on the sun. The weighted intensity is given in the body of the table, and the sum of the weights is the value listed at the head of the column. A more complicated weighting procedure which included "seeing" was used for the limb traces. Since the final weights for the limb traces bear no relationship to those for the complete curves, they are not given. However, for purposes of comparison, the limb runs of different wave length may be considered to be of equal weight and less reliable than the complete curves. In particular, the intensity values for $\cos\theta = 0.125$ and 0.100 are very unreliable.

It is impossible to make an exact estimate of the probable error of each intensity value

of the final limb-darkening-curves. In Table 2 are listed four-figure intensity values. The only justification for giving intensities to 0.01 per cent lies in the apparent high internal smoothness of each curve. An estimate of the relative accuracy of each value may be derived from the fluctuation of the observed mean intensities at cos $\theta = 1.0000$ and 0.9992. On this basis the probable error of each value is about 0.05 per cent. The real errors can be best estimated from Figure 6. For curves of weight 40 and above, the indi-

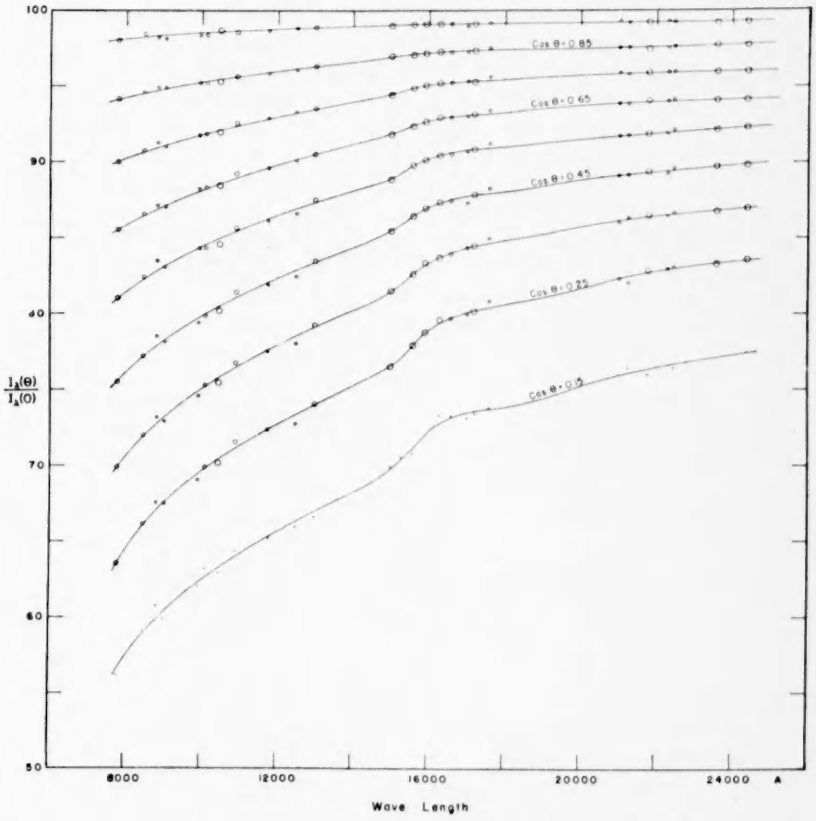

FIG. 6.—Observed values of $I_\lambda(\theta)/I_\lambda(0)$ plotted as a function of wave length. The largest circles have the greatest weight. The curves correspond to cos $\theta = 0.15$, 0.25, 0.35, 0.45, 0.55, 0.65, 0.75, 0.85, and 0.95.

vidual intensities have an estimated probable error of 0.2 per cent. However, even this value is too optimistic when we consider that the values depend on the determination of the limb point, the calibration of the receiver, and the accuracy of the corrections applied in the reductions described earlier. In absolute measure we must not expect the accuracy to be greater than 0.5–1.0 per cent.

The hump or break in the curves of Figure 6 at about 15,000 A also appears at the

TABLE 2 - OBSERVED LIMB DARKENING

	λ7793		λ8475		λ8853		λ9056		λ9955		λ10135		λ10478	
Cos θ	wt. 43		wt. 31		wt. 17		wt. 18		wt. 17		wt. 28		wt. 46	
1.0000	100.00		100.04		99.82		99.94		100.00		100.01		100.03	
0.9992	99.98		99.98		100.06		100.00		99.98		99.98		99.95	
0.9501	97.99		98.44		98.19		98.16		98.37		98.37		98.68	
0.8999	96.07		96.42		96.62		96.42		96.82		96.81		96.96	
0.8499	94.16		94.59		94.93		94.89		95.23		95.19		95.29	
0.8000	92.04		92.68		93.00		92.97		93.44		93.57		93.67	
0.7504	89.98		90.73		91.24		91.01		91.74		91.83		91.99	
0.7001	87.77		88.83		89.37		89.04		90.03		89.99		90.20	
0.6499	85.52		86.54		87.12		87.06		88.19		88.33		88.41	
0.6000	83.12		84.33		85.16		84.89		86.23		86.32		86.48	
0.5548	81.02		82.40		83.49		83.03		84.28		84.31		84.58	
0.5000	78.10		79.65		80.75		80.72		81.84		82.08		82.35	
0.4490	75.50	75.69	77.20	77.41	78.49	78.55	78.15	78.51	79.38	79.83	79.81	80.05	80.14	80.30
0.4012	72.98	72.95	74.70	74.92	75.95	75.87	75.40	76.80	77.26	77.24	77.69	77.95	77.92	78.07
0.3493	69.89	70.21	71.98	72.34	73.15	73.56	72.93	72.94	74.58	74.37	75.27	75.23	75.44	75.70
0.2998	66.84	67.22	69.12	69.39	70.39	70.49	70.40	70.28	71.96	71.32	72.47	72.84	72.79	72.91
0.2509	63.55	63.74	66.14	66.22	67.56	67.92	67.48	67.57	69.03	68.97	69.90	69.80	70.17	70.01
0.1990	59.61	60.18	62.50	62.55	63.87	64.44	64.22	63.57	65.79	66.10	66.71	66.47	66.42	66.62
0.1750		57.99		60.68		62.67		61.52		63.70		64.91		64.72
0.1506		56.21		59.12		60.74		59.94		62.05		63.23		62.91
0.1246		54.20		56.73		58.46		57.81		60.53		61.15		60.10
0.0999		50.63		53.51		55.64		54.85		59.91		58.28		57.15

	λ10911		λ11758		λ12515		λ13014		λ14998		λ15575		λ15950	
Cos θ	wt. 34		wt. 21		wt. 19		wt. 36		wt. 56		wt. 60		wt. 51	
1.0000	99.94		99.98		99.96		99.94		99.98		99.97		99.96	
0.9992	100.00		99.98		99.99		100.00		99.99		99.98		99.98	
0.9501	98.54		98.65		98.83		98.85		98.99		99.07		99.09	
0.8999	97.13		97.23		97.44		97.53		97.94		98.11		98.13	
0.8499	95.62		95.85		96.06		96.30		96.99		97.05		97.17	
0.8000	94.19		94.32		94.62		94.95		95.67		95.99		96.02	
0.7504	92.53		92.89		93.29		93.49		94.41		94.88		95.05	
0.7001	90.82		91.29		91.70		91.97		93.23		93.67		93.85	
0.6499	89.18		89.61		90.05		90.45		91.82		92.35		92.65	
0.6000	87.32		87.93		88.46		88.88		90.42		91.10		91.34	
0.5548	85.60		86.10		86.55		87.44		88.83		89.78		90.14	
0.5000	83.49		84.06		84.36		85.36		87.22		88.06		88.44	
0.4490	81.35	81.58	81.88	81.71	82.39	82.94	83.41	82.90	85.43	85.54	86.43	87.18	86.94	86.62
0.4012	79.21	79.14	79.91	79.59	80.69	80.66	81.49	80.87	83.52	83.62	84.63	84.93	85.22	85.85
0.3493	76.71	76.70	77.50	77.30	77.97	78.44	79.19	78.79	81.44	81.20	82.59	83.31	83.31	83.09
0.2998	74.19	74.34	74.86	74.80	75.42	75.97	76.73	76.67	79.05	79.21	80.21	81.22	81.04	80.49
0.2509	71.50	71.48	72.32	72.09	72.70	73.31	73.97	74.57	76.48	76.35	77.87	78.67	78.72	78.20
0.1990	68.17	67.93	69.01	68.78	69.20	69.85	70.71	70.63	73.23	73.13	74.67	74.99	75.72	74.74
0.1750		66.15		66.90		67.81		68.86		71.37		73.25		72.69
0.1506		64.39		65.53		65.94		66.59		69.89		70.73		70.54
0.1246		61.85		61.86		63.61		64.68		67.84		68.77		68.60
0.0999		58.92		59.77		61.63		62.76		64.09		65.92		65.96

TABLE 2 - OBSERVED LIMB DARKENING (Continued)

	λ16265		λ16579		λ17020		λ17185		λ17587		λ21028		λ21285	
Cos θ	wt. 50		wt. 28		wt. 20		wt. 68		wt. 20		wt. 20		wt. 20	
1.0000	99.93		100.00		100.05		100.03		100.05		99.85		100.03	
0.9992	100.01		99.97		99.94		99.96		99.95		100.05		99.95	
0.9501	99.10		99.10		98.98		99.11		99.21		99.33		99.20	
0.8999	98.24		98.12		98.15		98.27		98.34		98.52		98.42	
0.8499	97.28		97.23		97.27		97.31		97.57		97.56		97.58	
0.8000	96.26		96.18		95.90		96.29		96.58		96.80		86.75	
0.7504	95.18		95.20		95.31		95.28		95.61		95.90		95.79	
0.7001	94.07		94.04		94.17		94.32		94.48		94.91		95.06	
0.6499	92.92		92.91		93.01		93.12		93.42		93.86		93.84	
0.6000	91.63		91.66		91.82		91.97		92.32		92.79		92.80	
0.5548	90.41		90.49		90.68		90.85		91.24		91.73		91.77	
0.5000	88.91		89.05		89.19		89.35		90.14		90.47		90.47	
0.4490	87.34	87.24	87.40	87.57	87.27	87.73	87.85	87.72	88.26	88.00	89.11	89.40	89.16	89.16
0.4012	85.70	85.67	85.79	86.03	85.63	85.82	86.13	86.10	86.80	86.67	87.75	88.22	87.81	87.73
0.3493	83.66	83.77	83.90	84.25	84.31	84.06	84.41	84.09	84.97	84.41	85.98	86.25	86.33	86.06
0.2998	81.58	81.64	81.87	82.19	82.08	82.07	82.52	82.07	82.76	82.77	84.31	84.45	84.42	84.35
0.2509	79.55	79.45	79.63	79.73	79.92	79.73	80.17	79.80	80.80	80.89	82.24	82.36	82.20	82.28
0.1990	76.28	76.60	76.65	76.62	76.64	77.02	77.12	76.75	77.88	77.69	79.39	79.61	79.72	79.51
0.1750		74.73		74.91		75.21		75.19		76.05		77.79		78.35
0.1506		73.24		73.26		73.09		73.37		73.73		75.90		76.36
0.1246		70.40		70.36		69.74		71.42		71.55		72.77		73.38
0.0999		67.23		66.72		66.00		69.06		69.97		68.06		70.00

	λ21800		λ22115		λ22480		λ23595		λ24388	
Cos θ	wt. 60		wt. 20		wt. 19		wt. 45		wt. 62	
1.0000	100.01		100.00		100.03		99.99		100.00	
0.9992	99.97		99.98		99.96		99.97		99.97	
0.9501	99.28		99.23		99.24		99.23		99.30	
0.8999	98.31		98.33		98.26		98.54		98.54	
0.8499	97.45		97.56		97.63		97.77		97.71	
0.8000	96.79		96.72		96.67		96.81		96.81	
0.7504	95.89		95.93		95.93		95.96		96.03	
0.7001	95.02		94.90		95.05		95.07		95.11	
0.6499	94.07		94.01		94.18		94.13		94.15	
0.6000	92.96		92.94		93.08		93.18		93.14	
0.5548	91.88		91.97		92.17		92.18		92.32	
0.5000	90.75		90.54		90.80		90.86		90.97	
0.4490	89.39	88.90	89.24	89.20	89.65	89.21	89.72	89.32	89.87	89.90
0.4012	88.07	87.53	88.04	87.89	88.17	88.00	88.35	88.00	88.46	88.35
0.3493	86.46	85.85	86.42	86.17	86.67	86.27	86.78	86.50	86.96	96.82
0.2998	84.73	84.02	84.79	84.40	84.89	84.43	85.10	85.00	85.38	85.13
0.2509	82.79	82.16	82.91	82.73	83.10	82.80	83.26	82.86	83.52	83.04
0.1990	79.99	79.37	80.61	79.92	80.81	80.18	80.66	80.46	81.15	80.66
0.1750		77.91		78.33		78.88		79.15		79.18
0.1506		75.93		76.50		76.34		77.44		77.37
0.1246		73.77		74.71		73.41		75.83		75.89
0.0999		70.18		72.31		68.47		75.26		73.85

same wave lengths in the relative solar-energy distribution-curve for the center of the sun's disk (Pierce 1954). Thus the energy distribution for points near the limb must show a much greater break than that observed at the center of the disk. A detailed calculation is necessary in order to determine whether the negative hydrogen ion is sufficient to account for the break or whether additional absorbers are required. The concept that the observable extreme limb emits like a Planckian radiator may be incorrect. In fact, the steep temperature gradient with optical depth in the highest layers may prevent the appearance of the Planckian emission-curve in the observationally accessible layers.

I wish to express my thanks to my colleagues both in Ann Arbor and at Lake Angelus who encouraged this program and, in particular, to Dr. Robert R. McMath, whose interest and direction made possible this investigation. I wish also to thank Mr. William Livingston, who took part in the observing program.

REFERENCES

Abbot, C. G. 1908, *Ann. Smithsonian Inst.*, **2**, 214.
———. 1913, *Ibid.*, **3**, 157.
———. 1922, *Ibid.*, **4**, 221.
Minnaert, M.; van den Hoven van Genderen, E.; and van Diggelen, J. 1949, *B.A.N.*, **11**, 55.
Mohler, O. C.; Pierce, A. K.; Goldberg, L.; and McMath, R. R. 1950, *Photometric Atlas of the Near Infrared Solar Spectrum* λ 8465 *to* λ 25242 (Ann Arbor: University of Michigan Press), p. 2.
Münch, G. 1947, *Ap. J.*, **106**, 217.
Neven, L., and de Jager, C. 1951, *B.A.N.*, **11**, 291.
Peyturaux, R. 1952, *Ann. d'ap.*, **15**, 302.
———. 1953, *C.R.*, **236**, 896.
Pierce, A. K. 1954, *Ap. J.*, **119**, 312.
Pierce, A. K.; McMath, R. R.; Goldberg, L.; and Mohler, O. C. 1950, *Ap. J.*, **112**, 289.
Redman, R. O. 1938, *M.N.*, **98**, 614.
Van de Hulst, H. C. 1949, *The Atmospheres of the Earth and Planets*, ed. G. P. Kuiper (Chicago: University of Chicago Press, 1949), chap. 3, p. 71.
Wanders, A. J. M. 1934, *Zs. f. Ap.*, **8**, 108.
Zanstra, H. 1943, *M.N.*, **103**, 265.

PHOTOELECTRIC OBSERVATIONS OF THE PROFILE OF *Hα* IN THE SUN'S SPECTRUM

A. KEITH PIERCE
McMath-Hulbert Observatory, University of Michigan, Pontiac, Michigan
Received April 5, 1954

ABSTRACT

The profile of *Hα* in the sun's spectrum for the center of the disk is tabulated. The wings of the line show a depression of 1 per cent at ±40 A from the line center. The central core of the line is asymmetrical with the minimum intensity at −0.037 A.

Many photographic observations of the profile of *Hα* have been made. These have been summarized by de Jager (1952), who has added an extensive series of measures of his own. However, a very large amount of material is needed to overcome uncertainties due to plate grain, and the averaging process conceals interesting details. In addition, the absolute values depend on the nonlinear characteristic curve of the photographic plate. With the use of photoelectric techniques, additional accuracy is readily obtainable. This paper presents recent photoelectric observations of *Hα* in the solar spectrum.

EQUIPMENT

The work was carried out with the McGregor Tower telescope, which has an aperture of 30 cm and gives a solar image 13.8 cm in diameter. The existing infrared equipment was modified for use with a 1P21 photomultiplier and associated DC amplifier, which, when coupled to a Speedomax recorder, made it possible to obtain linear direct-intensity tracings. Through the kindness of Drs. I. S. Bowen and H. W. Babcock, we have been able to use an excellent 6 × 8-inch grating having 600 grooves per millimeter, ruled on aluminum by Dr. Babcock.

Tracings of the *Hg* λ 5461 and iodine absorption-band spectra in the green of the fourth order show a resolution of slightly greater than 250,000. But, because of the low sensitivity of the 1P21 cell at *Hα*, wider slits were used which reduced the resolving power to $R = 150{,}000$ for these observations. Tests of the grating showed no detectable scattered light at distances greater than 1 A from the core of the instrumental profile. In the fourth order the Rowland Ghosts are at ±1.24 and ±2.48 A. The respective intensities are 1.22 and 0.21 per cent of the central line.

WINGS OF *Hα*

The height of the continuum was determined by interpolating its position from tracings 200–300 A in length. This procedure was convenient, because the nature of the grating mounting (McMath and Mohler 1949) permits long-wave-length intervals to be strongly compressed. There remains some slight uncertainty in the interpolation because of the slowly varying sensitivity of the receiver with wave length. However, it is estimated that the position of the continuum could be determined with an error less than 0.5 per cent.

Observations made at the center of the sun's disk show a measurable depression in the line wing, amounting to 1 per cent at 40 A from the line center. Individual observations are shown by dots in Figure 1. Two different scales are used. The top scale, labeled at

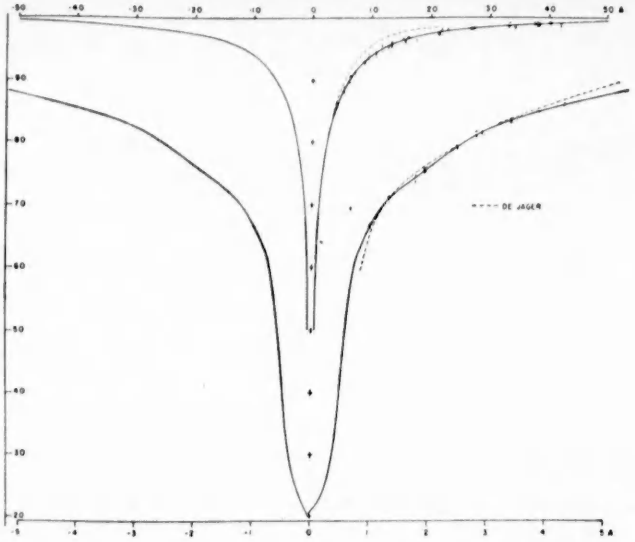

FIG. 1.—The observed profile of *Hα* in the extreme and intermediate wings of the line. Dots are individual observation points. The dashed line is from the recent photographic measurements of De Jager.

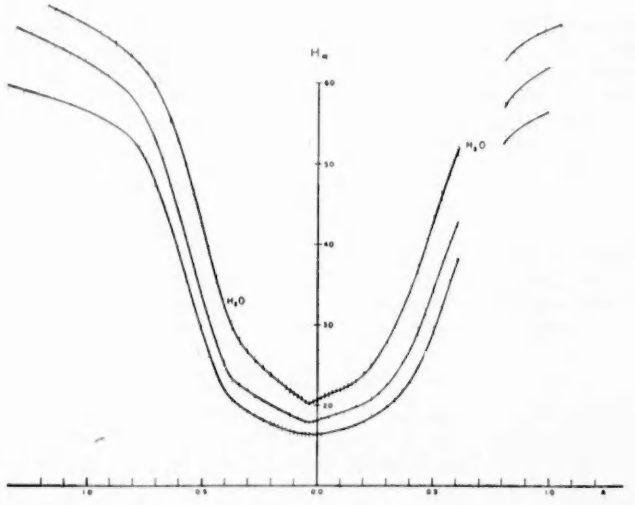

FIG. 2.—Observational points for *Hα* line core. The upper curve is for the sun's center and the two lower ones for points at 90 and 97 per cent of the radius toward the limb. The line asymmetry disappears at the limb.

"10 A Intervals," applies to the extreme wings; the bottom scale, in angstroms, applies to the intermediate wings. De Jager's photographic observations, represented by the dashed line, are in satisfactory agreement with the author's measures; yet there are systematic differences.

CORE OF *Hα*

The Doppler core of the lines was observed at $\cos \theta = 1.0, 0.42$, and 0.25 (see Fig. 2). At the center of the disk the central part of the line shows a distinct asymmetry with the minimum of intensity at -0.037 A. At this position there appears a variable feature whose strength, width, and shape give it the appearance of a weak absorption line. As illustrated by Figure 2, the asymmetry disappears at the limb. Numerous observations

FIG. 3.—Variations in the core of *Hα* for different parts of the disk near the center and for different days.

made on days with different water-vapor content in the earth's atmosphere exclude the possibility that the central feature is a water-vapor line. Besides, runs made in succession at different parts of the solar disk near the center show variations in the core profile (see Fig. 3).

In Table 1, I have listed the average intensity in *Hα* at different distances from the line center. The values have been corrected for the effect of ghosts and finite resolving power. At distances greater than 0.30 A from the center, the red or violet wing has been used to eliminate as far as possible the disturbing influence of blends. The general asymmetry of the line core, in the direction that the red part is considerably more rounded on the bottom than the steep violet part, is possibly caused by the integration of the slit over many floccular elements in vertical motion. Royds (1911) observed on *Hα* spectroheliograms that dark markings and the bright emission markings accompanying spot disturbances showed best when the second slit of the spectroheliograph was set 0.2 A to the violet of line center. When the slit was set an equal distance to the red, it was observed that the markings disappear and the image is much less contrasty.

S. Chandrasekhar (1945) has considered the formation of absorption lines in a moving atmosphere with a linear velocity gradient. His resulting profiles show a striking resemblance to our observed profile. The central feature can also be interpreted either as an absorption line, the minimum between emission components displaced to the red and violet of the line center, or a combination of these.

TABLE 1

CORRECTED INTENSITIES OF $H\alpha$
($\cos\theta = 1.00$)

$\Delta\lambda$	I	$\Delta\lambda$	I	$\Delta\lambda$	I	$\Delta\lambda$	I
45.0	99.3	5.0	87.9	0.95	66.2	−0.300	25.2
40.0	99.1	4.5	86.8	.90	65.1	− .250	23.5
35.0	98.8	4.0	85.5	.85	64.0	− .200	22.2
30.0	98.5	3.5	84.1	.80	62.7	− .150	21.0
25.0	98.1	3.0	82.3	.75	61.1	− .100	19.8
20.0	97.4	2.5	79.4	.70	58.6	− .050	18.6
18.0	97.1	2.0	76.0	.65	55.5	− .037	18.4
16.0	96.6	1.8	74.6	.60	51.3	.000	18.9
14.0	96.0	1.6	73.0	.55	46.2	+ .050	19.7
12.0	95.2	1.4	71.5	.50	41.0	+ .100	20.3
10.0	94.0	1.2	69.4	.45	36.9	+ .150	20.9
8.0	92.4	1.0	66.4	.40	32.5	+ .200	22.1
6.0	89.7			0.35	28.9	+ .250	24.0
						+0.300	26.1

It should be remembered that the entrance slit integrates on a finite portion of the sun, and thus a detailed discussion on interpretation should await more knowledge of the fine structure of the lower chromosphere.

This investigation started as a joint problem with Dr. McMath. He, however, was unable to continue because of other pressing work. I am glad to acknowledge with thanks his continued interest.

REFERENCES

Chandrasekhar, S. 1945, *Rev. Mod. Phys.*, **17**, 138.
Jager, C. de. 1952, *Recherches Astr. Obs. Utrecht*, **13**, Part 1.
McMath, R. R., and Mohler, O. C. 1949, *J. Opt. Soc. Amer.*, **39**, 903.
Royds, T. 1911, *M.N.*, **71**, 723.

SOME CHARACTERISTICS OF SOLAR FLARES*

CONSTANCE S. WARWICK
Sacramento Peak Station, Harvard College Observatory
Received March 15, 1954

ABSTRACT

Solar flares and limb events are studied in relation to radio noise at 200 Mc/sec and to SID's (sudden ionospheric disturbances). It is found that rising prominences are often associated with radio noise. SID's show a definite preferred association with the larger, brighter flares, and there is some indication that radio noise also favors these flares. However, either radio noise or an SID may be associated with a very small, faint flare. We find no lower limit (other than observational) of flare area or of intensity in the flare frequencies and no lower limit for association with radio noise or an SID. We conclude that any minimum value for area or for intensity of a brightening required for definition as a flare must be arbitrary.

A rapid rise to maximum and a long lifetime are found to be characteristic of large, bright flares. There is no significant asymmetry either in the number of flares appearing east or west of the solar meridian or in the number of coincidences with radio noise or fade-outs for flares near either limb. There is no significant difference between the number of coincidences with radio noise or fade-outs for flares near the limb and the number for flares near the center of the disk, indicating that the noise-producing radiation and the fade-out–producing agency are nondirectional.

OBSERVATIONS

Flare data are taken from the records of the Sacramento Peak flare patrol, which supplies *Hα* photographs at 5-minute (or shorter) intervals. We regard as a flare any sudden brightening that is seen on at least two successive frames of the film and that has an area at least 10^{-5} the area of the sun's hemisphere. We include, therefore, smaller and fainter flares than are reported by most observatories. There were 425 flares observed between February 28, 1951, and April 4, 1953. The flare areas are measured on the projected photograph, in millionths of the area of the sun's hemisphere. The photographic densities are estimated on an arbitrary scale from zero (disk brightness) to about 30 (the brightest flare yet observed at Sacramento Peak). In practice, the faintest recorded flares have intensity of 5, although some observers feel that any bright area with intensity less than 10 can be called only a plage. There is probably a general change in the intensity scale that depends on the level of flare activity; observers tend to call flares brighter when only few and faint flares have been observed for some months. Another uncertainty arises from the fact that a change in the temperature of the *Hα* filter causes a change of contrast that is difficult and sometimes impossible to distinguish from a true change in flare intensity.

Filaments and dark areas are observed on the *Hα* films. Only those that have been noted in the records as rapidly changing in position, shape, or intensity have been included here. Ascending (eruptive) prominences, puffs, and surges are observed visually and photographically. Again, only the events outstanding enough to be noted in the written records have been included.

The tapes from the Cornell laboratory at Sacramento Peak form the main source of radio data. On these are recorded the intensity of solar radio activity at 200 and at 55 Mc/sec. At 200 Mc the polarization (right- or left-circular) is recorded. The 55 Mc record in particular is obscured by interference from transmission lines and other local sources, so that only intense bursts that coincide within a few minutes with the optical activity and that occur at times of relatively low interference can be associated with the

* This research was sponsored by the Geophysics Research Directorate, Air Force Cambridge Research Center, Air Research and Development Command, under Contract AF19(604)-146.

optical observations. The data refer almost entirely to 200 Mc observations. The Sacramento Peak radio data have been supplemented by the published data for 200 Mc from the Cornell station at Ithaca (Cornell University 1951–1953*a*). The information on SID's is taken from the "F-series" publications of Central Radio Propagation Laboratories (National Bureau of Standards 1951–1953).

Because of the incompleteness and inhomogeneity of the data, only the crudest statistical discussion of the results has been attempted. The present results may be useful in indicating what lines of investigation may be fruitfully followed in more detail when exact flare photometry and the absence of local radio interference give us sharper observations.

ASSOCIATION OF SOLAR RADIO NOISE WITH *Hα* FEATURES

The radio data have been examined at the times of the optical events mentioned above, and the events have been classified as (*a*) associated with unusual radio activity, (*b*) associated with no unusual radio activity, or (*c*) having insufficient radio observations (no observation or excessive interference). The Cornell classification of types of radio

TABLE 1

Type of Event	Flares	Puffs and Surges	Large Ascending Prominences	Rapidly Changing Filaments and Dark Areas
No. with associated radio noise	185	28	9	5*
Percentage	64	80	75	
No. with no unusual radio activity	103	7	3	0
Percentage	36	20	25	
Total no.	288	35	12	5

* Of which 4 are associated with flares.

activity was used (Cornell University 1951*b*). Included as unusual activity are bursts, outbursts, beginnings, or intensifications of noise storms, rises in base level, and abrupt changes in polarization. The numbers and percentages of the different types of optical events with and without associated radio activity are listed in Table 1.

We may compare the percentage of flares found here to be associated with radio noise with the value found by Miss Dodson, Miss Hedeman, and Owren (1953). If we subtract from their total the flares associated with microbursts and with noise storms in progress (neither of which was included in the present study), 65 per cent of the flares remain associated with unusual noise. The value of 64 per cent found here is in good agreement with this result.

Again it should be stressed that, except in the case of flares, only unusual events of each type have been included. It seems clear, however, that limb activity must not be ignored in a search for sources of radio noise. Also, radio records may be helpful in relating flares to limb events.

The small observed number of rapidly changing dark areas and filaments, together with the fact that most of them are associated with flares, makes it difficult to say whether or not these events are themselves associated with radio noise. The features mentioned may be identified with the "active dark flocculi," which, it has been suggested, are seen as surges at the limb (Ellison 1942; Newton 1942; McMath and Mohler 1948; Dodson, Hedeman, and Owren 1953).

DEPENDENCE OF COINCIDENCE WITH RADIO NOISE OR SID ON INTENSITY AND AREA OF FLARE

Table 2 gives the intensity-area frequency distribution for flares with and without associated radio noise. The frequencies are given as percentages; the total number of flares is given in the lower right corner. The upper figures refer to flares without associated noise; the lower figures (in italics) to flares with noise.

It is seen that the maximum frequency is shifted slightly toward greater area and higher intensity for the flares with associated radio noise. One can make a rapid estimate of the significance of this shift by testing for association of radio noise with high intensity and with large flare area. The probability, P, that the observed association or a larger one will occur by chance is 0.21 for the association between radio noise and high flare intensity. For association between radio noise and large flare area, the value of P is 0.14. Although both associations are positive, neither is strong enough to be considered significant. Note also that there is no sharp cutoff at the low-intensity, small-area corner of

TABLE 2

Area	Intensity			Total
	5–10	11–20	21–30	
0–50	26	10	0	36
	23	*7*	*1*	*31*
51–100	22	13	1	36
	18	*17*	*1*	*36*
101–300	6	20	0	26
	8	*21*	*2*	*31*
>300	0	1	0	1
	0	*2*	*1*	*2*
Total	54	45	1	99
	49	*47*	*4*	*178*

the frequency diagram, either for quiet or for noisy flares. Flare frequency continues to rise up to our observational limit of intensity and area, and even the least observed flares may be associated with radio noise. Since we find no natural lower limit to the size or intensity of a brightening of the sort that has been called a flare, the observational limitations of each observatory should determine what it reports as a flare.

Because of the uncertainty of the radio data, it is possible that we have considered small bursts of radio noise to be associated with flares when the bursts are of the sort that can occur in the absence of a flare or that we have classified a flare as having no associated radio activity when a small burst is obscured by line noise. This fuzziness in the radio-noise classification of flares could obscure an association between noise and flare brightness or a lower limit of brightness or size of noise-associated flares. To check these possibilities, we present in Table 3 the frequency distribution in area and intensity of flares classified according to association with a "distinctive event" observed at Ithaca. The entries are percentages, with the total number given in the lower right corner. Although there is still a chance that a "distinctive event" may be assigned to a flare when the two events are actually unrelated, the unusual and definite character of these radio events makes this less likely than when all radio data are considered.

The "distinctive-event" classification of flares gives us a larger shift toward greater

area and intensity than is shown in Table 2. The association of "distinctive event" with flare intensity gives us a value for P of 0.06, while the association with area gives $P = 0.03$. The line below which an association is considered significant is conventionally drawn at $P = 0.05$. In view of the difficulty of classifying a flare either as having or not having associated radio noise, as well as the arbitrary nature of the intensity scale, the relations found here may well be significant. These results may be explained better by the results of Miss Dodson, Miss Hedeman, and Owren (1953). These authors found that the percentage of flares with associated radio noise at 200 Mc does not increase with flare importance but that distinctive radio events with high energy do tend to be associated with flares of greater importance. The "distinctive events" of Table 3 have, in general, higher energy than the radio events of Table 2 and so show the stronger association with larger flare area and intensity.

Table 4 shows the area-intensity frequency distribution, again in percentages, for flares with associated SID's (in italics) compared to that for flares with no SID. A flare

TABLE 3

Area	Intensity			Total
	0–10	11–20	21–30	
0–50	30	10	0	40
	20	*6*	*1*	*27*
51–100	21	14	1	36
	18	*20*	*0*	*38*
101–300	5	18	0	23
	7	*21*	*5*	*32*
>300	0	1	0	1
	0	*2*	*1*	*3*
Total	56	43	1	81
	44	*49*	*7*	*108*

was considered to be associated with an SID if the beginning times of SID and flare occurred within an interval of 15 minutes or if the SID began during the lifetime of the flare. If more than one flare met these conditions, the one with beginning time closest to that of the SID was considered to be the one associated with it.

There is a pronounced shift of the maximum frequency toward greater area and intensity for flares with SID's. The association of SID occurrence with high flare intensity and large area is real, with $P = 8 \times 10^{-5}$ for high intensity and $P < 1 \times 10^{-5}$ for large area. The absence of a lower limit in intensity and area for flares associated with SID's is evident; and we find no such limit, even when we consider a finer classification of flares in the lowest area and intensity class.

It should be pointed out that the SID's reported by C.R.P.L. are all severe effects of the sort that tend to disrupt radio communication. It is desirable that astronomers have the means to monitor radio-signal strengths and phase changes between ground and reflected waves, so that minor ionospheric effects can be studied in comparison with visual events. We might find then that every flare has associated with it a measurable change in height of the lowest ionized layer of the earth's atmosphere.

In view of the theory that SID's are caused by extreme ultraviolet radiation, it is not surprising that SID intensity is not strictly related to the *Hα* intensity of the associated

flare. Nor is it surprising that radio noise, presumably arising from a different level in the sun's atmosphere from that at which we observe the flare, has little dependence on flare energy.

GROUPS OF FLARES

There is a noticeable tendency for flares to keep reappearing in the same region on the sun. Flares were classed as members of a group if one or more other flares occurred in the same region (within about 5° of the first flare) on the same day; 59 per cent are found to fall into this class. As many as eight flares have been observed to occur in the same region on the same day. There is no obvious tendency for the flare of any given serial number to be brightest or to be associated with radio noise or an SID. The first, last, or an intermediate flare may be the most active of a series.

LIFETIME OF FLARE AND TIME OF RISE TO MAXIMUM RELATED TO OTHER CHARACTERISTICS

In Table 5 are given the mean values, obtained from all flares, of the total lifetime of the flare, the time from beginning to maximum intensity, and the ratio (time from beginning to maximum)/(total lifetime). The number of flares entering into the mean is

TABLE 4

Area	Intensity			Total
	0–10	11–20	21–30	
0–50	26 *9*	10 *6*	0 *0*	36 *15*
51–100	22 *7*	14 *7*	0 *2*	37 *17*
101–300	8 *0*	17 *54*	1 *7*	25 *61*
>300	0 *0*	1 *4*	0 *4*	2 *7*
Total	56 *17*	42 *70*	1 *13*	371 *54*

given in parentheses for each class. We see that as either intensity or area increases, the mean lifetime increases, and the mean value of the ratio (time of rise to maximum)/(total lifetime) decreases.

The mean values of the three quantities are given in Table 6 for flares with associated radio noise, compared to those without, and for flares with associated SID's, compared to all flares. The lifetime increases in the order: flares with no radio noise, flares with radio noise, flares with SID's; and the ratio (time of rise to maximum)/(lifetime) decreases in the same order.

SYMMETRY OF FLARE DISTRIBUTION

Evans, Yü, and Witte (1951) found that between February 15 and November 15, 1950, there were 151 flares observed east of the solar meridian and only 86 west of it. The probability that as large a difference or one larger will occur by chance is only 4×10^{-5}. Behr and Seidentopf (1952), working with data for the years 1935–1948, found

a smaller excess of eastern flares. The probability of occurrence of the excess observed by Behr and Siedentopf is 0.04 for all flares and 0.03 for flares of importance 2 or greater. Miss Dodson, Miss Hedeman, and Owren found among 194 flares in the years 1948–1950 for which they had 200 Mc/sec records, a few more flares west of the meridian than east, the small difference being insignificant. They point out, though, that in their study

TABLE 5

Area	Intensity			Mean
	0–10	11–20	21–30	
0–50	24^m 9^m 0.41 (91)	28^m 9^m 0.35 (35)	20^m 5^m 0.25 (1)	25^m 9^m 0.39 (127)
51–100	37^m 14^m 0.36 (70)	40^m 9^m 0.32 (48)	23^m 5^m 0.22 (1)	38^m 12^m 0.34 (119)
101–300	50^m 16^m 0.33 (27)	61^m 16^m 0.28 (73)	61^m 12^m 0.22 (6)	58^m 16^m 0.29 (106)
>300	.... (0)	106^m 26^m 0.25 (3)	120^m 24^m 0.18 (2)	112^m 25^m 0.22 (5)
Mean	32^m 12^m 0.38 (188)	48^m 13^m 0.31 (159)	65^m 13^m 0.21 (10)	40^m 12^m 0.34 (357)

TABLE 6

	Flares with No Associated Radio Noise	Flares with Associated Radio Noise	Flares with Associated SID	All Flares
Mean lifetime	40^m	42^m	54^m	40^m
Time of rise to maximum	13^m	11^m	10^m	12^m
Ratio	0.33	0.32	0.23	0.34

there is a larger proportion of flares of importance greater than 1, and of flares associated with SID's, among eastern flares. This difference is probably not significant, for we find that the probability of chance occurrence of the observed difference in numbers of flares of importance greater than 1 is 0.32. The value for the difference in numbers of flares accompanied by SID's is 0.05.

The Sacramento Peak flare data for the years 1951–1953 show 156 flares east of the

solar meridian and 130 west. The probability that this difference or a larger one will occur by chance is 0.12. Two possible explanations of the failure to confirm the east-west asymmetry are (1) that the asymmetry occurs only at the time of the sunspot cycle near maximum and (2) that the asymmetry is more pronounced for large, bright flares than for small, faint ones. The Sacramento Peak data do show a greater asymmetry in the year 1951 ($P = 0.17$) than in the years 1952 and 1953 ($P = 0.46$). However, the Evans, Yü, and Witte data, which are the only ones showing a clearly significant asymmetry, are for the year 1950. Tests for association of appearance east of the solar meridian with high intensity and with large area were applied to the Sacramento Peak data. For intensity, $P = 0.09$; for area, $P = 0.18$. Neither explanation seems to be satisfactory.

A more probable explanation, which has been suggested by Evans, Yü, and Witte, is that the observed asymmetry is actually less significant than it seems, because of the "clustering effect," or tendency of flares to recur in the same active region. We should test for significance of asymmetry by considering separately the number of active regions and the mean number of flares per region, east and west of the meridian. Evans, Yü, and Witte do not give the value of the mean number of flares per active region, but we can compute what the value would be for a given P and compare this to the value observed at Sacramento Peak. If the difference in number of active regions is three times the standard deviation, $P = 0.003$, and the number of flares per region is 1.7. If the value of P is to reach 0.05, the number of flares per cluster must be 2.0 (assuming equal mean numbers of flares per region east and west of the meridian). At Sacramento Peak, we have found a mean value of 1.65 flares per active region. The Boulder data were taken at a time near sunspot maximum, when we might expect a larger number of flares per region, as very active regions then dominate the solar activity. The cluster explanation of the asymmetry observed at Boulder does not seem unreasonable. Proper treatment of the data would almost certainly reduce the other two observations of asymmetry to insignificance.

SYMMETRY OF NOISE-PRODUCING FLARES

Hey, Parsons, and Phillips (1948) have found a greater proportion of coincidences with radio noise for flares appearing near the east limb than for those near the west limb. Similarly, Rydbeck and Stranz (1948) find a tendency for radio fade-outs to be more intense when associated with east-limb flares. The former authors have suggested that this is caused by a corpuscular stream which arcs between the sun and the earth and which must be traversed by radiation from the west limb but not from the east. The association coefficient for noise associated with position east of the meridian is negative, -1.57, with probability 0.12 of finding a coefficient numerically as large or larger. We conclude that there is no asymmetry of position for noise-associated flares. Hey, Parsons, and Phillips point out that the absorption of a corpuscular stream would increase with the wave length of the incident radiation. The fact that their radio data refer to 4.1 meters and ours to 1.5 may explain the failure to corroborate their results, although the negative correlation does not suggest this. The work of Miss Dodson, Miss Hedeman, and Owren (1953) has also shown symmetry for flares associated with 200 Mc events.

Of flares with associated SID's which appeared within 0.3 radius of either limb, we find eight near the east limb and twelve near the west limb. Of these, three eastern and six western flares were associated with complete fade-outs. When we group together flares occurring in the same active region, we find six separate regions near the east limb and seven near the west limb. The only way in which SID's associated with the eastern hemisphere are greater is in the intensity of the fade-out. The mean value given by C.R.P.L. (the ratio of the amplitude of the signal during the fade-out to the normal amplitude) is 0.045 for the east-limb flares and 0.050 for the west-limb flares. Again, we find no evidence of asymmetry in position of flares associated with SID's.

CENTRAL FLARES COMPARED TO LIMB FLARES

Finally we ask whether there is any difference in frequency of noise association between flares near the center of the disk and those near the limb. We classify the flares according to whether they have a radius vector equal to or greater than 0.5 or less than 0.5. The association between coincidence with radio noise and nearness to center has $P = 0.13$. There is no significant association of noise coincidence with distance of flare from the center of the disk and no evidence that radiation causing radio noise has directivity.

For flares with SID's, the association with small radius vector has probability $P = 0.23$. Again we conclude that there is no significant association between distance of flare from center of disk and association with an SID, in other words, that the radiation producing the SID is nondirectional.

In conclusion, we can list the general properties of an energetic flare: (1) rapid rise to maximum, (2) high intensity, (3) large area, (4) long lifetime, (5) associated radio noise(?), and (6) associated SID. However, any one of these characteristics may be missing when most of the others are present, or may appear alone when the others are missing.

REFERENCES

Behr, A., and Siedentopf, H. 1952, *Zs. f. Ap.*, **30**, 177.
Cornell University (School of Electrical Engineering). 1951–1953*a*, *Radio Astronomy Status Report*, Nos. 12–23.
———. 1951*b*, *Radio Astronomy Status Report*, No. 15.
Dodson, H. W.; Hedeman, E. R.; and Owren, L. 1953, *Ap. J.*, **118**, 169.
Ellison, M. A. 1942, *M.N.*, **102**, 11.
Evans, J. W.; Yü, C. S.; and Witte, B. 1951, *Preliminary Results of Flare Observations from 15 February 1950 to 15 November 1950* ("Special Reports," No. 34 [Harvard University Contract No. W19-122ac-17]).
Hey, J. S.; Parsons, S. J.; and Phillips, J. W. 1948, *M.N.*, **108**, 354.
McMath, R. R., and Mohler, O. 1948, *Observatory*, **68**, 110.
National Bureau of Standards. 1951–1953, *Ionospheric Data*.
Newton, H. W. 1942, *M.N.*, **102**, 2.
Rydbeck, O. E. H., and Stranz, D. 1948, *Tellus*, **1**, 6.

CORRELATION ANALYSES OF TURBULENT VELOCITIES AND BRIGHTNESS OF THE PHOTOSPHERIC GRANULATION

F. E. STUART AND J. H. RUSH*
High Altitude Observatory of Harvard University and University of Colorado
Received March 26, 1954

ABSTRACT

Data on the space distributions of turbulence velocities and brightness of photospheric granulation published by Richardson and Schwarzschild (1950) were subjected to correlation analyses. When large-scale fluctuations were minimized by smoothing operations, the remaining small-scale fluctuations of velocity and brightness were found to be correlated by a coefficient of −0.68. This result associated the bright granules with outward-moving material. The cross-correlogram function for smoothed brightness and velocity data revealed a maximum at 2300 km; the autocorrelogram function for the smoothed velocity data alone confirmed this result, suggesting the existence of a regular granular structure of this dimension. Autocorrelogram analyses of brightness fluctuations in the granulation, derived from plates obtained by W. A. Miller, revealed a maximum at about 14,000 km; this result is related to the finding by Frenkiel and Schwarzschild (1952) of a 15,000-km wave length in the velocity distribution referred to above.

I. INTRODUCTION

Since the pioneer work in solar photography by Janssen, there has been collected over the years only meager information concerning the solar granulation. One of the reasons for the scarcity of data is that, unless seeing conditions are excellent, the small granules cannot be observed. Moreover, obtaining reliable quantitative data on the evolution of these minutes features (1–2 seconds of arc) demands exceptional seeing over relatively long periods of time, and such conditions are rarely found anywhere. Most of the high-resolution photographs that have been used in studies of the granulation, such as those of Janssen (1896), Chevalier (1912), Keenan (1938, 1939), ten Bruggencate (1939), Macris (1953), and Miller (1953), have been exposed over broad spectral ranges for pictorial detail. These studies have yielded information on size, spacing, intensities, and lifetimes of the small granules and other granular features. None of these studies was spectrographic.

II. DATA OF RICHARDSON AND SCHWARZSCHILD

Richardson and Schwarzschild (1950) obtained at the Mount Wilson solar tower a spectrogram of the photosphere of exceptionally high resolution. The solar absorption lines on this plate are not straight but show a slight waviness due to Doppler shifts over intervals of granular dimensions. By measuring the shifts at 340 equally spaced points corresponding approximately to 330-km spacing at the sun, Richardson and Schwarzschild were able to compute the line-of-sight velocities of the granules lying along the line through the center of the disk defined by the spectrograph slit. They determined the corresponding fluctuations in brightness along this same line from a microdensitometer trace. Later, Frenkiel and Schwarzschild (1952) computed a turbulence spectrum from these same velocity data; in it they found clear evidence of a secondary maximum corresponding to a turbulence wave length of about 15,000 km.

Concerning the correlation between velocities and brightness obtained from this spectrogram, Richardson and Schwarzschild state: "the correlation between the brightness fluctuations and the velocities is rather weak; only the narrow regions of high upward velocities appear to have systematically higher brightness than average."

When we examined the graphs of these data, however, it appeared to us that the correlation between small-scale fluctuations of brightness and velocity (i.e., fluctuations cor-

* Now at Texas Technological College.

responding to the 1″–2″ granules) was good but that this correlation was masked by large-scale fluctuations in velocity that did not appear to be closely correlated with brightness. These large-scale variations probably are responsible for the secondary maximum at 15,000 km in the turbulence spectrum that was reported by Frenkiel and Schwarzschild.

To obtain a preliminary measure of the correlation between velocities and brightness for the small fluctuations only, we recalculated the tabulated results of Richardson and Schwarzschild, obtaining deviations from a running mean in the following manner. On a graph of the velocities, let y_m be the value of the velocity at one of the minima of the graph, and y_n the velocity at the following maximum. Points between the mth and nth point are replotted as deviations from the mean of y_m and y_n. Thus the mean value of the velocities at each successive pair of maxima and minima is used as a "running mean" from which new deviations of the intermediate points are computed. The new value at a maximum or minimum is taken as the deviation of y_m or y_n from the average of the two adjacent running means. Graphically, the result of this procedure is to shift all fluctuations so that they are symmetrical about the horizontal axis. If two sets of data are reduced in this way, then the correlation coefficient for the two resulting sets will be a measure of the correlation between fluctuations only, since the contribution of a particular fluctuation to the coefficient will have been made independently of the average value of the variable over a fluctuation.

We computed coefficients of correlation between velocities and brightness, first, as deviations from the over-all mean as given by Richardson and Schwarzschild and, second, as deviations from the running mean described above. Calling these coefficients r_1 and r_2, respectively, the results are

$$r_1 = -0.30\ , \qquad r_2 = -0.50\ .$$

These results supported our expectation of a significant correlation between the small-scale fluctuations. The negative sign implies that those granular features that are rising in the photosphere are the brighter.

We then computed the cross-correlogram function

$$r_{xy}(m) = \frac{\sum_i X_i Y_{i+m}}{\sqrt{\sum_i X_i^2 \sum_i Y_i^2}},$$

where X_i is the deviation of the ith velocity datum from the running mean, Y_i is the corresponding brightness deviation, and m is an integer expressing the degree of phase displacement between the two curves. If velocity and brightness are correlated, the value of the cross-correlogram function should be a maximum at $m = 0$, a condition corresponding to a direct point-for-point correlation between velocities and brightness; in fact, the correlation coefficients given above are identical with the cross-correlogram function at $m = 0$. If, however, maxima or minima tend to recur in both sets of data at a uniform interval of distance, then a secondary maximum in the value of the cross-correlogram function may be expected at a value of m corresponding to this repetitive interval. The dependence of the cross-correlogram function on m, as applied to the Richardson-Schwarzschild data adjusted by the running-mean procedure described earlier, is shown in Figure 1. The secondary maximum at approximately 2300 km indicates a definite tendency toward a repetitive granular configuration of this size.

Having used the simple running-mean procedure described above to determine that the surmise regarding small-scale correlation was tenable, we then used the conventional moving-average procedure for the same purpose of removing the large-scale velocity

fluctuations, in the hope that a stronger correlation would result. By the moving-average procedure, a new set of values of velocity and brightness was obtained from the following formula:

$$X'_i = X_i - \frac{1}{2k+1} \sum_{m=-k}^{k} X_{i+m},$$

where X_i is the deviation of the ith point from the over-all mean, and the second term is a moving average of $(2k + 1)$ points symmetrically distributed about the ith point. The attenuation characteristics of this operation depend on the value of k. Obviously, if $k = 0$, each point would be compared with its own value as a reference, and all deviations would become zero. Qualitatively, the greater the value of k, the greater will be the maximum spacing, or "wave length," of fluctuations that escape serious attenuation. For our computations the value $k = 3$ was chosen; this choice resulted in significant attenuation of wave lengths greater than approximately 5000 km.

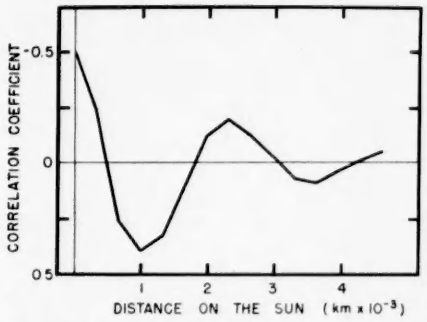

FIG. 1.—Cross-correlation function of velocity and brightness of granules, showing maximum at approximately 2300 km. The correlation coefficient is plotted against the phase shift (m) between the velocity- and brightness-curves, expressed in terms of distance on the sun.

A coefficient of correlation between velocity and brightness as deviations from the moving average was computed, yielding

$$r = -0.68 .$$

This result indicates that velocities and brightness of the small granules are strongly correlated. Graphs of the first 160 points of the adjusted data are shown in Figure 2 (the brightness-curve has been inverted so that the resulting correlation is positive). The high degree of correlation between the two curves is evident by inspection.

The autocorrelation function of the velocity data,

$$r(m) = \frac{\Sigma X_i X_{i+m}}{\Sigma X_i^2}$$

(where X_i is the deviation from the moving average of the ith datum), was found to have essentially the same shape as the curve in Figure 1 except that $r(0) = 1$ (as is always the case, because of the definition of this function). The secondary peak in $r(m)$ occurred for $m = 7$, corresponding to a distance at the sun of 2300 km, the same distance obtained from the cross-correlogram of Figure 1. These results indicate that the turbulence spectrum of velocities for the small granules consists of a *narrow* distribution of cell sizes cen-

tered about an average size of 2300 km. The random velocity computed from our reduced data is 0.17 km/sec, as compared with the value 0.37 km/sec obtained by Richardson and Schwarzschild.

The pictorial studies of the granulation mentioned earlier have yielded values of approximately 1″–2″ for the diameter of individual granules. If the width of the dark space between granules is approximately equal to the granule diameter, as seems reasonable on the basis of visual appraisal, then the average cell size, or center-to-center distance between granules, should be about 2″–4″. Thus our value of 3″ for the cell size from correlogram analyses agrees well with the results of the pictorial studies.

The fact that a well-defined cell dimension of 2300 km was obtained by two entirely different smoothing operations on the original data precludes the possibility that this result might be a spurious one introduced by the reduction procedures. Despite the strong evidence offered by Richardson and Schwarzschild, it is difficult to believe that a narrow distribution of cell dimensions about so large a mean (about 3″) is only the statis-

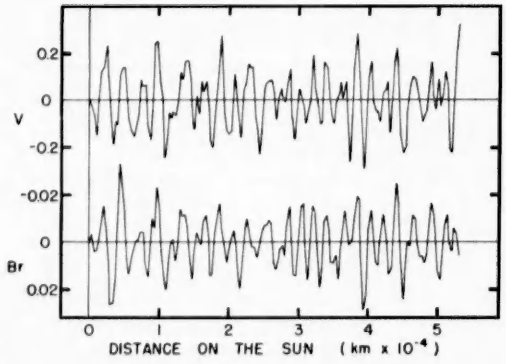

FIG. 2.—Graphical illustration of correlation between fluctuations in velocity (*V*) and brightness (*Br*) of small-scale granular detail, plotted as deviations from moving average of seven points.

tical "tail" of a much finer structure that is not resolved. Yet, without quantitative information on the loss of definition caused by instrumental and seeing effects, one cannot be sure that this is not the case. An alternative possibility is that the granular structure consists of at least three superimposed orders of cellular organization: the hypothetical small granules of the order of 200 km in diameter, not yet resolved; the 2300-km cells indicated here; and cells of approximately 15,000 km in diameter, to be discussed in the next section.

III. DATA FROM MILLER'S PLATES

We have analyzed eight photometrically calibrated white-light photographs of the solar disk on slow orthochromatic plates, taken by W. A. Miller, of R.C.A. laboratories, to determine whether or not there exists a regularly spaced fluctuation in brightness corresponding to the maximum at 15,000 km in the turbulence spectrum of Frenkiel and Schwarzschild. It is interesting to note that these plates, the quality of which is comparable to that of the excellent plates obtained by Janssen, were exposed at Rocky Point, Long Island, a locality that is practically at sea-level and close to the metropolitan areas of the East Coast. Furthermore, the best seeing conditions, sometimes persisting through several hours, occur only during periods of haze.

Microdensitometer traces were made along two straight lines running approximately north-south and east-west through the center of the disk. The density traces were converted into discrete data by dividing each trace into 96 intervals of approximately 2400 km each and determining by eye-estimate the average density over each interval. These average densities were then reduced to relative brightness, and the autocorrelation function was computed for the brightness data from each trace:

$$r(m) = \frac{\Sigma X_i X_{i+m}}{\Sigma X_i^2},$$

where X_i is the deviation from the mean of relative brightness. The brightness data from the majority of traces were reduced by the preliminary running-mean procedure described earlier, before being used to compute the correlogram. Figure 3 shows one of the correlograms obtained from a trace that was subjected to this operation. In all cases in which the running mean was used, the result clearly indicated the presence of brightness

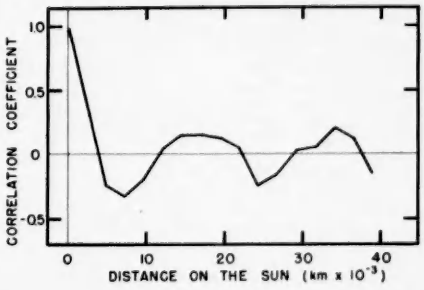

FIG. 3.—Autocorrelation function of fluctuations in brightness of large-scale granular detail, showing secondary maxima at approximately 17,000 and 34,000 km.

fluctuations with a mean wave length of approximately 14,000 km. Comparison of the correlograms of the same trace with and without the use of the running mean showed that this operation produced a significant enhancement of the 14,000-km maximum. Since the running mean involved intervals of irregular lengths determined by the data itself, it does not appear to have been capable of introducing a spurious periodicity into the correlogram. Further, the fact that the correlations between brightness and velocity, discussed in the preceding section, were revealed by the use of the running mean and still further enhanced by the moving-average procedure supports the validity of the periodicities revealed by the use of the running mean.

The fluctuations in brightness that defined the 14,000-km structure were not nearly so marked as those of the small granules. On the plates we analyzed, the r.m.s. deviation from the mean averaged about 1 per cent of the mean surface brightness. This quantity was not constant from one plate to the next but varied between the limits of $\frac{1}{2}$ and 2 per cent. Some of this variation, however, must be attributed to differences in seeing effects from one plate to another. The dimension of the large structure was by no means constant either, but varied from 10,000 to 17,000 km. Comparisons of results from the two traces at right angles on each plate revealed no consistent orientation effects.

We subjected Richardson and Schwarzschild's brightness data to autocorrelation analysis after smoothing by the running-mean procedure. The resulting curve showed no significant indication of a 15,000-km wave length. The reason for this disagreement with

the results from the velocity data and from Miller's plates is not clear. Our traces extended over about 15 wave lengths, twice the length of Richardson and Schwarzschild's trace. This difference is a statistical advantage for the longer traces, but it does not account for so great a discrepancy in results. More significant, probably, is the fact that Richardson and Schwarzschild's brightness measurements were made in a narrow strip of the continuum between absorption lines, while ours were made on orthochromatic plates in white light.

We should like to acknowledge our indebtedness to Drs. Martin Schwarzschild, David Hawkins, Walter Orr Roberts, and William A. Miller, whose suggestions and assistance have contributed substantially toward these results. The research has been supported in part by the Radio Corporation of America.

REFERENCES

Bruggencate, P. ten. 1939, *Zs. f. Ap.*, **19**, 59.
Chevalier, S. 1912, *Ann. Obs. Zô-Sé*, **8**, CI.
Frenkiel, F. W., and Schwarzschild, M. 1952, *Ap. J.*, **116**, 422.
Janssen, J. 1896, *Ann. Obs. Meudon*, **1**, 103.
Keenan, P. C. 1938, *Ap. J.*, **88**, 360.
———. 1939, *ibid.*, **89**, 604.
Macris, C. 1953, *Ann. d'ap.*, **16**, 19.
Miller, W. A. 1953, *A.J.*, **58**, 223.
Richardson, R. S. and Schwarzschild, M. 1950, *Ap. J.*, **111**, 351.

A STATISTICAL INVESTIGATION OF SUNSPOT OBSERVATIONS WITH SPECIAL REFERENCE TO H. ALFVÉN'S SUNSPOT MODEL

P. WHITTLE
University Institute of Statistics, Uppsala, Sweden
Received March 30, 1953; revised May 26, 1954

ABSTRACT

After a brief account of the properties of the autoregressive scheme, a double autoregression is fitted to the observed sunspot intensities in the northern and southern solar hemispheres. The results obtained confirm H. Alfvén's theory of sunspot generation and give evidence of a number of new phenomena.

I. INTRODUCTION

Sunspot series have been subjected to at least two statistical analyses: those of Yule (1927) and of Wold and Galvenius (1947). The analysis by Yule, based on an autoregressive scheme, aimed at a graduation of the data and not in the construction of a detailed physical model. Wold and Galvenius were concerned with the testing of a particular hypothesis; to that end they examined the spot intensity as a function of latitude at a certain stage of each of the six cycles available. In this paper we shall follow a complementary method, in that we shall examine the observational series for every recorded instant for two solar latitudes, situated symmetrically north and south of the equator. The justification for this is that the sunspot phenomenon is a time-dependent one, and it is reasonable to suppose that we can reach an understanding of its mechanism best by following its course in time; and this we can do by using the well-developed methods of time-series analysis which are now available.

The observations analyzed consist of two time series, giving the total spot area for a series of 6-monthly periods from 1886 to 1945 and for two belts of latitude, 16°–21° N., and 16°–21° S., inclusive. Observations are taken only for a relatively narrow belt, since the phenomena we shall study are definitely latitude-dependent. The terms of the two series will be denoted by N_t, S_t ($t = 1, 2, \ldots, 120$). We shall have occasion to work with sums and differences, $x_t = N_t + S_t$; $y_t = N_t - S_t$. The values of these quantities and their correlograms are given in Appendix I. Since the unit of time adopted is 6 months, the length of the sunspot cycle will be approximately 22 units. Before commencing the analysis proper, we shall give a brief account of the relevant properties of the autoregressive scheme.

II. THE AUTOREGRESSIVE SCHEME

Suppose that one has a series of observations $\ldots, x_{t-1}, x_t, x_{t+1}, \ldots$, taken at equal intervals of time. Let x_t have an expectation zero; this entails no loss of generality. Suppose, further, that the observations are so generated that x_t can be represented as a linear function of $x_{t-1}, x_{t-2}, \ldots, x_{t-p}$ plus a disturbance variate, i.e.,

$$x_t + a_1 x_{t-1} + a_2 x_{t-2} + \ldots + a_p x_{t-p} = \epsilon_t , \tag{1}$$

where the a's are constant coefficients and the ϵ's constitute a random series of uncorrelated variates. It is then said that x_t obeys a *linear autoregression of order p*.

An autoregressive series displays, in general, pronounced periodic tendencies. However, in common with many physical series, the curve is not exactly sinusoidal but continually undergoes random changes in amplitude and phase. The great virtue of assumption (1) is that it provides an explanation of this observed quasi-periodicity.

The quasi-periods T of the autoregression are determined by the values of $T = 2\pi/\omega$, for which

$$F(\omega) = |1 + a_1 e^{i\omega} + a_2 e^{2i\omega} + \ldots + a_p e^{ip\omega}|^{-2} \tag{2}$$

is a maximum. It is thus obvious that a series with a given dominant quasi-period (e.g., the 11-year period of the sunspot cycle) could be conceived as being generated by any one of an infinite number of autoregressions, since all that is required is that $F(\omega)$ possess a sufficiently strong maximum at the ω value corresponding to the given T. However, these different autoregressions will generate curves of different wave form, i.e., of different harmonic content.

Now the restriction to a set of discrete instants of time $\ldots, t-1, t, t+1, \ldots$, should be regarded as an approximation to some other relation of continuous nature. Thus a second-order autoregression can be regarded as an approximation to a second-order stochastic differential equation (cf. Doob 1949):

$$\frac{d^2x_t}{dt^2} + b_1\frac{dx_t}{dt} + b_2 x_t = \epsilon_t, \tag{3}$$

where b_1 and b_2 are constants, and ϵ_t is again a purely random variate (not identical with the ϵ_t of [1]). Equation (3) will also, in general, generate a disturbed harmonic curve (the oscillation of a "disturbed pendulum"; cf. Yule 1927); and, given b_1 and b_2, an autoregression may be found which would, in the absence of disturbances, generate a series of the same period and damping.

However, an autoregression need not necessarily correspond to a differential equation, it may also correspond to some variety of difference equation (with other time lags than those occurring in the autoregression itself) or even an equation of mixed type (a so-called "differential-difference equation"):

$$\frac{dx_t}{dt} + c_1 x_t + c_2 x_{t-\tau} = \epsilon_t. \tag{4}$$

The relevance of this to the sunspot problem will be apparent later.

III. THE FORM OF THE OSCILLATIONS IN TOTAL INTENSITY

By graduating Wolfer's data for the total sunspot intensity with a second-order autoregression, Yule obtained a fit which was spectacularly successful compared with that yielded by previous methods, which had all attempted to represent the oscillation by a finite number of sinusoidal terms. The oscillations were thus regarded as comparable to those of a disturbed pendulum. This is an analogy which is often suggested; but too much importance should not be attached to it in this particular case.

Now, in Alfvén's model of a sunspot, a mechanism is postulated which should lead to a rather different wave form from that of the "disturbed-pendulum" model. It is supposed that when a magneto-hydrodynamic whirl enters one of two unstable regions ("activity regions") situated north and south of the sun's center, it is amplified and then proceeds outward along a line of force to the sun's surface, where it produces a spot. The amplification of the original disturbance produces a recoil whirl which passes through the opposite activity region (initiating yet a new disturbance in doing so) to the surface of the opposite hemisphere. Here it produces a spot, situated roughly symmetrical to the first but lagging behind it by a time equal to the time taken to traverse the distance between the two regions. This transit time is postulated to be equal to the length of the sunspot cycle, roughly 11 years. Thus the spot pattern in one hemisphere should approximately reproduce itself in the opposite hemisphere 11 years later. Wold and

Galvenius in their statistical analysis confirmed the existence of this phenomenon, thus giving powerful support to Alfvén's theory.

However, the postulated mechanism should show itself in another way, which can be tested even more directly, namely, in the wave form of the intensity oscillations. For the oscillation is thought of as being produced, not by a mechanism analogous to that of a pendulum or a resonant circuit, but by repeated reflection between two regions. This means that the spot intensity at a given moment is as much determined by its value 11 years previously as by its values in an immediately preceding interval of time, so that the quantitative relation is rather of type (4) than of type (3).

We can test this point by fitting two different types of autoregression to the total intensity, $x_t = N_t + S_t$. If the "pendulum" model were the correct one, then the total intensity should be representable approximately by an autoregression

$$x_t + a_1 x_{t-1} + a_2 x_{t-2} = \epsilon_t . \tag{5}$$

On the other hand, if Alfvén's theory holds, then a term in x_{t-22} should be necessary, so that if we fit an autoregression,

$$x_t + a_1 x_{t-1} + a_2 x_{t-2} + a_{22} x_{t-22} = \epsilon_t , \tag{6}$$

we should find that a_{22} is significantly negative. (It should be realized that the fact that x_t and x_{t-22} are strongly positively correlated does not necessarily imply that a_{22} will be nonzero. This will be the case only if x_t has a *direct* dependence on x_{t-22}.)

Upon fitting an autoregression of type (6), including also a term in x_{t-44} to see whether the relevant past extends over more than one cycle, we find

$$x_t = 0.547 x_{t-1} - 0.068 x_{t-2} + 0.411 x_{t-22} - 0.011 x_{t-44} \tag{7}$$

(see Appendix II for details of fitting and testing techniques). The coefficient of x_{t-22} is large. It remains to be seen whether it is significantly large. For this purpose we assume that x_{t-22} term to be superfluous and compare the estimates of the residual variance obtained upon fitting autoregressions with lags 1, 2, and 1, 2, 22. These are, respectively, $v_1 = 0.409773$ and $v_2 = 0.326866$, so that

$$\psi^2 = 117 \log_e \left(\frac{0.409773}{0.326866} \right) = 26.45 . \tag{8}$$

On the hypothesis of a second-order autoregression, the probability of obtaining a value of ψ^2 as large as or larger than 26.45 is extremely small, only 5×10^{-7}. That is, the "pendulum" hypothesis is quite untenable, and Alfvén's hypothesis gives a vastly improved fit.

The coefficient of x_{t-2} in equation (7) is so small as scarcely to seem necessary. To test its significance, we fit an autoregression with lags 1, 22, and find the corresponding residual variance to be 0.329716. Comparing this with the value for the 1, 2, 22 autoregression, we have

$$\psi^2 = 117 \log_e \left(\frac{0.329716}{0.326866} \right) = 1.01 . \tag{9}$$

The probability on the 1, 22 hypothesis that $\psi^2 \geq 1.01$ is about 0.30. This is quite reasonable, so the conclusion is that the x_{t-2} term is superfluous.

The coefficient of x_{t-1} is significantly large. This is evidence of a certain "neighbor correlation," which is quite simply a consequence of the fact that the observed series are fairly continuous in nature, so that neighboring terms do not differ greatly.

IV. THE OSCILLATION BETWEEN HEMISPHERES

We shall now attempt to set up a scheme which represents the mechanism in greater detail, with the object of deciding whether the whirls actually are reflected between the hemispheres, as Alfvén's theory supposes.

To do this, we shall set up a *double* autoregression, i.e., represent N_t as a linear function of $N_{t-1}, N_{t-2}, \ldots, S_t, S_{t-1}, S_{t-2}, \ldots$ plus a disturbance term, so that a relation holds,

$$AN_t + BS_t = \epsilon_t , \tag{10}$$

where $AN_t = a_0N_t + a_1N_{t-1} + \ldots$, and $BS_t = b_0S_t + b_1S_{t-1} + \ldots$. Now it is reasonable to suppose, at least as a first approximation, that the sun is symmetric about its equator, so that a relation

$$BN_t + AS_t = \epsilon_t' \tag{11}$$

must also hold, where ϵ_t' is another disturbance term, with the same variance as ϵ_t. Further, we lose no generality by supposing ϵ_t and ϵ_t' uncorrelated, since equations (10) and (11) may be transformed linearly so as to bring this about. These equations together constitute the complete model.

Now, adding and subtracting equations (10) and (11), we find

$$(A + B)x_t = \epsilon_t + \epsilon_t' ; \qquad (A - B)y_t = \epsilon_t - \epsilon_t' . \tag{12}$$

Since ϵ_t and ϵ_t' are uncorrelated, so are $\epsilon_t + \epsilon_t'$ and $\epsilon_t - \epsilon_t'$. That is, the series x_t and y_t develop independently of each other, so that if we fit autoregressions to these two series separately, we shall obtain estimates of $A + B$ and $A - B$, from which estimates of A and B may be derived.

The question now is, Which lags should be included in these two regressions? There are a priori reasons for believing that the sunspot intensity at any given instant of time is largely determined by its values in the immediate past and in the preceding cycle, so that we should expect lags of perhaps 1–3 and 20–24 to be significant. However, in order to avoid such a priori reasoning, autoregressions to x_t and y_t were fitted, in which all lags from 1 to 26 have been included. Thus, we obtain autoregressions of the type

$$\begin{aligned} x_t &= c_1x_{t-1} + c_2x_{t-2} + \ldots + c_{26}x_{t-26} + (\text{error}) , \\ y_t &= d_1y_{t-1} + d_2y_{t-2} + \ldots + d_{26}y_{t-26} + (\text{error}) . \end{aligned} \tag{12a}$$

Adding the two relations, we have

$$\begin{aligned} N_t = {} & \tfrac{1}{2}(c_1 + d_1)N_{t-1} + \tfrac{1}{2}(c_2 + d_2)N_{t-2} + \ldots + \tfrac{1}{2}(c_{26} + d_{26})N_{t-26} \\ & + \tfrac{1}{2}(c_1 - d)S_{t-1} + \tfrac{1}{2}(c_2 - d_2)S_{t-2} + \ldots + \tfrac{1}{2}(c_{26} - d_{26})S_{t-26} + (\text{error}), \end{aligned} \tag{13}$$

that is, a representation of N_t in terms of *past* values of N_t and S_t. Equation (13) does not correspond directly to either (10) or (11); it corresponds to the equation when S_t is eliminated from them. This is just what we required: for the coefficients of representation (13) indicate the degree of direct dependence of N_t upon $N_{t-1}, \ldots, N_{t-26}, S_{t-1}, \ldots, S_{t-26}$, assuming that lags of higher order are redundant. A similar representation for S_t may be deduced by subtracting the two equations (12).

The estimated values of the coefficients are given in Table 1. These are represented graphically in Figure 1, in which all coefficients less than 0.07 in absolute value have been

omitted. The following features may be noted: (*a*) The coefficients of N_{t-1}, S_{t-1}, S_{t-22}, and those of N_{t-20} and N_{t-25} are large; (*b*) the isolated maximum at S_{t-22} is immediately followed by three strongly negative coefficients; (*c*) the smaller coefficients which remain resolve themselves into groups beginning at $s = 4$, 9, and 14 for the autoregressive coefficients and $s = 4$, 11, and 17 for the cross-regression coefficients. The intervals between these latter groups are thus 4, 5, 5 and 5, 7, 6, which suggests a periodicity. As

TABLE 1

AUTOREGRESSION COEFFICIENTS

s	Coeff. N_{t-s}	Coeff. S_{t-s}	s	Coeff. N_{t-s}	Coeff. S_{t-s}
1	+0.325	+0.214	14	+0.072	−0.002
2	− .060	+ .045	15	− .105	− .030
3	+ .063	+ .018	16	− .059	− .023
4	− .092	+ .128	17	+ .083	+ .095
5	− .035	+ .090	18	− .078	− .084
6	− .066	− .133	19	− .105	+ .090
7	+ .023	+ .045	20	+ .206	+ .001
8	− .045	− .027	21	+ .075	− .020
9	− .089	− .041	22	+ .087	+ .217
10	− .024	+ .025	23	+ .001	− .160
11	− .049	+ .108	24	− .039	− .154
12	− .001	− .057	25	+ .228	− .173
13	−0.019	+0.007	26	−0.106	+0.093

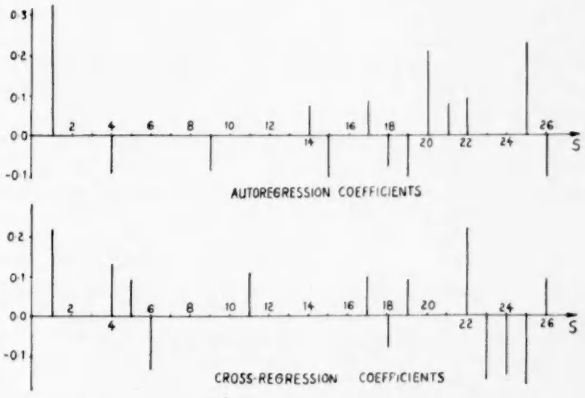

FIG. 1.—Autoregression and cross-regression coefficients

pointed out at the end of Section III, the effect noted under *a* is evidence for the fact that the observed series are relatively smooth. While this is the sort of thing that one expects, it nevertheless requires explanation. Several possible explanations suggest themselves: The train of whirls may suffer some sort of smoothing process on its passage from the core to the surface, or there may be a genuine correlation between the intensities of successive whirls, due to the fact that the reserve of latent energy in the activity regions also varies relatively smoothly with time. The fact that the coefficient of S_{t-1} is large indi-

cates the existence of a coupling between the intensities in the northern and southern hemispheres at any given time. This requires explanation.

The large S_{t-22} coefficient provides direct evidence of the repeated reflection, which is the essential feature of Alfvén's hypothesis. If an 11-year reflection really takes place, then the spot intensity in the one hemisphere should exhibit a direct dependence upon the intensity in the other hemisphere 11 years previously, and this is just the effect observed. The magnitude of this S_{t-22} coefficient is evidently crucial for the hypothesis, and we shall examine its statistical significance more closely in the next section.

The large coefficients of N_{t-20} and N_{t-25} are quite unexpected: They suggest that the intensity at a certain time in a certain hemisphere is partly determined by the intensity in the same hemisphere roughly 11 ± 1 years previously. We shall not attempt to explain this effect, although one possible mechanism will be discussed later in the section.

The effect noted under *b* implies that, although a strong spot in the southern belt is accompanied by increased activity in the northern belt 11 years later, during the subsequent $1\frac{1}{2}$ years (i.e., from 11 to $12\frac{1}{2}$ years after the occurrence of the southern spot) there will be decreased activity in the northern belt. This may be interpreted as a "fatigue effect." However, if this were the fact, we should expect the transmitted whirls to be as much affected as the reflected ones, so that the southern spot would be immediately followed by decreased activity in the same belt. This means that the early autoregression coefficients should be negative, something which is not observed. There may be two explanations of this, however: first, this manifestation of the fatigue effect is partly offset by the continuity effect; second, the production of a strong whirl may not leave the region in an exhausted state but may well leave it in a relatively homogeneous state, since it will be the more active parts of the region which will have contributed most energy. A subsequent whirl will then be amplified fairly uniformly (see Alfvén 1950, p. 131), so that the recoil disturbance is more drawn out and less intense than it would otherwise have been. The transmitted whirl will be as concentrated as ever, however, so it will be only the recoil whirl which will seem to have been weakened.

Finally, the presence of regularly occurring groups of coefficients noted under *c* suggests the injection of disturbances from some outside source. As an example, consider the so-called *moving average*,

$$x_t = \epsilon_t - c\epsilon_{t-\tau}. \tag{14}$$

Eliminating $\epsilon_{t-\tau}$, $\epsilon_{t-2\tau}$, etc., we transform equation (14) to an infinite autoregression,

$$x_t + cx_{t-\tau} + c^2x_{t-2\tau} + \ldots = \epsilon_{t-\tau}. \tag{15}$$

We thus see that a scheme of type (15) leads to an autoregression of infinite order in which regularly repeated coefficients occur. Similarly, the repetition of coefficients in the graph at roughly 5 units interval suggests that a disturbance which enters the system at time t enters it again at time $t + 5$, just as in equation (15) the disturbance ϵ_t which affects x_t will, a time τ later, affect $x_{t+\tau}$.

This could possibly be accounted for by some sort of a center of disturbance situated asymmetrically between the two regions, so that a disturbance propagated in both directions reaches one hemisphere 5 units ($2\frac{1}{2}$ years) before it reaches the other. It would be this center of disturbance which stimulated the two active regions to oscillation, just as a succession of random blows will stimulate a pendulum to oscillation. An attempt to explain the smaller coefficients by such a mechanism leads to an agreement which is satisfactory qualitatively, but not quantitatively.

If we suppose that whirls traveling through a center of disturbance are also partially reflected by it, we can then explain the coefficients of N_{t-20} and N_{t-25}. On the basis of

this extremely tentative suggestion, one could calculate the distances of the two active regions and center of disturbance from the equatorial plane. For suppose that these distances are p, q, and r (all measured in the same direction and in "propagation years," i.e., the number of years required for a whirl to traverse them). Then

$$p - q = 11\,, \qquad 2(p - r) = 10\,, \qquad 2(r - q) = 12.5\,, \qquad 2r = 2.5\,. \tag{16}$$

These equations express the fact that the transit time between the regions is 11; that it will take a whirl 10 years to travel from the first active region to the center of disturbance and back again; that it will take the same whirl $12\frac{1}{2}$ years for the second region; that the center of disturbance is $2\frac{1}{2}$ years nearer one of the hemisphere surfaces than the other.

Solving the last three relations of (16) we find $p = 6\frac{1}{4}$, $q = -5$, and $r = 1\frac{1}{4}$. This gives $p - q = 11\frac{1}{4}$, in good agreement with the first relation, so that the four equations may be said to be consistent. The mid-point between the two regions has co-ordinate $(p + q)/2 = \frac{5}{8}$. Thus, according to this calculation, the disturbance center is displaced $1\frac{1}{4}$ "years" from the equatorial plane, and the activity regions are displaced half as much in the same direction. These last suggestions are, of course, only one of many interpretations of the observed facts and should therefore be considered to be highly tentative.

V. TESTING OF THE REFLECTION EFFECT

As stated in the previous section, it is the size of the S_{t-22} coefficient which proves or disproves the hypothesis of an interhemisphere reflection. However, to establish the hypothesis, it is not sufficient to prove that the coefficient is significant, but it must also be shown to be significantly larger than the corresponding N_{t-22} coefficient. For, suppose that there were no differential effect between hemispheres, so that the northern and southern intensities varied together, both being dependent upon some common cause. Then a dependence of N_t upon S_{t-22}, for example, would be accompanied by an equally strong dependence upon N_{t-22}. The fact that these two dependences actually differ is an indication of a differential effect, and we wish to see whether the effect is so strong as to be unmistakable.

The difference between the N_{t-22} and S_{t-22} coefficients is simply equal to the coefficient of y_{t-22} in the second equations (12), so that the problem reduces to an examination of this coefficient, following the method outlined in Appendix II. Actually, we have simplified the calculations by including only those lags which are obviously of importance, i.e., 1, 20, 22, 23, 24, and 25; but this will have little effect upon the result of the test. Denoting the estimate of the residual variance obtained upon fitting an autoregression with lags $p, q, r, \ldots$, by $v(p, q, r, \ldots)$, we have

$$v(1, 20, 22, 23, 24, 25) = 0.704801$$

and

$$v(1, 20, 23, 24, 25) = 0.741972\,, \tag{17}$$

so that

$$\psi^2 = 114 \log_e \left(\frac{0.741972}{0.704801}\right) = 5.855\,. \tag{18}$$

The probability that $\psi^2 \geq 5.855$ on the hypothesis that lag 22 is superfluous is only 0.016, so that the y_{t-22} coefficient is clearly significant. Actually, since we are not testing the hypothesis that the coefficient is nonzero but that it is negative, the result is significant at a level of 0.008.

The conclusion is, then, that there is a genuine differential effect, corresponding to a repeated reflection of the type proposed by Alfvén. It should be noted, however, that all

tests have been made under the assumption of solar symmetry and are strictly valid only on this assumption. Further, in using the autoregressive technique, we have tacitly assumed that the data are representable in the form (1), with a residual ϵ_t of constant variance. It is not likely that the situation is quite so simple, however, since examination of the sunspot intensity record shows that the variance of the smaller fluctuations increases with a general rise in intensity. A radical modification of existing methods would be required to account for this. However, since the different effects found in the autoregressive analysis are produced rather by the wave form of the main 11-year oscillation than by the presence of these minor fluctuations, we may expect that the conclusions arrived at would be substantially confirmed by a more refined analysis.

The author wishes to express his gratitude to Professor H. Alfvén for help with the preparation of the observational material, to Professor H. Wold for facilities granted in connection with the numerical computations, and to both for stimulating discussion at various times.

APPENDIX I

TABLE 2

THE 120 VALUES OF $x_t = N_t + S_t$, ARRANGED IN COLUMNS

1579	104	747	87	160
465	20	112	0	130
92	3	8	0	2173
257	0	0	304	4213
0	0	0	446	6065
0	58	40	2631	9371
0	58	17	2183	12803
675	111	79	8828	5331
26	19	593	12551	5967
1632	849	2096	7308	8033
4389	2442	7444	6112	5413
7157	5323	7148	4569	7469
6041	3029	5278	4368	1171
3141	4940	4000	5970	2786
7887	3436	8350	1613	448
10255	3246	8675	4169	1366
5509	4252	5011	2626	343
4762	4649	5986	423	118
3747	4653	4505	114	0
3675	1998	999	128	0
3943	1208	1433	0	0
2186	1361	1237	0	1725
725	1643	516	0	3288
78	454	175	0	4404

TABLE 3

THE 120 VALUES OF $y_t = V_t - S_t$, ARRANGED IN COLUMNS

−1475	+ 8	+ 105	− 87	− 160
+ 147	− 20	− 92	0	− 108
+ 14	− 3	− 8	0	−1653
− 257	0	0	− 102	+ 695
0	0	0	− 210	+ 65
0	− 58	+ 40	+2601	+1785
0	− 58	+ 17	+1091	+4137
− 675	− 111	+ 79	− 152	−1393
+ 26	+ 19	+ 455	−2067	+2357
+ 900	− 49	+1270	+2838	+ 727
+1671	+ 6	+2690	+ 46	−3253
+3243	−2045	−4136	−2549	− 569
− 187	+ 977	−1352	−1456	− 653
− 699	− 840	+1382	+ 344	−1140
−3687	− 480	−1572	− 901	− 184
−1885	− 694	+1423	+ 509	+ 246
− 413	+2402	+ 283	− 4	+ 343
−2008	+ 581	− 486	+ 359	+ 118
+ 583	−1883	−3301	− 114	0
+1401	−1616	− 667	+ 128	0
−1751	−1058	− 365	0	0
−1144	− 811	− 253	0	+ 161
− 653	−1571	+ 268	0	−2962
+ 33	− 264	− 175	0	−2190

TABLE 4

THE FIRST 26 AUTOCORRELATION COEFFICIENTS OF x_t

+0.7681	−0.1142	−0.6295	−0.0654	+0.6828
+ .5796	− .2914	− .5990	+ .1617	+ .7315
+ .4428	− .4471	− .5214	+ .2819	+ .5808
+ .2800	− .5848	− .3720	+ .4191	+ .4332
+0.1158	−0.6372	−0.2343	+0.5851	+ .3473
				+0.1843

TABLE 5

THE FIRST 26 AUTOCORRELATION COEFFICIENTS OF y_t

+0.0982	−0.0836	−0.0994	−0.0705	+0.1500
− .0952	+ .0484	+ .0135	+ .0224	− .0895
+ .0278	+ .0271	+ .0487	− .0543	+ .1777
− .1537	− .0374	+ .0463	− .0822	+ .2328
−0.1629	−0.0253	−0.0135	+0.1616	+ .2826
				−0.1518

APPENDIX II

Suppose that a given observational series $(x_1, x_2, x_3, \ldots, x_n)$ has autocorrelation coefficients $r_1, r_2, r_3, \ldots$. Then the coefficients of an autoregression with lags $p, q, r, \ldots, u$, namely,

$$x_t = a_p x_{t-p} + a_q x_{t-q} + a_r x_{t-r} + \ldots + a_u x_{t-u} ,$$

are estimated by the Yule-Walker relations (see Wold 1938, p. 104),

$$\begin{aligned}
r_p &= a_p + r_{q-p} a_q + r_{r-p} a_r + \ldots + r_{u-p} a_u , \\
r_q &= r_{q-p} a_p + a_q + r_{r-q} a_r + \ldots + r_{u-q} a_u , \\
r_r &= r_{r-p} a_p + r_{r-q} a_q + a_r + \ldots + r_{u-r} a_u , \\
&\cdots\cdots\cdots\cdots\cdots\cdots\cdots\cdots\cdots\cdots \\
r_u &= r_{u-p} a_p + r_{u-q} a_q + r_{u-r} a_r + \ldots + a_u ,
\end{aligned}$$

and the residual variance of the scheme fitted is proportional to the ratio

$$v = \begin{vmatrix} 1 & r_p & r_q & \ldots & r_u \\ r_p & 1 & r_{q-p} & \ldots & r_{u-p} \\ r_q & r_{q-p} & 1 & \ldots & r_{u-q} \\ \cdot & \cdot & \cdot & \ldots & \cdot \\ \cdot & \cdot & \cdot & \ldots & \cdot \\ \cdot & \cdot & \cdot & \ldots & \cdot \\ r_u & r_{u-p} & r_{u-q} & \ldots & 1 \end{vmatrix} \div \begin{vmatrix} 1 & r_{q-p} & \ldots & r_{u-p} \\ r_{q-p} & 1 & \ldots & r_{u-q} \\ \cdot & \cdot & & \cdot \\ \cdot & \cdot & & \cdot \\ \cdot & \cdot & & \cdot \\ r_{u-p} & r_{u-q} & & 1 \end{vmatrix} .$$

Suppose that in this way α coefficients are fitted. To test the joint significance of any β of these coefficients, a scheme is fitted in which these β coefficients are excluded, leading to another estimate of the residual variance, v^1, say. Then, if it is true that the theoretical values of the coefficients under test is, in fact, zero,

$$\psi^2 = (n - \alpha) \log_e \left(\frac{v^1}{v} \right)$$

is approximately distributed as χ^2 with β degrees of freedom (Whittle 1952; see also Walker 1952). Thus a value of ψ^2 which is significantly large according to the χ^2 table indicates that the coefficients under test are necessary to the representation of x_t, while a value in the neighborhood of expectation indicates that they can be dispensed with. Similar tests may be derived for a multiple series (Whittle 1953).

A number of minor variants of the autocorrelation coefficient are in use; the one employed in the present calculations was

$$r_s = \frac{n}{n-s} \frac{\sum_1^{n-s} x_t x_{t+s} - \left(\sum_1^{n-s} x_t \right) \left(\sum_1^{n-s} x_{t+s} \right) / (n-s)}{\sum_1^n x_t^2 - \left(\sum_1^n x_t \right)^2 / n} .$$

REFERENCES

Alfvén, H. 1950, *Cosmical Electrodynamics* (Oxford: Oxford University Press). Also contains references to the original papers.

Doob, J. L. 1949, *The First Berkeley Symposium* (University of California Press, Berkeley).

Walker, A. M. 1952, *J. R. Stat. Soc.*, *B*, **14**, 117.

Whittle, P. 1952, *Biometrika*, **39**, 309.

———. 1953, *J. R. Stat. Soc.*, *B*, **15**, 125.

Wold, H. 1938, *A Study in the Analysis of Stationary Time Series* (Uppsala).

Wold, H., and Galvenius, I. 1947, *Ark. f. Mat.*, Vol. **34A**, No. 24.

Yule, G. U. 1927, *Phil. Trans.*, *A*, **226**, 267.

THE STRUCTURE OF THE OWL NEBULA

R. MINKOWSKI AND L. H. ALLER
Mount Wilson and Palomar Observatories and University of Michigan Observatory
Received April 13, 1954

ABSTRACT

Isophotic contours are measured on direct photographs of NGC 3587 secured with the 200-inch reflector. The Owl Nebula shows a very smooth structure with no sharp filaments or condensations. The object may be interpreted as a globe in which the density falls off uniformly at large distances from the center. Regions closer to the center exhibit a symmetry, which is, however, not radial. There appear to be two condensations symmetrically placed with respect to the center. Estimates of the electron density suggest $N_e \sim 50/\text{cm}^3$, which is comparable with the densities found in bright diffuse nebulae in our own and other galaxies. The probable mass of the object is also discussed. Attention is called to the similarity between the Owl Nebula and the object described by Jones and Emberson.

INTRODUCTION

One of the intrinsically largest, although also one of the faintest, of the planetary nebulae is NGC 3587, the "Owl Nebula." A century ago, Sir John Herschel (1858) wrote of this object as follows:

> The light of this stupendous globe is perfectly equable (except just at the edge, where it is slightly softened), and of considerable brightness. Such an appearance would not be presented by a globular space uniformly filled with stars or luminous matter, which structure would necessarily give rise to an apparent increase of brightness towards the center in proportion to the thickness traversed by the visual ray. We might, therefore, be induced to conclude its real constitution to be either that of a hollow spherical shell or of a flat disc, presented to us (by a highly improbable coincidence) in a plane precisely perpendicular to the visual ray.

Direct photographs of this object show a smooth structure uninterrupted by small condensations and filaments of the type so common to many planetaries (see Fig. 2). The variations of brightness that occur on the main disk of the nebula lack the crisp outlines characteristic of the features found in most planetaries. Photographs in the light of different radiations show no evidence of any stratification. The different monochromatic images would appear to be of comparable sizes and appearances.

ISOPHOTIC CONTOURS

Tracings of a direct photograph in the [*O* III] radiations made with the balanced-beam isophotometer (Williams and Hiltner 1940) confirm the conclusions drawn from a visual inspection of the plate. There is nothing that might be called a "fine structure"; the gradients are all smooth and uniform. The contours in Figure 1 are given for an approximate log I scale. The original plate had no photometric calibration, so we have adopted the calibration-curve from other plates of the same emulsion-filter combination that were developed under exactly the same conditions. The values of the relative log I are indicated for each contour.

An inspection of these curves reveals at once that the hypothesis of a radially symmetrical density distribution will not work, even as a first approximation. As the simplest working hypothesis we might assume one kind of radial symmetry along a line passing through the two bright condensations and another type of radial symmetry in the plane perpendicular thereto, except, of course, for the central regions (Fig. 2). The density of emission histograms constructed on such a hypothesis suggests that the maximum emission per unit volume in the plane containing the two bright condensations is at least

twice that in the other plane (see Fig. 3). A hypothesis of a simple shell in which the density depends only on the radius will not work; the globe is roughly a shell structure with two smooth, bright, condensations placed symmetrically on opposite sides of the central star and inside the shell (see Fig. 4).

DENSITY AND TEMPERATURE

The electron temperature may be estimated from the relative intensities of the 4363 and green nebular lines by the method employed by Menzel, Aller, and Hebb (1941) with the improved target areas computed by M. J. Seaton (1953). The relative intensities of the stronger nebular emissions were given some years ago by one of us, (Minkowski 1942) $I(N_1 + N_2) = 129$, $I(4363) = 1.3$. Hence $T_e = 13{,}600°$ K.

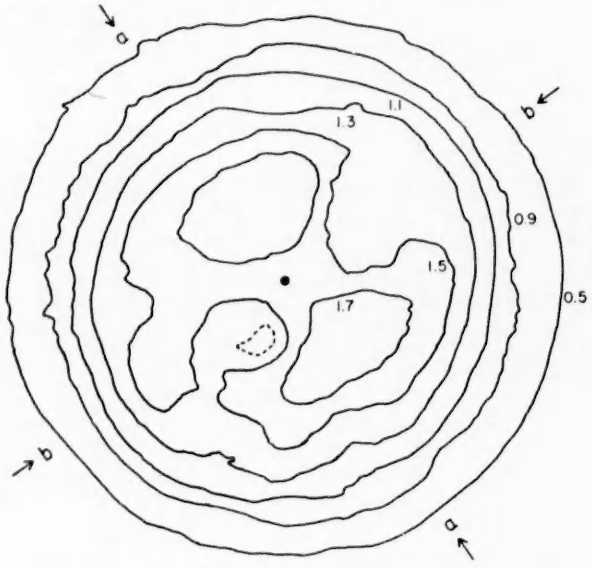

FIG. 1.—Isophotic contours of the Owl Nebula. Except for the faintest contour, isophotes are drawn for intervals in $\Delta \log I$ of approximately 0.2. A black dot indicates the central star. Lines drawn from points *a* and *b* through the central star indicate directions along which the density analyses were attempted (2".4 per mm).

An estimate of the electron density requires a knowledge of the surface brightness of the nebula and of its distance. The distance of the nebula is given by Berman (1937) as 3630 parsecs. Since the angular diameter is 200", the radius of the nebula comes out as 5.4×10^{18} cm, or about 1.7 parsecs.

The surface brightness has not been measured directly. The only available estimate is that by Curtis (1918), who gives a "relative exposure" of 100. This surface brightness may be reduced roughly in terms of c.g.s. flux units by calibrating the reciprocals of the Curtis relative exposures with the photoelectrically measured surface brightnesses (Liller and Aller 1954) for those objects for which accurate measures are available. It is found that a relative exposure of 100 corresponds to about $S = 3 \times 10^{-3}$ ergs/cm^2 sec for the green nebular lines. We now use the relation between surface brightness in a Balmer line,

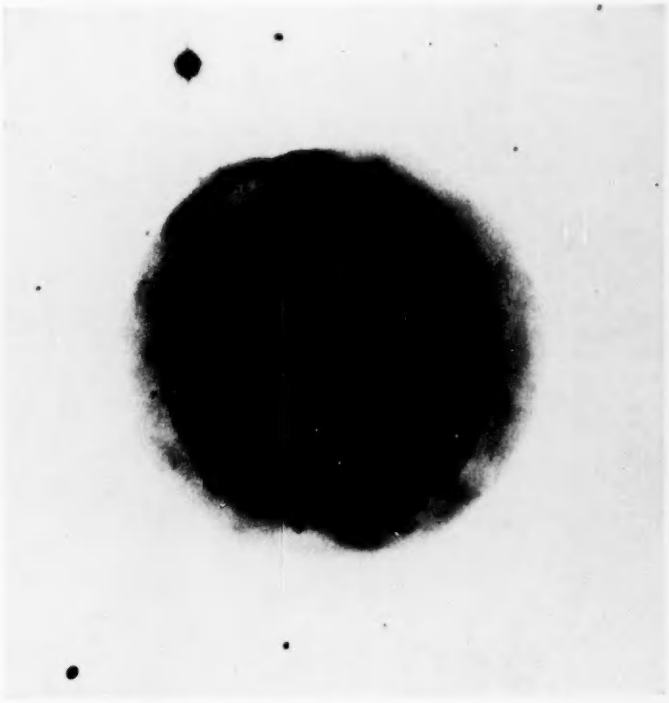

FIG. 2.—The Owl Nebula. Photographed in $H\alpha$ with the 200-inch reflector (3".2 per mm)

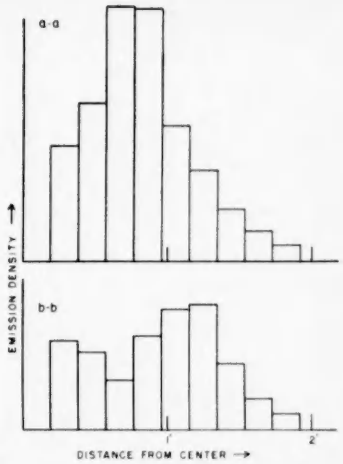

FIG. 3.—Emission density histograms for two mutually perpendicular directions in the Owl Nebula. The great differences between the density distributions along the directions indicated in Fig. 1 show that the assumption of a radially symmetrical distribution is untenable. It was assumed that the density was radially symmetrical in the outer portions of the nebula along the two directions analyzed. The densities can be regarded as only of qualitative significance.

FIG. 4.—Schematic drawing of the emission density in the Owl Nebula. This sketch is intended to depict a shell with two symmetrically placed, large, rather diffuse condensations of higher emission per unit volume.

specifically $H\beta$, and the ion and electron density (e.g., Liller and Aller 1954, eq. [3]) to compute N_e. In this way we find for the assumed distance of the Owl Nebula a mean electron density of $N_e = 43/\text{cm}^3$. The corresponding mass turns out to be about twice that of the sun and substantially larger than that of smaller, brighter planetary nebulae.

Berman (1937) remarks that he has probably overestimated the distance of this object. If we suppose that the distance is one-third the value given by Berman, the radius A will be 1.8×10^{18} cm, N_e will be $75/\text{cm}^3$, and the total mass will be about 0.15 that of the sun. Pending improved distance estimates, we are inclined to view the smaller distance as closer to the actual value. The Owl Nebula remains a giant among planetaries, however.

The density of NGC 3587 appears to be comparable with that of the brighter diffuse nebulae in our own and other galaxies, e.g., NGC 604 in the Triangulum Spiral. Its size is also comparable with the dimensions of the diffuse nebulae. The most remarkable feature of the object, however, is its apparent lack of any small-scale fine structure of the type so characteristic of other large planetaries, such as NGC 7293 in Aquarius or the Dumbbell Nebula in Vulpecula.

The Reynolds numbers for the planetaries are so high that any detectable internal motion must be turbulent unless suppressed by magnetic fields, Coriolis forces, or other restraints. It is difficult to understand why the Owl Nebula does not show a turbulent structure. Perhaps the sizes of the filaments are below the resolution of the plate, as may occur in NGC 7027. Speculation on this point is unwarranted until the internal motions have been measured.

After the analysis of the structure of the Owl Nebula was completed, the photograph of the faint planetary shown in Figure 5 was obtained on plates of the National Geographic Society–Palomar Observatory sky survey. This object, discovered by R. B. Jones and R. Emberson (1939), shows in a striking way a distribution of surface brightness which can hardly be interpreted in any other way than that it is a symmetrical hollow sphere with two symmetrical condensations, seen almost at right angles to the plane of the condensations. The Owl Nebula is apparently a very similar object seen in a somewhat different projection.

We are indebted to Mrs. Nancy Boggess for making the tracings with the balanced-beam isophotometer. Thanks are due to the Horace H. Rackham School of Graduate Studies for a grant to purchase a Brown Recorder for the balanced-beam isophotometer. The reductions of the observations of NGC 3587 and of other planetaries have been carried out with the aid of a contract between the University of Michigan and the Office of Naval Research.

REFERENCES

Berman, L. 1937, *Lick Obs. Bull.*, **18**, 57.
Curtis, H. D. 1918, *Pub. Lick Obs.*, Vol. **13**, Part 3, Fig. 23.
Herschel, Sir John. 1858, *Outlines of Astronomy* (London: Longmans, Green & Co.).
Jones, R. B., and Emberson, R. 1939, *Harvard Coll. Obs. Bull.*, **911**, 11.
Liller, W., and Aller, L. 1954, *Ap. J.*, **120**, 48.
Menzel, D. H.; Aller, L. H.; and Hebb, M. H. 1941, *Ap. J.*, **93**, 230.
Minkowski, R. 1942, *Ap. J.*, **95**, 243.
Seaton, M. J. 1953, *Proc. R. Soc. London, A*, **218**, 400.
Williams, R. C., and Hiltner, W. A. 1940, *Pub. U. Michigan Obs.*, **8**, 45.

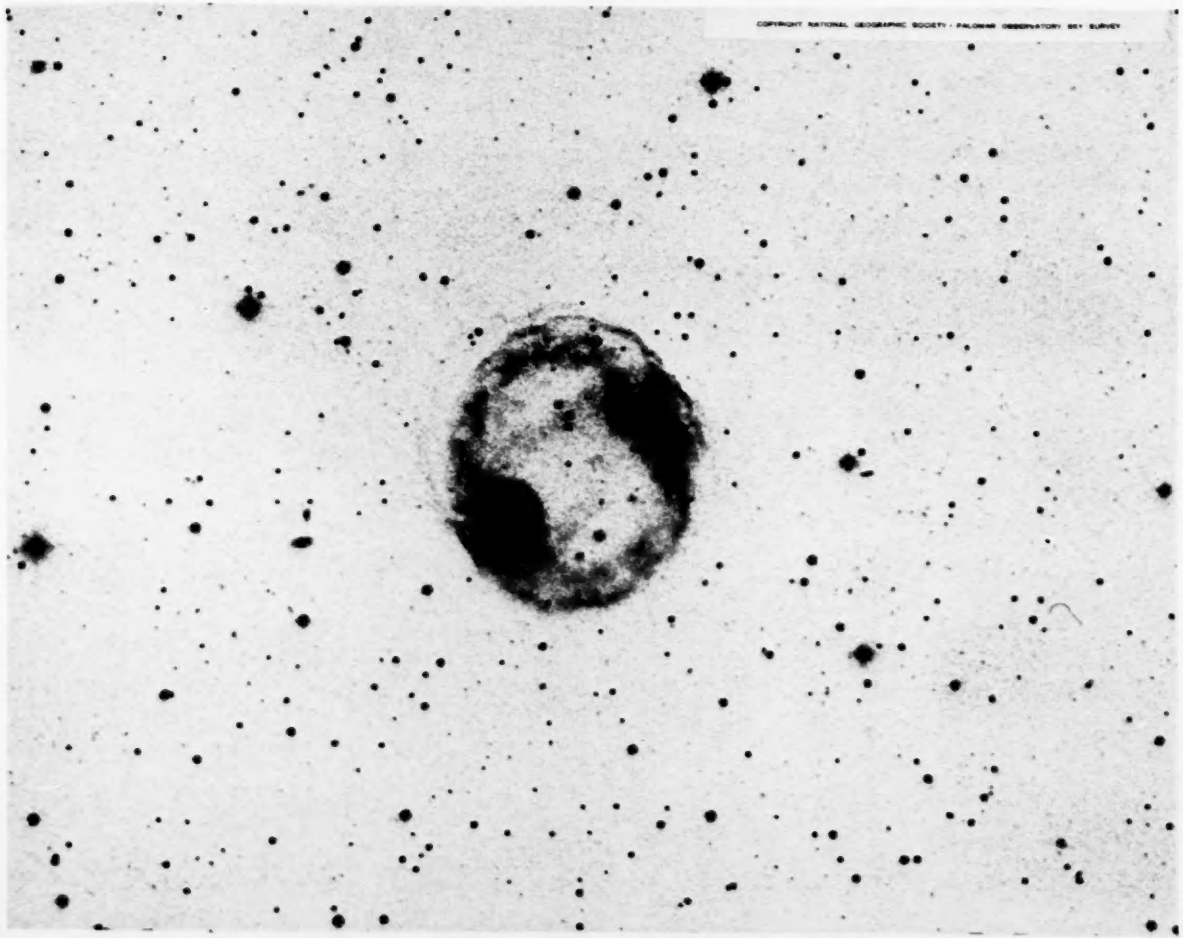

FIG. 5.—The planetary nebula ($\alpha = 7^h50^m0$; $\delta = +53°40'9$). This faint object, discovered by R. B. Jones and R. Emberson (1939), was photographed in $H\alpha$ radiation in the sky survey. The nebula is fainter in the blue and some of the fine detail which is presumably due to [N II] is missing in the blue photographs. Otherwise no differences in the images can be seen; i.e., there are no stratification effects (8.7 per mm).

WOLF-RAYET AND OTHER SPECTRA OF EARLY TYPE IN THE 1μ REGION

FREEMAN D. MILLER
University of Michigan Observatory
Received April 15, 1954

ABSTRACT

Objective-prism and slit spectrograms have been obtained in the wave-length range 9000–11000 A for a variety of spectra of early type. The nitrogen and carbon sequences of Wolf-Rayet stars are sharply differentiated in this wave-length range: the principal emission features are to be attributed to *He* I, *He* II, and C III. λ 10830 of *He* I is found in the spectra of P Cygni, γ Cassiopeiae, and β Lyrae. At the dispersions employed, only the Paschen series in absorption is seen in spectra of α Lyrae and α Aquilae.

INTRODUCTION

The characteristics of N and late M spectra photographed with the combined 4° and 6° objective prisms of the Curtis Schmidt on I-Z(2) plates have been described in an earlier note (Miller 1953*a*). Spectra of stars of early type form the subject of this communication.

Our experience in warm-weather work with the hypersensitized I-Z(2) emulsion may be of interest. The plates of N and M stars were taken at air temperatures below 0° C; those of the present program at temperatures above +15° C. The first of the latter were badly fogged, although a plate kept in a box at the telescope and developed unexposed was fog-free. This hinted at a solution of the difficulty: by exposing through a filter, warm-weather fogging was eliminated. In our plateholders, the addition of a filter incloses the plate in an airtight box with a volume of 140 cc. By preventing circulation of warm air over the emulsion, plate fog is minimized.

On a number of the Schmidt plates, spectra of α Lyrae were superposed. Paschen 6 and 7, together with telluric bands, served to establish a wave-length scale for the program stars. The zero point for each of the latter is necessarily somewhat uncertain, since the telluric features on which it depends are diffuse and sometimes in underexposed spectral regions.

Through the kindness of Dr. Keller, director of the Perkins Observatory, the writer had full use of the 69-inch reflector equipped with the two-prism spectrograph, for a week in August, 1953. The neon comparison spectrum and dispersion of 512 A/mm at Paschen 6, as compared with 1450 A/mm for the Schmidt plates, made this material of the greatest value in interpreting the objective-prism spectra. The observing program included a number of stars of late spectral type which are not referred to in the present discussion.

Table 1 lists the spectrograms available for each star; those of the first seven were generally unwidened. Exposures for the Schmidt plates range from 5 to 90 minutes, and for the slit spectrograms from 15 minutes to 4 hours. The plate taken with the 4° objective prism was useful only in estimating relative intensities of emission lines. The numerous plates for α Lyrae are due to its use as wave-length standard on objective-prism plates and as test star in focusing the slit spectrograph.

Typical objective-prism spectrograms are illustrated in Figure 1. On plates made with the combined objective prisms, the distance between P6 and P7 is 0.65 mm. The striking difference between the WN and WC spectra will be noted. The resolution obtained with the objective prisms may be judged by comparing the microdensitometer tracings of

spectra of α Lyrae shown in Figure 2, *b* and *c* The first is from a Perkins spectrogram, the second from a typical objective-prism plate.

WN SPECTRA

The spectrum of HD 192163 (Fig. 1, *b*) is typical of the four stars of the nitrogen sequence. The two strong emissions are designated A and B for convenient reference. The wave-length difference between these features can be measured with fair precision on the objective-prism plates, the mean value being

$$\delta\lambda_{AB} = 703\text{A} \pm 9 \text{ (m.e.)} .$$

On the 4-hour, weakly exposed slit spectrogram, the wave lengths of both features were measured. The images are diffuse and faint; the uncertainty in the wave lengths may be estimated as of the order of ± 15 A.

In Table 2 are the wave lengths and line widths measured on the slit spectrogram and, in the third line, the wave length of B derived by adding the wave-length difference measured on Schmidt plates to the wave length of A in the first line.

The inaccuracy inherent in the study of these spectra at low dispersion is indicated by comparison of wave lengths in Table 2 with those derived provisionally by the writer

TABLE 1

OBSERVATIONAL MATERIAL

Star	Spectrum	Curtis 4°+6°	Schmidt 4°	Perkins 2-Prism
HD 192163	WN6	3	1	1
HD 193077	WN6	1	1	.....
HD 193576	WN6	1	.....	.....
HD 193928	WN6	.....	1	.....
HD 192641	WC7	1	.....	.....
HD 193793	WC6	1	.....	2
P Cyg	B1ep	3	.....	.....
γ Cas	B0 IVp	1	.....	2
β Lyr	Bep	4	.....	.....
α Lyr	A0V	6	.....	6
α Aql	A7V	.....	.....	2

from objective-prism plates alone (Miller 1953*b*). The two sets of wave lengths differ systematically by 67 A, consistent with the estimated uncertainty of ±40 A for the provisional results, due to near invisibility of telluric bands which provided the zero point.

The line widths in Table 2 may be compared with those for the same star at shorter wave lengths. Beals (1930) finds widths of the order of 30–40 A for lines near λ 4000. If the widths are assumed proportional to wave length, the proportionality constant is close to 0.008, which predicts widths of about 80 A in the 1 μ region. The widths listed in Table 2 are thus consistent with those at shorter wave length. The relative intensities of A and B differ from one star to another as shown in Table 3.

The continuum between A and B on the objective-prism plates has been compared visually with spectra of stars of early type on the same plates. There is no indication that in this wave-length range the WN stars are abnormally bright, and it seems that there are no moderately strong emission lines contributing to this part of the spectrum. The continuum is invisible on the slit spectrogram.

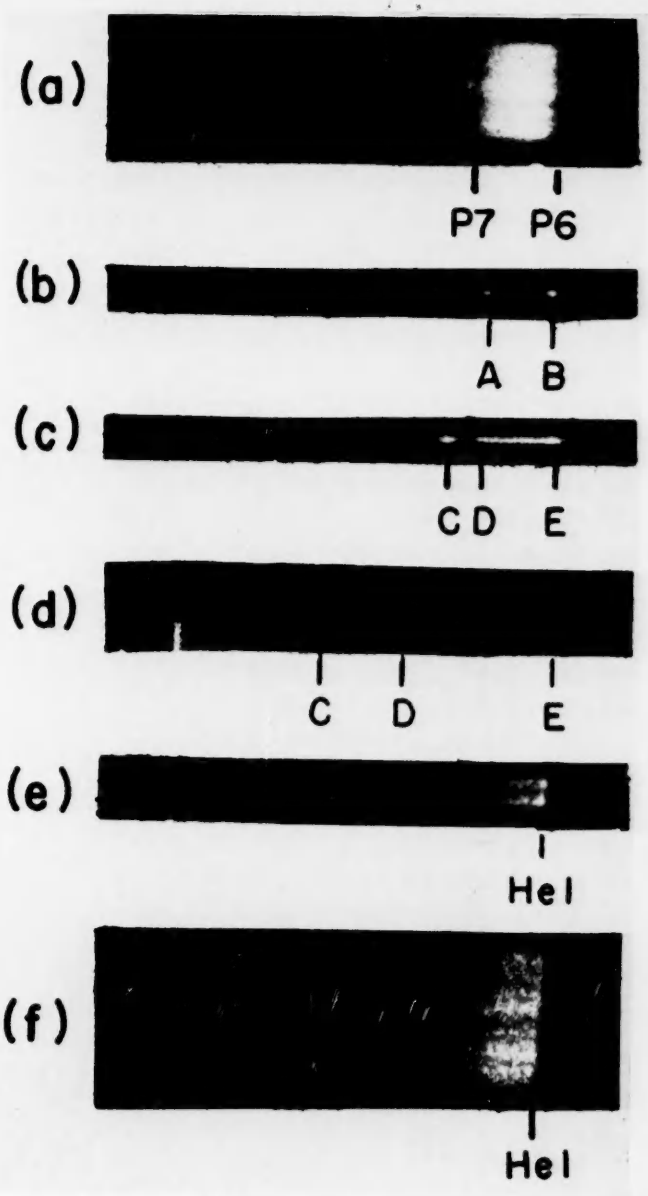

FIG. 1.—*a*, α Lyr; *b*, HD 192163 WN6; *c*, *d*, HD 193793 WC6; *e*, P Cyg; *f*, β Lyr. *d* with Perkins reflector, 2-prism spectrograph; remaining spectra with combined prisms, Curtis Schmidt.

THE WC STAR HD 193793

A single underexposed objective-prism spectrogram of HD 192641 confirms the marked difference in the appearance of WC and WN spectra illustrated in Figure 1, *b* and *c*, but is not suited to measurement.

The features measured are lettered in Figure 1, *c* and *d*, which are reproductions of spectrograms of HD 193793 made with the Schmidt and Perkins reflectors, respectively. *C* is a strong emission line. *D* marks the short-wave-length limit of a region of enhanced

TABLE 2

WAVE LENGTHS IN WN SPECTRA

	A	B
λ(Perkins)	10,126	10,850
$\Delta\lambda$(Perkins)	90	100
λ(Schmidt)		10,829

TABLE 3

RELATIVE INTENSITIES IN WN SPECTRA

HD 192163	B clearly stronger	HD 193576	A slightly stronger
HD 193077	A slightly stronger	HD 193928	B slightly stronger

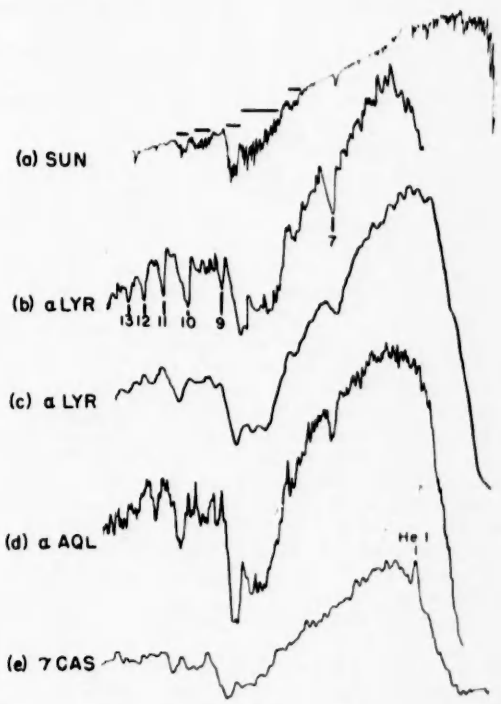

FIG. 2.—*a*, Snow telescope, infrared spectrograph; *b*, Perkins reflector, 2-prism spectrograph, Paschen lines marked; *c*, combined prisms, Curtis Schmidt; *d* and *e*, Perkins reflector, 2-prism spectrograph.

intensity which is terminated by what appears to be another emission feature at *E*. In Figure 1, *d*, a plate defect gives feature *D* the appearance of an isolated emission line.

Wave lengths measured on the slit spectrograms, mean widths, and wave lengths obtained by combining differential measures on the Schmidt plate with the wave length of *C* in the third line are given in Table 4.

The provisional wave lengths (Miller 1953*b*) differ systematically by 25 A from those in the third line of Table 4. The estimated zero-point uncertainty in the provisional wave-length system is as mentioned above, ±40 A.

Beals (1930) has measured line widths in the spectrum of this star. Considering width proportional to wave length, his factors for *C* III and *He* II lead to widths of 166 and

TABLE 4

WAVE LENGTHS IN SPECTRUM OF WC STAR HD 193793

	C	*D*	*E*		*C*	*D*	*E*
λ (Perkins No. 8640)	9726	10,066	.....	Δλ (mean)	127	.....	.....
λ (Perkins No. 8659)	9724	10,041	.....	λ (Schmidt)	.....	10,038	10,875
λ (mean)	9725	10,054	.....				

93 A, respectively, at 9725 A. The 127 A width of feature *C* is thus consistent with measures at shorter wave lengths.

On both Schmidt and slit spectrograms, there is a marked discontinuity at point *D*, which is not characteristic of emulsion sensitivity. It appears that longward of λ 10040 there must be a series of emissions which are unresolved on the present plates.

WN AND WC SPECTRA—IDENTIFICATIONS

The wave-length and intensity data described in preceding paragraphs is necessarily of low weight compared with that which can easily be obtained for shorter wave lengths. Nevertheless, the striking dissimilarity of the spectra of stars of the nitrogen and carbon sequences suggests that it should be possible to interpret the conspicuous features in terms of the carbon-nitrogen differentiation. The identifications listed below were proposed by Dr. Leo Goldberg as probable explanations of the emission bands summarized in Tables 2 and 4.

The emission lines designated A and B in the spectra of the WN stars may be attributed to λ 10124 *He* II and λ 10830 *He* I, respectively; the wave-length agreement is excellent. Beals (1930) classifies these stars according to the intensity ratio 5875 *He* I/5411 *He* II and assigns the first two and the fourth stars in Table 3 above to OW6, intensity ratio 0.3. HD 193576 is classed as OW5, intensity ratio 0.1. The corresponding ratio in our spectra is *B*/*A*; it is, in fact, smaller for HD 193576 than for HD 192163 and HD 193928. The ratio for HD 193077 is also smaller, contrary to Beal's classification. In our spectra, the *B*/*A* ratio certainly does not appear to vary by a factor of 3, and the correlation between *B*/*A* and Beal's classifications is extremely weak.

The principal contribution to feature *C* in the WC spectra should be from the *C* III multiplet $2s3p^3P^0$–$2sd^3D$, with six lines between λ 9702 and λ 9720. On the slit spectrogram this band extends from λ 9662 to λ 9789. Other high-excitation lines of *C* III may also be present, for example, the multiplet $2p3p^3D-2p3d^3F^0$ with six lines between λ 9697 and λ 9758.

The short- and long-wave-length limits of the continuous strip of emission between points *D* and *E* are undoubtedly set by λ 10124 *He* II and λ 10830 *He* I. Leading contributors to the intervening emission should be the two strong transitions, *C* III λ 10291, $2p3s^1P^0-2p3s^1P$, and *C* II λ 10506, $2s^24f^2F^0-2s^25d^2D$.

OCCURRENCE OF λ 10830 OF *He* I

P Cygni, γ Cassiopeiae, and β Lyrae were observed with the Schmidt, in anticipation of the occurrence of emission features in their spectra. The plate of γ Cassiopeiae was taken under unfavorable conditions at low altitude, and no emission lines appeared in its spectrum. It was, nevertheless, included in the program at the Perkins Observatory. A sharp emission line appears on the two slit spectrograms, taken on JD 2434612 and 2434616, respectively. The mean wave length of the line on these plates is λ 10831, and it is certainly to be identified with *He* λ 10830. A tracing of a slit spectrogram of the star is reproduced as Figure 2, *e*.

An objective-prism spectrogram of P Cygni is reproduced as Figure 1, *e*. The strong emission line has a measured wave length, referred to the telluric bands, of 10843 A. Within the zero-point uncertainty, this agrees with *He* I λ 10830. The line is conspicuous on all plates, two of which were taken on JD 2434555 and the third 28 days later.

Spectra were obtained of β Lyrae with the Schmidt on dates corresponding to values of cycle and phase 2790.630, 2790.786, 2790.941, and 2791.320 (Rossiter 1934). Figure 1, *f*, shows the appearance of the spectrum on the first date. On each plate an emission line of moderate strength is seen, whose wave length referred to the telluric A band is 10847 A. As in the case of P Cygni, this agrees, within the observational uncertainty, with the wave length of λ 10830 of *He* I. The plates at phases 0.320 and 0.630 are of comparable density and quality; the intensity of the emission line appears to be about the same as these two phases. The intensity of λ 10830 on our plates is in agreement with its appearance on the microphotometer tracing lately published by Barocas and Righini (1954). On two slit spectrograms made with the 122-cm reflector of the Asiago Observatory at a dispersion of 570 A/mm, they find that, 2.1 and 4.1 days after primary minimum, the density of the photographic image of λ 10830 exceeds that at any other point in the infrared spectrum of the star. The phase of their second plate coincides closely with the fourth in our series, but was taken about a month earlier.

ABSORPTION SPECTRA, CLASS A

Unwidened spectra of α Lyrae and α Aquilae in the wave-length range covered by the present material were obtained some years ago by Morgan and Wooten (1934) at a dispersion similar to that of our objective-prism plates. Their program was an investigation of the energy distribution in the continuous spectrum. More recently, Kuiper, Wilson, and Cashman (1947) have published a tracing of α Canis Majoris (made with a lead sulfide cell as receiver and the McDonald reflector) which shows the conspicuous absorption lines of Paschen 6 and 7 in the 1μ region, as well as Paschen 5 at longer wave length.

Figure 1, *a*, is a typical 5-minute exposure of α Lyrae with the combined objective prisms: the Paschen series and a number of telluric features are well visible. Paschen 6 is easily seen on the original plates but is difficult to reproduce; it falls at a point where the combined atmospheric transmission and plate sensitivity is decreasing rapidly, as may be seen from the position of λ 10830 of *He* I in the tracing of γ Cassiopeiae (Fig. 2, *e*).

A number of slit spectrograms of α Lyrae and α Aquilae were obtained in the course of the work at Perkins Observatory. Tracings are reproduced in Figure 2, *b* and *d*. Telluric bands are conspicuous in the spectra to longward of 9000 A. To assist in sorting out these features, Dr. Mohler, of the McMath-Hulbert Solar Observatory, arranged for the recording of a number of relatively low-dispersion tracings of the solar spectrum with the Mount Wilson Snow telescope and infrared spectrometer. For this purpose, the grating was rotated rapidly by hand. The resulting dispersion is somewhat variable with wave length, but the tracings are entirely adequate for comparison with the stellar spectrograms. One such tracing is included as Figure 2, *a*, reduced in scale to agree roughly with the prismatic dispersion from 0.9 to 1.0 μ. Telluric bands which also appear in the stellar spectrograms are marked by horizontal lines.

With the telluric bands eliminated, only the Paschen series remains in the spectra of the two stars of class A. Paschen 6, as stated above, is located on the steep slope of the observed intensity-curve and appears as an inflection (e.g., Fig. 2 *c*, *d*) in the tracings. Paschen 8 is lost in the complex structure of the telluric bands; Paschen 10 overlies, and in these stars, dominates, the telluric band, which falls at the same wave length.

The writer is indebted to the director and staff of the Perkins Observatory for their interest and co-operation in the observing program at that institution; to Dr. Mohler and Mr. Mitchell, the observer, for the solar tracings; to Dr. Leo Goldberg for discussion of identifications; and to Dr. D. B. McLaughlin for a variety of helpful comments and suggestions.

REFERENCES

Barocas, V., and Righini, G. 1954, *Observatory*, **74**, 73.
Beals, C. S. 1930, *Pub. Dom. Ap. Obs. Victoria*, **4**, 271.
Kuiper, G. P.; Wilson, W.; and Cashman, R. J. 1947, *Ap. J.*, **106**, 243.
Miller, F. D. 1953*a*, *Ap. J.*, **118**, 572.
———. 1953*b*, *A.J.*, **58**, 222.
Morgan, W. W., and Wooten, B. A. 1934, *Ap. J.*, **80**, 229.
Rossiter, R. A. 1934, *Pub. Obs. U. Michigan*, **5**, 67.

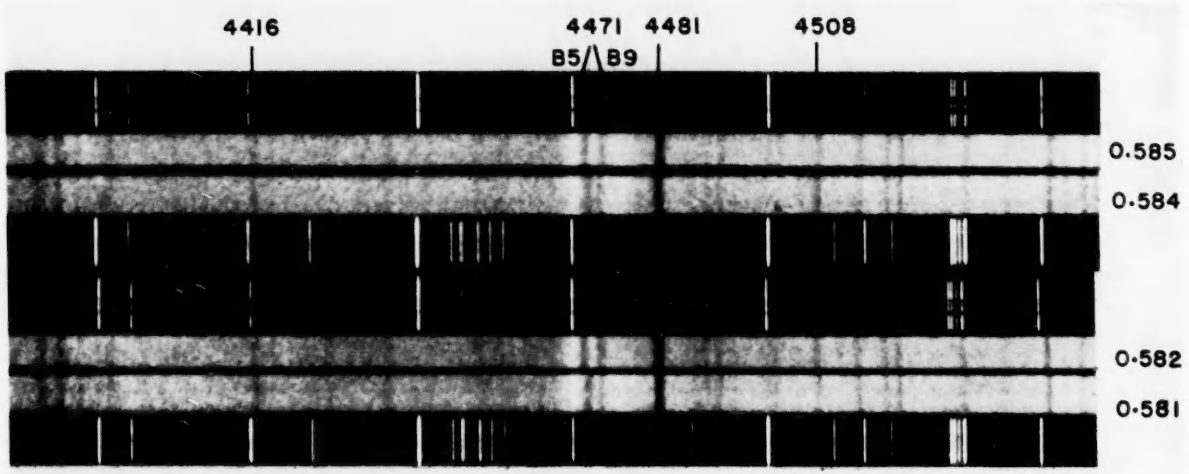

Fig. 1

FIG. 1.—Spectrum of β Lyrae at phases 0.585 and 0.582 on November 2, 1952, and at phases 0.584 and 0.581 on October 20, 1952. The B5 absorption line *He* I 4471 shows different velocity shifts on these two days, despite the fact that the phases are very nearly the same.

THE SPECTRUM OF BETA LYRAE

ERIKA BÖHM-VITENSE
Berkeley Astronomical Department and University of Kiel, Germany
Received March 15, 1954

ABSTRACT

The B5 absorption component of β Lyrae shows rapid changes in radial velocity between successive cycles and also during a single cycle when the exposures are separated by 1 or 2 hours. The absorption line *Fe* II 4351 yields an average rotational velocity of the order of 40–50 km/sec. This line appears to be slightly broader during the elongations than near secondary eclipse. If this difference in rotational broadening is attributed to the ellipticity of the B8 component, the resulting ratio of the axes should be somewhat less than the photometric value of 1.33. From the weakening of the equivalent width of the same line at elongation, as compared to the equivalent width measured at secondary minimum, a value of approximately 20 per cent is obtained for the fraction of the light at maximum which is caused by the secondary component and the gaseous stream.

The main features of the spectrum of β Lyrae were explained by O. Struve (1941). The system consists of a B9 star, which is supposed to be a supergiant, and a small, invisible star of a later spectral type, perhaps F. These two stars are surrounded by a gaseous shell, which is probably built up of material streaming from the larger, primary, to the smaller, secondary, star and of which only a small part returns to the primary star.

The present investigation is based on 50 plates, taken by D. McNamara and myself with the Mills spectrograph of the Lick Observatory, and on some coudé plates taken by O. Struve at Mount Wilson. Several pairs of plates were obtained at nearly the same phases but in different cycles. In Figure 1 we compare four spectrograms at phases near 0.58 *P*. The line *He* I 4471 is double, one component being that of the B9 star, the other that of the B5 shell; but the separations are very different on these two plates. The B5 line is displaced by about 1A, which corresponds to a difference in radial velocity of about 60 km/sec.

Figure 2 represents the profiles of the lines λ 4471 and $H\gamma$ on an intensity scale. These two lines show the same effects. The difference between the radial-velocity shifts of the B5 lines on October 20 and November 2 will be noticed, and, furthermore, there is a slight difference in Doppler shift as the phase changes from 0.582 to 0.585 on November 2. Since this difference is present in both lines, it is probably real. It is concluded that changes of radial velocity may occur in the B5 shell within even a single hour. These rapid changes may be responsible for the large scatter in the radial-velocity measurements of the shell lines. It is also probable that they are related to the large scatter in the light-curve of β Lyrae.

With regard to the question of the ellipticity of the primary star and the luminosity of the secondary, I examined principally the line *Fe* II 4351, because this is one of the few lines on our plates which can be followed through the whole cycle. Figure 3 shows a plot of the line profiles measured on the photometer tracings of 33 plates. The well-known broadening of the line around primary minimum cannot be an effect of the geometry of the system, since it is not present during secondary minimum. This broadening must be due to highly turbulent matter which is probably connected with the ingoing and outgoing streams. At the same time the lines are deepened; evidently more absorbing atoms are present along the line of sight than during other phases. As this broadening is not visible at phase 0.112, this turbulent material must be at a fairly large distance from the star, because at this phase it is not projected upon the surface of the primary

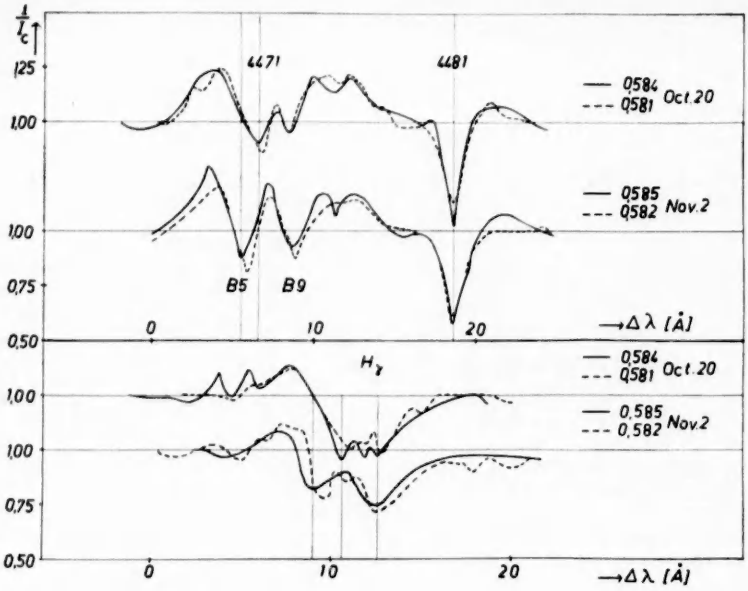

FIG. 2.—The observed profiles of the lines *He* I 4471, *Mg* II 4481, and *Hγ* on October 20 and November 2, 1952.

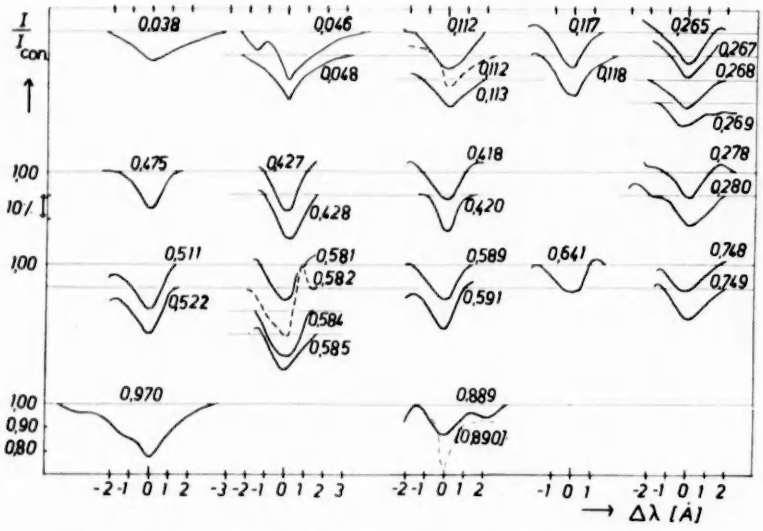

FIG. 3.—Observed profiles of the absorption line *Fe* II 4351 at different phases

star. The distance from the center of the star must be greater than 1.5 times the radius of the star.

Since the very broad *Fe* II lines near primary minimum do not originate in the star itself, they cannot be used for determining the ellipticity of the star. Because of ellipticity, the lines should be more broadened by rotation during the elongations than during the minima. Actually, during the elongations the lines may be slightly broader than near the secondary eclipse, perhaps by a factor of 1.2. If this difference is attributed to ellipticity, the ratio of the axes should be less than the photometric value of 1.33.

During secondary minimum the β Lyrae system is 0.38 mag. fainter than during elongation; hence, taking into account the ellipticity, the secondary star, together with the extra gas concentrated around it, must contribute at least 15 per cent to the maximum light if uniform surface brightness of the primary star is assumed. To explain the decrease of line depth near elongation as the effect of the light of the secondary star and the concentrated gas around it, it would be necessary for these sources to contribute 26 per cent to the total maximum light. A value of 19 per cent is derived from the change of the equivalent width of the line.

If it is assumed that the original line, without rotational broadening, has an infinitesimally small width, an upper limit for the rotational velocity of 90 km/sec is derived. If, as seems likely, the periods of revolution and rotation are equal, this rotational velocity corresponds to a radius of 25 $\odot$. Allowing for the width of the original line, the true equatorial velocity of rotation would be approximately 40 or 50 km/sec, as given by Struve. This would make the B star even smaller and would raise the question of whether it is really a normal supergiant.

I am grateful to Dr. O. Struve for having suggested this problem and for many interesting discussions. I also wish to thank Dr. C. D. Shane for making it possible for me to work at the Lick Observatory and Dr. G. H. Herbig for advice in the observational work. Finally, I am grateful to the American Association of University Women for an international grant and to the United States Department of State for financial assistance in my traveling expenses.

REFERENCES

Struve, O. 1941, *Ap. J.*, **93**, 104.
———. 1934, *Observatory*, **57**, 268.
———. 1952, *Pub. A.S.P.*, **64**, 180.

ROTATION OF THE PRIMARY OF BETA LYRAE

RICHARD I. MITCHELL
Berkeley Astronomical Department, University of California
Received March 15, 1954

ABSTRACT

A study of the profile of *Mg* II 4481 of β Lyrae does not show the effect of ellipticity. A rotational velocity of 40 km/sec is found.

Photoelectric observations of β Lyrae, analyzed by Z. Kopal (1941) and others, indicate that the primary is a prolate ellipsoid with a ratio of minor axis to major axis of about $\frac{3}{4}$. In the preceding article Dr. Erika Böhm-Vitense has discussed the profiles of the line *Fe* II 4351. This paper will consider the rotational profile of the line *Mg* II 4481 which was previously used by G. Wares (quoted by Struve 1934). This line has the advantage of being stronger in absorption than *Fe* II 4351. It is, however, complicated at certain phases by the emission component of *He* I 4472 (Struve 1941). There is also a very weak absorption component of *Mg* II 4481, which belongs to the so-called B5 spectrum. Nevertheless, a study of the line profile of *Mg* II 4481 as a function of phase is of considerable interest.

Figure 1 shows the theoretical profile of *Mg* II 4481 calculated by the standard graphical method (Struve 1930). The star was assumed spherical with uniform surface brightness. The nonrotational profile of *Mg* II 4481 was assumed to be the same as in β Orionis (Hiltner and Williams 1946).

Figure 2 shows what might be expected in the case of β Lyrae, again if there were no limb darkening and if the equatorial rotational velocity at secondary eclipse were 50 km/sec, as was recently suggested by Struve (1952).

TABLE 1

Phase	Mean Half-Half-Width (A)	Standard Deviation (A)	Phase	Mean Half-Half-Width (A)	Standard Deviation (A)
0.266	0.67	±0.02	0.590	0.71	±0.06
.419	.62	.01	.748	.56	.01
0.511	0.62	0.06	0.826	0.76	0.11

The observed profiles were obtained from the Mills three-prism spectrograms taken at the Lick Observatory by D. H. McNamara. These plates have a dispersion of 10 A/mm. Six different stages are represented by eleven plates. The instrumental profile for all plates gave a Gaussian curve with a dispersion of 0.09 A, which could be safely neglected.

The mean profiles in Figure 3 are in fairly good agreement. There is an apparent increase in equivalent width at phase 0.511, but this effect is probably caused by the secondary eclipse. Because it is difficult in this system to determine how much of the light is

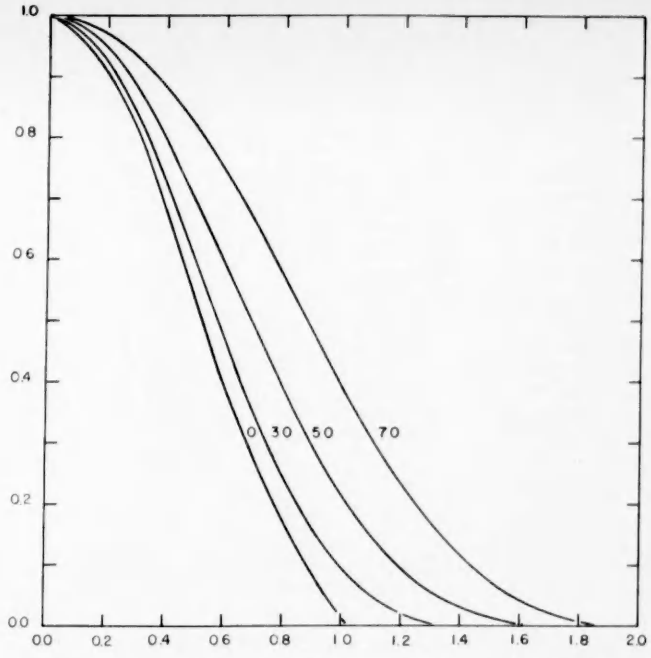

FIG. 1.—Computed profiles of *Mg* II 4481 for rotational velocities of 0, 30, 50, and 70 km/sec. Relative intensity is measured vertically, and wave length in angstroms is measured horizontally.

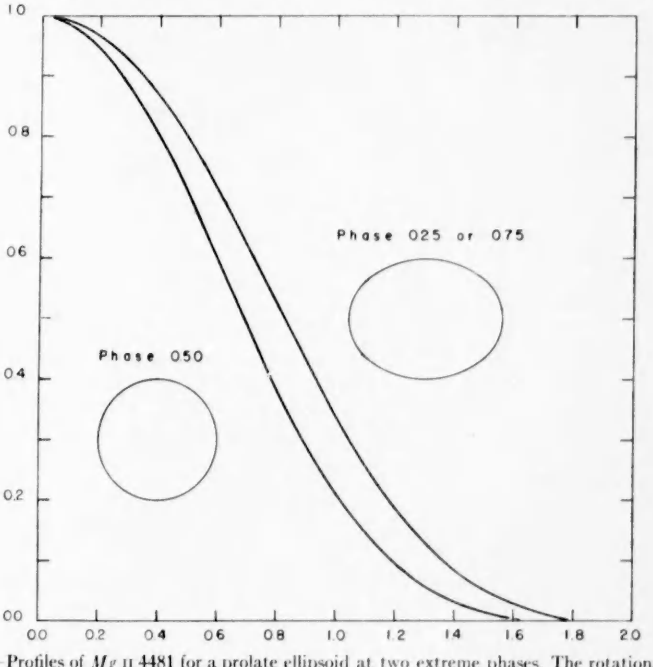

FIG. 2.—Profiles of *Mg* II 4481 for a prolate ellipsoid at two extreme phases. The rotational velocity at phase 0.50 is 50 km/sec. Relative intensity is measured vertically, and wave length in angstroms is measured horizontally.

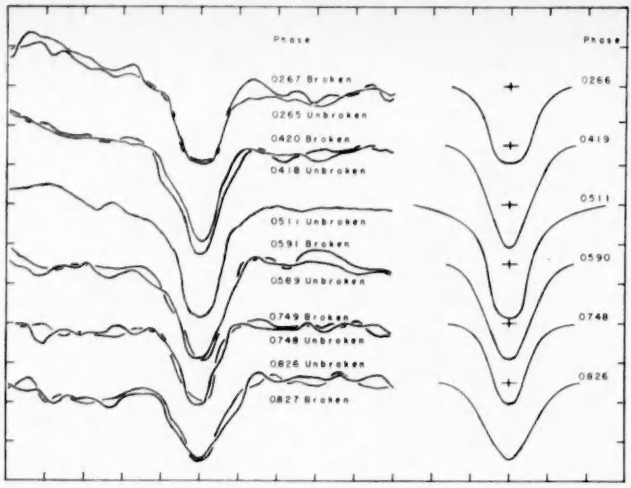

FIG. 3.—The observed profiles of *Mg* II 4481 on the left, and mean profiles on the right. Intensity is plotted vertically, with zero intensity seven units below the continuum of each line. Each horizontal unit corresponds to 1.045 A. Note the emission of *He* I 4472 on the left at phase 0.266.

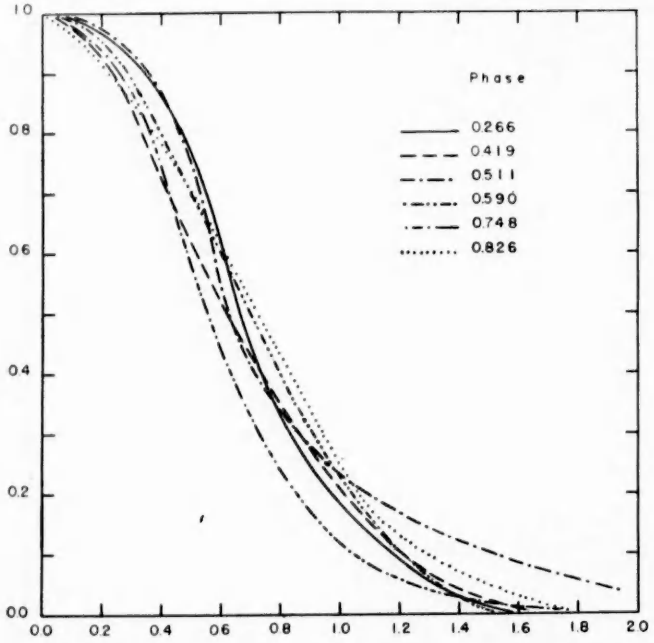

FIG. 4.—The mean observed profiles of *Mg* II 4481. Relative intensity is measured vertically, and wave length in angstroms is measured horizontally.

due to the primary and how much is due to the extensive gas stream and the secondary, the line profiles were adjusted in Figure 4 to have a central intensity of 1.0. There is no systematic trend with phase. The mean half-width for all profiles at half the central intensity is 0.62 ± 0.07 A. Table 1 gives half-half-widths for each phase.

From Figure 1 the mean velocity of rotation is 40 km/sec. From Figure 2, computed with a velocity of 50 km/sec, the maximum expected variation in wave length is 0.15 A, about twice the observed variation. Hence the observations do not show the expected effect of ellipticity. This seems to be at variance with Dr. Böhm-Vitense's conclusion that a small elliptical effect may be present in *Fe* II 4351. It is possible that the two lines are produced by different mechanisms or are formed in different gaseous layers. It is also possible that emission and absorption in the gas stream distort the profile of the primary. Another possibility is that the limb darkening is such that the star appears much smaller, thus preventing accurate spectroscopic observation of ellipticity. This latter hypothesis does not conflict with previous interpretations of β Lyrae as a very massive supergiant.

I wish to thank Dr. Otto Struve for suggesting this problem.

REFERENCES

Hiltner, W., and Williams, R. 1946, *Photometric Atlas of Stellar Spectra* (Ann Arbor: University of Michigan Press), Book IV.
Kopal, Z. 1941, *Ap. J.*, **93**, 92–103.
Struve, O. 1930, *Ap. J.*, **72**, 1–18.
———. 1934, *Observatory*, **57**, 265–274.
———. 1941, *Ap. J.*, **93**, 104–117.
———. 1952, *Pub. A.S.P.*, **64**, 180–183.

PHOTOELECTRIC AND SPECTROSCOPIC OBSERVATIONS OF UX URSAE MAJORIS*

MERLE F. WALKER†
MOUNT WILSON AND PALOMAR OBSERVATORIES
CARNEGIE INSTITUTION OF WASHINGTON
CALIFORNIA INSTITUTE OF TECHNOLOGY
AND
GEORGE H. HERBIG
Lick Observatory, University of California
Received March 15, 1954

ABSTRACT

Some eighteen hundred photoelectric observations of the eclipsing variable UX UMa were made (by Walker) in three colors with the 60- and 100-inch reflectors at Mount Wilson and are described in Section I. They show the asymmetry and stillstand on the rising branch of principal minimum that were discovered by Linnell. Eclipse is preceded by an increase in light of 0.10 mag. and is (at the present time) followed by a rise of about half that amount. The rapid, irregular fluctuations in the light of the system, also discovered by Linnell, were confirmed; their durations range from 1 to 20 minutes, while their amplitudes in the ultraviolet may be as large as 0.18 mag. They are less conspicuous at longer wave lengths. The depth of primary minimum is not always the same; furthermore, its depth increases, the shorter the wave length of observation. No secondary minimum has been observed. In Section II are described spectroscopic observations made (by Herbig) with a continuous-recording technique and a low-dispersion (430 A/mm at $H\gamma$) spectrograph at the 36-inch Crossley reflector of the Lick Observatory. The spectrum of the primary star is of type O, with very wide and shallow absorption lines. Narrow absorption is observed at the *H* lines in the ultraviolet (particularly *H*8–*H*11) during the later parts of some cycles. The radial velocity given by these narrow *H* lines is approximately constant, with a value of about +350 to +400 km/sec. Weak emission at $H\beta$ and rather strong emission at *He* II λ 4685, neither of which is of constant intensity, vary in velocity throughout the cycle. The increases in brightness of UX UMa before and after primary minimum are due to an intensification of the continuous spectrum and are not accompanied by an enhancement of the emission lines. The variation of the spectrum of UX UMa through the eclipse cycle, like the details of the light-curve, is not always the same. A tentative model that seems to explain some of the features of this remarkable system is discussed in Section III.

I. INTRODUCTION AND PHOTOMETRIC OBSERVATIONS

The very short period (4^h43^m) of the eclipsing variable UX Ursae Majoris, together with its Algol-type light-curve, indicate that the two components must be unusually small and dense. The observations of Struve (1948) have shown, moreover, that the spectroscopic behavior of the system is peculiar. It was felt, accordingly, in view of the presently unique nature of the object, that the collection of more observational information was highly desirable.

The earlier work on UX UMa has been reviewed by Linnell (1950), and the most recent discussions of the system have been by him and by Parenago (1950). Linnell obtained the first photoelectric observations of the star in 1949. More recently, a very extensive series of photoelectric observations in three colors was made by Johnson, Perkins, and Hiltner (1954) during the years 1951–1953. The observations of UX UMa described in the present paper were made without knowledge of the work of Johnson *et al.*, and the discussion and conclusions are based for the most part on our own results. We were much interested, however, in reading (through the kindness of Dr. Hiltner) the Johnson, Perkins, and Hiltner paper in advance of publication, and we have attempt-

* *Contributions from the Lick Observatory*, Ser. II, No. 54.

† Carnegie Fellow, 1952–1954.

ed to arrive at conclusions that are in harmony with both the McDonald observational results and our own material.

Photoelectric observations of UX UMa were obtained on seven nights in 1953 with a photometer attached to either the 60- or the 100-inch reflector of the Mount Wilson Observatory. The specific purposes of the investigation were threefold: (1) to study the peculiar features of the light-curve discovered by Linnell (1949, 1950); (2) to increase our knowledge of the star by obtaining light-curves in yellow, blue, and ultraviolet light; and (3) to attempt to correlate the features of the light-variation with changes in the spectrum or velocity of the star, by use of measurements of the light secured simultaneously with spectroscopic observations made at the Lick Observatory.

The photometer was used with an Emitron 5659 end-on multiplier tube, which was operated without refrigeration. The three filters were: yellow, 1.7 mm of Schott GG 11; blue, 1 mm of Schott BG 12 plus 2 mm of Schott GG 13; ultraviolet, 2.6 mm of Corning 9863. The output of the multiplier tube was amplified and displayed on a Brown recording potentiometer geared to a chart speed of 12 inches per hour.

The photometer mounting is provided with an eyepiece for offset guiding during the observations. The procedure adopted was to monitor the variable almost continuously, with only occasional breaks to observe the sky or the extinction stars. The emphasis was placed upon obtaining very complete and detailed light-curves in a given color. Usually only one color was observed on any one night. However, on two nights yellow and ultraviolet observations were obtained for the purpose of investigating the variation in the color of the star throughout the 5-hour period.

In reducing the observations, the brightness of the star was in most cases read, for convenience, on the minute and half-minute. The accuracy of reading the time from the recorder sheet was about ± 3 seconds. The observations were corrected for extinction, with coefficients derived each night from a red and a blue comparison star, but the data have been left on the instrumental system. The primary comparison star was BD+52°1722, which also served as the blue extinction star. A near-by red star was used as the second comparison star.

The (approximately eighteen hundred) individual measurements of the magnitude of UX UMa through the yellow, blue, and ultraviolet filters are given in Tables 1, 2, and 3, respectively. The tables list the magnitude difference, UX UMa *minus* BD+52°1722, together with the heliocentric Julian date of the observation and the phase computed from the elements of Johnson, Perkins, and Hiltner (1954):

$$\text{Minimum} = \text{JD } 2427341.2221 + 0^{d}196671379E\,.$$

The individual light-curves, plotted against the phase expressed in units of the period, are shown in Figures 1–7. The observations on April 23 were obtained with the 100-inch telescope and the others with the 60-inch reflector.

The observations confirm the existence of the asymmetry of the rising branch of the light-curve between 0.03 and $0.10P$ and of the stillstand between 0.05 and $0.07P$ discovered by Linnell. They differ from Linnell's observations in showing that at the present time the primary eclipse is preceded by an increase in light of 0.10 mag., in all colors, which occurs between phases 0.73 and $0.92P$. Primary minimum begins at phase $0.92P$. This amplitude and duration are approximately twice the height and length of the rise that follows the eclipse; this following "shoulder" occurs between 0.11 and $0.18P$. The total interval between the beginning of the shoulder before eclipse and the end of the shoulder following the minimum is $0.45P$, which agrees with the interval of $0.48P$ found by Linnell. A comparison of the present observations with those of Linnell and of Johnson *et al.* suggests that the interval of anomalous brightness has shifted relative to the phase of minimum light since Linnell's observations in 1949.

TABLE 1

YELLOW OBSERVATIONS

Heliocentric JD 2434+	Heliocentric Phase	Δ Mag	Heliocentric JD 2434+	Heliocentric Phase	Δ Mag	Heliocentric JD 2434+	Heliocentric Phase	Δ Mag
485.76020	0.2894	+2.777	490.74546	0.6376	+2.760	490.90865	0.4673	+2.740
.76992	.3388	2.782	.74615	.6411	2.781	.91907	.5203	2.747
.77895	.3847	2.752	.74789	.6499	2.748	.91976	.5238	2.761
.78902	.4359	2.803	.74962	.6587	2.729	.92080	.5291	2.790
.79180	.4501	2.786	.75032	.6623	2.730	.92115	.5309	2.780
.79735	.4783	2.824	.75240	.6729	2.763	.92150	.5327	2.748
.80187	.5013	2.834	.75379	.6799	2.738	.92184	.5344	2.739
.80812	.5330	2.799	.75517	.6869	2.748	.92254	.5379	2.738
.81263	.5560	2.784	.75587	.6905	2.730	.92323	.5414	2.738
.87548	.8755	2.644	.75900	.7064	2.723	.93400	.5962	2.744
.87895	.8932	2.736	.76490	.7364	2.730	.93608	.6068	2.760
.87930	.8950	2.674	.76664	.7453	2.718	.93851	.6191	2.782
.88207	.9091	2.692	.76907	.7576	2.757	.94997	.6774	2.769
.88520	.9250	2.722	.76976	.7611	2.746	.95206	.6880	2.762
.88575	.9278	2.733	.77046	.7647	2.718	.95414	.6986	2.729
.88728	.9355	2.752	.77184	.7717	2.746	.95553	.7057	2.739
.88777	.9380	2.741	.78157	.8212	2.642	.95622	.7092	2.739
.89562	.9780	3.489	.78296	.8282	2.680	.95691	.7127	2.737
.89596	.9797	3.514	.79407	.8847	2.652	.95796	.7180	2.699
.89735	.9867	3.704	.79684	.8988	2.654	.95823	.7194	2.690
.89770	.9885	3.703	.79823	.9059	2.653	.95934	.7251	2.710
.89874	.9938	3.763	.80687	.9483	2.765	.95969	.7268	2.737
.89909	.9956	3.761	.80935	.9624	2.939	.96073	.7321	2.725
.90048	.0027	3.751	.80969	.9641	2.966	.96108	.7339	2.730
.90082	.0044	3.748	.81108	.9712	3.180	.96351	.7463	2.689
.90194	.0101	3.677	.81143	.9730	3.233	.96490	.7533	2.701
.90221	.0115	3.647	.81247	.9783	3.371	.96525	.7551	2.704
.90256	.0132	3.608	.81282	.9801	3.428	.96636	.7608	2.696
.90395	.0203	3.444	.81316	.9818	3.493	.96664	.7622	2.686
.90430	.0221	3.386	.81420	.9871	3.606	.96691	.7636	2.681
.90457	.0235	3.328	.81455	.9889	3.633	.96941	.7763	2.683
.90569	.0292	3.205	.81490	.9906	3.673	.97983	.8292	2.662
.90603	.0309	3.157	.81594	.9959	3.723	.98087	.8345	2.663
.90624	.0320	3.126	.81629	.9977	3.728	.98886	.8752	2.647
.90742	.0380	3.015	.81642	.9984	3.723	.99060	.8840	2.648
.90812	.0415	3.005	.81768	.0048	3.717	.99164	.8893	2.639
.90916	.0468	2.952	.81802	.0065	3.711	518.67894	.6688	2.776
.90950	.0485	2.932	.81816	.0072	3.705	.67963	.6723	2.813
.90985	.0503	2.924	.81906	.0118	3.653	.68033	.6759	2.834
.91089	.0556	2.887	.81941	.0136	3.593	.68137	.6812	2.848
.91124	.0574	2.884	.81976	.0154	3.553	.68172	.6829	2.837
.91332	.0679	2.845	.82115	.0224	3.371	.68241	.6864	2.796
.91506	.0768	2.840	.82150	.0242	3.322	.68380	.6935	2.799
.91575	.0803	2.827	.82185	.0260	3.251	.68449	.6970	2.799
.91714	.0874	2.802	.82289	.0313	3.102	.68866	.7182	2.862
.91784	.0909	2.791	.82324	.0330	3.082	.68935	.7217	2.847
.92151	.1086	2.720	.82428	.0383	3.022	.69074	.7288	2.836
.92270	.1156	2.769	.82462	.0401	2.993	.69144	.7324	2.803
.92339	.1192	2.743	.82497	.0418	2.973	.69318	.7412	2.789
.92548	.1298	2.719	.82601	.0471	2.892	.69457	.7483	2.772
.92687	.1368	2.727	.82636	.0489	2.881	.69873	.7694	2.756
.92756	.1404	2.756	.82671	.0507	2.872	.70047	.7783	2.744
.92895	.1474	2.746	.82775	.0560	2.858	.70602	.8065	2.749
.92964	.1509	2.786	.82809	.0577	2.852	.70741	.8136	2.727
.93659	.1863	2.762	.82948	.0648	2.821	.70810	.8171	2.720
.93728	.1898	2.760	.82983	.0666	2.811	.70949	.8241	2.720
.93937	.2004	2.751	.83156	.0754	2.816	.71435	.8489	2.733
.94078	.2533	2.765	.83365	.0860	2.799	.71574	.8559	2.732
.95157	.2640	2.773	.83643	.1001	2.752	.71644	.8595	2.698
.95256	.2675	2.756	.83782	.1072	2.732	.71713	.8630	2.711
.95464	.2780	2.733	.83990	.1177	2.722	.71852	.8701	2.687
.95534	.2816	2.752	.84129	.1248	2.756	.72304	.8930	2.700
.96506	.3310	2.786	.84963	.1672	2.730	.72373	.8965	2.700
.96749	.3434	2.745	.85136	.1760	2.747	.72442	.9001	2.736
.97721	.3928	2.779	.86038	.2219	2.770	.72477	.9018	2.710
.97895	.4017	2.778	.86212	.2307	2.767	.72512	.9036	2.693
.98138	.4140	2.753	.86420	.2413	2.771	.72547	.9054	2.693
490.70865	.4504	2.745	.87324	.2873	2.739	.72804	.9230	2.725
.71283	.4716	2.752	.87601	.3014	2.775	.72963	.9265	2.740
.71629	.4892	2.745	.87879	.3155	2.734	.73033	.9301	2.742
.72949	.5564	2.741	.88921	.3685	2.737	.73241	.9407	2.780
.73434	.5810	2.730	.89198	.3826	2.744	.73380	.9477	2.839
.73643	.5917	2.731	.89407	.3932	2.753	.73449	.9513	2.870
.74338	.6270	2.730	.90379	.4426	2.724	.73518	.9548	2.900
.74476	.6340	2.739	.90657	.4567	2.735	.73588	.9583	2.950

TABLE 1

YELLOW OBSERVATIONS

Heliocentric JD 2434+	Heliocentric Phase	Δ Mag	Heliocentric JD 2434+	Heliocentric Phase	Δ Mag	Heliocentric JD 2434+	Heliocentric Phase	Δ Mag
518.73623	0.9601	+3.000	518.80185	0.2938	+2.813	518.93657	0.9788	+3.423
.73727	.9654	3.087	.80672	.3185	2.821	.93692	.9805	3.532
.73761	.9671	3.128	.80741	.3220	2.813	.93727	.9823	3.566
.73796	.9689	3.180	.80860	.3291	2.830	.93762	.9841	3.624
.73831	.9708	3.235	.80949	.3326	2.811	.93797	.9859	3.648
.73866	.9725	3.280	.81435	.3573	2.798	.93970	.9947	3.761
.73901	.9742	3.332	.81505	.3609	2.810	.94005	.9965	3.794
.73935	.9760	3.380	.81474	.3644	2.805	.94040	.9982	3.810
.73970	.9777	3.439	.81713	.3714	2.832	.94074	.0000	3.800
.74005	.9795	3.491	.81782	.3750	2.846	.94109	.0017	3.772
.74040	.9813	3.548	.82199	.3962	2.806	.94144	.0035	3.769
.74074	.9830	3.590	.82269	.3997	2.808	.94178	.0052	3.736
.74109	.9848	3.630	.82338	.4032	2.814	.94213	.0070	3.788
.74144	.9866	3.652	.82477	.4103	2.812	.94248	.0088	3.768
.74178	.9883	3.687	.82546	.4138	2.812	.94283	.0106	3.722
.74213	.9901	3.723	.83206	.4474	2.845	.94317	.0123	3.687
.74248	.9919	3.760	.83241	.4491	2.815	.94352	.0141	3.666
.74282	.9936	3.775	.83727	.4739	2.843	.94387	.0159	3.586
.74317	.9954	3.787	.83797	.4774	2.848	.94526	.0229	3.413
.74352	.9972	3.800	.83935	.4844	2.836	.94561	.0247	3.334
.74387	.9989	3.799	.84456	.5109	2.830	.94595	.0264	3.282
.74421	.0007	3.792	.84700	.5233	2.826	.94630	.0282	3.235
.74456	.0025	3.782	.85185	.5480	2.818	.94664	.0300	3.165
.74491	.0042	3.763	.85255	.5515	2.826	.94699	.0317	3.112
.74525	.0060	3.730	.85324	.5551	2.834	.94734	.0335	3.100
.74560	.0077	3.715	.85463	.5621	2.836	.94769	.0353	3.091
.74734	.0166	3.567	.85532	.5656	2.836	.94838	.0388	3.069
.74768	.0183	3.512	.86054	.5922	2.802	.94908	.0424	3.013
.74803	.0201	3.462	.86227	.6010	2.792	.94977	.0459	2.986
.74838	.0219	3.410	.86296	.6045	2.772	.95047	.0494	2.969
.74873	.0237	3.347	.86852	.6327	2.807	.95116	.0529	2.936
.74908	.0254	3.302	.86922	.6363	2.809	.95185	.0564	2.930
.74942	.0272	3.250	.87130	.6469	2.789	.95255	.0600	2.909
.74977	.0289	3.200	.87824	.6822	2.782	.95394	.0671	2.909
.75012	.0307	3.147	.87894	.6857	2.796	.95463	.0706	2.919
.75047	.0325	3.110	.87963	.6892	2.817	.95533	.0741	2.930
.75081	.0342	3.080	.88171	.6998	2.813	.96088	.1024	2.799
.75116	.0360	3.056	.88241	.7034	2.810	.96227	.1094	2.804
.75185	.0395	3.012	.88310	.7069	2.841	.96713	.1341	2.774
.75255	.0431	2.970	.88727	.7281	2.794	.96921	.1447	2.789
.75324	.0466	2.947	.88796	.7316	2.777	.96991	.1483	2.830
.75394	.0502	2.942	.88866	.7352	2.770	.97025	.1500	2.856
.75463	.0537	2.921	.88935	.7387	2.774	542.68731	.7423	2.735
.75532	.0572	2.915	.89144	.7493	2.735	.69009	.7565	2.755
.75671	.0642	3.879	.89213	.7528	2.752	.69078	.7600	2.745
.75741	.0678	2.877	.89699	.7775	2.752	.69148	.7635	2.748
.75810	.0713	2.869	.89769	.7811	2.760	.69217	.7670	2.755
.75880	.0749	2.868	.89838	.7846	2.741	.69287	.7706	2.795
.76297	.0961	2.799	.89977	.7916	2.715	.69356	.7741	2.739
.76366	.0996	2.762	.90046	.7951	2.749	.69425	.7776	2.739
.76435	.1031	2.741	.90602	.8234	2.725	.69495	.7812	2.735
.76505	.1066	2.791	.90672	.8270	2.719	.69564	.7847	2.734
.76574	.1102	2.769	.90880	.8376	2.726	.69634	.7883	2.732
.76713	.1172	2.773	.91366	.8623	2.700	.69703	.7918	2.759
.76782	.1207	2.782	.91435	.8658	2.702	.69773	.7953	2.747
.76852	.1243	2.766	.91644	.8764	2.678	.70050	.8094	2.731
.76991	.1314	2.778	.91713	.8799	2.683	.70120	.8130	2.716
.77060	.1349	2.823	.92199	.9046	2.706	.70189	.8165	2.705
.77130	.1384	2.778	.92269	.9082	2.714	.70259	.8200	2.718
.77685	.1666	2.798	.92338	.9117	2.702	.70328	.8235	2.729
.77755	.1702	2.807	.92477	.9188	2.710	.70398	.8271	2.732
.77894	.1773	2.826	.92546	.9223	2.727	.70537	.8342	2.735
.77963	.1808	2.812	.92616	.9258	2.736	.70606	.8377	2.714
.78519	.2090	2.816	.92685	.9293	2.770	.70675	.8412	2.718
.78588	.2126	2.817	.93102	.9505	2.804	.70745	.8447	2.704
.78796	.2231	2.811	.93172	.9541	2.922	.71092	.8624	2.673
.78866	.2267	2.811	.93241	.9576	2.963	.71162	.8659	2.705
.78935	.2302	2.817	.93380	.9647	3.078	.71231	.8695	2.711
.79630	.2655	2.806	.93414	.9664	3.110	.71300	.8730	2.691
.79699	.2690	3.806	.93449	.9682	3.162	.71370	.8765	2.676
.79769	.2726	2.814	.93484	.9700	3.206	.71439	.8800	2.686
.79838	.2761	2.814	.93518	.9717	3.256	.71648	.8907	2.709
.79977	.2832	2.835	.93553	.9735	3.321	.71717	.8942	2.725
.80046	.2867	2.792	.93588	.9752	3.384	.71995	.9083	2.735
.80116	.2902	2.823	.93623	.9770	3.425	.72064	.9118	2.735

TABLE 1

YELLOW OBSERVATIONS

Helioc JD 2434+	Helioc Phase	Δ Mag	Helioc JD 2434+	Helioc Phase	Δ Mag	Helioc JD 2434+	Helioc Phase	Δ Mag
542.72134	0.9154	+2.694	542.75398	0.0813	+2.872	542.83106	0.4732	+2.824
.72203	.9189	2.705	.75467	.0848	2.872	.83523	.4945	2.825
.72273	.9224	2.703	.75536	.0883	2.828	.83592	.4980	2.854
.72412	.9295	2.725	.75606	.0919	2.820	.83662	.5015	2.841
.72481	.9330	2.746	.75675	.0954	2.795	.83731	.5050	2.823
.72550	.9365	2.763	.75745	.0990	2.781	.83870	.5121	2.820
.72620	.9401	2.776	.75814	.1025	2.775	.83939	.5156	2.855
.72689	.9436	2.800	.75884	.1060	2.750	.84009	.5192	2.849
.72759	.9471	2.826	.75953	.1095	2.759	.84078	.5227	2.847
.72794	.9489	2.843	.76023	.1131	2.739	.84425	.5403	2.804
.72828	.9507	2.854	.76092	.1166	2.753	.84495	.5439	2.816
.72863	.9524	2.877	.76300	.1272	2.784	.84564	.5474	2.806
.72898	.9542	2.899	.76370	.1308	2.798	.84634	.5509	2.832
.72933	.9560	2.918	.76717	.1484	2.784	.84773	.5580	2.824
.72967	.9577	2.928	.76787	.1520	2.802	.84842	.5615	2.823
.73002	.9595	2.968	.76856	.1555	2.803	.84912	.5651	2.829
.73037	.9613	2.998	.76925	.1590	2.785	.84981	.5686	2.821
.73072	.9631	3.025	.76995	.1625	2.789	.85398	.5898	2.830
.73106	.9648	3.050	.77134	.1696	2.780	.85467	.5933	2.814
.73141	.9666	3.100	.77203	.1731	2.782	.85537	.5969	2.818
.73175	.9683	3.142	.77273	.1767	2.781	.85606	.6004	2.816
.73210	.9701	3.187	.77342	.1802	2.786	.85675	.6039	2.814
.73245	.9719	3.220	.77412	.1837	2.792	.85814	.6109	2.800
.73280	.9736	3.270	.77481	.1872	2.811	.85884	.6145	2.796
.73384	.9789	3.434	.77550	.1907	2.800	.85953	.6180	2.789
.73419	.9807	3.484	.77967	.2120	2.802	.86370	.6392	2.825
.73453	.9824	3.534	.78037	.2155	2.797	.86439	.6427	2.821
.73488	.9842	3.599	.78106	.2190	2.789	.86509	.6463	2.826
.73523	.9860	3.614	.78175	.2225	2.788	.86578	.6498	2.826
.73558	.9878	3.653	.78245	.2261	2.784	.86717	.6569	2.793
.73592	.9895	3.658	.78384	.2332	2.776	.86787	.6604	2.801
.73627	.9913	3.681	.78453	.2367	2.797	.86856	.6639	2.795
.73662	.9931	3.709	.78523	.2402	2.795	.86925	.6674	2.814
.73697	.9948	3.714	.78904	.2596	2.776	.87342	.6886	2.786
.73731	.9966	3.719	.78939	.2614	2.796	.87412	.6922	2.813
.73766	.9983	3.730	.79009	.2649	2.816	.87481	.6957	2.799
.73800	.0001	3.733	.79078	.2684	2.816	.87550	.6992	2.783
.73835	.0019	3.738	.79148	.2720	2.825	.87689	.7063	2.790
.73870	.0036	3.723	.79217	.2755	2.824	.87759	.7098	2.806
.73905	.0054	3.728	.79356	.2826	2.818	.87828	.7133	2.793
.73939	.0071	3.708	.79425	.2861	2.817	.87898	.7169	2.792
.73974	.0089	3.683	.79495	.2896	2.814	.88245	.7345	2.736
.74009	.0107	3.652	.79565	.2932	2.798	.88314	.7381	2.739
.74044	.0125	3.627	.79600	.2950	2.772	.88384	.7416	2.740
.74078	.0142	3.585	.79981	.3144	2.840	.88453	.7451	2.766
.74113	.0160	3.571	.80050	.3179	2.827	.88523	.7487	2.775
.74148	.0178	3.512	.80120	.3214	2.828	.88592	.7522	2.775
.74183	.0196	3.477	.80189	.3249	2.834	.88731	.7593	2.740
.74217	.0213	3.411	.80328	.3320	2.838	.88800	.7628	2.721
.74252	.0231	3.235	.80398	.3356	2.838	.88870	.7663	2.751
.74356	.0283	3.200	.80467	.3391	2.845	.88939	.7698	2.755
.74391	.0301	3.152	.80537	.3426	2.855	.89287	.7875	2.726
.74425	.0319	3.114	.80884	.3603	2.814	.89356	.7910	2.729
.74460	.0336	3.100	.80953	.3638	2.817	.89425	.7945	2.757
.74495	.0354	3.071	.81023	.3673	2.828	.89495	.7981	2.716
.74530	.0372	3.051	.81092	.3708	2.825	.89564	.8016	2.714
.74564	.0389	3.064	.81231	.3779	2.824	.89634	.8052	2.712
.74599	.0407	3.041	.81300	.3814	2.813	.89703	.8087	2.725
.74634	.0425	3.022	.81370	.3850	2.803	.89842	.8157	2.726
.74669	.0443	3.020	.81439	.3885	2.811	.89912	.8193	2.742
.74703	.0460	3.005	.81474	.3903	2.812	.89981	.8228	2.754
.74738	.0478	2.990	.81787	.4062	2.819	.90050	.8263	2.748
.74773	.0495	2.981	.81856	.4097	2.832			
.74808	.0513	2.964	.81925	.4133	2.821			
.74842	.0531	2.959	.81995	.4168	2.808			
.74877	.0548	2.949	.82134	.4238	2.823			
.74912	.0566	2.939	.82203	.4273	2.820			
.74947	.0584	2.920	.82273	.4309	2.814			
.74981	.0601	2.917	.82342	.4344	2.81*			
.75016	.0619	2.909	.82620	.4485	2.814			
.75050	.0636	2.909	.82689	.4520	2.829			
.75120	.0672	2.888	.82759	.4556	2.833			
.75189	.0707	2.883	.82828	.4591	2.822			
.75259	.0743	2.879	.82967	.4662	2.844			
.75328	.0778	2.872	.83037	.4697	2.820			

TABLE 2

BLUE OBSERVATIONS

Heliоc JD 2434+	Heliоc Phase	Δ Mag	Heliоc JD 2434+	Heliоc Phase	Δ Mag	Heliоc JD 2434+	Heliоc Phase	Δ Mag
484.66718	0.7316	+2.355	484.76301	0.2190	+2.381	484.83245	0.5721	+2.395
.66787	.7353	2.348	.76370	.2226	2.391	.83314	.5756	2.395
.66856	.7388	2.357	.76440	.2261	2.379	.83384	.5792	2.390
.66926	.7424	2.349	.76509	.2296	2.383	.83453	.5827	2.384
.66843	.7906	2.263	.76578	.2331	2.376	.83522	.5898	2.397
.66912	.8942	2.271	.76648	.2367	2.377	.83662	.5933	2.400
.69981	.8977	2.277	.76717	.2402	2.375	.83731	.5968	2.419
.70051	.9013	2.281	.76856	.2473	2.379	.83801	.6004	2.397
.70815	.9401	3.332	.76926	.2508	2.376	.84148	.6180	2.427
.70884	.9436	2.362	.76995	.2543	2.375	.84218	.6216	2.416
.70954	.9472	2.381	.77064	.2578	2.376	.84287	.6251	2.411
.71023	.9507	2.401	.77134	.2614	2.375	.84356	.6286	2.412
.71093	.9542	2.478	.77620	.2861	2.380	.84496	.6313	2.413
.71162	.9577	2.519	.77690	.2897	2.375	.84495	.6357	2.404
.71301	.9648	2.887	.77829	.2967	2.380	.84565	.6392	2.403
.71440	.9719	2.830	.77898	.3002	2.407	.84634	.6428	2.394
.71509	.9754	2.997	.77968	.3038	2.402	.84704	.6463	2.394
.71578	.9789	3.114	.78037	.3073	2.389	.84773	.6498	2.401
.71648	.9825	3.216	.78106	.3108	2.390	.84842	.6533	2.413
.71717	.9860	3.297	.78176	.3144	2.384	.84912	.6569	2.401
.71787	.9895	3.366	.78245	.3179	2.374	.84981	.6604	2.420
.71925	.9965	3.410	.78314	.3214	2.374	.85050	.6639	2.441
.72064	.0036	3.443	.78384	.3250	2.379	.85189	.6710	2.418
.72134	.0072	3.396	.78592	.3355	2.390	.85259	.6745	2.399
.72203	.0107	3.346	.78662	.3391	2.390	.85328	.6780	2.398
.72272	.0142	3.277	.78731	.3426	2.399	.85398	.6816	2.408
.72342	.0177	3.199	.78801	.3462	2.401	.85467	.6851	2.408
.72411	.0213	3.071	.79148	.3638	2.408	.85536	.6886	2.415
.72481	.0248	2.944	.79218	.3674	2.384	.85606	.6922	2.398
.72550	.0283	2.825	.79357	.3744	2.399	.85676	.6957	2.407
.72619	.0318	2.716	.79426	.3779	2.390	.86025	.7134	2.404
.72689	.0354	2.674	.79495	.3814	2.399	.86093	.7169	2.411
.72759	.0389	2.627	.79565	.3850	2.396	.86162	.7204	2.400
.72829	.0425	2.600	.79634	.3885	2.408	.86231	.7239	2.405
.72898	.0460	2.580	.79704	.3921	2.410	.86301	.7275	2.393
.72968	.0496	2.557	.79773	.3956	2.407	.86370	.7310	2.399
.73037	.0531	2.543	.79842	.3991	2.406	.86440	.7346	2.406
.73106	.0566	2.414	.79912	.4026	2.399	.86509	.7381	2.408
.73176	.0602	2.416	.79981	.4062	2.386	.86578	.7416	2.392
.73245	.0637	2.423	.80051	.4097	2.389	.86648	.7452	2.380
.73315	.0672	2.431	.80398	.4274	2.394	.86717	.7487	2.362
.73384	.0707	2.413	.80467	.4309	2.374	.86856	.7557	2.366
.73523	.0778	2.381	.80884	.4521	2.377	.86925	.7592	2.355
.73592	.0813	2.375	.80954	.4556	2.390	.86995	.7628	2.335
.73662	.0849	2.359	.81093	.4627	2.390	.87064	.7663	2.350
.73731	.0884	2.353	.81162	.4662	2.407	.87134	.7699	2.355
.73800	.0919	2.345	.81231	.4697	2.413	.87482	.7876	2.334
.74148	.1096	2.330	.81301	.4733	2.418	.87551	.7911	2.325
.74218	.1131	2.337	.81370	.4768	2.403	.87620	.7946	2.307
.74357	.1202	2.339	.81440	.4803	2.398	.87690	.7981	2.312
.74426	.1237	2.363	.81509	.4838	2.388	.87759	.8016	2.322
.74495	.1272	2.365	.81578	.4874	2.406	.87829	.8052	2.339
.74565	.1308	2.363	.81648	.4909	2.407	.87898	.8087	2.359
.74634	.1343	2.352	.81717	.4944	2.407	.87968	.8123	2.360
.74704	.1378	2.360	.81856	.5015	2.410	.88037	.8158	2.354
.74773	.1414	2.373	.81925	.5050	2.412	.88106	.8193	2.347
.74842	.1449	2.378	.81995	.5086	2.389	.88176	.8228	2.332
.74912	.1484	2.385	.82064	.5121	2.403	.88245	.8264	2.325
.74981	.1519	2.390	.82134	.5156	2.408	.88314	.8299	2.346
.75051	.1555	2.386	.82203	.5192	2.409	.88384	.8334	2.372
.75189	.1625	2.373	.82273	.5227	2.394	.88453	.8369	2.369
.75259	.1661	2.365	.82620	.5404	2.413	.88523	.8405	2.368
.75328	.1696	2.397	.82690	.5439	2.401	.88592	.8440	2.346
.75398	.1731	2.400	.82759	.5474	2.395	.88662	.8476	2.323
.75467	.1766	2.402	.82829	.5510	2.391	.88731	.8511	2.294
.75954	.2014	2.348	.82898	.5545	2.396	.88801	.8546	2.314
.76023	.2049	2.304	.82968	.5580	2.405	.89218	.8758	2.281
.76093	.2085	2.337	.83037	.5616	2.391	.89287	.8793	2.276
.76162	.2120	2.364	.83106	.5651	2.400	.89357	.8829	2.269
.76232	.2155	2.383	.83176	.5686	2.398	.89426	.8864	2.262
						.89495	.8899	2.259

TABLE 2

BLUE OBSERVATIONS

Helioc JD 2434+	Heliоc Phase	Δ Mag	Heliоc JD 2434+	Heliоc Phase	Δ Mag	Heliоc JD 2434+	Heliоc Phase	Δ Mag
484.89665	0.8935	+2.285	484.96440	0.2430	+2.405	519.72648	0.9952	+3.520
.89834	.8970	2.281	.96509	.2466	2.389	.72682	.9969	3.540
.89904	.9005	2.277	.96578	.2501	2.383	.72717	.9987	3.525
.89973	.9040	2.280	.96648	.2536	2.382	.72752	.0004	3.540
.89942	.9076	2.279	.96717	.2571	2.389	.72787	.0022	3.535
.89912	.9111	2.278	.96786	.2606	2.390	.72821	.0039	3.541
.89981	.9146	2.270	.97343	.2890	2.417	.72856	.0057	3.500
.90259	.9288	2.287	.97412	.2925	2.423	.72890	.0075	3.460
.90328	.9323	2.307	.97481	.2960	2.340	.72925	.0092	3.423
.90815	.9570	2.501	.97551	.2995	2.421	.72960	.0110	3.400
.90884	.9605	2.537	.97620	.3030	2.420	.72995	.0128	3.362
.90954	.9641	2.596	.97690	.3066	2.427	.73030	.0146	3.340
.91023	.9676	2.675	.97759	.3101	2.416	.73064	.0163	3.277
.91093	.9712	2.802	.97967	.3207	2.388	.73203	.0234	3.046
.91162	.9747	2.966	.98037	.3242	2.407	.73238	.0252	2.960
.91231	.9782	3.107	.98106	.3277	2.406	.73273	.0269	2.900
.91301	.9817	3.223	.98175	.3313	2.408	.73307	.0287	2.833
.91370	.9853	3.332	.98245	.3348	2.419	.73342	.0304	2.774
.91440	.9888	3.397	.98314	.3383	2.422	.73377	.0322	2.717
.91509	.9923	3.444	519.67682	.7426	2.343	.73412	.0340	2.660
.91578	.9958	3.503	.67752	.7462	2.356	.73446	.0357	2.651
.91648	.9994	3.511	.67821	.7533	2.356	.73481	.0375	2.633
.91717	.0029	3.501	.67960	.7568	2.381	.73516	.0393	2.621
.91787	.0065	3.466	.68030	.7603	2.396	.73585	.0428	2.601
.91856	.0100	3.437	.68446	.7815	2.396	.73655	.0464	2.590
.91925	.0135	3.331	.69175	.8186	2.394	.73724	.0499	2.586
.92064	.0205	3.133	.69210	.8203	2.394	.73794	.0534	2.576
.92134	.0241	2.979	.69280	.8239	2.278	.73863	.0569	2.553
.92204	.0277	2.827	.69349	.8274	2.277	.73932	.0604	2.534
.92273	.0312	2.702	.69418	.8345	2.287	.74002	.0640	2.519
.92343	.0347	2.642	.69835	.8521	2.269	.74037	.0658	2.541
.92412	.0382	2.607	.69905	.8557	2.295	.74071	.0675	2.523
.92482	.0418	2.579	.69974	.8592	2.303	.74106	.0693	2.530
.92551	.0453	2.559	.70044	.8627	2.334	.74280	.0781	2.492
.92620	.0488	2.544	.70113	.8663	2.331	.74349	.0816	2.482
.92690	.0524	2.524	.70182	.8698	2.309	.74384	.0834	2.476
.92759	.0559	2.515	.70217	.8715	2.290	.74696	.0993	2.449
.92828	.0594	2.513	.70252	.8733	2.317	.74731	.1011	2.420
.92898	.0629	2.510	.70287	.8751	2.289	.74766	.1028	2.400
.92967	.0664	2.509	.70321	.8768	2.283	.74835	.1064	2.396
.93106	.0735	2.435	.70391	.8804	2.293	.74905	.1099	2.391
.93245	.0806	2.431	.70738	.8980	2.302	.74974	.1134	2.400
.93314	.0841	2.413	.70807	.9015	2.295	.75044	.1170	2.385
.93384	.0877	2.397	.70946	.9086	2.325	.75182	.1240	2.382
.93453	.0912	2.377	.71016	.9122	2.304	.75252	.1276	2.404
.93523	.0947	2.352	.71085	.9157	2.344	.75321	.1311	2.412
.93592	.0982	2.347	.71363	.9298	2.337	.75391	.1346	2.402
.93801	.1089	2.332	.71432	.9333	2.358	.75807	.1553	2.393
.93870	.1124	2.327	.71502	.9369	2.358	.75877	.1593	2.396
.94286	.1335	2.362	.71641	.9439	2.373	.75946	.1628	2.405
.94356	.1371	2.373	.71710	.9475	2.412	.76085	.1699	2.404
.94425	.1406	2.378	.71780	.9510	2.457	.76155	.1735	2.413
.94495	.1441	2.367	.71849	.9545	2.480	.76294	.1770	2.413
.94565	.1477	2.359	.71919	.9581	2.536	.76571	.1946	2.431
.94634	.1512	2.361	.71988	.9616	2.598	.76641	.1981	2.443
.94704	.1548	2.373	.72057	.9651	2.666	.76710	.2017	2.449
.94912	.1653	2.368	.72092	.9669	2.708	.76780	.2052	2.434
.94981	.1689	2.349	.72127	.9687	2.750	.76815	.2070	2.441
.95051	.1724	2.364	.72231	.9739	2.942	.76953	.2140	2.424
.95120	.1759	2.354	.72266	.9757	3.009	.76988	.2158	2.450
.95189	.1794	2.346	.72300	.9775	3.077	.77057	.2193	2.441
.95259	.1830	2.362	.72335	.9792	3.147	.77127	.2229	2.419
.95328	.1865	2.366	.72370	.9810	3.214	.77196	.2264	2.415
.95884	.2148	2.369	.72405	.9828	3.268	.77266	.2300	2.421
.95954	.2183	2.378	.72439	.9845	3.319	.77717	.2529	2.449
.96023	.2218	2.396	.72474	.9863	3.347	.77753	.2547	2.447
.96092	.2253	2.390	.72509	.9881	3.304	.77821	.2582	2.433
.96162	.2289	2.386	.72544	.9899	3.436	.78030	.2688	2.430
.96231	.2324	2.388	.72578	.9916	3.466	.78099	.2723	2.457
.96470	.2395	2.417	.72613	.9934	3.490	.78168	.2758	2.458

TABLE 2

BLUE OBSERVATIONS

Heliocentric JD 2434+	Heliocentric Phase	Δ Mag	Heliocentric JD 2434+	Heliocentric Phase	Δ Mag	Heliocentric JD 2434+	Heliocentric Phase	Δ Mag
519.78516	0.2935	+2.441	519.86641	0.7066	+2.424	519.92196	0.9891	+03.54
.78585	.2970	2.444	.86710	.7101	2.422	.92231	.9909	3.57
.78655	.3006	2.442	.86780	.7137	2.429	.92266	.9927	3.59
.78724	.3041	2.462	.86849	.7173	2.439	.92300	.9944	3.62
.78828	.3094	2.481	.86919	.7208	2.448	.92335	.9962	3.65
.78863	.3112	2.450	.86988	.7243	2.452	.92370	.9979	3.63
.78932	.3147	2.459	.87544	.7526	2.413	.92405	.9997	3.65
.79002	.3182	2.467	.87613	.7561	2.404	.92439	.0014	3.64
.79766	.3571	2.447	.87682	.7596	2.415	.92474	.0032	3.63
.79974	.3677	2.433	.87752	.7631	2.423	.92509	.0050	3.61
.80044	.3712	2.441	.87891	.7702	2.410	.92544	.0068	3.58
.80113	.3747	2.441	.87960	.7737	2.411	.92578	.0085	3.56
.80530	.3959	2.445	.88030	.7773	2.401	.92613	.0103	3.54
.80599	.3994	2.444	.88099	.7808	2.399	.92648	.0121	3.477
.80669	.4030	2.436	.88238	.7878	2.371	.92682	.0138	3.438
.80807	.4100	2.458	.88307	.7914	2.370	.92717	.0156	3.395
.80877	.4136	2.445	.88377	.7949	2.359	.92752	.0174	3.317
.81363	.4383	2.462	.88446	.7984	2.370	.92856	.0226	3.111
.81432	.4418	2.443	.89002	.8267	2.330	.92891	.0244	3.069
.81502	.4453	2.457	.89071	.8302	2.346	.92925	.0262	2.969
.81571	.4489	2.444	.89141	.8338	2.350	.92960	.0279	2.899
.81710	.4559	2.450	.89349	.8443	2.405	.92995	.0297	2.843
.81780	.4595	2.452	.89418	.8478	2.404	.93030	.0315	2.801
.81849	.4630	2.468	.89835	.8690	2.392	.93064	.0332	2.768
.81919	.4665	2.458	.89905	.8726	2.384	.93099	.0350	2.748
.81988	.4701	2.455	.89974	.8761	2.367	.93134	.0368	2.719
.82057	.4736	2.456	.90044	.8797	2.385	.93168	.0385	2.686
.82127	.4771	2.453	.90113	.8832	2.377	.93203	.0403	2.667
.82266	.4842	2.475	.90148	.8850	2.384	.93238	.0421	2.659
.82335	.4877	2.483	.90252	.8902	2.368	.93307	.0456	2.631
.82821	.5124	2.477	.90321	.8938	2.355	.93377	.0491	2.586
.82891	.5160	2.477	.90391	.8973	2.370	.93446	.0526	2.575
.82960	.5195	2.476	.90460	.9008	2.377	.93516	.0562	2.563
.83168	.5301	2.469	.90877	.9220	2.364	.93585	.0597	2.552
.83238	.5336	2.483	.90946	.9255	2.369	.93655	.0633	2.527
.83794	.5619	2.495	.91016	.9291	2.381	.93724	.0668	2.512
.83863	.5654	2.494	.91085	.9326	2.389	.93863	.0739	2.516
.84002	.5725	2.473	.91155	.9362	2.397	.94314	.0968	2.419
.84071	.5760	2.479	.91224	.9397	2.403	.94349	.0986	2.411
.84141	.5795	2.489	.91432	.9502	2.483	.94418	.1021	2.409
.84210	.5830	2.476	.91502	.9538	2.562	.94488	.1056	2.396
.84280	.5866	2.463	.91571	.9573	2.589	.94974	.1303	2.422
.84349	.5901	2.475	.91641	.9609	2.628	.95044	.1339	2.418
.84766	.6113	2.449	.91710	.9644	2.689	.95113	.1374	2.407
.84835	.6148	2.444	.91745	.9662	2.717	.95182	.1409	2.415
.84905	.6184	2.446	.91780	.9679	2.780	.95252	.1445	2.419
.85113	.6289	2.448	.91814	.9697	2.848	.95321	.1480	2.411
.85182	.6325	2.446	.91849	.9714	2.907	.95877	.1763	2.469
.85668	.6572	2.460	.91884	.9732	2.992	.95946	.1798	2.432
.85877	.6678	2.502	.91918	.9750	3.058	.96016	.1833	2.454
.85946	.6713	2.486	.91953	.9767	3.150	.96085	.1868	2.446
.86016	.6749	2.486	.91988	.9785	3.199	.96571	.2115	2.446
.86155	.6819	2.454	.92092	.9838	3.417			
.86224	.6854	2.452	.92127	.9856	3.461			
.86571	.7031	2.432	.92162	.9874	3.488			

TABLE 3

ULTRA VIOLET OBSERVATIONS

Heliocentric JD 2434+	Heliocentric Phase	Δ Mag	Heliocentric JD 2434+	Heliocentric Phase	Δ Mag	Heliocentric JD 2434+	Heliocentric Phase	Δ Mag
485.76298	0.3035	+1.629	490.75046	0.6630	+1.618	490.90726	0.4602	+1.601
.77305	.3547	1.617	.75066	.6640	1.626	.90761	.4620	1.612
.78173	.3989	1.603	.75101	.6658	1.657	.90796	.4638	1.632
.78971	.4394	1.627	.75136	.6676	1.697	.90830	.4655	1.646
.79284	.4554	1.599	.75170	.6693	1.697	.90934	.4708	1.625
.79874	.4854	1.686	.75274	.6746	1.720	.90969	.4726	1.613
.80360	.5101	1.682	.75309	.6764	1.700	.91004	.4744	1.611
.80950	.5401	1.682	.75344	.6781	1.697	.91038	.4761	1.599
.81471	.5666	1.653	.75448	.6834	1.677	.91073	.4779	1.593
.81687	.5826	1.552	.75622	.6923	1.644	.91390	.5245	1.668
.82034	.9003	1.619	.75969	.7099	1.643	.92046	.5274	1.663
.82277	.9126	1.564	.76525	.7382	1.656	.92219	.5362	1.600
.82603	.9292	1.563	.76560	.7400	1.673	.92393	.5450	1.658
.82659	.9320	1.636	.76594	.7417	1.695	.92462	.5485	1.655
.82805	.9395	1.599	.76733	.7488	1.710	.93469	.5997	1.689
.82867	.9426	1.593	.76803	.7523	1.733	.93712	.6121	1.707
.83631	.9815	2.517	.76872	.7558	1.744	.93920	.6226	1.730
.83666	.9832	2.557	.77080	.7664	1.706	.95102	.6827	1.714
.83700	.9850	2.633	.77115	.7682	1.733	.95310	.6933	1.656
.83805	.9903	2.724	.77150	.7700	1.760	.95483	.7021	1.692
.83839	.9920	2.763	.77219	.7735	1.742	.95657	.7110	1.745
.83944	.9973	2.848	.77254	.7753	1.716	.95677	.7120	1.711
.83978	.9991	2.843	.77288	.7770	1.703	.95726	.7145	1.653
.84013	.0009	2.843	.78192	.8229	1.526	.95761	.7163	1.622
.84117	.0062	2.742	.78226	.8247	1.551	.95810	.7188	1.618
.84152	.0080	2.704	.78261	.8265	1.568	.95837	.7201	1.620
.84186	.0094	2.680	.78365	.8317	1.571	.95865	.7215	1.629
.84291	.0150	2.518	.79548	.8919	1.517	.95900	.7233	1.646
.84325	.0167	2.485	.79892	.9094	1.473	.96004	.7286	1.703
.84360	.0185	2.397	.80692	.9501	1.557	.96038	.7303	1.712
.84464	.0238	2.128	.80726	.9518	1.594	.96122	.7346	1.680
.84499	.0256	2.085	.81039	.9677	1.816	.96143	.7356	1.660
.84534	.0274	2.026	.81074	.9695	1.881	.96177	.7374	1.640
.84645	.0330	1.865	.81178	.9748	2.146	.96212	.7392	1.626
.84673	.0344	1.827	.81213	.9765	2.235	.96386	.7480	1.606
.84707	.0362	1.783	.81351	.9836	2.505	.96421	.7498	1.609
.84846	.0432	1.733	.81386	.9854	2.565	.96455	.7515	1.613
.84881	.0450	1.732	.81525	.9924	2.734	.96560	.7569	1.653
.84930	.0521	1.716	.81559	.9941	2.745	.96594	.7586	1.656
.84955	.0539	1.700	.81663	.9994	2.802	.96622	.7600	1.655
.84959	.0592	1.648	.81698	.0012	2.737	.96705	.7643	1.619
.84994	.0609	1.648	.81733	.0030	2.780	.96737	.7657	1.611
.85028	.0627	1.668	.81837	.0083	2.715	.96872	.7727	1.554
.85063	.0644	1.696	.81872	.0101	2.665	.97011	.7798	1.573
.85437	.0733	1.686	.81892	.0111	2.624	.97045	.7815	1.606
.85645	.0839	1.645	.82046	.0189	2.396	.98053	.8328	1.532
.85953	.0944	1.631	.82081	.0207	2.329	.98157	.8381	1.554
.86200	.1121	1.626	.82220	.0278	1.973	.98955	.8787	1.500
.86409	.1227	1.579	.82254	.0295	1.910	.99129	.8875	1.525
.86478	.1262	1.584	.82358	.0348	1.798	.99233	.8928	1.526
.86617	.1333	1.598	.82393	.0366	1.784	541.69363	.6898	1.723
.86825	.1439	1.592	.82532	.0436	1.714	.69641	.7040	1.735
.86874	.1464	1.620	.82567	.0454	1.695	.69710	.7075	1.708
.86978	.1933	1.600	.82705	.0524	1.634	.69780	.7111	1.699
.93867	.1968	1.594	.82740	.0542	1.630	.69849	.7146	1.721
.94006	.2039	1.614	.82844	.0595	1.616	.69919	.7181	1.735
.94075	.2074	1.631	.82879	.0613	1.613	.70057	.7251	1.758
.95043	.2569	1.621	.83018	.0683	1.621	.70127	.7287	1.726
.95117	.2604	1.607	.83052	.0701	1.621	.70474	.7463	1.647
.95325	.2710	1.637	.83260	.0806	1.608	.70543	.7498	1.643
.95395	.2745	1.630	.83435	.0895	1.619	.70613	.7534	1.656
.95603	.2851	1.602	.83712	.1036	1.596	.70682	.7569	1.679
.95673	.2887	1.625	.83886	.1125	1.567	.70717	.7587	1.705
.96645	.3381	1.639	.84059	.1213	1.600	.70752	.7605	1.684
.96853	.3487	1.728	.84198	.1283	1.613	.70821	.7640	1.652
.97825	.3981	1.656	.85032	.1707	1.577	.70891	.7675	1.664
.98034	.4087	1.615	.85206	.1796	1.591	.70960	.7711	1.643
.98207	.4175	1.633	.86142	.2272	1.605	.71030	.7746	1.693
490.70935	.4540	1.660	.86316	.2360	1.593	.71099	.7781	1.672
.71351	.4751	1.659	.86490	.2449	1.601	.71238	.7852	1.736
.71490	.4822	1.653	.87482	.2943	1.604	.71308	.7887	1.700
.71698	.4928	1.672	.87740	.3084	1.581	.71377	.7923	1.668
.73087	.5634	1.659	.87948	.3190	1.570	.71863	.8170	1.669
.73573	.5881	1.653	.89060	.3795	1.557	.71932	.8205	1.665
.74401	.6305	1.633	.89337	.3896	1.590	.72002	.8240	1.635
.74685	.6446	1.749	.89545	.4002	1.614	.72071	.8275	1.627
.74754	.6481	1.714	.90448	.4461	1.623	.72210	.8346	1.645
.74823	.6516	1.665	.90483	.4479	1.631	.72280	.8382	1.645
.74893	.6552	1.633	.90518	.4497	1.620	.72349	.8417	1.645
.74958	.6585	1.620	.90553	.4514	1.608	.72419	.8452	1.646
			.90587	.4532	1.601			

TABLE 3

ULTRA VIOLET OBSERVATIONS

Helioc JD 2434 +	Helioc Phase	Δ Mag	Helioc JD 2434 +	Helioc Phase	Δ Mag	Helioc JD 2434 +	Helioc Phase	Δ Mag
541.72488	0.8487	+1.684	541.76272	0.0411	+1.854	541.82766	0.3713	+1.722
.72557	.8523	1.711	.76307	.0429	1.823	.82835	.3748	1.757
.72592	.8540	1.738	.76342	.0447	1.801	.82905	.3784	1.745
.72627	.8558	1.713	.76377	.0465	1.806	.82974	.3819	1.725
.72696	.8593	1.691	.76412	.0483	1.804	.83044	.3855	1.724
.72766	.8629	1.658	.76446	.0500	1.778	.83182	.3925	1.660
.72835	.8664	1.612	.76481	.0518	1.760	.83252	.3960	1.676
.72870	.8682	1.569	.76516	.0536	1.758	.83321	.3996	1.713
.72905	.8699	1.561	.76551	.0553	1.769	.83391	.4031	1.666
.72974	.8735	1.620	.76585	.0571	1.777	.83460	.4066	1.632
.73044	.8770	1.629	.76655	.0606	1.766	.83530	.4102	1.650
.73321	.8947	1.623	.76724	.0641	1.766	.84016	.4349	1.679
.73460	.8982	1.608	.76794	.0677	1.754	.84085	.4384	1.722
.73530	.9017	1.626	.76863	.0712	1.759	.84155	.4420	1.731
.73599	.9052	1.656	.76932	.0747	1.760	.84190	.4437	1.698
.73669	.9088	1.653	.77002	.0783	1.731	.84224	.4455	1.725
.73738	.9123	1.632	.77071	.0818	1.720	.84259	.4473	1.754
.73807	.9158	1.642	.77141	.0853	1.720	.84363	.4525	1.772
.73877	.9194	1.583	.77210	.0888	1.727	.84432	.4560	1.758
.73946	.9229	1.626	.77280	.0924	1.706	.84502	.4596	1.749
.74016	.9264	1.650	.77349	.0959	1.696	.84571	.4631	1.743
.74085	.9299	1.682	.77419	.0995	1.676	.84641	.4667	1.763
.74155	.9335	1.684	.77488	.1030	1.653	.84676	.4685	1.798
.74224	.9370	1.677	.77557	.1065	1.618	.85057	.4878	1.749
.74294	.9406	1.679	.77627	.1100	1.601	.85127	.4914	1.730
.74363	.9441	1.686	.77696	.1135	1.629	.85196	.4949	1.718
.74467	.9494	1.716	.77766	.1171	1.641	.85266	.4985	1.705
.74502	.9511	1.745	.77835	.1206	1.649	.85335	.5020	1.733
.74537	.9529	1.765	.77905	.1242	1.660	.85405	.5055	1.718
.74571	.9546	1.768	.77974	.1277	1.661	.85544	.5126	1.743
.74606	.9564	1.774	.78044	.1312	1.665	.85613	.5161	1.753
.74641	.9582	1.783	.78113	.1348	1.654	.85682	.5196	1.756
.74675	.9599	1.813	.78460	.1524	1.675	.85752	.5232	1.759
.74710	.9617	1.832	.78530	.1560	1.677	.86099	.5408	1.709
.74745	.9635	1.862	.78599	.1595	1.674	.86169	.5444	1.713
.74780	.9653	1.910	.78669	.1630	1.656	.86238	.5479	1.712
.74814	.9670	1.951	.78738	.1665	1.686	.86307	.5514	1.698
.74849	.9688	1.996	.78807	.1700	1.701	.86377	.5549	1.705
.74884	.9706	2.041	.78877	.1736	1.691	.86446	.5584	1.693
.74919	.9723	2.101	.78946	.1771	1.694	.86655	.5691	1.694
.74953	.9741	2.181	.79016	.1807	1.651	.86724	.5726	1.707
.74988	.9759	2.250	.79051	.1824	1.626	.86794	.5761	1.673
.75023	.9776	2.360	.79085	.1841	1.654	.86863	.5797	1.666
.75057	.9794	2.419	.79155	.1877	1.671	.87210	.5973	1.684
.75092	.9811	2.479	.79294	.1948	1.696	.87280	.6009	1.661
.75127	.9829	2.546	.79363	.1983	1.660	.87349	.6044	1.698
.75162	.9847	2.595	.79432	.2018	1.657	.87419	.6079	1.697
.75196	.9864	2.621	.79780	.2195	1.678	.87488	.6114	1.720
.75231	.9882	2.656	.79849	.2230	1.661	.87627	.6185	1.663
.75266	.9900	2.696	.79919	.2266	1.675	.87696	.6220	1.646
.75300	.9917	2.755	.79988	.2301	1.675	.87766	.6256	1.660
.75335	.9935	2.805	.80057	.2336	1.673	.88182	.6467	1.701
.75370	.9953	2.835	.80127	.2372	1.692	.88252	.6503	1.716
.75405	.9971	2.855	.80266	.2442	1.673	.88321	.6538	1.652
.75439	.9988	2.867	.80335	.2477	1.682	.88391	.6573	1.683
.75474	.0006	2.854	.80682	.2654	1.640	.88460	.6609	1.703
.75509	.0023	2.848	.80752	.2689	1.641	.88599	.6679	1.707
.75544	.0041	2.811	.80821	.2724	1.641	.88669	.6715	1.711
.75578	.0059	2.801	.80891	.2760	1.677	.88738	.6750	1.719
.75613	.0076	2.770	.80960	.2795	1.714	.88807	.6785	1.742
.75717	.0129	2.610	.81030	.2831	1.741	.88877	.6821	1.750
.75752	.0147	2.590	.81065	.2848	1.743	.89224	.6997	1.741
.75787	.0165	2.540	.81099	.2866	1.731	.89294	.7033	1.721
.75821	.0182	2.492	.81238	.2936	1.695	.89363	.7068	1.722
.75856	.0200	2.429	.81307	.2972	1.693	.89432	.7103	1.683
.75891	.0218	2.333	.81377	.3007	1.671	.89502	.7138	1.646
.75925	.0235	2.247	.81724	.3184	1.723	.89571	.7173	1.661
.75960	.0253	2.176	.81794	.3219	1.751	.89710	.7244	1.601
.75995	.0271	2.083	.81863	.3254	1.760	.89780	.7280	1.601
.76030	.0288	2.025	.81932	.3289	1.726	.89849	.7315	1.614
.76064	.0306	1.978	.82002	.3325	1.705	.89884	.7333	1.639
.76099	.0323	1.966	.82141	.3396	1.693	.90266	.7527	1.682
.76134	.0341	1.959	.82210	.3431	1.716	.90335	.7562	1.636
.76168	.0359	1.939	.82280	.3466	1.704	.90405	.7598	1.595
.76203	.0376	1.914	.82349	.3501	1.706	.90474	.7633	1.607
.76238	.0394	1.893	.82696	.3678	1.730			

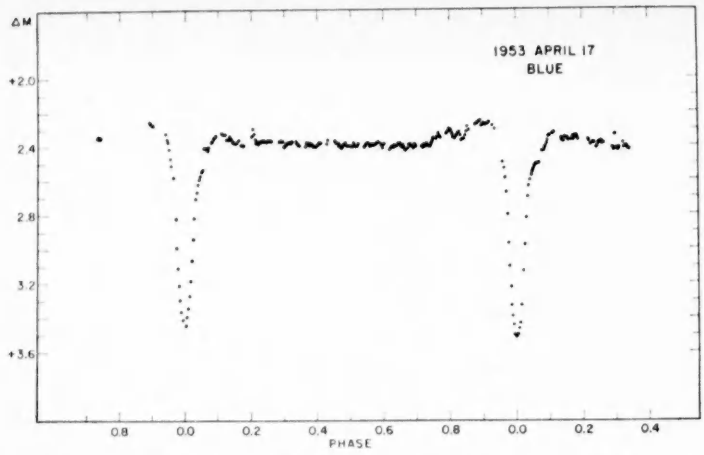

FIG. 1.—Photometric observations of UX UMa. The ordinate is the magnitude difference, UX UMa *minus* BD+52°1722, reduced to no atmosphere. The abscissa is the phase computed from zero phase = Minimum = JD 2427341.2221 + 0^d19667137 9*E*.

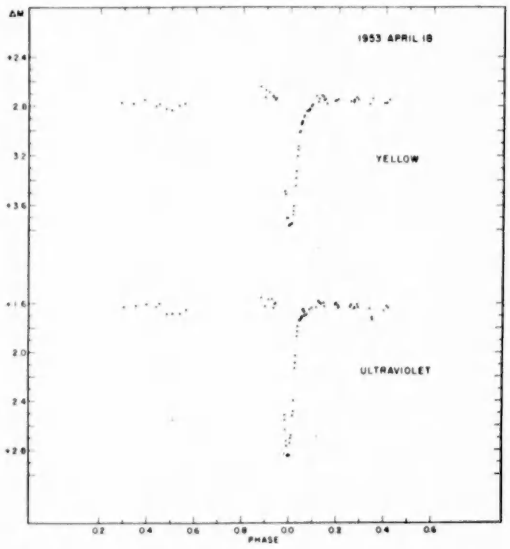

FIG. 2.—Photometric observations of UX UMa. Ordinate and abscissa as in Fig. 1

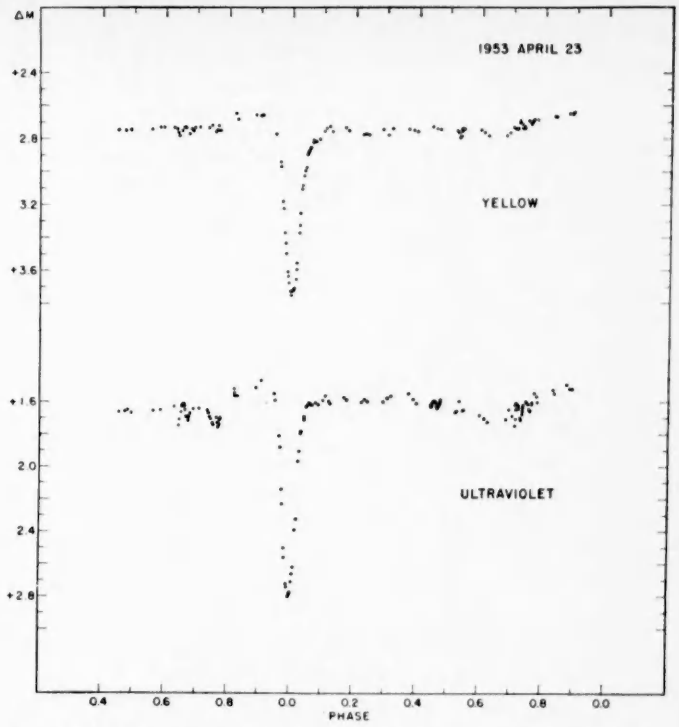

FIG. 3.—Photometric observations of UX UMa. Ordinate and abscissa as in Fig. 1

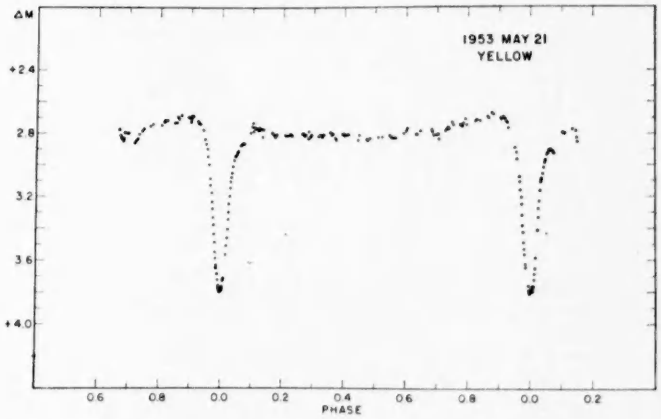

FIG. 4.—Photometric observations of UX UMa. Ordinate and abscissa as in Fig. 1

The light-curves show clearly the short-period, intrinsic fluctuations discovered by Linnell. Their lengths range between 1 and 20 minutes, and their amplitudes (in the ultraviolet) between 0.01 and 0.18 mag. Their amplitude in yellow light is about 0.4 as large as in ultraviolet. Fluctuations shorter than about 1 minute in length may be present, but very quick changes such as these tend to become indistinguishable from variations due to seeing. These rapid changes occur throughout the cycle, but there may be a tendency for the largest to fall between phases 0.4 and 0.9*P*.

Another feature of the light-curve brought out by the present investigation (and also pointed out by the McDonald workers) is a gradual decrease in the light of the star from

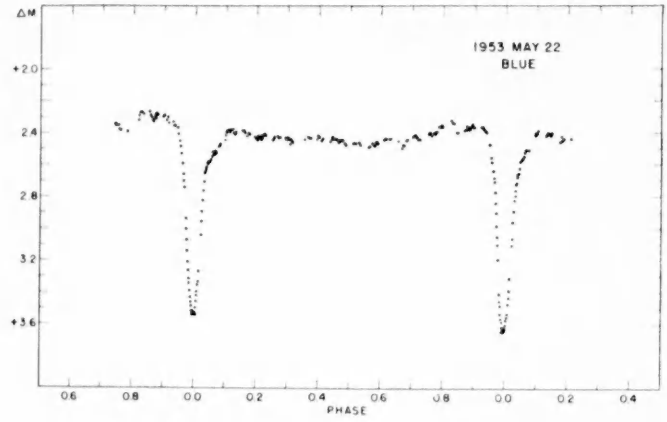

FIG. 5.—Photometric observations of UX UMa. Ordinate and abscissa as in Fig. 1

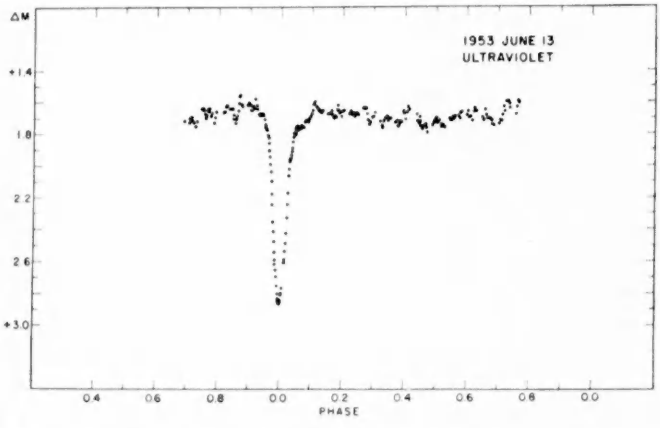

FIG. 6.—Photometric observations of UX UMa. Ordinate and abscissa as in Fig. 1

phase 0.19 until 0.73P, when the shoulder preceding eclipse begins. No secondary minimum has been detected.

The depth of primary minimum, measured from the light-level between phases 0.2 and 0.4P, is about 1.0 mag. in the yellow, 1.1 mag. in the blue, and 1.2 mag. in the ultraviolet. The depth of minimum is not always the same, even for two successive cycles. Examples are the light-curves of May 21 and June 14 in the yellow and the two minima observed on May 22 in the blue.

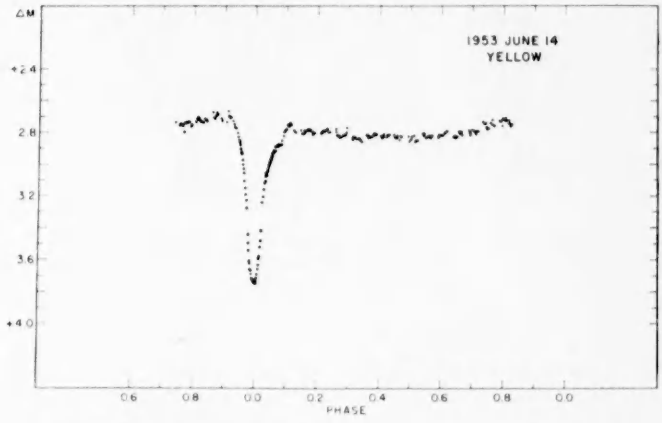

FIG. 7.—Photometric observations of UX UMa. Ordinate and abscissa as in Fig. 1

TABLE 4

OBSERVED MINIMA OF UX URSAE MAJORIS

Helioc. JD 2434+	O−C (Day)	Color	Helioc. JD 2434+	O−C (Day)	Color
484.71988	−0.00005	B	518.7438	−0.0003	Y
484.91650	− .00010	B	518.9409	+ .0001	Y
485.89956	− .00040	Y	519.72732	− .00011	B
485.89973	− .00023	UV	519.92399	− .00011	B
490.81668	− .00006	UV	541.75455	− .00008	UV
490.81674	0.00000	Y	542.73792	−0.00006	Y

The observed times of minimum light are listed in Table 4, together with the residuals from the elements given earlier, in the sense of observed *minus* predicted date. The largest residual is only 0.0004 day. The large residuals, which have been reported elsewhere (Walker 1953), were obtained by measuring the times of minimum light directly on the original Brown potentiometer sheets; they have not been substantiated by the complete reduction of the observations. Most of the large residuals result from asymmetries and disturbances of the lower portion of the light-curve at primary minimum, which changes from cycle to cycle. It is not clear whether these irregularities have the same origin as the short-period fluctuations observed outside eclipse. The present re-

sults are not adequate to confirm or deny the existence of the variation in the time of minimum light with wave length, found by Johnson and his co-workers.

If the color of UX UMa between phases 0.2 and 0.4P is regarded as normal, then the two-color light-curves of April 18 and April 23 reveal the following ultraviolet-yellow color variations:

1. As already mentioned, the star is redder than normal during primary eclipse, between phases 0.98 and 0.02P.

2. The observations of April 23 indicate that the star was redder than normal between phases 0.4 and 0.9P. This result is probably connected with the presence of large intrinsic light-fluctuations during this interval. As already mentioned, these fluctuations have about 0.4 the range in the yellow that they exhibit in the ultraviolet. Within this phase interval, the star appeared reddest during the minima of the rapid variations.

3. The ultraviolet brightness of the star is greater than normal between phases 0.03 and 0.09P, during the asymmetric portion of the ascending branch of primary minimum. Maximum ultraviolet brightness coincides with the occurrence of the stillstand between phases 0.05 and 0.07P.

4. The color is normal on the shoulder after eclipse and at the top of the shoulder before eclipse.

Because of the peculiarities of the light-curve, it does not seem worth while at this time to attempt to improve upon the solution that was made by Linnell for the geometrical elements of the eclipsing system.

II. SPECTROSCOPIC OBSERVATIONS

The first published spectroscopic observations of UX UMa were made by G. P. Kuiper (1941), who described the spectrum as that of "a subdwarf primary with very faint lines of type B3." A later low-dispersion spectrogram taken by O. Struve (1945) showed "only broad H absorption lines." A spectrogram taken by N. U. Mayall in 1948 with the same spectrograph that was used in the present investigation shows only a featureless early-type continuous spectrum. This plate was exposed at phase 0.24P.[1] A new series of nine spectrograms was obtained by Struve (1948)[2] with a dispersion of 330 A/mm at $H\gamma$, and our knowledge of the spectroscopic properties of the system has rested, up to the present time, upon Struve's brief discussion of these observations.

The new Lick observations were made with the nebular spectrograph of the Crossley reflector, which gives a dispersion of 430 A/mm at $H\gamma$. The emulsion used was Eastman IIa-O, baked for 3 days at 50° C. In order to secure as complete a record as possible of any transient changes that might take place in the spectrum of UX UMa, the star was moved once, slowly and uniformly, along a long slit at the proper rate to produce a well-exposed spectrogram. The uniform motion was produced with the aid of a moving wire in the guiding eyepiece. This wire was advanced by a micrometer screw a small distance every 2 minutes, and a guide star was kept on this moving intersection. It would have been possible to obtain the spectrum of an entire cycle, with good time resolution, on a single spectrogram. In order to cut down the contribution of sky radiations, however, three separate exposures, each 90–100 minutes in length and about 0.65 mm wide, were used to cover each cycle. The three spectra were combined in printing (see Figs. 8 and 9) to produce a nearly continuous record of the spectroscopic changes of UX UMa over an interval of almost 5 hours. This method of observing has, in addition to the advantage of nearly continuous recording, the feature of making visible weak lines that might not be seen on narrower spectra. Sixteen spectrograms were obtained on seven nights in

[1] The phases in this section are computed from the elements of Johnson, Perkins, and Hiltner that were used in Sec. I.

[2] Reproductions of Struve's spectrograms have been published by A. P. Linnell (1949).

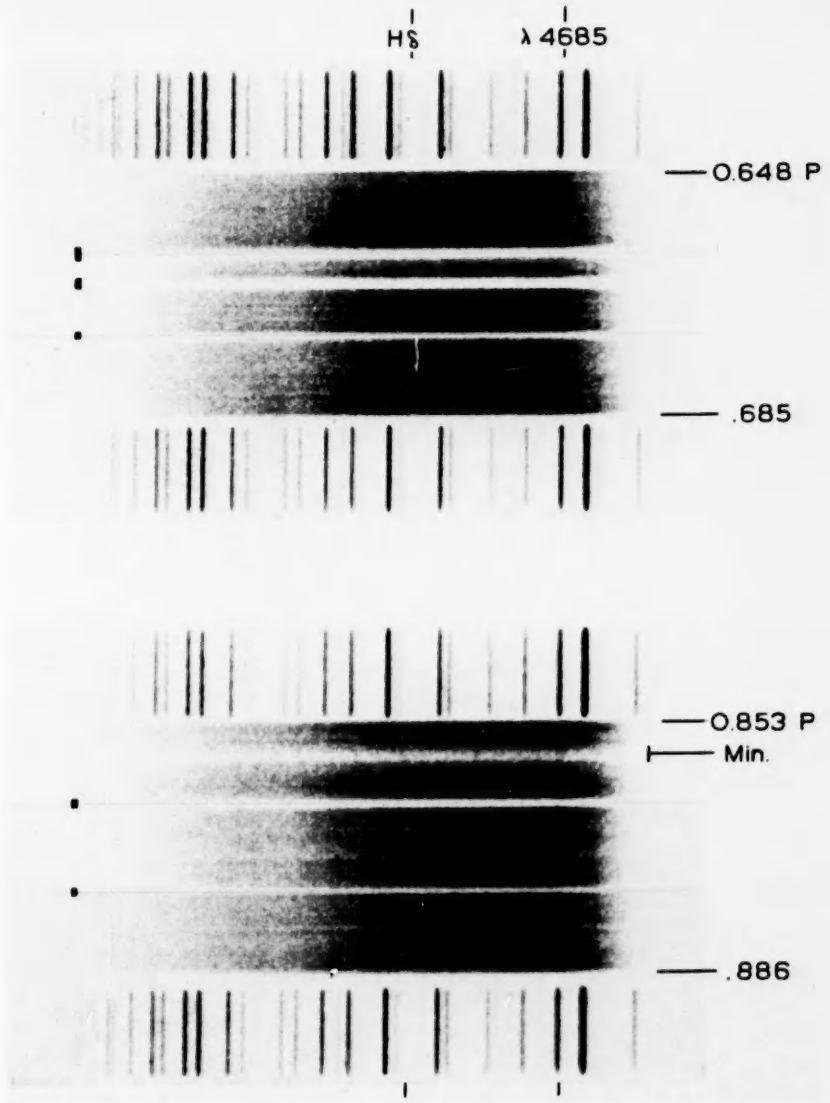

FIG. 8.—The spectrum of UX Ursae Majoris. *Above:* The spectrum on April 15, 1953, beginning at phase 0.648P at the top and continuing with a constant time scale to phase 0.685P in the following cycle, at the bottom. The black marks near the left edge indicate gaps in the spectrum that were caused by actual interruptions of the exposure. Most of the other horizontal streaks were caused by guiding irregularities. The depression at λλ 3750–3850 is at least partly spurious (see text). *Below:* The spectrum on May 11, 1953, arranged and marked in the same manner. *Min.* marks the position of primary minimum.

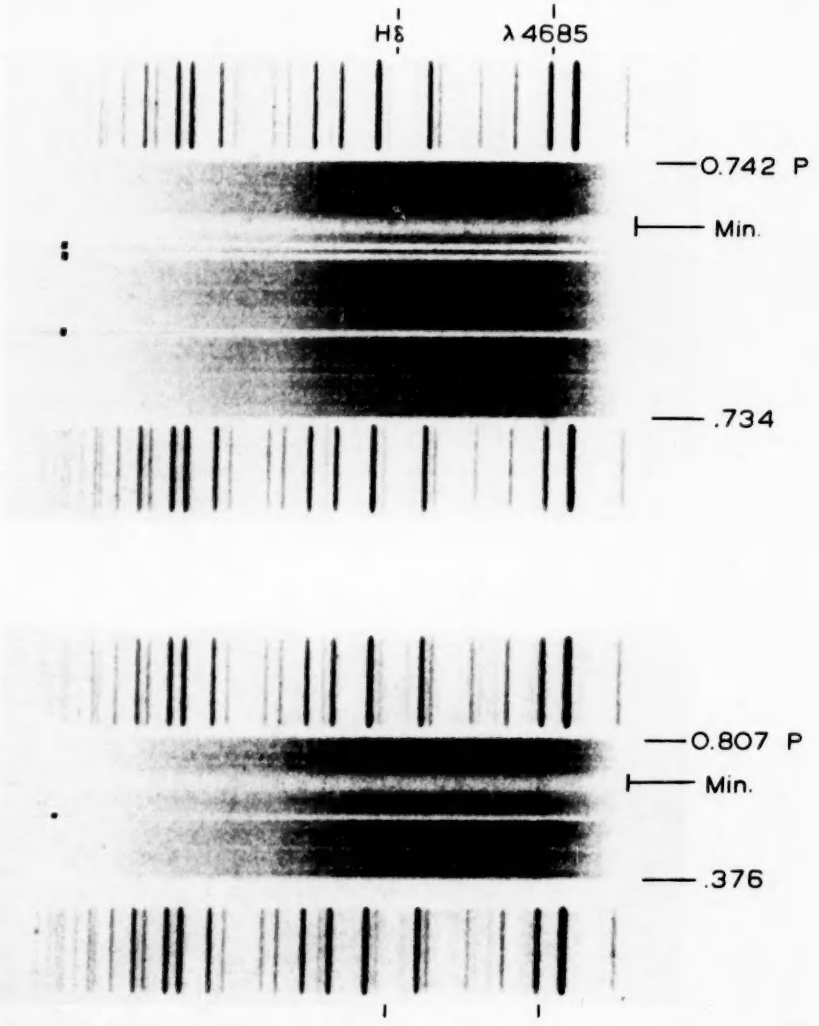

FIG. 9.—The spectrum of UX Ursae Majoris. *Above:* The spectrum on June 13, 1953, beginning at phase 0.742*P* at the top and continuing with a constant time scale to phase 0.734*P* in the following cycle, at the bottom. The black marks near the left edge indicate gaps in the spectrum that were caused by actual interruptions of the exposure. Most of the other horizontal streaks were caused by guiding irregularities. *Min.* marks the position of primary minimum. The depression at λλ 3750–3850 is, at least partly, spurious (see text). *Below:* The spectrum on June 14, 1953, arranged and marked in the same manner.

April, May, and June, 1953, with this technique, and the details of these observations are given in Table 5.

The continuous spectrum of UX UMa is that of a rather blue star: on plates exposed properly for the photographic region, the continuum extends well to shortward of λ 3500. Rather weak emission of variable intensity is present at $H\beta$ for most of the cycle; but the most conspicuous, as well as the most nearly permanent, line feature on the Lick spectrograms is *He* II λ 4685 in emission. Unless the spectrum of UX UMa has changed, it is remarkable that λ 4685 was not seen by the earlier spectroscopic observers. Broad, very shallow absorption lines can usually be seen at $H\gamma$, $H\delta$, and $H\epsilon$ throughout

TABLE 5

SPECTROGRAPHIC OBSERVATIONS OF UX URSAE MAJORIS

Plate No.	UT (Geocentric)		JD (Heliocentric) 2434000+	Phase (Periods)
	Date 1953	Exposure		
CS-1485	Apr. 15	4^h21^m–5^h54^m5	482.684–.749	0.648–0.979
1486*a*		6 04.5–7 38	482.756–.821	.014–.345
1486*b*		7 42 –9 15	482.824–.888	.360–.685
1492*a*	May 11	4 24 –5 56	508.685–.749	.853–.179
1492*b*		6 02 –7 37.5	508.753–.820	.199–.540
1493		7 41 –9 16.5	508.822–.888	.550–.886
1496*a*	May 16	5 29.5–6 59	513.730–.792	.505–.821
1496*b*		7 08 –8 39.5	513.798–.862	.851–.176
1498	May 17	6 42 –8 15.5	514.780–.845	.844–.175
1500*a*	June 5*	5 00 –6 31.5	533.708–.772	.086–.411
1500*b*		6 35.5–8 07	533.775–.838	.427–.747
1502*a*	June 13†	4 53.5–6 25	541.704–.767	.742–.063
1502*b*		6 28 –7 59.5	541.769–.833	.073–.399
1503		8 02.5–9 34	541.835–.899	.409–.734
1504*a*	June 14‡	4 48.5–6 18	542.700–.762	.807–.122
1504*b*		6 20 –7 29.5	542.764–.812	0.132–0.376

* Clouds. McDonald photoelectric observations. † Mount Wilson photoelectric observations.

‡ McDonald and Mount Wilson photoelectric observations.

most of the cycle, except for a short time after minimum light, when they are very weak or absent. During the later phases of some cycles, narrow absorption lines were observed at the higher *H* lines.

The variation of the spectrum through the eclipse cycle, which was discovered by Struve, is not always the same. Therefore, a condensed description of the changes of several spectral features throughout the individual cycles is given in Table 6. In this table, a solid horizontal rule crossing a single column indicates that the corresponding phase is better defined than is one marked by a dotted line. The heavy rules completely across the table at top and bottom indicate the phases when the observations began and ended, respectively. The cycles are designated by their numbers in the equation of Johnson, Perkins, and Hiltner for the time of minimum.

The observations described in Table 6 lead to the following conclusions:

1. The spectrum of UX UMa varies throughout the 0.197-day eclipse cycle, but, al-

though the details of this variation are not the same in every cycle, the general pattern is similar.

2. The narrow *H* absorption lines of high quantum number (*H*8 and higher) were found in about half the cycles observed. They appear first at phases approximately midway in the cycle. They persist until minimum light, after which they have always disappeared. The very wide, shallow *H* absorption lines, seen best at *Hδ*, are usually visible for most of the cycle except at phases just following minimum light. These broad lines have been seen or suspected every cycle, and they do not seem to be affected by the appearance or nonappearance of the lines of higher quantum number. It is likely that the two sets of features have, in general, different places of origin: the wide lines probably

TABLE 6

VARIATIONS IN THE SPECTRUM OF UX URSAE MAJORIS

APRIL 15, 1953: $E = 36311\text{–}2$*

PHASE (PERIODS)	*Hβ* EMISSION	λ 4685 EMISSION	*H* ABSORPTION		λ 4471 ABSORPTION
			Hδ	*H*8–*H*10	
0.648					
0.7–	Faintly present	Faint	Fairly strong, wide	Fairly strong	Present
0.8–					
0.9–					
0.0–	Minimum				
0.1–	Faintly present	Faint		Absent	Present?
0.2–					
0.3–	Increase in strength	Increase in strength	Faintly present; wide, shallow	*H*8 present	
0.4–					Present
0.5–				Present?	
0.6–	Fairly strong	Fairly strong			
0.685					

* Minimum was missed while plateholders were being changed and the focus of the star on the slit checked. The K line of Ca II was present in absorption from phase 0.2 to 0.7*P*. Weak emission to shortward of λ 4685 was present from about phase 0.7 to 0.3 or 0.4. These spectrograms are reproduced in the upper part of Fig. 8.

TABLE 6—*Continued*

MAY 11, 1953: $E = 36443.4$†

Phase (Periods)	*Hβ* Emission	λ 4685 Emission	*H* Absorption		λ 4471 Absorption
			Hδ	*H*8–*H*10	
0.853					
0.9—	Weakly present?	Strong, diffuse	Present	Present	Present
0.0—			Minimum		
0.1—			Probably absent	Probably absent	
0.2—	Very weak				
0.3—					
0.4—		Strong			
0.5—		Diffuse	Faintly present; wide, shallow	Faint	Faintly present
0.6—					
0.7—	Fairly strong				
0.8—		Diffuse			
0.886					

† For about 10 minutes while the variable was near the bottom of primary minimum, the continuous spectrum was too faint to register and only the rather diffuse emission lines *Hβ* through *Hε* (and possibly *H*8 and *H*9 as well) and λ 4685 were visible. The presence of very weak emission to shortward of λ 4685 was suspected from 0.2 to 0.4*P*, and perhaps later. These spectrograms are reproduced in the lower part of Fig. 8.

TABLE 6—*Continued*

MAY 16, 1953: $E = 36469.70$‡

Phase (Periods)	$H\beta$ Emission	λ 4685 Emission	*H* Absorption		λ 4471 Absorption
			$H\delta$	$H8$–$H10$	
0.505					
0.6—					
0.7—	Weak	Moderately strong; diffuse	Faintly present; wide	Very faint or absent	Absent
0.8—					
0.9—	Very weak or absent		Present?		Present?
0.0—	Minimum				
0.1—	Present?	Moderately strong	Very faint or absent	Absent	(Plate defect)
0.176					

‡ At minimum light, $H\beta$, $H\gamma$, and λ 4685 were weakly present in emission. A bright line may have been present to shortward of λ 4685 just preceding and following minimum.

MAY 17, 1953: $E = 36474.5$§

Phase (Periods)	$H\beta$ Emission	λ 4685 Emission	*H* Absorption		λ 4471 Absorption
			$H\delta$	$H8$–$H10$	
0.844					
0.9—	Very faint or absent	Moderately weak	Present; wide	Present	Absent
0.0—	Minimum				
0.1—	Weak	Moderately weak; diffuse?	Present?	Absent	Faintly present?
0.175					

§ At minimum light, λ 4685 was, as usual, the strongest emission line, followed by $H\beta$, $H\gamma$, and $H\delta$. Emission was present to shortward of λ 4685 from about phase 0.9*P* to just before minimum.

TABLE 6—*Continued*

JUNE 5, 1953: $E_c = 36571$

Phase (Periods)	*Hβ* Emission	λ 4685 Emission	*H* Absorption		λ 4471 Absorption
			*H*δ	*H*8–*H*10	
0.086					
0.2—	Weak	Moderately strong	Very faint	Absent	Fairly strong
0.3—					Weak
0.4—					
0.5—		Weak	Faint, wide		
0.6—	(Plate defect)	Medium strength			Absent
0.7—					
0.747					

TABLE 6—*Continued*

JUNE 13, 1953: $E = 36611.2$[1]

Phase (Periods)	*Hβ* Emission	λ 4685 Emission	*H* Absorption		λ 4471 Absorption
			Hδ	*H*8–*H*10	
0.742					
0.8—	Weak	Strong	Faint, wide	Weak	Faintly present?
0.9—					
0.0—	Minimum				
0.1—	Weak				
0.2—			Faint		
0.3—	Increase in strength	Strong			Faintly present
0.4—				*H*8 present	
0.5—	Strong	Diffuse	Moderately strong; wide		
0.6—					Probably absent
0.7—	Moderately strong	Strong			
0.734					

[1] The *He* II line λ 4685 and the *H* lines from *Hβ* to *H*8 are in emission at minimum light. Emission to shortward of λ 4685 was present after about phase 0.8*P*, through minimum, and probably after minimum as well. These spectrograms are reproduced in the upper part of Fig. 9.

TABLE 6—*Continued*

JUNE 14, 1953: $E = 36616.7$#

Phase (Periods)	$H\beta$ Emission	λ 4685 Emission	*H* Absorption		λ 4471 Absorption
			$H\delta$	$H8$–$H10$	
0.807					
0.9—	Absent	Moderately weak	Very wide, shallow	Fairly strong	Faint
0.0—	Minimum				
0.1—	Absent	Moderately weak	Faintly present?	Absent	Moderately strong
0.2—	Very faintly present	Diffuse			
0.3—			Absent		
0.376					

λ 4685 is fairly strong in emission at minimum light, while the bright Balmer lines $H\beta$ through $H\epsilon$ or $H8$ appear only faintly. These spectrograms are shown in the lower part of Fig. 9.

originate in the primary star, while the ultraviolet lines may be produced in an extended envelope, as was suggested by Struve.

3. Of all the spectral features studied, bright *He* II λ 4685 most nearly maintains a constant intensity throughout the cycle, but it is stronger in some cycles than in others. Compare, for example, the upper and lower panels of Figure 8.

4. No obvious pattern for the intensity variations of the $H\beta$ emission line has been discovered, except that the line has a tendency to be stronger at intermediate phases (0.4–0.7*P*) than it does in the neigborhood of minimum light.

5. The somewhat diffuse emission spectrum observed at minimum light (λ 4685 is the strongest line, followed by the *H* lines) has a much slower Balmer decrement than that observed outside eclipse. It is unlikely that the spectrum at minimum could be produced from that just before eclipse simply by removing the continuous spectrum of the primary star.

The spectrograms taken on nights when simultaneous Mount Wilson or McDonald photoelectric observations were also available have been examined in an effort to detect any spectral changes that might be correlated with the "flares" observed in the light-curve. Only one very tentative correlation could be found: there is some reason to suspect that the seemingly erratic widenings of the λ 4685 emission line may occur at about the same time as the flares in the light-curve. Unfortunately, the present material is too scanty to make possible a firm statement. If this association of λ 4685 width with short-lived maxima in the light-curve is real, it is very reminiscent of the phenomenon of "nitrogen flaring" observed in certain novae during their decline in light (Wright 1930). In novae, the flaring affects *He* II λ 4685 as well as the fluorescent *N* III lines, and it is associated with temporary increases in the light of the star, as is suspected to be the case in UX UMa.

A word of caution must be inserted with regard to the spectra of UX UMa reproduced

in Figures 8 and 9. Test exposures of artificial light-sources having continuous spectra have been obtained with the Crossley nebular spectrograph, after the light was first reflected from the primary mirror. These spectrograms show the presence of a wide, very shallow absorption band lying approximately between λ 3750 and λ 3850. The wide absorption shown at about this position in the spectra of UX UMa seems to be somewhat stronger than in the test exposures which may be due to reinforcement in the star by the overlapping wings of broad *H* lines. Nevertheless, there can be little doubt that the conspicuous depression in the near ultraviolet, seen in Figures 8 and 9, is, to a large extent, of instrumental or photographic origin.

The Lick spectrograms were not intended for the determination of the radial velocity

TABLE 7

RADIAL-VELOCITY MEASUREMENTS OF UX URSAE MAJORIS

Plate No.	Phase Interval (Periods)	*Hβ* Emission (Km/Sec)	λ 4685 Emission (Km/Sec)	*H* Absorption Lines (Km/Sec)
CS-1485	0.65–0.81	—	—	+440 *Hε*, *H*8, *H*10
	.81– .98	—	+260:*d*	+430 *Hε*, *H*8, *H*9, *H*10
1486*a*	.24– .34	−140	+150:*d*	+360 *H*8
1486*b*	.36– .47	—	−210	—
	.47– .58	—	− 80	—
	.58– .68	−460	−190:	—
1492*a*	.85– .98	—	−480:*d*	+430 *H*8, *H*9
	.98– .02	—	− 50:	—(*Hγ*, *Hδ* emission = +20 km/sec)
	.02– .18	−130	−250	—
1492*b*	.20– .30	—	+ 60:*d*	—
	.30– .40	−170:	+ 60	+430: *H*8*
	.40– .54	−440	− 50	+350 *H*8, *H*9, *H*10
1493	.55– .66	−360	+180:*d*	+300? *Hε*
	.66– .77	− 30	−280:	—
	.77– .89	—	−750?*d*	+440 *Hε*, *H*9
1496*a*	.50– .61	−170	—*d*	—
	.61– .71	+200:	−500	—
	.71– .82	+100:	−210:*d*	—
1496*b*	.85– .98	—	+270:*d*	—
	.98– .02	—	−210:	—
	.02– .18	—	− 50:*d*	—
1498	.84– .98	—	+400	+260: *H*8
	.98– .02	—	+ 40:	—(*Hγ* emission = +90 km/sec)
	.02– .18	+ 20	—	—
1502*a*	.74– .85	—	+140:*d*	+420 *Hε*, *H*8, *H*9, *H*11
	.85– .98	—	+ 60	—
	.98– .02	−130:	+ 70:	—(*Hγ*, *Hδ*, *Hε*, *H*8 emission = −90 km/sec)
1502*b*	.10– .22	—	+340:	—
	.22– .30	—	+160:*d*	—
	.30– .40	—	+300	—
1503	.41– .55	−440	−200:*d*	—
	.55– .73	−150	−250	—
1504*a*	.81– .98	—	—	+250: *H*8
	.98– .02	—	—	—
	.02– .12	—	−210:	—
1504*b*	.13– .25	—	−360:	—
	0.25–0.38	—	−670?*d*	—

* *H*8 phase, 0.37–0.42.

of UX UMa, because it was felt that the present observational technique, which involved only one passage of the star along the slit, might introduce guiding error into the radial velocities. Observations of early-type stars of constant velocity with the same technique, however, have failed to reveal any serious systematic errors ascribable to this procedure. Nevertheless, the unusual character of the radial-velocity results for UX UMa makes it desirable that they be independently confirmed.

The spectrum of UX UMa is very difficult to measure for radial velocity, because of the weakness of its features. This fact, coupled with the low dispersion that had to be

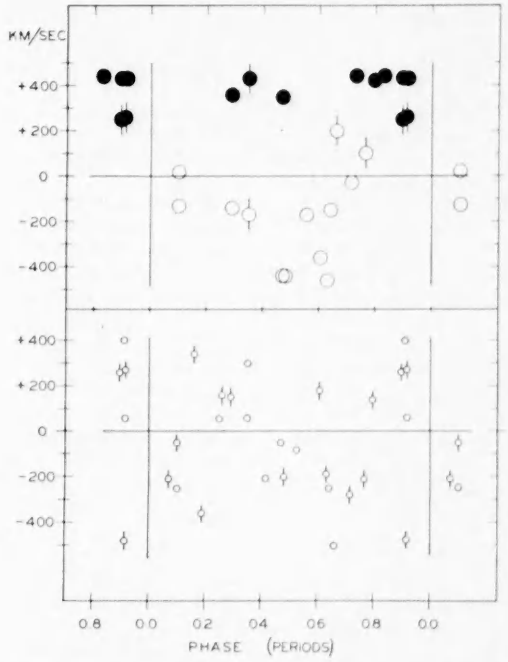

FIG. 10.—Radial velocities measured in the spectrum of UX Ursae Majoris. In the upper panel, the open circles represent the velocities obtained from the $H\beta$ emission line, while the filled circles indicate the velocities measured for the high-quantum number H absorption lines. The smaller open circles in the lower panel show the velocities obtained from the *He* II λ 4685 emission line. In both panels, a vertical bar through a point indicates a measurement of lower weight. The sizes of the circles and the length of the vertical bars are not intended to correspond to the uncertainties of the velocities in either panel.

used (on the present plates, at $H\beta$ a displacement of 1 μ corresponds to a velocity of 39 km/sec), is responsible for the very low precision of the velocities. Only three features could be measured with any consistency: emission $H\beta$, λ 4685, and the high H absorption lines. The very wide, shallow features observed at $H\gamma$, $H\delta$, and $H\epsilon$ were too indefinite for velocity determination. In Table 7, a dash indicates that the corresponding line was unmeasurable or not seen. A colon follows velocities of lower weight than those not so indicated, and a *d* in the column for λ 4685 indicates that the line was not well defined at that time. The data of Table 7 are plotted in Figure 10.

If the velocities are taken at their face value, then these conclusions may be drawn from the data:

1. The displacements of the *Hβ* emission line suggest a velocity variation with a minimum at phase 0.5 or 0.6*P*. Unfortunately, this line is usually quite faint between phase 0.8*P* and minimum light; this fact accounts for the lack of measures in that interval, which would be of great value in establishing the reality of the velocity variation.

2. The displacements of the *H* absorption lines of higher quantum number (*H*8–*H*11, and sometimes *Hε*) correspond to an approximately constant velocity of +350 to +400 km/sec. The real uncertainty of these velocities is much larger than one would infer from the rather small dispersion about their mean.

3. Much of the scatter in the displacement of λ 4685 is due to its frequently diffuse character. There is no conspicuous regularity to its velocity variation, but there may be a tendency for its displacement to change in approximately the same way as does that of the *Hβ* emission line.

It is difficult to assign a spectral type to the primary component of UX UMa because significant features in its spectrum undergo interference from other lines that should not be considered in the classification. For example, the radial-velocity evidence shows that the high *H* absorption lines are not formed in the primary star, and hence they must be disregarded. It is of interest that, on some occasions, a very weak emission has been observed shortward of λ 4685. This emission probably is a blend of the *N* III lines at λλ 4634–4641, although an identification with *C* III λλ 4647–4651 cannot be ruled out. On some plates there is also an apparent emission line near λ 4525. A similar feature at that wave length, found on low-dispersion spectra of stars of spectral type near O6, is apparently a gap between weak absorption lines. Therefore, the spectrum of UX UMa resembles that of an Of star with bright *Hβ*; but, since the radial-velocity information has not served to demonstrate clearly an association of the *He* II emission with the primary star, the f designation is only tentative. The lack of a conspicuous Balmer jump and the weakness of the wide *H* lines are, however, in harmony with a classification of the primary star as of type O rather than early B. The assignment to type O is substantiated by the presence of the high-excitation lines of *He* II and, probably, *N* III; for, whether they originate immediately in the primary component or not, that star probably is the source of their excitation.

III. INTERPRETATION AND DISCUSSION

Possible interpretations of the features of the light-curve of UX UMa have been discussed by Linnell. He suggested that the bright shoulder on the light-curve between phase 0.7*P* and primary minimum and the lesser (in 1953) shoulder following minimum were due either to a hot spot on the primary star or to a luminous region some distance above its surface. We propose to discuss and extend the second possibility in the light of the more extensive information now available. We advance for consideration an interpretation of the observational features of UX UMa in terms of the model shown schematically in Figure 11. For lack of better information, the relative dimensions and masses of the components that were used in the construction of Figure 11 are those determined by Linnell; but, in view of the difficulty in discussing the peculiar light-curve of this variable and doubt as to the applicability of the ordinary mass-luminosity relationship, these values may very well not be correct. If the hump preceding minimum light is due to the presentation at the most favorable aspect of a mass of hot material situated well above the surface of the primary and (in 1953) located asymmetrically with respect to the line joining the two stars, then the asymmetry on the rising branch of primary minimum between phases 0.03 and 0.10*P* is due to the occultation of this bright region by the fainter star. The phase of the asymmetry shows that the bright region must effectively lie about 1 radius above the surface of the primary, as was pointed out by Linnell. The extension of the bright region in the direction perpendicular to the orbit plane may vary, so that

the only correlation to be expected between the intensity of the shoulders and that of the asymmetry is that the asymmetry should never occur unless the bright shoulders are present; but the converse may not always be true.

It is clear that the radiation of the postulated hot cloud is essentially continuous with wave length, for the spectra show that only the continuum grows stronger just before minimum (see especially Fig. 9, *top*), and there is no enhancement of the bright lines at this phase. The sudden appearance at about phase $0.7P$ of the contribution of this bright region must be due, not to its appearance from behind the disk of the brighter star, but

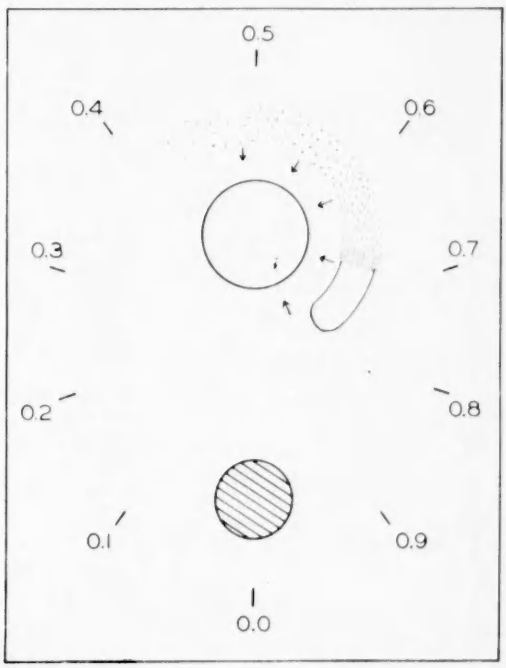

FIG. 11.—Schematic diagram of proposed model of the system of UX Ursae Majoris. The relative dimensions and separation of the components correspond to the elements of Linnell; the disk of the fainter star is shaded. The stippled portion of the cloud near the primary star is cooler than the part not so marked. The arrows indicate material falling into the bright star from the cloud. Phases are indicated around the edges of the diagram and are in units of the period.

rather to its being uncovered by an extensive region of cooler gas that is seen projected upon the disk of the primary at earlier phases. After minimum, the bright region is occulted by the secondary component, and the anomalous ultraviolet brightness of the system at this phase may be explained if we suppose that the color of the bright cloud is redder than that of the primary star. The less favorable aspect of the bright region after minimum would explain the smaller shoulder following eclipse.

In this picture, the cooler mass of gas that hides the hot region until phase $0.7P$ may also be responsible for the gradual reddening of the system between about 0.4 and $0.9P$, and it is presumed to be associated with the gas that produces the high-quantum number

H absorption lines. This cooler cloud may merge continuously with the hotter, and both are shown as parts of a continuous arc in Figure 11. Certainly, as one considers regions of the cooler cloud that are projected upon the disk at earlier phases, the blocking effectiveness of the cloud decreases until its last vestiges, the high *H* absorption lines, are only occasionally seen at phases earlier than about 0.4 or 0.5*P*. The large positive displacement of these lines (+350 to +400 km/sec) suggests that they are produced by cool gas descending from the surrounding cloud to the primary star.

The facts that the bright *Hβ* line usually is strongest between phases 0.4 and 0.7*P* and that its velocity variation reaches a minimum value near phase 0.6*P* indicate that the *Hβ* emission originates somewhere in that portion of the arc of cool gas that is approaching the observer at phase 0.6*P*. It may be that some contribution to *He* II λ 4685 is produced in the same region, but the rather small variation of the strength of λ 4685 with phase suggests that it must, in general, be of more widespread origin. The process responsible for the maintenance of the luminous region apparently does not operate smoothly, as shown by the changes in the spectrum and light-curve in different cycles. The possibility of a considerable change in the nature or location of the luminous region is indicated by the existence of abnormal cycles such as that whose light-curve was observed by Johnson *et al.* on May 29, 1952. A more gradual change in the characteristics of the hypothetical gaseous cloud must be responsible for the weakening of the shoulder that follows minimum, and the strengthening of the shoulder that precedes eclipse, which seem to have taken place since Linnell's observations in 1949 (see Sec. I). Finally, we do not believe that it is clear which star is the source of the material in the arc or cloud which we have postulated around the brighter component in order to explain the observations.

REFERENCES

Johnson, H. L.; Perkins, Barbara; and Hiltner, W. A. 1954, *Ap. J. Suppl.*, **1**, 91 (No. 4).
Kuiper, G. P. 1941, *Pub. A.A.S.*, **10**, 206.
Linnell, A. P. 1949, *Sky and Telescope*, **8**, 166.
———. 1950, *Harvard Circ.* No. 455.
Parenago, P. P. 1950, *Peremennye Zvezdy*, **7**, 196.
Struve, O. 1945, *Ap. J.*, **102**, 85, n. 64.
———. 1948, *ibid.*, **108**, 153.
Walker, M. F. 1953, *Carnegie Inst. Washington Yearbook*, **52**, 15.
Wright, W. H. 1930, *Pub. Lick Obs.*, **14**, 88–90 and Pl. VI.

A DETERMINATION OF LOWER LIMITS TO THE ABUNDANCE RATIO OF CARBON 12 TO CARBON 13 IN THE ATMOSPHERES OF G8–K5 GIANT STARS*

JOHN D. SCHOPP
Princeton University Observatory
Received February 15, 1954; revised March 12, 1954

ABSTRACT

An analysis was made of high-dispersion Mount Wilson spectrograms for twenty-eight red giant stars of spectral types of G8–K5. Photoelectric color indices for these stars were measured at the Princeton University Observatory. Depth measurements were made on $C^{12}N^{14}$ lines and on a feature coinciding with an expected $C^{13}N^{14}$ line, all in the 0,0 band of *CN* near λ 3883. When transformed via pseudo-curves of growth, obtained from *Fe* I lines, these depths yielded relative numbers of absorbing molecules, which made it possible to determine for each star a lower limit to the abundance ratio of carbon 12 to carbon 13. These lower limits are conservative and may, in fact, be much lower than the true abundance ratios. Of the twenty-eight stars, only seven yield ratios less than 6.5. These seven stars are all of spectral type K2 or later, and all have relatively weak *CN* strength; hence no useful lower limit to the C^{12}/C^{13} abundance ratio could be obtained for them. For all the remaining twenty-one stars, with sufficient strength in the *CN* band, lower limits greater than 6.5 were found. This is in excess of the equilibrium ratio of 4 or 5 now predicted for matter involved in the carbon cycle. For these stars, which presumably represent normal red giants in general, the conclusion might be drawn that if the carbon cycle has ever operated in the interiors, there has been little or no mixing between the interiors and the atmospheres. In this respect the normal red giants seem to differ from the majority of the R- and N-type stars.

I. INTRODUCTION

The existence of the carbon isotope of mass 13 was first shown by King and Birge (1930) in 1929 from a study of laboratory spectra. Carbon 13 was subsequently identified by Sanford (1929) in the spectra of several R- and N-type giants. A summary of the subsequent research on the abundance of C^{13} has been given by McKellar (1949).

The results this far have indicated that the abundance ratio of C^{12} to C^{13} is certainly not uniform in all sources and that, in fact, it usually seems to fall into one of two main groups. In the cases of all examined terrestrial sources, meteorites, and the sun (Greenstein, Richardson, and Schwarzschild 1950), the ratio is quite high, tending to be of the order of 90 where accurate ratios could be determined, and from 15 to 90 where only a lower limit to the abundance ratio could be set. The other group of C^{12}/C^{13} abundance ratios is consistently small, of the order of 3; these have been found exclusively in the atmospheres of class R- and N-type stars, although not all stars of these types show the low ratios. In 1948, McKellar (1949) investigated the spectra of twenty-one R-type stars and determined the C^{12}/C^{13} abundance ratios from measurements in the 1,0 band of the C_2 molecule near λ 4740. His results indicate quite strongly that either the R-type stars have C^{12}/C^{13} abundance ratios of the order of 3, or else the ratio is not less than 30.

This paper extends the study of C^{12}/C^{13} abundance ratios to normal red giants of spectral types G8–K5. In these stars either the 1,0 band of C_2 is extremely weak, or it is nonexistent; hence the same techniques as those applied by McKellar could not be used. The 0,0 band of the molecule *CN* near λ 3883, however, is sufficiently strong in the red giants, that quantitative results on the abundance ratio have been obtained.

* This research was supported by contract with the Office of Naval Research.

II. OBSERVATIONS AND MEASUREMENTS

Grating spectrograms for the stars listed in Table 1 were obtained at the coudé focus of the 100-inch telescope of the Mount Wilson Observatory during the summer and fall of 1951, with Dr. M. Schwarzschild as guest investigator. A total of 112 exposures on the twenty-eight stars were used. About half that number of additional exposures were rejected, because they had densities unsuitable for photometric purposes. The dispersion

TABLE 1

PROGRAM STARS, COLOR INDICES, AND LOWER LIMITS ON C^{12}/C^{13} RATIOS

NAME	m	SPEC. (ROMAN 1952; MORGAN AND ROMAN 1950)	C.I.$_J$	T_{eff}	$-\log(1-I_{line}/I_{cont})$		$\Delta_{c\ of\ 2}$	Δ_{comp}	LOWER LIMIT C^{12}/C^{13}
					$C^{13}N^{14}$	$C^{13}N^{13}$			
β Aql	3.9	G8 IV	0.870	4871	0.165	0.774	1.71	0.45	18.0
o Tau	4.1	G8 III	0.892	4789	.130	.480	1.74	.45	19.5
γ Psc	3.8	G8 III	0.915	4711	.145	.655	1.82	.46	23.0
η Her*	3.6	G8 III–IV	0.936	4664	.141	.523	1.46	.47	9.8
μ Peg	3.7	K0 III	0.934	4664	.136	.559	1.74	.47	18.5
α^2 Cap	4.1	G9 III	0.937	4649	.140	.535	1.63	.47	14.5
o Psc	4.5	K0 III	0.961	4575	.108	.433	1.62	.48	14.0
ϵ Oph	3.3	G8 III	0.975	4532	.133	.598	1.83	.48	22.5
δ Tau	3.9	K0 III	0.985	4503	.099	.417	1.60	.48	13.0
λ And*	4.3	G8 III–IV	1.008	4447	.217	.774	1.43	.50	8.5
ϵ Cyg*	2.9	K0 III	1.032	4393	.129	.453	1.46	.50	9.1
η Cyg	4.0	K0 III	1.038	4366	.114	.493	1.66	.50	14.5
β Cet	2.2	K0 III	1.038	4366	.140	.448	1.33	.50	6.8
λ Peg	4.1	G8 II–III	1.076	4287	.109	.388	1.49	.52	9.3
η Eri	4.0	K1 III–IV	1.098	4224	.128	.677	1.86	.52	22.0
α Ari*	2.2	K2 III	1.147	4115	.118	.492	1.72	.54	15.0
κ Oph	3.4	K2 III	1.152	4103	.099	.390	1.47	.54	8.5
γ And A	2.3	K2 III	(1.160)	(4080)	.162	.418	1.04	.55	3.1
η Cet	3.6	K2 III	1.167	4068	.118	.442	1.55	.55	10.0
β Oph	2.9	K2 III	1.166	4068	.103	.372	1.42	.55	7.4
109 Her	3.9	K2 III	1.180	4034	.127	.506	1.58	.55	10.5
ι Cet	3.8	K2 III	1.218	3956	.132	.450	1.39	.56	6.8
δ And	3.8	K3 III	1.267	3860	.143	.452	1.28	.59	4.9
α Sct	4.1	K3 III	1.314	3768	.155	.372	1.07	.60	3.0
π Her	3.4	K3 II	1.414	3571	.180	.490	0.95	.64	2.0
ι Aur*	2.9	K3 II	1.494	3418	.233	.529	0.83	.67	1.4
γ Aql	2.8	K3 II	1.499	3410	.203	.535	1.00	.67	2.2
α Tau	1.1	K5 III	1.513	3385	0.331	0.596	0.48	0.68	0.6

* Indicates a standard star for the color program. The C.I. for And A, indicated by parentheses, was taken from Becker (1933).

used was 10.3 A/mm, and Eastman IIa-O emulsion was used for all exposures. The spectrograph slit-width was set to correspond to 0.016 mm on the plate, and a uniform density over a width of about 0.18 mm was obtained by trailing. Exposure times of the calibration-step spectra were selected so that they differed from the effective stellar exposures by less than a factor of 3. The calibration optics was carefully collimated and checked every night for uniformity.

Four exposures were taken for each star, two to cover the "band region" from λ 3920 to λ 3870 and two to cover the "iron-line region" from λ 4100 to λ 3980. The two regions could not be covered with the same exposures because of the rapid decrease in intensity of the radiation from the G and K giants in the deep blue and ultraviolet. Most of the exposure times for the band region ran from 4 to 30 minutes, and for the iron-line region from 2 to 15 minutes.

All plates were registered on the microdensitometer of the Mount Wilson Observatory. A slit-width was chosen to correspond to about 0.005 mm on the plate, and a magnification of 100 was used. The iron-line region and the band region were covered by separate

TABLE 2

Fe I LINES

λ	Mult. No. (Moore 1945)	E.P.	$\log (x_0/p_e)_\odot$ (Bell 1951)	$\log (x_0/p_e)_{4000}$
4091.56	357	2.82	+0.71	−0.71
90.96	695	3.35	+0.57	− .52
89.23	422	2.94	+0.73	− .62
88.57	906	3.62	+0.68	− .68
87.10	694	3.32	+1.00	− .42
84.50	698	3.32	+1.80	+ .23
80.88	557	3.28	+0.52	− .64
80.22	558	3.27	+0.96	− .48
79.85	359	2.85	+1.05	+ .33
73.77	558	3.25	+1.08	− .26
70.78	558	3.23	+1.41	+ .23
67.99	559	3.20	+1.69	+ .63
67.28	217	2.55	+1.43	+ .54
66.99	358	2.82	+1.99	+ .54
65.39	698	3.42	+0.63	− .39
62.45	359	2.83	+1.52	+ .56
59.72	767	3.53	+0.96	− .34
51.92	700	3.38	+0.85	− .08
36.38	279	2.75	−0.14	− .67
16.43	560	3.27	+0.78	− .38
11.72	153	2.44	+0.37	− .51
11.42	218	2.55	+0.57	− .22
09.72	72	2.21	+1.71	+ .74
07.28	277	2.75	+1.25	+ .23
01.67	72	2.17	+1.35	+0.44

registrations. The calibration steps were registered twice for each region, once at the beginning and once at the end of the wave-length range, the former being done just prior to, and the latter immediately following, the recording of the spectrum. In all cases the two calibration-curves were nearly enough alike that they could be combined into a mean calibration-curve for each registration of a region.

Measurements on registrations of the iron-line region were of two kinds, continuum measurements and depth measurements of *Fe* I lines. The continuum was determined by selecting twenty-one points which were consistently high for stars of all spectral types represented. Ten of these points lay between λ 4099 and λ 4080, and eleven lay between λ 4020 and λ 3988. Deflections for these points were measured, and the averages for the first ten and for the second eleven points were transformed to log I values by the calibra-

tion-curves. A continuum was then defined for each iron-line region registration by a straight line drawn in the log I versus λ diagram through two points, which were determined by the log I values and the mean wave lengths of the two groups of measured high points. From this line were read the values of log I_{cont} at the wave lengths of the various *Fe* I lines.

For the purpose of constructing curves of growth, the depths of the twenty-five *Fe* I lines listed in Table 2 were determined. These depths, expressed as $-\log (1-I_{line}/I_{cont})$, are given in Table 3. Each entry represents the mean of measurements on two plates. The accuracy of the depth measurements could be judged from the differences found between the two plates of the same star. These differences gave ± 0.017 for the probable error of each log $(1-I_{line}/I_{cont})$ value (mean of two plates) as given in Table 3. Some of these errors were caused by systematic differences between the two plates for the same star, which averaged 0.011 for the twenty-eight stars.

Measurements on the band-region registrations also consisted of two kinds, continuum measurements and depth measurements of features in the *CN* band near λ 3883. The continuum was determined by eleven points between λ 3915 and λ 3883 which were consistently high for stars throughout the spectral range covered. Unlike the high points used to determine the iron-line region continuum, which straddle all the *Fe* I lines, the band-region high points occur on only one side of the band features measured. In this case the continuum was considered constant and equal to the log I from the average deflection of these eleven points. It was necessary to adopt this procedure because on the

TABLE 3

Fe I LINE DEPTHS, IN TERMS OF $-\log (1-I_{line}/I_{cont})$

λ	β Aql	α Tau	γ Psc	η Her	μ Peg	α^2 Cap	α Psc	ϵ Oph	δ Tau	λ And
4091.56	0.541	0.548	0.486	0.541	0.596	0.544	0.445	0.570	0.533	0.529
90.96	.529	.440	.506	.470	.452	.480	.398	.512	.405	.529
89.23	.465	.470	.495	.507	.480	.551	.410	.523	.470	.514
88.57	.553	.456	.588	.524	.596	.506	.456	.547	.470	.707
87.10	.422	.382	.404	.398	.446	.434	.324	.418	.386	.451
84.50	.206	.269	.240	.255	.267	.270	.227	.292	.219	.268
80.88	.535	.465	.567	.504	.554	.512	.421	.541	.484	.524
80.22	.363	.394	.394	.376	.426	.418	.350	.456	.379	.460
79.85	.329	.299	.318	.318	.332	.304	.264	.329	.274	.324
73.77	.350	.362	.353	.364	.332	.346	.310	.383	.273	.386
70.78	.287	.304	.335	.288	.307	.297	.257	.334	.259	.300
67.99	.219	.248	.257	.212	.230	.196	.178	.234	.184	.255
57.28	.285	.216	.254	.224	.252	.227	.212	.225	.212	.308
66.99	.250	.232	.233	.222	.252	.224	.204	.231	.195	.259
65.39	.402	.444	.438	.430	.429	.442	.413	.474	.382	.462
62.45	.274	.232	.254	.234	.228	.246	.208	.240	.206	.274
59.72	.421	.366	.383	.445	.379	.390	.346	.394	.320	.441
51.92	.342	.297	.330	.304	.300	.339	.255	.326	.290	.414
36.38	.618	.612	.704	.566	.602	.580	.490	.573	.455	.742
16.43	.470	.417	.429	.442	.433	.406	.338	.446	.369	.448
11.72	.499	.440	.484	.486	.495	.472	.394	.517	.429	.524
11.42	.478	.406	.448	.523	.465	.421	.390	.480	.394	.468
09.72	.189	.210	.172	.190	.187	.182	.155	.212	.165	.190
07.28	.344	.298	.268	.307	.312	.321	.295	.316	.297	.326
01.67	0.297	0.219	0.266	0.256	0.276	0.248	0.206	0.250	0.228	0.304

TABLE 3—*Continued*

λ	ε Cyg	η Cyg	β Cet	λ Peg	η Eri	α Ari	κ Oph	γ And	η Cet	β Oph
4091.56	0.522	0.480	0.519	0.574	0.494	0.526	0.512	0.438	0.448	0.476
90.96	.442	.423	.360	.387	.396	.427	.390	.312	.353	.356
89.23	.422	.433	.454	.470	.435	.448	.491	.312	.514	.526
88.57	.511	.470	.482	.462	.429	.501	.456	.437	.421	.406
87.10	.353	.414	.374	.360	.348	.341	.356	.283	.351	.366
84.50	.210	.220	.225	.252	.208	.223	.212	.200	.196	.224
80.88	.438	.476	.470	.437	.482	.495	.492	.366	.402	.486
80.22	.329	.358	.348	.386	.374	.374	.390	.298	.346	.376
79.85	.261	.214	.265	.290	.197	.212	.228	.147	.174	.224
73.77	.290	.297	.274	.326	.277	.293	.272	.232	.246	.290
70.78	.257	.252	.252	.300	.226	.250	.212	.204	.195	.227
67.99	.166	.172	.174	.222	.172	.180	.160	.141	.166	.162
67.28	.205	.198	.196	.181	.202	.189	.189	.105	.174	.183
66.99	.189	.188	.207	.234	.191	.208	.193	.158	.170	.190
65.39	.386	.382	.406	.450	.364	.370	.337	.310	.321	.343
62.45	.214	.190	.200	.224	.192	.202	.166	.124	.158	.164
59.72	.312	.332	.271	.376	.272	.369	.340	.332	.294	.350
51.92	.276	.278	.278	.350	.294	.295	.290	.250	.266	.248
36.38	.474	.496	.474	.551	.456	.445	.425	.386	.444	.374
16.43	.350	.347	.369	.410	.338	.347	.330	.290	.324	.329
11.72	.427	.417	.402	.452	.400	.379	.372	.310	.392	.368
11.42	.362	.398	.386	.382	.388	.360	.348	.248	.328	.328
09.72	.146	.145	.137	.182	.128	.140	.141	.088	.132	.129
07.28	.246	.246	.258	.278	.252	.255	.272	.177	.222	.232
01.67	0.218	0.214	0.203	0.228	0.231	0.210	0.210	0.152	0.218	0.238

λ	109 Her	ε Cet	δ And	α Set	π Her	ε Aur	γ Aql	α Tau
4091.56	0.635	0.450	0.474	0.494	0.388	0.480	0.506	0.648
90.96	.476	.320	.345	.370	.266	.320	.342	.373
89.23	.580	.398	.501	.481	.314	.346	.356	.519
88.57	.580	.401	.400	.523	.363	.449	.480	.602
87.10	.500	.305	.307	.356	.248	.307	.284	.369
84.50	.255	.210	.216	.232	.166	.227	.210	.287
80.88	.556	.384	.414	.430	.316	.344	.362	.551
80.22	.518	.310	.342	.366	.253	.330	.329	.512
79.85	.250	.180	.152	.164	.122	.152	.154	.162
73.77	.402	.242	.238	.280	.208	.274	.272	.348
70.78	.262	.193	.180	.192	.152	.200	.184	.210
67.99	.208	.141	.132	.142	.110	.152	.142	.164
67.28	.238	.150	.174	.156	.108	.124	.129	.199
66.99	.210	.164	.160	.168	.152	.174	.185	.224
65.39	.425	.321	.292	.302	.262	.296	.299	.283
62.45	.200	.150	.149	.152	.120	.152	.146	.188
59.72	.398	.300	.287	.299	.278	.350	.374	.421
51.92	.353	.251	.254	.262	.217	.302	.259	.316
36.38	.531	.386	.410	.446	.362	.434	.414	.505
16.43	.410	.287	.318	.344	.272	.318	.292	.413
11.72	.489	.341	.344	.352	.263	.288	.298	.390
11.42	.377	.312	.274	.278	.229	.230	.225	.256
09.72	.171	.112	.106	.109	.076	.098	.102	.136
07.28	.257	.212	.192	.198	.170	.194	.182	.240
01.67	0.244	0.181	0.162	0.189	0.149	0.176	0.163	0.242

short-wave-length side of λ 3883 there were absolutely no points in the spectrum which were high enough to be considered in determining a continuum. Thus a possible error is introduced in the determination of depths in the *CN* band; but the error is on the side of producing ultimately a smaller numerical upper limit to the ratios of C^{12}/C^{13}.

Depths were determined in the $C^{12}N^{14}$ band for the first four lines listed in Table 4 (see also Fig. 1), all of which seem free from blends. The fifth line, $K'' = 58$, listed for the $C^{12}N^{14}$ band was strongly blended with an *Fe* I line and therefore was not measurable.

TABLE 4

$C^{12}N^{14}$ LINES

No.	λ (Uhler *et al.* 1915)	K''	E.P.	Relative *gf* Values		
				4871	4115	3385
1	3880.791	44	0.4653	29.04	23.67	17.86
	3880.731					
	3880.670	12	.0367	21.98	21.65	21.17
				51.02	45.32	39.03
2	3880.450	45	.4864	28.26	22.86	17.01
	3880.392					
	3880.327	11	.0310	20.44	20.15	19.78
				48.70	43.01	36.79
3	3880.092	46	.5081	27.42	21.99	16.10
	3880.033					
	3879.964	10	.0258	18.80	18.60	18.30
				46.22	40.59	34.40
4	3879.712	47	.5302	26.60	21.06	15.23
	3879.654					
	3879.579	9	.0212	17.12	16.96	16.74
				43.72	38.02	31.97
8	3874.190	58	0.8042	17.05	12.06	7.37
	3874.123					

The isotopic doublet due to $C^{13}N^{14}$, corresponding to $K'' = 58$, has a shift of about 0.18 A to the red from its $C^{12}N^{14}$ counterpart. This shifted wave length coincides with a "window" reaching nearly to the continuum, which is free from any other absorption lines. Although no actual absorption line was found at this wave length, the "depth" of the top of this window, below the continuum, was determined as an upper limit to the possible depth for the $C^{13}N^{14}$ feature. The mean depth of the four lines in the $C^{12}N^{14}$ band and the depth of the window which possibly contains $C^{13}N^{14}$ absorption are listed in the sixth and seventh columns of Table 1.

For all measurements in both the iron-line and the band regions, the deflections were read at the place in the center of the line or at the top of the high point where it had a width on the registration of 0.5 mm. This method was adopted to help eliminate errors due to the random occurrence of grains in the plates.

III. COLORS AND TEMPERATURES

In order to construct pseudo-curves of growth so that depth measurements could be transformed into relative abundances, it was necessary to obtain an internally consistent set of temperatures. To this end the color of each star was measured and subsequently transformed into an effective temperature.

Color indices for twenty-seven of the program stars were determined photoelectrically at the 23-inch refractor of the Princeton University Observatory. These colors are listed

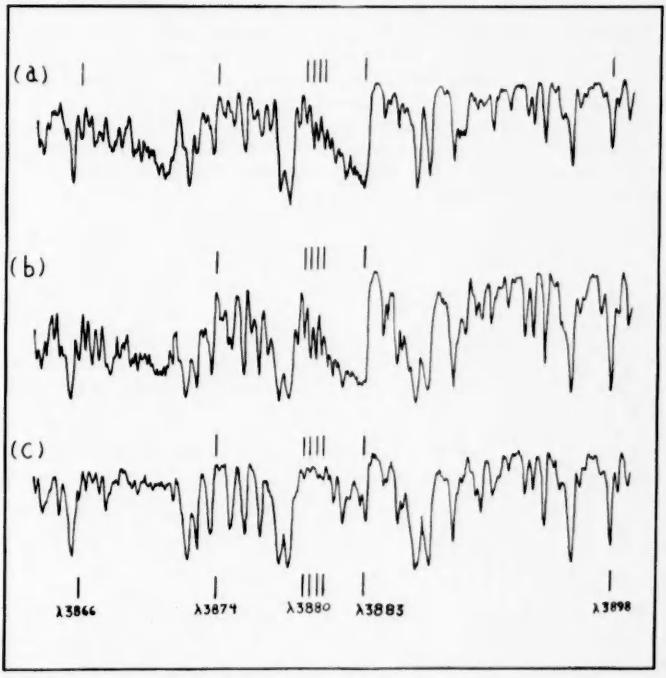

FIG. 1.—Tracings of the region λλ 3866–3898, containing the 0,0 band of *CN*. The stars represented are (*a*) *o* Tau, G8; (*b*) κ Oph, K2; (*c*) α Tau, K5. The feature at λ 3883 marks the head of the *CN* band; those at λ 3880 are the $C^{12}N^{14}$ lines; and the feature at λ 3874 is the $C^{13}N^{14}$ window.

in the fourth column of Table 1 and represent the results of seventeen nights of observing between May, 1952, and January, 1953. A 1P21 phototube and Corning filters, Nos. 5330, m-823, and 3388, were used for the blue and the yellow observations, respectively.

Five stars, indicated in Table 1 by asterisks, were selected from the program to serve as color standards and to provide, at the same time, the zenith extinction in the blue and in the yellow for each night. The minimum number of independent observations on any star was four, each standard star being observed at least sixteen times. In order to record α Tau, the telescope objective had to be diaphragmed to an effective aperture of about 12 inches. The star γ And A was not observed at Princeton because the diameter of the diaphragm used for the program was not small enough to block entirely the light from γ And B.

The Princeton colors were tied to the new Johnson (1952) color system through eight stars common to both programs by the equation

$$\text{C.I.}_J = -0.114 + 1.100\ \text{C.I.}_P .$$

Residuals for the eight stars give a probable error of ± 0.004 mag. For all the program stars, the deviations of observations from the mean for each star give a probable error of ± 0.009 mag. The final mean color for each standard star has a probable error of ± 0.002 mag. and for each of the remaining stars, ± 0.004 mag.

The method followed in transforming color indices into effective temperatures, T_{eff}, was one outlined by Kuiper (1938). The colors obtained at Princeton were transformed to Becker's (1933) photoelectric color system. This was possible with high accuracy because of the large number of stars common to both programs. With the Becker colors, a value of c_2/T_{eff} was obtained from data given by Becker (1935). Small corrections to the value of c_2/T_{eff} were made according to Kuiper's outline. The color index given by Becker for γ And A was used directly. The values for T_{eff} finally obtained appear in the fifth column of Table 1.

IV. PSEUDO-CURVES OF GROWTH

In order to construct pseudo-curves of growth, it was necessary to have, in addition to the *Fe* I line depths and a value of T_{eff} for each star, the relative numbers of absorbing atoms. For this purpose, relative stellar log $(x_0/p_c)_T$ values were derived from values of log $(x_0/p_c)_\odot$ given by B. Bell (1951) for the sun, where $x_0 = N a_v\,(k_c/k_0)$, or essentially the relative number of absorbing atoms, and p_c is the continuous absorption coefficient, taken in this paper to be constant over the short-wave-length range considered.

The following procedure was used in obtaining the values of log $(x_0/p_c)_T$. The four stars, α Tau, 109 Her, ϵ Cyg, and o Tau were chosen as representative of the temperature range. For each of the four temperatures, the solar values of log $(x_0/p_c)_\odot$, listed in the fourth column of Table 2, were corrected by the equation

$$\log\left(\frac{x_0}{p_c}\right)_* = \log\left(\frac{x_0}{p_c}\right)_\odot - \left(\frac{5040}{T} - \frac{5040}{5713}\right)\text{E.P.}$$

These values of log $(x_0/p_c)_*$ were then plotted against the *Fe* I line depths for the four stars, and preliminary pseudo-curves of growth were drawn. These curves were used to obtain new temporary values of log $(x_0/p_c)'_*$. The four sets of temporary log $(x_0/p_c)'_*$ values were reduced to the common temperature of 4000° and then averaged. From these values, listed in the fifth column of Table 2, values of log $(x_0/p_c)_T$ for each star were obtained by the equation

$$\log\left(\frac{x_0}{p_c}\right)_T = \log\left(\frac{x_0}{p_c}\right)_{4000} - \left(\frac{5040}{T} - \frac{5040}{4000}\right)\text{E.P.}$$

Pseudo-curves of growth then represented the relations between *Fe* I line depths and values of log $(x_0/p_c)_T$.

The *Fe* I lines measured fell mostly on the flat portion of the curve of growth. The weakest lines seemed just to reach the linear portion. It was necessary in the majority of cases to extrapolate the pseudo-curves of growth at the strong-line end, at the most by 0.49 in terms of log $(x_0/p_c)_T$, in order to include the measurements of the $C^{12}N^{14}$ lines. In only three cases did the curves need to be extrapolated at the weak-line end, at the most by 0.21, in order to include the measurements of the $C^{13}N^{14}$ feature.

V. ANALYSIS, RESULTS, AND CONCLUSIONS

With the pseudo-curves of growth it was now possible to transform depths in the *CN* band into relative numbers of absorbing molecules. It is seen in the third column of Table 4 that all the features considered are the combinations of either two or three unresolved molecular lines, and thus some assumption must be made regarding their blending or lack of blending in the stellar atmosphere. If it is assumed that the components are completely blended into single lines by the atmospheric turbulence, then the measured depths reflect the actual relative abundances of the absorbing molecules, and these depths can be used straightway in the pseudo-curves of growth. If, however, the other extreme case is considered, i.e., that the components absorb as completely separate lines and are then smeared into one line by the instrumental profile, the assigned depths, when transformed via the pseudo-curves of growth, yield too many absorbing molecules for saturated lines on the flat portion of the curve of growth (such as the strong $C^{12}N^{14}$ lines, but not the weak $C^{13}N^{14}$ features). From the size of the separation in wave length of adjacent components, which is 0.07 A at the most, it follows that turbulent velocities of the order of 5 km/sec are necessary in order that the components may be blended and absorb as single lines. The assumption was here made that these velocities do, in fact, exist in the atmospheres of the red giants. This does not seem unreasonable and is approximately borne out from a study of the widths of the *Fe* I lines at their half-depths. As a result, the depths in the *CN* band were applied directly to the pseudo-curves of growth.

The $C^{12}N^{14}$ lines were of nearly enough equal strengths that, for simplicity and greater weight, the depths of the four measured lines were averaged prior to entering the pseudo-curves of growth. The sixth and seventh columns of Table 1 give the mean depth of the four $C^{12}N^{14}$ lines and the depth of the $C^{13}N^{14}$ window, respectively, for each star. The column headed $\Delta_{c\ \mathrm{of}\ g}$ in Table 1 gives the difference, for each star, in the log $(x_0/p_e)_T$ values obtained for these depths from the pseudo-curves of growth.

The lower limits to the ratios of the numbers of absorbing molecules, referred to as C^{12}/C^{13} in Table 1, were obtained by numerically relating the results from the pseudo-curves of growth with the relative gf values for the $C^{12}N^{14}$ and $C^{13}N^{14}$ features in the following way:

$$\log \frac{C^{12}}{C^{13}} = \log \frac{(x_0/p_e)_{12}}{(x_0/p_e)_{13}} - \log \frac{gf_{12}}{gf_{13}}$$

$$= \Delta_{c\ \mathrm{of}\ g} - \Delta_{\mathrm{computed}} .$$

The equation, modified from one in Herzberg (1939), used to compute the relative gf values for each line listed in Table 4 was

$$gf \propto (K' + K'' + 1)\ 10^{-2.35\times10^{-4}K''(K''+1)\theta} ,$$

where K'' and K' are the total angular-momentum quantum numbers of the lower and upper states of the transition, respectively, and $\theta = 5040/T$. The gf values for each line were computed separately for the temperature of each of the twenty-eight stars and are listed for three representative values of T_{eff} in Table 4. They were then added to obtain the total relative gf values for each measured feature. The relative gf value for the $C^{12}N^{14}$ line, $K'' = 58$, is taken to be equal to that for the $C^{13}N^{14}$ line, $K'' = 58$, the isotopic line, looked for at the measured window. Differences in the values of log gf for the mean of the four $C^{12}N^{14}$ lines and for the one $C^{13}N^{14}$ window are listed under Δ_{comp} in Table 1.

Lower limits to the abundance ratios, C^{12}/C^{13}, were finally obtained by taking the differences between $\Delta_{c\ \mathrm{of}\ g}$ and Δ_{comp} for each star and are listed in the last column of Table 1.

The results in Table 1 show that all the stars but seven have lower limits to the C^{12}/C^{13} ratio in excess of 6.5. The seven exceptions are all of spectral class K2 or later and show relatively weak $C^{12}N^{14}$ features. The combined effects of decreasing strength of the $C^{12}N^{14}$ band with decreasing T_{eff} and of increasing differences in the computed gf values of the four $C^{12}N^{14}$ lines and the one $C^{13}N^{14}$ line tend to make the abundance test less sensitive in these cases.

For the remaining twenty-one stars, presumably representative of normal red giants, the results give lower limits to the abundance ratio, C^{12}/C^{13}, in excess of 6.5. This is definitely higher than the value 4, which is approximately the equilibrium ratio predicted for material involved in the carbon-nitrogen cycle (Chandrasekhar 1951). Hence

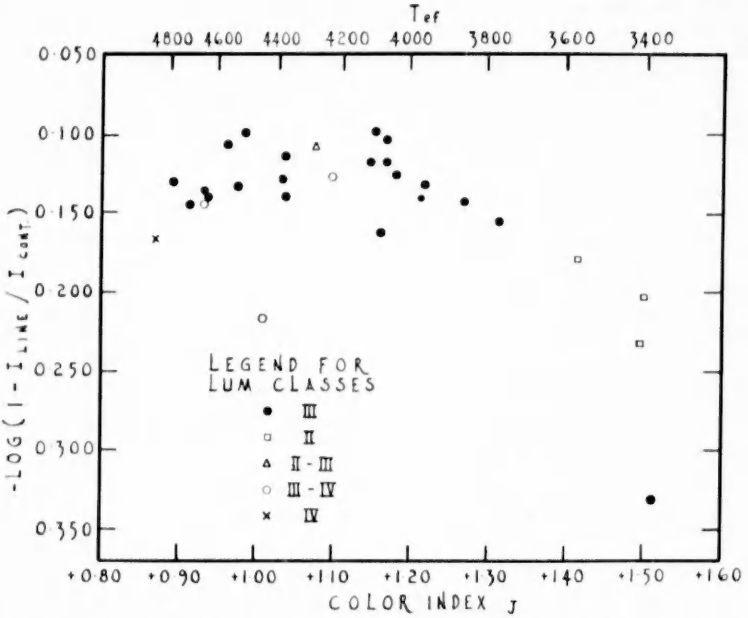

FIG. 2.—Relation between line depths in the λ 3883 band of $C^{12}N^{14}$ and color indices on the Johnson system, for the program stars.

for these stars it can probably be concluded that if the carbon-nitrogen cycle is now operating in the interior or has operated there in the past, there has been little, if any, mixing between the interior and the atmosphere. In respect to the C^{12}/C^{13} abundance ratios and probably in respect to the interior-atmosphere mixing, these normal red giants differ, therefore, from the majority of the R- and N-type giants (McKellar 1949).

The data available do not permit a reliable estimate of the factor by which the true C^{12}/C^{13} ratios exceed the lower limits here derived. In particular, it is possible that $C^{12}/C^{13} = 90$ for all the stars in this program.

Besides the main result, these additional minor points follow from the present observations. From the measured depths of the four $C^{12}N^{14}$ lines it was found that the λ 3883 band reaches a maximum strength in normal red giants somewhere between spectral types K0 and K2, as shown in Figure 2. This corresponds to the C.I.$_J$ range, +1.00 to +1.15. No significant difference was found in the λ 3883 band strengths between low-

velocity giants and the two giants of luminosity class III with space velocities in excess of 70 km/sec, γ Psc and α Sct. The high-velocity star (class III–IV), λ And, does, however, definitely have weak λ 3883 absorption.

The author wishes to express his deep gratitude to Dr. Martin Schwarzschild, Dr. Lyman Spitzer, Jr., and Dr. Uco van Wijk for their generous help and advice. Thanks are also due to Dr. Roscoe F. Sanford for loaning the author some of his plates of R-type stars, and to Mrs. Mary Anna Reeves who assisted a great deal with the reductions.

REFERENCES

Becker, W. 1933, *Veröff. Berlin-Babelsberg*, Vol. **10**, Heft 3.
———. 1935, *ibid.*, Heft 6, p. 8, Table 4.
Bell, B. 1951, *Special Report No. 35* (AMC Contract W 19-122ac-17).
Chandrasekhar, S. 1951, *Astrophysics*, ed. J. A. Hynek (New York: McGraw-Hill Book Co.), p. 636.
Greenstein, J. L.; Richardson, R. S.; and Schwarzschild, M. 1950, *Pub. A.S.P.*, **62**, 15.
Herzberg, G. 1939, *Molecular Spectra and Molecular Structure* (New York: Prentice-Hall Book Co., Inc.), p. 133.
Johnson, H. L. 1952, *Ap. J.*, **117**, 313.
King, A. S., and Birge, R. T. 1930, *Ap. J.*, **72**, 19.
Kuiper, G. P. 1938, *Ap. J.*, **88**, 469.
McKellar, A. 1949, *Pub. Dom. Ap. Obs. Victoria*, Vol. **7**, No. 26.
Moore, C. E. 1945, *Contr. Princeton U. Obs.*, No. 20.
Morgan, W. W., and Roman, N. G. 1950, *Ap. J.*, **112**, 362.
Roman, N. G. 1952, *Ap. J.*, **116**, 122.
Sanford, R. F. 1929, *Pub. A.S.P.*, **41**, 271.
Uhler, H. S., and Patterson, R. A. 1915, *Ap. J.*, **42**, 434.

RED SHIFT IN THE SPECTRUM OF 40 ERIDANI B*

DANIEL M. POPPER
Department of Astronomy, University of California, Los Angeles
Received March 12, 1954

ABSTRACT

Measurement of 42 hydrogen lines on 27 spectrograms of 40 Eri B leads to an observed red shift, $\Delta\lambda/\lambda$, of 7×10^{-5}, corresponding to a velocity of 21 km/sec. This is to be compared to the value of 17 km/sec predicted on the basis of general relativity from the mass and radius of the star. The difference between observed and predicted values is less than the sum of their uncertainties, which are considerable fractions of the values themselves.

INTRODUCTION

The available observational material concerning displacements of lines in spectra of white-dwarf stars of known mass is meager and uncertain. Adams (1925; Strömberg 1926) on the basis of four spectrograms and Moore (1928) on the basis of 3 spectrograms have published observations of Sirius B, giving a red shift of 20 km/sec. Although the well-known observational difficulties caused by the light of Sirius A are considerable, the agreement between the results of the two experienced observers seems to indicate a reliable determination. Recently, however, lack of confidence has been expressed (e.g., Einstein 1950;[1] Gamow and Critchfield 1949) in the validity of this result, partly because of theoretical difficulties (e.g., Mestel 1952). On the basis of two spectrograms with lines of poor quality, Münch (1944) has obtained a velocity giving a red shift of 22 ± 9 km/sec for the white dwarf 40 Eri B.

It appears desirable to obtain a more nearly definitive determination of the red shift for a white dwarf. Much the most favorable case is 40 Eri B. After Sirius B, it is the brightest known white dwarf (9.5 mag.). There is no danger of contamination of its spectrum from the light of 40 Eri A or C, and the radial velocity of the system is known from observations of A, which has a proper motion and parallax in common with the binary system BC.

OBSERVATIONS

Between December, 1949, and January, 1953, 37 prismatic spectrograms of 40 Eri B were obtained at Mount Wilson, 22 with the 60-inch reflector (dispersion 78 A/mm at $H\gamma$) and 15 with the 100-inch (dispersion 67 A/mm at $H\gamma$). A number of the 60-inch observations were made by Dr. E. C. Yowell, whose assistance is gratefully acknowledged. Exposure times of $1\frac{1}{2}$–4 hours on baked Kodak IIa-O plates were employed in an effort to fill in the wings of the very broad hydrogen lines. In this way the relatively narrow cores (Kuiper 1935; Babcock 1948) stand out in enhanced contrast. There is no possibility that light from either 40 Eri A (4.5 mag., K1) or 40 Eri C (11.0 mag., M6) contaminates the spectrum of the white dwarf. Although star A is 4 mag. brighter in the blue and has numerous sharp lines in its spectrum, its distance of 82″ places it safely out of the way. Star C is more than 4 mag. fainter than star B in the blue, and nearly 7″ away in a position angle near 180°, which is perpendicular to the slit length. No trace of such a strong line in the spectra of stars A and C as *Ca* I 4226 could be detected in any of the spectrograms of B.

* This investigation was carried out under a co-operative arrangement with the Mount Wilson and Palomar Observatories.

[1] "The shifting of spectral lines toward the red [predicted by general relativity theory] . . . is not yet confirmed" (passage written in 1948).

In addition to the spectrograms of 40 Eri B, on each night of observation a plate was taken of 40 Eri A, and, starting in January, 1951, of one or both of the standard velocity stars, HD 36591 (5.3 mag., B2) and η Leo (3.6 mag., A0). These latter stars were chosen to test for possible systematic errors in velocities obtained from measures of hydrogen lines.

The spectrograms of all four stars were measured with a magnification of 14 times. Each spectrogram was measured twice, and the mean displacement obtained for each measured line. Only the hydrogen lines, $H\delta$, $H\gamma$, and $H\beta$, could be measured in the spectrum of 40 Eri B. At the time of measurement each line was assigned a weight according to the reliability of its appearance. Mean displacements for the different lines and for each of the two sets of plates (60-inch and 100-inch) are given for 40 Eri B in Table 1. The second group of values, being weighted means of only the better lines, is considered the more reliable and is adopted. The other is included to show the effects of choice of lines. The adopted results are obtained from sixteen 60-inch and eleven 100-inch spectrograms.

TABLE 1

MEASURED DISPLACEMENTS OF LINES IN SPECTRUM OF 40 ERI B

Telescope	Line	All Lines				Better Lines			
		No. of Plates	Sum of Weights	Mean Displ. (Km/Sec)	P.e. of Mean (Km/Sec)	No. of Plates	Sum of Weights	Mean Displ. (Km/Sec)	P.e. of Mean (Km/Sec)
60-inch	$H\delta$	16	4.6	−13	5	3	1.0	− 7	8
	$H\gamma$	21	10.6	−22	4	13	5.2	−26	4
	$H\beta$	22	8.4	−18	6	6	3.0	−31	4
100-inch	$H\delta$	8	3.1	−12	4	3	1.2	−15	5
	$H\gamma$	13	7.4	−26	3	10	6.0	−25	4
	$H\beta$	11	5.6	−17	6	7	3.8	−22	5

The probable error of the velocity from a single line of unit weight corresponds, on the average, to a displacement of 0.0022 mm on the plate. This value may be compared with the weighted mean difference between two measures of the same line, which is 0.0017 mm. For the sharper lines of the standard stars, the mean difference is 0.0011 mm. These results indicate that the scatter of measured displacements can be adequately accounted for by accidental errors of measurement. The small number of good lines in the case of $H\delta$ is a result of the small number of plates on which this line shows a core comparable with those of $H\gamma$ and $H\beta$. Part, though apparently not all, of this effect results from the generally weaker exposures at shorter wave lengths.

Since we are interested in the apparent velocity of 40 Eri B relative to the center of mass of the system BC, differential velocities with respect to 40 Eri A, which shows a common parallax and proper motion, should suffice. The hydrogen lines in the spectrum of 40 Eri A, however, are badly blended on plates of the dispersion used, so that direct differences of velocity could not be evaluated. Furthermore, appreciable systematic differences of velocity among the fifteen lines measured in the spectrum of 40 Eri A were found when the wave lengths recommended by the Mount Wilson spectroscopy division were used. Hence I feel that an apparent difference in velocity between stars A and B can best be evaluated by adopting the known velocity of A and investigating possible systematic effects in the measures of B. Spectrograms of HD 36591 and of η Leo, which have strong hydrogen lines and well-determined velocities in the Lick system, were used for the purpose. The corrections to measured velocities indicated by the measures of these

spectrograms are shown in Table 2. Only results from lines of reliable appearance are included. The systematic corrections are disappointingly large. In Table 3 we give the final results of the measurements, both corrected and uncorrected. The weights listed are those of the adopted displacements of Table 1 adjusted, for each telescope, for differences in linear displacement on the plate corresponding to 1 km/sec of velocity.

Giving low weight to the uncorrected values, I finally adopt for the apparent velocity of 40 Eri B, −21 km/sec. A computation of the probable error of this result, when each of the 42 measured lines is treated as an independent determination, yields ±1.9 km/sec. Because of the differences between the results from the different hydrogen lines and

TABLE 2

CORRECTIONS

Telescope	Line	No. of Plates	Correction To Reduce to Lick System (Km/Sec)	P.e. (Km/Sec)
60-inch	$H\delta$	11	−1.3	1.4
	$H\gamma$	19	+5.3	1.2
	$H\beta$	7	+1.8	4.8
100-inch	$H\delta$	14	+6.1	1.4
	$H\gamma$	17	+5.4	1.2
	$H\beta$	13	+0.4	2.8

TABLE 3

RESULTS OF MEASUREMENTS BEFORE AND AFTER CORRECTION

Telescope	Line	Weight	Uncorrected Displacement (Km/Sec)		Corrected Displacement (Km/Sec)	
60-inch	$H\delta$	1.2	−7	−26 (weighted mean)	−8	−21 (weighted mean)
	$H\gamma$	5.2	−26		−21	
	$H\beta$	2.2	−31		−29	
100-inch	$H\delta$	1.5	−15	−22 (weighted mean)	−9	−19 (weighted mean)
	$H\gamma$	6.0	−25		−20	
	$H\beta$	2.7	−22		−22	

because of the unexpectedly large systematic corrections, ±4 km/sec is considered as a more realistic estimate.

After these reductions had been completed, Dr. J. L. Greenstein made available to me three plates of this star exposed at Mount Palomar with a dispersion of 38 A/mm and one with a dispersion of 18 A/mm. Only $H\gamma$ could be measured. The mean apparent velocity from these plates is −23 km/sec, while the rough value by Münch, quoted above, is −20 km/sec. The inclusion of these values would not alter the adopted velocity.

The radial velocity of 40 Eri A in the Lick system is −42 km/sec, so that the apparent difference in velocity, B *minus* A, for a mean epoch of 1951 is +21 km/sec, with an estimated uncertainty of ±4 km/sec. The corresponding value of $\Delta\lambda/\lambda$ is 7×10^{-5}, where $\Delta\lambda$ is the red shift in wave-length units.

DISCUSSION

Known effects which could give rise to an apparent velocity difference between 40 Eri B and 40 Eri A are (1) relative motion, (2) mass motions in the atmosphere of A or B, (3) asymmetrical line-absorption coefficient, and (4) gravitational red shift. Since star A is a normal dwarf and star B a white dwarf, we shall assume that effect 2 is not present. The others will be considered in turn.

From the orbit of 40 Eri BC published by van den Bos (1926) and the similar orbit by Artukhina (1948), the radial-velocity amplitude of B about the center of mass of BC is 1.3 km/sec. At the epoch of the spectrograms the radial component of B was 0.4 km/sec, the sign being unknown. This motion is so small relative to both the observed red shift and its uncertainty that it can be neglected. The parallax (0".20) and proper motion ($\mu_\alpha \cos \delta$: 2".2; μ_δ : 3".4) of component A of 40 Eri are known to be equal to those of BC to within small fractions of the values themselves, so that it is certain that A is a member of the same system as B and C. Van den Bos (1926) has analyzed the double-star measures of B relative to A and finds, after correcting for orbital motion of B in the system BC, a relative motion of 6" per century approximately normal to the line joining stars A and B. At a distance of 5 parsecs this motion corresponds to a tangential speed of 1.4 km/sec. There is no way of knowing whether a radial component of a similar order of magnitude may be present. The relative velocity of escape is about 2.5 km/sec. We shall assume that this component of radial motion is also small relative to the measured red shift. It would have been desirable to determine the radial velocity of 40 Eri C on the Lick system as a further check. Because of the faintness of this component, however, this check is not practicable with the available equipment.

Since 40 Eri A is a normal K dwarf and since K dwarfs show no unexplained systematic residual velocity on the Lick system, we can assume that the apparent velocity difference between stars A and B results entirely from effects 3 and 4 in B. The principal causes of line broadening of hydrogen lines in stellar atmospheres are rotation and interatomic Stark effect. The former has no unsymmetrical effects. For very large electric fields, the second-order Stark effect, which is unsymmetrical, can become appreciable.[2] Theory and experiment agree (Rausch von Trauenberg and Gebauer 1929) that the longward shift in $H\gamma$ from this cause is approximately

$$\Delta\lambda = \frac{3E^2}{10^{11}} \text{A},$$

where E is the field strength in volts per centimeter. The average effective field experienced by an atom depends on the density of perturbing ions. An estimate of the ion density may be obtained by application of the Inglis-Teller relation in the case of a spectrum with strong hydrogen lines. Combining the relevant formulas (e.g., Aller 1953, pp. 308–317) gives, for the longward shift in $H\gamma$,

$$\log \Delta\lambda = 7.64 - 10 \log n_m ,$$

where n_m is the quantum number of the upper energy level of the highest observable member of the Balmer series. The numerical constant has not been evaluated for lines other than $H\gamma$, since most of the weight of the observations is in this line. The value of n_m in the spectrum of 40 Eri B is at least 9 (Kuiper 1941). Through the co-operation of Dr. H. W. Babcock, I was able to make a tracing of his 10 A/mm plate of 40 Eri B (Babcock 1948). A faint trace of $H10$ is visible. Hence n_m is greater than 9, and $\Delta\lambda$ is less than 0.012 A, which corresponds to a red shift of 0.8 km/sec. Moreover, the cores of the H lines, which were measured, must be produced at lower densities than the wings, the

[2] I am indebted to Dr. L. Spitzer for calling my attention to this fact.

overlapping of which determines n_m. We conclude that the shift resulting from asymmetrical line broadening can be neglected.

Thus gravitation appears to be the only known effect which can produce the observed red shift. It remains to compare the observed value with that predicted by general relativity, which is $0.635\ \mathfrak{M}/R$ km/sec. $\mathfrak{M}$ and R are the mass and radius of the star, respectively, in solar units. The available data for $\mathfrak{M}$ and R are discussed briefly in the next paragraphs.

Artukhina (1948) has corrected van den Bos's (1926) orbit of 40 Eri BC on the basis of a few additional observations and a reconsideration of the assigned weights. Although her elements differ but little from those of van den Bos, a definitive orbit will not be obtained until a considerably greater fraction of the period, 250 years, has been covered by observations. Artukhina's elements, combined with the most recent value of the parallax of the system, $0''.201 \pm 0''.002$ (Lippencott 1952) give 0.63 ± 0.05 for the combined mass of B and C. Van den Bos gives, for the mass ratio,

$$\frac{\mathfrak{M}_C}{\mathfrak{M}_B + \mathfrak{M}_C} = 0.31 \pm 0.02 .$$

This value is based on two completely independent determinations, one (0.32) obtained from the double-star measures of B with respect to A, and the other (0.29) from parallax plates (Alden 1925). We adopt for the mass of 40 Eri B, in solar units, 0.43 ± 0.04. Since the probable error is obtained only from the internal consistency of the observations, a more realistic value would be somewhat greater than ± 0.04.

The radius of 40 Eri B must be evaluated from the apparent magnitude, parallax, and surface brightness of the star. The magnitude of 40 Eri B on the V system (Johnson and Morgan 1953) is 9.50 (D. L. Harris, unpublished), and the parallax is $0''.201$. The surface brightness has been evaluated from independent observations and by different methods by Kuiper (1941) and by Berger, Chalonge, Divan, and Fringant (1952). Kuiper evaluated the effective temperature by spectrophotometry of the continuous spectrum. His value is 13,500°. In this case the bolometric correction must be assumed known. Berger and associates obtain the "brightness temperature" at λ 5400 from the color temperature of the continuum, the "surface" temperature corresponding to an energy-curve defined by the intensities at the centers of the hydrogen lines, and the residual intensities of the hydrogen lines. Their value is 13,000°. In this case the bolometric correction is not needed. The values of the radius, R, recomputed with Harris' improved magnitude of 40 Eri B and his unpublished revision of the magnitude of the sun on the V system are, respectively, 0.017 and 0.015 solar radii. It is my opinion that before complete confidence can be placed in such determinations, a theory for the atmosphere of 40 Eri B must be developed which will predict satisfactorily the form of the continuous spectrum and the profiles of the absorption lines, including their cores. The surface brightness would emerge as a parameter, from which the radius could be calculated. For the present we adopt

$$R = 0.016 \pm 0.002 \text{ solar radii} .$$

It is well known (e.g., Kuiper 1941) that this value of the radius agrees with that predicted for a degenerate star of the mass of 40 Eri B without appreciable hydrogen (Chandrasekhar 1939; Rudkjøbing 1952). A mass of 0.43 ± 0.04 corresponds to a radius of 0.015 ± 0.001 (Chandrasekhar) or 0.014 ± 0.001 (Rudkjøbing). Hence if 40 Eri B conforms to this theory and has no hydrogen in the interior, the radius of the sphere of degenerate matter must be close to the adopted radius of the star, 0.016.

The gravitational red shift predicted for 40 Eri B from the mass and radius adopted is 17 ± 3 km/sec, the estimated uncertainty being computed from the uncertainties given for $\mathfrak{M}$ and R. This value is to be compared to the observed value of 21 ± 4 km/sec. The

significance of the estimated uncertainties is not easy to assess. We conclude that the observed red shift, which we have attributed entirely to the gravitational effect, agrees with the predicted value within the uncertainties of both and, if allowance is made for all uncertainties, that the ratio of observed to predicted values must be well within the range $\frac{1}{2}$–2.

Walker (1951) has extended the theory of kinematic relativity into the realm of dynamics through a principle of least action. The results agree with those of general relativity for planetary motions and for the deflection of light-rays, but they predict twice as large a red shift as does general relativity. This prediction appears to be contradicted by the observations, as does the conclusion of Findlay-Freundlich (1954) concerning the magnitude of the relativity red shift.

REFERENCES

Adams, W. S. 1925, *Proc. Nat. Acad. Sci.*, **11**, 382.
Alden, H. L. 1925, *Pop. Astr.*, **33**, 164.
Aller, L. H. 1953, *Astrophysics* (New York: Ronald Press).
Artukhina, N. M. 1948, *Astr. Zhur.*, **25**, 180.
Babcock, H. W. 1948, *Pub. A.S.P.*, **60**, 369.
Berger, J.; Chalonge, D.; Divan, L.; and Fringant, A.-M. 1952, *C.R.*, **235**, 348; *Contr. Inst. Ap. de Paris*, ser. A, No. 128.
Chandrasekhar, S. 1939, *Introduction to the Study of Stellar Structure* (Chicago: University of Chicago Press), chap. xi.
Einstein, A. 1950, *Out of My Later Years* (New York: Philosophical Library).
Findlay-Freundlich, E. 1954, *Phil. Mag.*, **45**, 303.
Gamow, G., and Critchfield, C. L. 1949, *Theory of Atomic Nucleus and Nuclear Energy Sources* (London: Oxford University Press), p. 293 n.
Johnson, H. L., and Morgan, W. W. 1953, *Ap. J.*, **117**, 313.
Kuiper, G. P. 1935, *Pub. A.S.P.*, **47**, 312.
Kuiper, G. P. 1941, *Colloquium on Novae and White Dwarfs* ("Actualités Scientifiques et Industrielles," No. 897).
Lippencott, S. L. 1952, *A.J.*, **56**, 202.
Mestel, L. 1952, *M.N.*, **112**, 582.
Moore, J. H. 1928, *Pub. A.S.P.*, **40**, 229.
Münch, G. 1944, *Ap. J.*, **99**, 271.
Rausch von Trauenberg, H., and Gebauer, R. 1929, *Zs. f. Phys.*, **54**, 307; **56**, 254.
Rudkjøbing, M. 1952, *Pub. Copenhagen Obs.*, No. 160.
Strömberg, G. 1926, *Pub. A.S.P.*, **38**, 44.
van den Bos, W. H. 1926, *B.A.N.*, **3**, 127.
Walker, A. G. 1951, *Nature*, **168**, 961.

VISUAL BINARIES FOR THE MASS-LUMINOSITY RELATION

K. Aa. Strand
Dearborn Observatory
AND
R. G. Hall*
Yerkes Observatory
Received May 14, 1954

ABSTRACT

Twenty-three visual binaries have been listed for which accurate data are now available for the determination of the correlation between luminosity and mass.

Since the publication by Kuiper (1938*b*), considerable progress has been made in the determination of improved data for several of the stars listed in his Table 1. The improvements consist in most cases in the determination of the mass ratios and parallaxes

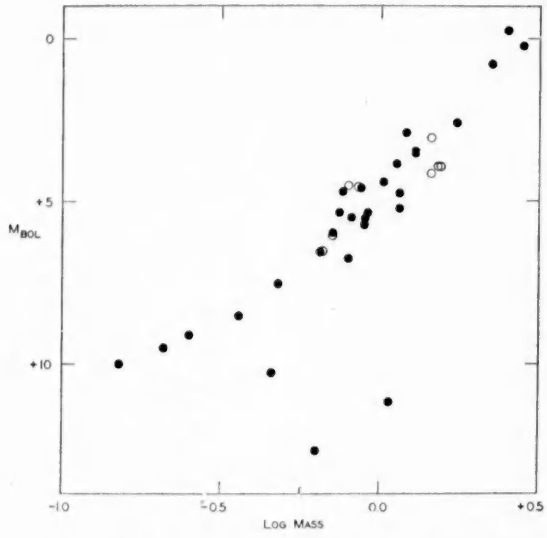

Fig. 1.—Empirical mass-luminosity relation for visual binaries

from long series of photographic plates, while in certain cases the photographic observations were also used to improve the orbits (η Cas, α CMi, 70 Oph, and Kr 60).

Kuiper's original list contained binaries for which the orbits could be considered as reliable, or at least the error in $3 \log a'' - 2 \log P$ to be small, and which had parallaxes larger than $0''.045$ with a probable error of less than 10 per cent of the parallax. In the correlation of the mass and the luminosity for these objects the probable errors in the

* Now at U.S. Naval Observatory, Washington, D.C.

TABLE 1

VISUAL BINARIES FOR THE MASS-LUMINOSITY RELATION

α_{1900}	Star	Period (Year)	Semi-major axis	Parallax with p.e.	$Mb/(Ma+Mb)$	m_{AB}	Δ_m	Spec.	$M_{bol\,A}$	log Ma	$M_{bol\,B}$	log Mb	Δ log Ma, b
0^h30^m1	13 Cet	6.95	0".236	0".058 ± .005	0.435	+5.24	0.6	F7	+ 4.51	−0.10		−0.21	±0.13
0 43.0	η Cas	480	11.993	.182 ± .005	.390	+3.45	3.86	G0 V, K5+	+ 4.72	− .12	+ 7.52	− .32	.05
4 10.7	o_2 Eri BC	247.92	6.894	.201 ± .003	.31	+9.37	1.48	B9, M5e	+10.26	− .34	+ 9.5	− .68	.03
5 09.3	α Aur	0.2847	0.0559	.074 ± .003	.53	+0.19	0.15	G8, F6	− 0.25	+ .40	+ 0.23	+ .45	.07
6 40.7	α CMa	49.94	7.62	.377 ± .003	.326	−1.47	10.05	A1 V, A5	+ 0.79	+ .35	+11.14	+ .03	.02
7 34.1	α CMi	40.65	4.548	.287 ± .004	.268	+0.34	10.3	F5 IV,	+ 2.59	+ .24	+12.4–12.9	− .20	.02
7 47.1	9 Pup	23.18	0.58	.060 ± .004	.495	+5.27	0.7	G1 V,	+ 4.55	− .07		− .08	.11
9 26.8	ψ Vel	34.11	0.920	.062 ± .006	.49	+3.7	0.9	F0,	+ 3.05	+ .16		+ .14	.14
11 12.9	UMa	59.86	2.536	.126 ± .006	.50	+3.77	0.45	G0 V, G0 V	+ 4.76	+ .06	+ 5.21	+ .06	.09
12 36.6	γ Vir	171.37	3.746	.089 ± .006	.492	+2.98	0.02	F0 V, F0 V	+ 3.47	+ .11	+ 3.49	+ .11	.09
13 44.5	Σ 1785	155.0	2.42	.075 ± .006	.487	+7.26	0.49	K6, K6	+ 6.03	− .15	+ 6.52	− .18	.13
14 32.8	α Cen	80.09	17.593	.761 ± .004	.465	−0.20	1.37	G4, K1	+ 4.39	+ .01	+ 5.72	− .05	.02
14 46.8	ξ Boo	149.95	4.884	.145 ± .004	.465	+4.51	2.15	G8 V, K5	+ 5.36	− .04	+ 6.76	− .10	.05
16 37.5	ζ Her	34.38	1.369	.103 ± .004	.398	+2.82	2.64	G0 IV, K0 V	+ 2.89	+ .08	+ 5.48	− .09	.05
17 09.2	Fu 46	13.12	0.71	.147 ± .007	.444	+9.4	0.38	M3,	+ 8.5	− .44		− .54	.08
17 12.1	Melb 4 AB	42.09	1.82	.142 ± .005	.411	+5.9	1.5	K5,	+ 6.0	− .15		− .31	.07
17 34.0	26 Dra	74.16	1.50	.073 ± .004	.446	+5.23	2.61	G0 V,	+ 4.58	− .06		− .15	.08
18 04.0	70 Oph	87.85	4.551	.199 ± .004	.421	+3.97	1.75	K1 V, K5 V	+ 5.53	− .05	+ 6.56	− .19	.03
18 03.2	99 Her	56.40	1.03	.058 ± .004	.36	+5.04	3.40	F7 V,	+ 3.86	+ .05		− .20	.08
18 53.3	σ 648	59.8	1.26	.059 ± .004	.47	+5.17	1.78	G0,	+ 4.15	+ .16		+ .11	.11
21 09.6	δ Equ	5.70	0.26	.056 ± .004	.492	+4.50	0.0	F8 V, F8 V	+ 3.94	+ .19	+ 3.94	+ .18	.10
22 24.2	Kr 60	44.46	2.386	.253 ± .003	.382	+9.59	1.58	M4+, M6	+ 9.1	− .60	+10	− .82	.02
23 56.9	85 Peg	26.27	0.83	0.083 ± .004	0.491	+5.75	3.04	G2 V,	+ 5.34	−0.13		−0.15	0.07

luminosity do not exceed ± 1.2 mag (1938*b*). Certain binaries included in Kuiper's list have been excluded, primarily for the lack of a reliable mass ratio, while others have been added because of improved data since 1938. The orbital data and the parallaxes were determined from a careful evaluation of published material, as well as from unpublished investigations by the authors (η Cas and Σ 1785).

In Table 1, the columns listed in order are: (1) R.A. (1900); (2) name of binary; (3) period; (4) semi-major axis; (5) parallax with its probable error; (6) mass of B-component in terms of total mass; (7) combined visual magnitude on the international photovisual system according to Kuiper, with some new data added from recent work by Johnson and Morgan (1953); (8) magnitude difference based on data by Kuiper and, for the wider pairs, from photovisual determinations by Ferwerda and Kooreman (1946); (9) spectra on the revised Yerkes atlas system (MK), where luminosity classes are given, otherwise the data by Kuiper; (9) bolometric magnitudes as derived from the visual magnitudes, with correction to bolometric according to the tables by Kuiper (1938*a*); (10) logarithm of mass of the brighter components; (10–11) bolometric magnitudes and masses for the fainter components; (12) probable errors of the logarithm of mass of either component.

The bolometric magnitudes and masses listed in Table 1 are plotted in Figure 1. The values for which the probable errors of the logarithm of the masses are less than 0.10 (errors in mass less than 25 per cent) are plotted as solid dots, otherwise as open circles. The components of ξ UMa were excluded in the graph, since they are spectroscopic binaries. Excluding the positions of the three white dwarfs, the diagram displays, in general, a close relationship between luminosity and mass.

Although bolometric magnitudes are lacking for nine fainter components for which no spectra are available, there is some evidence that the brighter components are more luminous than the fainter components of the same mass. This is consistent with the evolutionary tracks computed by Schönberg and Chandrasekhar (1942) and with recent photometric work by Johnson (1953).

REFERENCES

Ferwerda, J. G., and Kooreman, C. J. 1946, *B.A.N.*, **10**, 169.
Johnson, H. L. 1953, *Ap. J.*, **117**, 361.
Johnson, H. L., and Morgan, W. W. 1953, *Ap. J.*, **117**, 313.
Kuiper, G. P. 1938*a*, *Ap. J.*, **88**, 429.
———. 1938*b*, *ibid.*, p. 472.
Schönberg, M., and Chandrasekhar, S. 1942, *Ap. J.*, **96**, 161.

GALACTIC CLUSTERS AND STELLAR EVOLUTION

HAROLD L. JOHNSON
Lowell Observatory
Received March 12, 1954; revised April 12, 1954

ABSTRACT

The color-magnitude diagrams for the galactic clusters suggest evolutionary tracks for individual stars that exhibit the same general trends shown by the theoretical tracks computed by Sandage and Schwarzschild. The agreement of theory with observation is perhaps more satisfactory for the galactic clusters than for the globular clusters.

I. INTRODUCTION

The photoelectric observations on the individual stars in several galactic clusters, most of which have already been published, permit some tentative conclusions regarding possible evolutionary paths for stars of Baade's population type I. The clusters have been chosen to represent, as well as possible, the principal regions of the H-R diagram for stars later than about A0. It is for these stars that it has been possible to suggest evolutionary paths; it is not possible, on the basis of data available at present, to make such suggestions for the stars earlier than spectral class A0.

II. ASSUMPTIONS

In order to make it possible to draw conclusions regarding stellar evolution from the cluster color-magnitude diagrams, it is necessary, first, to make several basic assumptions. These assumptions are: (1) that the stars in each individual cluster are all of the same age; (2) that the various regions of the H-R diagram occupied by the several clusters are different primarily because the clusters are of different ages; (3) that the main sequences of the several clusters may legitimately be fitted together; and (4) that the few clusters considered here may be accepted as representative of galactic clusters in general.

The first two assumptions are obviously essential to any discussion of cluster color-magnitude diagrams in terms of stellar evolution, and no further justification seems to be required. The third assumption seems to be a reasonable one, which underlies all discussions of cluster diagrams; the moving clusters, such as the Hyades and the Ursa Major nucleus, provide some justification for this assumption. Regarding the fourth assumption, it may be said that the clusters discussed here were selected from the list given by Trumpler (1930) as representative of the clusters in that list. With the exception of M67, no further justification seems to be necessary; M67 will be discussed later. Other well-known clusters might have been included also, but, since the present clusters are believed to be representative, they probably would not add anything more of significance.

III. EVOLUTIONARY MODELS TO BE TESTED

The cluster color-magnitude diagrams will be regarded principally in the light of the theoretical evolutionary tracks proposed by Sandage and Schwarzschild (1953). According to the inhomogeneous models proposed by these authors, a star evolves first by rising in luminosity from the main sequence to a maximum of about 1 mag. increase and then turns to the right and slightly downward. The reader is referred to figure 3 in the paper by Sandage and Schwarzschild. The cluster diagrams will be examined to see whether this theory is consistent with the observations.

Another theory that may have application to the color-magnitude diagrams for the galactic clusters is that of B. Strömgren (1933), according to which the differences between the galactic clusters might be interpreted in terms of differing hydrogen content.

IV. THE OBSERVATIONS

The clusters that have been chosen as representative are: M39 (Johnson 1953*a*), Praesepe (Johnson 1952), NGC 752 (Johnson 1953*b;* stars of membership classes 1 and 2 are plotted), the Coma Berenices star cluster (Weaver 1952; additional observations made at the Lowell Observatory to transform to the *B, V*-System), the Pleiades (Johnson and Morgan 1953), NGC 2362 (Johnson and Morgan 1953), and M67 (unpublished). The color-magnitude diagrams for M39 (*open circles*) and Praesepe (*filled circles*) are shown in Figure 1. The inclosed areas plus the line representing the main sequence will be used later for schematic representations of the clusters. Similarly, the color-magnitude diagrams for the Coma cluster (*open circles*) and NGC 752 (*filled circles*) are shown in Figure 2, while Figure 3 shows the photoelectric observations on M67.

Only a few of the M67 stars fainter than $M_v = +2$ have been observed photoelectrically; several of the brighter stars, thought by Becker and Stock (1953) not to be members of the cluster on the basis of their three-color photometry, have been omitted from the diagram. The distance modulus for M67, obtained by fitting the cluster main sequence to that for the near-by stars, is 10 mag. The giant sequence is populated by stars indistinguishable spectroscopically from near-by giant stars of similar absolute magnitudes (D. M. Popper, private communication).

V. COMPOSITE COLOR-MAGNITUDE DIAGRAMS

A composite schematic diagram for the clusters is shown in Figure 4, where the clusters are identified by their numbers in the table accompanying the figure. The giant stars present in the Coma cluster, Praesepe and NGC 752, have been plotted individually.

The positions of M39 (*3*), the Coma cluster (*4*), and Praesepe (*5*) with respect to the main sequence indicate that the first stage in the evolution of these stars is a general "peeling-off" from the main sequence, with the brightest stars in each cluster evolving most rapidly. The four F- and G-type giant stars, distributed at approximately equal intervals between Praesepe and the group of K giants, suggest a path by which the K giants in the clusters may have evolved. On this hypothesis, NGC 752 (*6*), whose principal group of stars occurs at about F2 and which has more K giants than Praesepe, represents a later stage in the evolution of stars, while M67 (*7*) would be the oldest of the clusters on the diagram.

Generally speaking, the appearance of Figure 4 is in accord with the theoretical evolutionary tracks computed by Sandage and Schwarzschild (1953). Certain discrepancies, however, do exist. The early stages in the departure from the main sequence and the much more rapid motion to the right along the horizontal track (the speed of evolution in different parts of the tracks should vary inversely as the numbers of stars found in corresponding parts of the diagram) are in reasonable agreement, but the theory does not predict the sudden slowing-down in the region of the K giants. This sudden increase in the number of stars, starting at about G8, shows very strongly among the bright stars (Roman 1952). Another difference is that the late-type subgiants predicted by the theory do not exist either in clusters or among the bright stars. Of course, this may mean only that such stars would be so old that none have yet evolved to that stage.

The earlier portions of the empirical evolutionary tracks, discussed earlier, show the same general trends that would be expected from Strömgren's theory. He has not, however, carried the computations beyond the earlier stages.

The cluster M67 is at galactic latitude $+33°$, which corresponds, for a distance modulus of 10 mag., to a distance from the galactic plane of 500 parsecs. Shapley (1930)

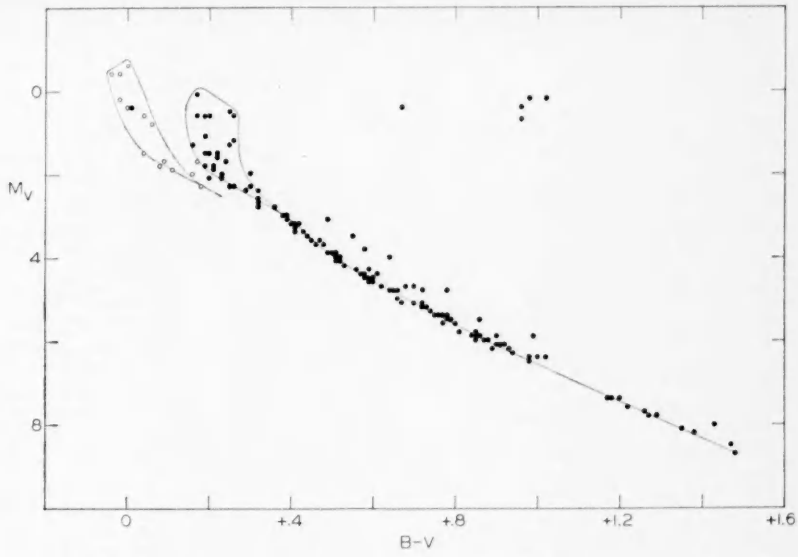

FIG. 1.—The color-magnitude diagram for M39 (*open circles*) and Praesepe (*filled circles*)

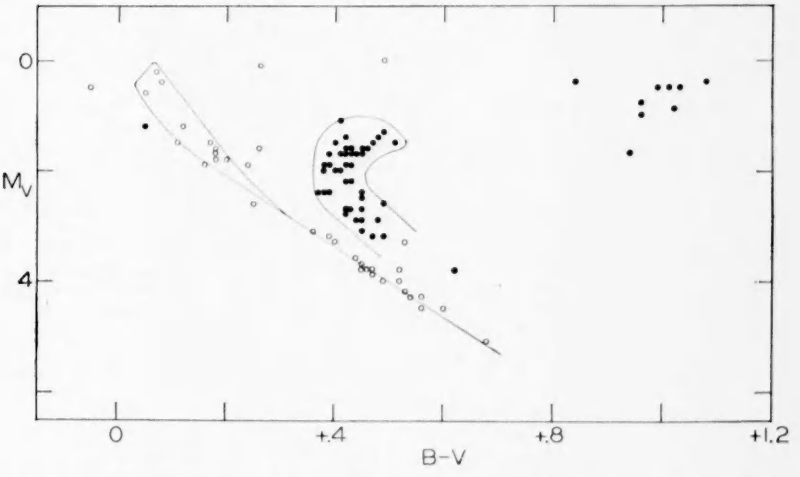

FIG. 2.—The color-magnitude diagrams for the Coma cluster (*open circles*) and NGC 752 (*filled circles*).

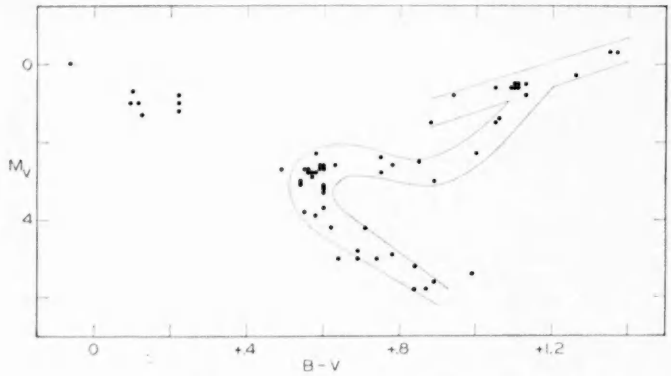

FIG. 3.—The color-magnitude diagram for M67

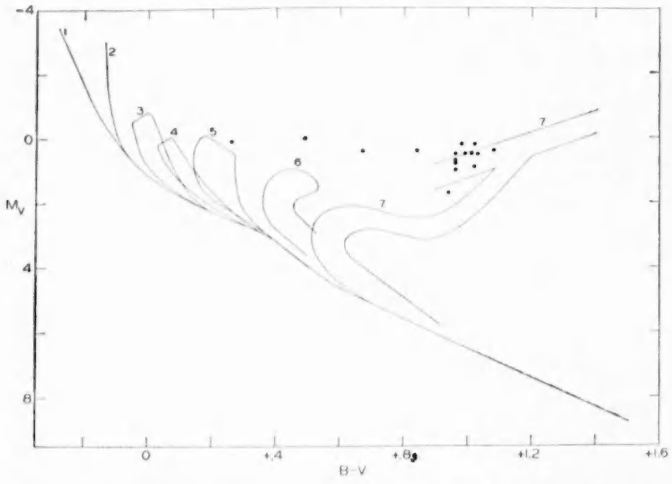

FIG. 4.—The composite schematic color-magnitude diagram for the clusters. The clusters are identified as follows:

1, NGC 2362
2, Pleiades
3, M39
4, the Coma cluster
5, Praesepe
6, NGC 752
7, M67

has considered it to be a galactic cluster, while Becker and Stock (1953) and Ebbighausen (1940) have pointed out the similarity of its H-R diagram to those for globular clusters. While the M67 diagram is similar to the globular-cluster diagrams (Arp, Baum, and Sandage 1952; Baum 1952), in that there is a fairly well-populated giant sequence with a sequence of subgiants leading up to it, the similarity ends there. The members of the M67 giant sequence are ordinary giant stars of luminosity class III on the MK system, both spectroscopically and photometrically; the corresponding sequences in the globular clusters are much brighter, extending up to $M_v = -3$ (Baum 1952). The subgiant sequence in M67 fits in quite well with the few near-by subgiants; the subgiant sequences in globular clusters, on the other hand, pass directly through the very thinly populated Hertzsprung gap, which M67 respects. We must conclude that M67 is more closely related to the stars of population type I than to the globular clusters. If the evolutionary hypothesis proposed above is correct, M67 may represent a very advanced stage in the evolution of stars of population type I.

We turn now to Figure 5, where the bounded area represents schematically the regions of Figure 4 in which the galactic cluster stars fall. The open circles represent the brighter components of double stars (Johnson 1953*c*), whose absolute magnitudes have been computed on the assumption that the fainter components are normal main-sequence stars. The filled circles are near-by stars with accurately determined parallaxes (Johnson and Morgan 1953; see Table 8 on p. 335; four additional subgiants for which $0''.050 < \pi < 0''.100$ have been included). The near-by stars were selected to be representative of stars which appear in different parts of the color-magnitude diagram, and the relative numbers of stars in various parts of the diagram are not in proportion to the relative frequencies of such stars in space. The double stars may be more representative in this respect, since most of the physical pairs in Aitken's catalogue that had separations exceeding about $8''$ and that were in a particular part of the sky were measured. Four blue stars from the Ursa Major cluster and three yellow giants from the Hyades cluster are included, but the parallaxes for these stars were found by purely geometrical considerations, not by reference to the cluster H-R diagrams. With the exception of a few stars below the main sequence around $B-V = +0.8$, these two groups of stars agree well with the bounded area defined by the cluster stars. There are two differences: (1) the scatter above the main sequence does not seem to be so great for the double and near-by stars as it is for the cluster stars; and (2) some of the near-by subgiants are redder than the subgiant sequence of M67.

The crosses in Figure 5 represent mean values for spectral types G5–K5, inclusive, for the high-velocity giant stars investigated by Keenan and Keller (1953). It is evident that the giants of the high-velocity group, of the near-by stars, the bright stars (Roman 1952), M67, and the galactic clusters form a homogeneous group so far as location in the color-magnitude diagram is concerned. The considerable difference between these giant stars and those of globular clusters is shown in Figure 6, where the bounded area is taken from Figure 5 but has been corrected to include the near-by subgiants; the hatched area represents the schematic giant sequences given for the globular clusters M3 and M92 by Baum (1952). It does not seem possible to explain the giant sequences in globular clusters on the simple evolutionary hypothesis put forth here.

VI. CONCLUSIONS

The color-magnitude diagrams for the galactic clusters suggest an apparently logical evolutionary process that connects the young stars of population type I with the presumably older stars in M67 and in the high-velocity group. The evolutionary tracks that are suggested are in accord schematically with the theoretical tracks computed by Sandage and Schwarzschild. The densities of stars in the various parts of the color-magnitude diagram are in accord with the theoretical times of evolution, except for the

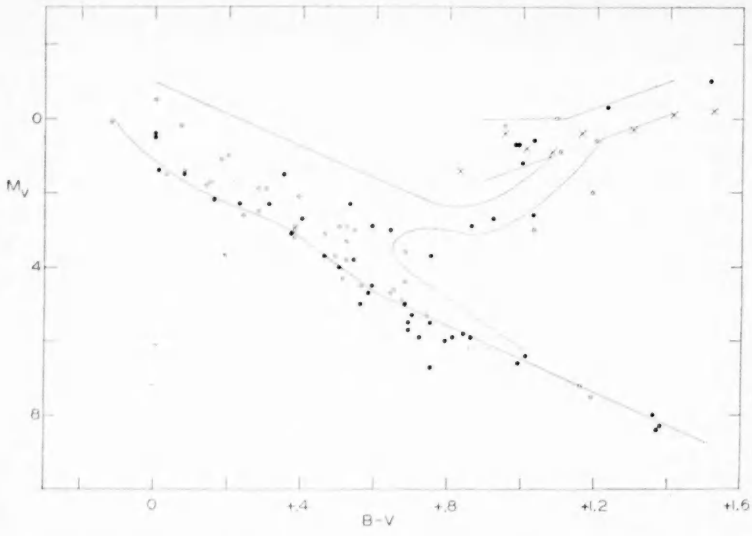

FIG. 5.—The composite color-magnitude diagram for the clusters (*bounded area*), brighter components of double stars (*open circles*), stars with accurately known parallaxes (*filled circles*), and means for high-velocity stars (*crosses*).

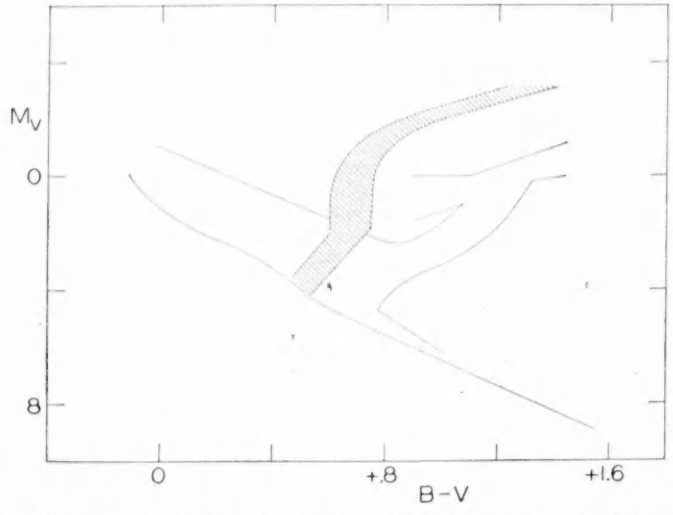

FIG. 6.—Schematic color-magnitude diagram showing the bounded area from Fig. 5 and the schematic giant sequence for globular clusters.

K giant stars. The semi-empirical correction in the theoretical evolutionary tracks that Sandage and Schwarzschild found necessary to explain the giant sequences in the globular clusters does not seem to be required to explain the diagrams of the galactic clusters. In this connection one's attention should be called to the considerable differences between the spectra of globular-cluster stars and spectra of high-velocity (Keenan and Keller 1953) and low-velocity stars (Baum 1952).

I wish to thank Dr. D. M. Popper for several valuable discussions during the preparation of this paper.

REFERENCES

Arp, H. C.; Baum, W. A.; and Sandage, A. R. 1952, *Ap. J.*, **57**, 4.
Baum, W. A. 1952, *A.J.*, **57**, 222.
Becker, W., and Stock, J. 1953, *Zs. f. Ap.*, **31**, 316.
Ebbighausen, E. G. 1940, *Ap. J.*, **91**, 244.
Johnson, H. L., 1952, *Ap. J.*, **116**, 640.
Johnson, H. L. 1953*a*, *Ap. J.*, **117**, 353.
———. 1953*b*, *Ibid.*, p. 356.
———. 1953*c*, *Ibid.*, p. 361.
Johnson, H. L., and Morgan, W. W. 1953, *Ap. J.*, **117**, 313.
Keenan, P. C., and Keller, G. 1953, *Ap. J.*, **117**, 241.
Roman, Nancy G. 1952, *Ap. J.*, **116**, 122.
Sandage, A. R., and Schwarzschild, M. 1953, *Ap. J.*, **116**, 463.
Shapley, Harlow. *Star Clusters* (New York: McGraw-Hill Book Co., 1930).
Strömgren, B. 1933, *Zs. f. Ap.*, **7**, 222.
Trumpler, R. J. 1930, *Lick Obs. Bull.*, **14**, 154, Table 3.
Weaver, H. F. 1952, *Ap. J.*, **116**, 612.

EVOLUTION OF MASSIVE STARS

R. J. TAYLER*
Princeton University Observatory
Received March 15, 1954

ABSTRACT

The evolution is considered of massive stars with opacity due to electron scattering. As the stars evolve, the convective core retreats, and a zone of continuously varying composition is set up between the core and the envelope. Ten models have been obtained with core hydrogen content changing from 100 to 6 per cent. The evolutionary tracks of the models have been plotted in the H-R diagram. It is found that, although the individual tracks are very different from those found by other authors, the H-R diagram for stars of different masses but of the same age exhibits the well-known "knee," which occurs at the point of 11 per cent over-all reduction of hydrogen content.

I. INTRODUCTION

The course of stellar evolution is largely determined by the existence or nonexistence of general mixing currents in stellar interiors. If there are efficient mixing currents, a star will remain effectively homogeneous over long periods of time, and its theoretical properties are well known. Such homogeneous models are unable to explain the observed positions of the giants in the Hertzsprung-Russell diagram, and recently the great importance of inhomogeneous models has been realized (Oke and Schwarzschild 1952, this paper contains a list of references to previous papers; Sandage and Schwarzschild 1952; Schwarzschild, Rabinowitz, and Härm 1953; Roy 1952). It appears that a single discontinuity of composition can explain the properties of red giants, but the origin of such a discontinuity must be explained. With the assumption of general mixing, this could be explained by a process of accretion. However, Sweet (1950) has recently shown that the rate of circulation in meridian planes of a star is less than was believed by Eddington. As a result, stars may remain virtually unmixed, and inhomogeneities will arise naturally in the course of evolution. The evolution of unmixed stars was considered by Schönberg and Chandrasekhar (1942), and a further series of models has been obtained by Sandage and Schwarzschild (1952).

An initially homogeneous star, with a convective core and a high temperature-dependent law of energy generation, evolves by the conversion of hydrogen into helium in the core. There are two possible courses when this evolution commences: the mass of the convective core may either increase or decrease. In the former case, the core being well mixed by convection, a discontinuity of molecular weight will be set up at the core boundary, and the star will be divided into zones of differing composition. In the latter case convection will die out in the outer regions of the core; as this material will already have converted some of its hydrogen, a continuous gradient of molecular weight will be set up. There will be a uniform envelope with the same mass as the original envelope, a radiative zone of variable composition, and a convective zone, the last two containing the material of the original convective region.

That in fact the core mass decreases is suggested by available model sequences in which a composition discontinuity has been assumed at the surface of the core. For Kramers' opacity, sequences have been obtained by Schönberg and Chandrasekhar (1942), Harrison (1944), and Roy (1952), while the present author has obtained a sequence for Schwarzschild's modification of Kramers' law. In all these sequences, as the molecular weight in the core increases, the mass of the convective core decreases, showing that an intermediate zone with continuously varying molecular weight must, in fact,

* Commonwealth Fund Fellow.

have been set up. Thus these sequences must be regarded only as approximations to the actual evolutionary series.

In this paper is derived an evolutionary model sequence in which account is taken of the intermediate zone. A star was chosen in which electron opacity predominates throughout. The relative importance of electron opacity increases with the mass of the star, and in this case the importance of radiation pressure also rises. We have, therefore, taken account of the contribution of radiation pressure, which means essentially that the sequence of models applies only to one value of the mass ($9.9\,M_\odot$). Including the homogeneous starting model, ten successive models for the star have been obtained, as the hydrogen in the interior is gradually exhausted and the convective core shrinks in size.

II. ASSUMPTIONS AND EQUATIONS

The models here considered consist of a helium-enriched core in convective equilibrium surrounded by a zone of variable composition in radiative equilibrium and an envelope of pure hydrogen, also in radiative equilibrium. The following simplifying assumptions have been made: (1) energy generation is by the carbon cycle; (2) except in the convective regions, there is no mixing; (3) the central temperature for all models of the sequence is 2×10^7 °K; (4) the opacity is due to electron scattering only; (5) the initial composition has been taken as 100 per cent hydrogen, though a small proportion of heavy elements must be present; and (6) degeneracy never becomes important. Radiation pressure is not neglected.

In the subsequent work the following definitions and equations are used.

Homology variables.—The solutions were obtained in homology variables introduced by Bondi and Bondi (1949) and defined by

$$S = \frac{4\pi P r^4}{GM_r^2}, \qquad Q = \frac{Pr}{GM_r\rho}, \qquad \mathfrak{N} = \frac{P}{T}\frac{dT}{dP}, \tag{1}$$

where the third variable replaces the Bondis' variable N, to which $\mathfrak{N}$ reduces when radiation pressure is neglected and when there are no inhomogeneities. As radiation pressure is not neglected, we require a further variable introduced by the Bondis,

$$Z = \frac{aT^3}{3\rho}\left(\frac{\mu H}{k}\right), \tag{2}$$

where Z is the ratio of radiation pressure to gas pressure.

Subscripts.—s = surface; c = center; 1 = inner interface, between the convective core and zone of variable composition; 2 = outer interface between intermediate zone and envelope.

Equations.—Bondi and Bondi have derived the necessary equations in homology variables in the case of constant composition, and these can easily be extended to include variable composition. The hydrostatic equation and equation of mass conservation reduce to

$$\frac{S}{Q}\frac{dQ}{dS} = \frac{S + \mathfrak{N} - Q + Z(4\mathfrak{N} - 1)}{1 + 2S - 4Q} + \frac{5S}{3 + 5X}\frac{dX}{dS}, \tag{3}$$

where we have used

$$\mu = \frac{4}{3 + 5X}. \tag{4}$$

Z satisfies the equation

$$\frac{S}{Z}\frac{dZ}{dS} = \frac{(Z+1)(4\mathfrak{N} - 1)}{(1 + 2S - 4Q)}. \tag{5}$$

In a radiative region with electron-scattering opacity,

$$\kappa = \kappa_{00}(1+X) \qquad \kappa_{00} = 0.19\ , \tag{6}$$

the energy-transport relation leads to

$$\mathfrak{N} = \frac{\kappa_{00}(1+X)L_s}{16\pi c}\left(\frac{\mu H}{k}\right)^2\left(\frac{4\pi aG}{3}\right)^{1/2}\frac{Q^2}{S^{1/2}Z^{3/2}(1+Z)^{1/2}}, \tag{7}$$

while, in a convective region,

$$\gamma = \tfrac{5}{3}, \qquad \mathfrak{N} = \frac{2+10Z+8Z^2}{5+40Z+32Z^2}. \tag{8}$$

Limit of convection.—Stability will cease in the inhomogeneous zone when

$$\left(\frac{dT}{dr}\right)_{\text{rad}} > \left(\frac{dT}{dr}\right)_{\text{adiab}}\ ,$$

where we have taken as our criterion, for stability against convection, that there must be stability not only for simple vertical displacements of elements but also for the accidental mixing of such an element with its surroundings which will destroy the inhomogeneity (cf. Öpik 1950, p. 582). This relation reduces to

$$\mathfrak{N}_{\text{rad}} > \mathfrak{N}_{\text{adiab}}\ . \tag{9}$$

Inclosed mass.—There is an expression for the inclosed mass in terms of homology variables:

$$M_r^2 = \frac{3}{4\pi aG^3}\left(\frac{k}{\mu H}\right)^4\frac{SZ(1+Z)^3}{Q^4}. \tag{10}$$

III. CONSTRUCTION OF MODELS

The equations for the envelope possess a two-parameter family of solutions which fulfil the surface conditions $S = Q = 0$. Developing these solutions at the surface with S as independent variable and A and Z_s as the two independent parameters, one finds

$$\begin{aligned} Q &= AS^{1/4} + A\left(\frac{5+4Z_s}{8}\right)S^{5/4} + O(S^{6/4})\ , \\ Z &= Z_s + \tfrac{1}{2}Z_s(Z_s+1)S + \frac{104}{45}AZ_s(Z_s+1)S^{5/4} + O(S^{6/4})\ , \\ \mathfrak{N} &= \tfrac{1}{4} + \tfrac{1}{8}S + \frac{2A}{9}S^{5/4} + O(S^{6/4})\ , \end{aligned} \tag{11}$$

and from equations (7) and (10) the luminosity and mass can be expressed in terms of A and Z_s by

$$L_s = \frac{4\pi c}{\kappa_{00}(1+X_s)}\left(\frac{k}{\mu H}\right)^2\frac{3^{1/2}}{(4\pi aG)^{1/2}}\frac{Z_s^{3/2}(1+Z_s)^{1/2}}{A^2}, \tag{12}$$

$$M_s^2 = \frac{3}{4\pi aG^3}\left(\frac{k}{\mu H}\right)^4\frac{Z_s(1+Z_s)^3}{A^4}. \tag{13}$$

For stars of a given mass there is a single infinity of possible envelope solutions whose parameters satisfy equation (13).

In the convective regions there is a one-parameter family of solutions which satisfy the central boundary conditions:

$$Q = \frac{S}{3} + O(1) , \qquad Z = Z_c + O\left(\frac{1}{S}\right). \tag{14}$$

When $Z_c = 0$, the single central solution reduces to the Lane-Emden solution for polytropic index 1.5. Core solutions for several values of Z_c were obtained by numerical integration.

Convective-core solutions and complete homogeneous stellar models have previously been obtained by Henrich (1941, 1942, 1943). As a starting model for our evolutionary sequence, we require a homogeneous model, and, in fact, several homogeneous models of different masses were obtained and compared with Henrich's results. One of our models was almost directly comparable with one of his, and agreement was entirely satisfactory.

The envelopes for the evolutionary sequence were obtained as follows: The mass of the star was defined by the envelope with surface parameters

$$A = 0.215, \qquad Z_s = 0.01 ; \tag{15}$$

and this leads, according to equation (13), to a mass,

$$M_s = 9.9\, M_\odot . \tag{16}$$

Parameters for further envelopes are obtained from relation (13). The envelopes are obtained by numerical integration, using starting values obtained by series (11). The differential equations form a second-order system, but the algebraic relation (7) may be replaced by an equivalent differential equation. Though this procedure is less accurate than an algebraic evaluation of $\mathfrak{N}$, it makes the equations easier to handle and will be justified, provided that the value of $\mathfrak{N}$ obtained by quadrature agrees with that obtained from equation (7). This proved to be the case, and both methods were used for obtaining envelopes. Ten envelopes were obtained with A values between 0.210 and 0.255 at intervals of 0.005.

By interpolation between the first two of these envelopes, a unique solution was obtained which fits, continuously in S, Q, Z, and $\mathfrak{N}$, to a convective core and is thus the homogeneous starting model of our sequence. The corresponding value of A was found to be $A = 0.211$.

The second model of the sequence was constructed as follows: The neighboring envelope, corresponding to $A = 0.215$, was used to the point where it contained the same mass as the radiative part of the first model (this point was reached before condition [9] for convective instability was satisfied). Beyond this point the integration had to be carried through the new transition zone with variable hydrogen content. The hydrogen content was taken to be linear, with the variable

$$u = -\ln \frac{M_r}{M_s} \tag{17}$$

used by Roy (1952); so that in the transition zone we have

$$\frac{dX}{du} = \text{Const.}, \tag{18}$$

$$\frac{dX}{dS} = \frac{1}{1 + 2S - 4Q} \frac{dX}{du} . \tag{19}$$

The integration was carried out for a trial value of dX/du. The corresponding curve in the S, Q plane cuts the one-parameter family of convective-core solutions (14), and at one such intersection it will have the same value of Z as do the core solutions. If the values of $\mathfrak{R}$ are also equal, then the intermediate zone fits smoothly to the convective core. This last condition will not, in general, be fulfilled for an arbitrary trial value of dX/du. Hence several integrations (3 or 4), with 10–20 steps each, had to be carried out for subsequent trial values until the required intermediate zone could be obtained by interpolation between the last two integrations.

The variation of composition in this transition zone defines the variation in the first part of the transition zone of the next model, and the remainder of the transition zone is constructed as above. In all, including the homogeneous starting model, ten models have been obtained, and the mathematical characteristics of these models are listed in Table 1.

TABLE 1

	0	I	II	III	IV	V	VI	VII	VIII	IX
A	0.211	0.215	0.220	0.225	0.230	0.235	0.240	0.245	0.250	0.255
Z_s	0.0091	.0100	0.0109	0.0119	0.0130	0.0141	0.0153	0.0165	0.0179	0.0193
S_2	0.9035	.8470	0.8110	0.7670	0.7190	0.6790	0.6320	0.5878	0.5456	0.5093
Q_2	0.4099	.4099	0.4189	0.4237	0.4275	0.4338	0.4355	0.4378	0.4407	0.4428
Z_2	0.0176	.0189	0.0212	0.0233	0.0256	0.0285	0.0309	0.0336	0.0368	0.0399
$\mathfrak{R}_2$	0.3813	.3763	0.3744	0.3711	0.3670	0.3641	0.3598	0.3558	0.3513	0.3475
S_1		.9640	1.0295	1.0797	1.1276	1.1614	1.1841	1.1947	1.1793	1.1376
Q_1		.4319	0.4543	0.4724	0.4892	0.5018	0.5101	0.5144	0.5098	0.4963
Z_1		.0200	0.0237	0.0275	0.0320	0.0381	0.0444	0.0523	0.0629	0.0757
$\mathfrak{R}_1$		.3790	0.3757	0.3725	0.3688	0.3641	0.3597	0.3545	0.3481	0.3413
$-(dX/du)_1$		.718	0.940	0.862	0.842	0.880	0.778	0.744	0.696	0.628
Z_c	0.030	.035	0.040	0.045	0.051	0.060	0.068	0.078	0.093	0.109
X_c	1.000	0.925	0.832	0.743	0.642	0.538	0.430	0.312	0.185	0.062

Figure 1 shows the change in hydrogen content and the retreat of the convective core as the star evolves.

IV. PHYSICAL PROPERTIES OF MODELS

To pass from the solution in terms of homology variables to physical variables, one quadrature is required. From the definitions of the homology variables, we obtain

$$\ln Q_1 = \ln \frac{P_c r_s}{G M_s \rho_c} - \int_0^{s_1} \frac{(Q-S)\,dS}{S(1+2S-4Q)} - \int_{s_1}^{\infty} \frac{[\mathfrak{R}+Z(4\mathfrak{R}-1)]\,dS}{S(1+2S-4Q)}, \tag{20}$$

where we have taken this relation at the boundary of the convective core. An essentially similar relation holds at all points (Bondi and Bondi 1949). The luminosity, L_s, and mass, M_s, are already known from equation (12) and (13); T_c is assumed constant; and this, combined with Z_c, gives P_c and ρ_c according to equation (2). Thus from equation (20) we can obtain the radius of the star, r_s.

The effective temperature can now be found from

$$L_s = \pi a c r_s^2 T_e^4 . \tag{21}$$

The fractional mass contained in the core is known by applying equation (10) to the inner interface, and the fractional radius can be obtained from one of the terms evaluated in equation (20) above

$$\ln \frac{r_1}{r_s} = -\int_0^{s_1} \frac{Q\,dS}{S(1+2S-4Q)}. \tag{22}$$

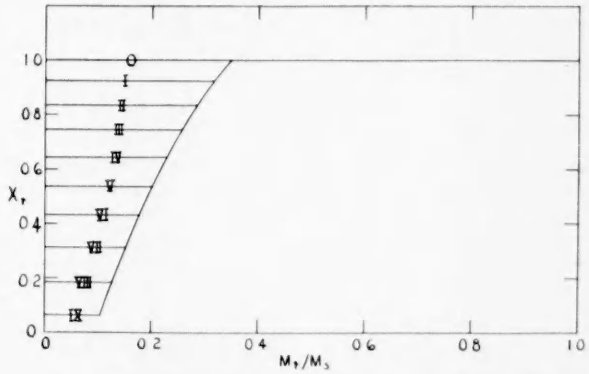

FIG. 1.—The variation of hydrogen content from center (*left*) to surface (*right*). The composition of the envelope is constant for all models of the sequence, and this is shown by the horizontal line at the right of the figure. The numbered horizontal lines at the left show the hydrogen content and extent of the convective cores of the successive models. The horizontal lines are joined by a curve showing the varying composition in the intermediate zone.

TABLE 2

	0	I	II	III	IV	V	VI	VII	VIII	IX
$r_s/R_\odot$	4.20	4.41	4.82	5.23	5.72	6.32	7.08	8.06	9.33	11.42
M_{bol}	−4.07	−4.15	−4.24	−4.34	−4.43	−4.52	−4.60	−4.69	−4.77	−4.85
T_e	21,100	21,000	20,500	20,100	19,600	19,100	18,400	17,600	16,600	15,300
ρ_c	4.0	3.7	3.4	3.2	3.1	2.9	2.8	2.7	2.7	2.7
M_{core}/M_s	0.351	0.316	0.286	0.258	0.229	0.204	0.177	0.151	0.126	0.104
r_{core}/r_s	0.295	0.276	0.249	0.225	0.200	0.176	0.152	0.127	0.104	0.080
X_{core}	1.000	0.925	0.832	0.743	0.642	0.538	0.430	0.312	0.185	0.062
Mass burned/M_s	0.000	0.025	0.053	0.077	0.102	0.124	0.145	0.164	0.182	0.196
Time/10^7 years	0.00	0.79	1.61	2.28	2.86	3.36	3.79	4.16	4.48	4.78

By integrating the hydrogen content over the mass, the fractional mass of hydrogen burned (M_B/M_s) in any model of the sequence may be found, and the time taken at any stage in the evolution may be obtained as follows:

$$\text{Time} = 0.007\, c^2 \int \frac{dM_B}{L}. \tag{23}$$

The results of all these calculations are shown in Table 2.

We are now in a position to consider the validity of the assumptions which were made in Section II. The assumption that energy generation is confined to the core is most likely to break down in the later models of the sequence when the central hydrogen content is depleted. The law of energy generation,

$$\epsilon = \epsilon_{00} X \rho T^{18}, \tag{24}$$

was integrated through the core of the last model of the sequence, and it was found that at the boundary of the core the ratio of the rate of energy production to the mean rate of energy production in the core is approximately 1 to 100; and, provided that this rate does not increase outside the core, we can at least write

$$\frac{\text{Core production}}{\text{Envelope production}} > 10 .$$

This result will give a very extreme upper limit to the envelope production. We can now consider the way in which the rate of energy production is changing at the boundary of the core, and we find that in all but the last model the rate of energy production continues to fall as the zone of increasing hydrogen content is entered. Thus the amount of energy generated outside the core is certainly small in all but the last model, and even in this model the initial rise is likely to be countered by the rapid fall of energy production farther out in the envelope.

Next we can check on the assumed constancy of the central temperature throughout the sequence. With the knowledge that the energy production is essentially confined to the core, we may assume the luminosity to be approximately proportional to $\epsilon_{00} X_c \rho_c T_c^{18}$ (in this we omit the last model). Thus we find that the central temperature will rise by 16 per cent and the radius will have been overestimated by 16 per cent in model VIII of the sequence. This will have only a small effect on the tracks in the H-R diagram.

The neglect of photoelectric opacity can never be entirely justified for the outermost parts of the models. Assuming 1 per cent heavy elements, in the form of a Russell mixture, and using the tables of Morse (1940), an estimate was made, for the initial and final models, of the temperatures below which Kramers' opacity predominates. The critical temperature for the homogeneous star is approximately 3×10^6 °K, and that for the final model, 10^6 °K. These figures show that Kramers' opacity does make an important contribution in the outer regions of the early stars of the sequence. The tabulated values of ρ_c show that degeneracy is indeed nonexistent.

V. CONCLUSIONS AND COMPARISONS

Figure 2 shows the 10 models of the sequence plotted in the H-R diagram; superimposed is the H-R diagram of the models studied by Sandage and Schwarzschild (1952), with the starting point of one of their models arbitrarily placed at our starting point. The differences are immediately apparent. In the early stages their model evolves to a limiting isothermal core containing 12 per cent of the total mass of the star (Schönberg-Chandrasekhar limit); the transition zone is neglected, and the brightness of the star rises by 1 mag., while the effective temperature is virtually constant. Only when the gravitational contraction is taken into account, does the star move to the right in the H-R diagram. Our series extends until 19.6 per cent of the mass has been converted into helium; but at this stage no isothermal region has yet been set up. Movement to the right in the H-R diagram is immediately much more rapid, but the total change in luminosity is only 0.8 mag.

In view of this great difference between the two evolutionary tracks, it seemed worth

while to compute the H-R diagram for stars of different masses but of the same age. Strictly, our models apply only to stars of 9.9 solar masses; but over a limited mass range little inaccuracy should be introduced by applying the homologies

$$L \propto M^3, \qquad r \propto M, \qquad T_c \propto M^{1.4}, \qquad \text{Time} \propto \frac{M}{L}.$$

We can then obtain an H-R diagram for stars of different masses at time = 4.78×10^7 years.

The plot obtained is shown in Figure 3. It can be seen that, despite great differences in the tracks of individual stars in the H-R plane between these and the Sandage-Schwarz-

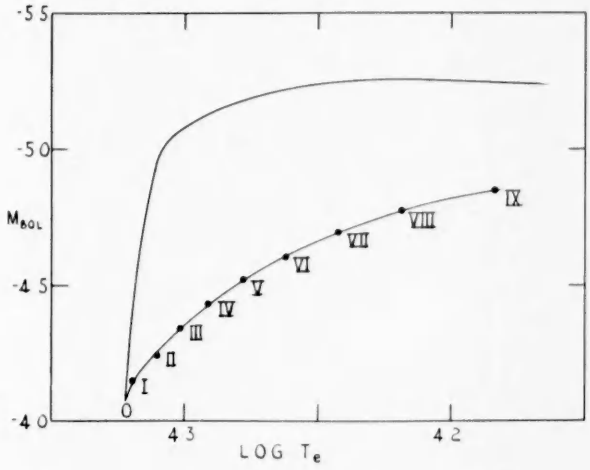

FIG. 2.—The evolutionary tracks in the H-R diagram. The upper curve shows the H-R diagram for evolution to the Schönberg-Chandrasekhar limit followed by the gravitationally contracting models of Sandage and Schwarzschild. The lower curve is the H-R diagram for models of the present sequence, with positions of the successive models marked with Roman numerals.

schild results, the locus at fixed time is very similar. In particular, it exhibits the well-known "knee," and the position of the knee corresponds to a star which has burned about 11 per cent of its hydrogen. This figure is again close to the result obtained by Sandage and Schwarzschild.

Let us consider now when a zone of variable composition is likely to be of importance. In large stars, in which electron opacity predominates, the models given in this paper are applicable to a first approximation. For stars of smaller mass Kramers' opacity becomes more important, and the extent of the intermediate zone will certainly diminish (pure Kramers' opacity: mass of initial convective core, 14.5 per cent; mass of Schönberg-Chandrasekhar limit isothermal core, 10 per cent), and it will take a further investigation to determine the effect of this smaller transition zone. As still smaller stars are considered, energy generation by the proton-proton reaction will become more important than the carbon cycle, and the convective core will still further reduce in size until it disappears

altogether (Tayler 1952; Naur and Osterbrock 1953). In a homogeneous star with Kramers' opacity and no convective core, energy production is important through at least 40 per cent of the mass; and if such a star evolves without mixing, there must inevitably be an extensive zone of variable composition.

What can we expect to happen as a star evolves beyond the stage which we have reached in our sequence? As the hydrogen content of the core is reduced, energy production outside the core will become more important, since the outward increase of hydrogen content will offset the fall in temperature. The shell burning of hydrogen will commence, and, in fact, this stage has already been reached in the last model of our sequence, since in this model the energy generation increases slightly with increasing r in the inner portion of the transition zone.

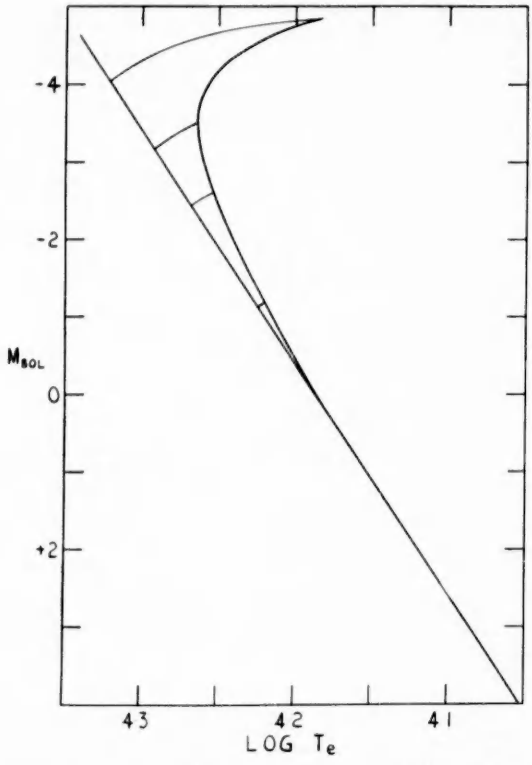

FIG. 3.—Instantaneous H-R diagram at time 4.78×10^7 years. The straight line at the left of the diagram is the original main sequence; the thick curve at the right is the locus for stars of varying masses at time 4.78×10^7 years. The connecting curves are the evolutionary tracks of individual stars.

This work was commenced at Cambridge during the tenure of a maintenance allowance from the Department of Scientific and Industrial Research and was completed at Princeton on a Commonwealth Fund Fellowship; I am grateful to both these organizations for the support I have received. My thanks are due to Professor Martin Schwarzschild for many helpful discussions and advice on the presentation of the paper.

REFERENCES

Bondi, C. M., and Bondi, H. 1949, *M.N.*, **109**, 62.
Harrision, M. H. 1944, *Ap. J.*, **100**, 343.
Henrich, L. R. 1941, *Ap. J.*, **93**, 483.
———. 1942, *ibid.*, **96**, 106.
———. 1943, *ibid.*, **98**, 192.
Morse, P. M. 1940, *Ap. J.*, **92**, 27.
Naur, P., and Osterbrock, D. E. 1953, *Ap. J.*, **117**, 306.
Öpik, E. J. 1950, *M.N.*, **110**, 559.
Oke, J. B., and Schwarzschild, M. 1952, *Ap. J.*, **116**, 317.
Roy, A. E. 1952, *M.N.*, **112**, 484.
Sandage, A. R., and Schwarzschild, M. 1952, *Ap. J.*, **116**, 463.
Schönberg, M., and Chandrasekhar, S. 1942, *Ap. J.*, **96**, 161.
Schwarzschild, M.; Rabinowitz, I.; and Härm, R. 1953, *Ap. J.*, **118**, 326.
Sweet, P. A. 1950, *M.N.*, **110**, 548.
Tayler, R. J. 1952, *M.N.*, **112**, 387.

THE STRUCTURE OF STARS WITH NEGLIGIBLE CONTENT OF HEAVY ELEMENTS

ANDERS REIZ
Yerkes Observatory and Lund Observatory
Received March 31, 1954

ABSTRACT

In order to explain the location in the H-R diagram of the population II high-velocity subdwarfs of F type, recently studied by Miss Roman, in terms of their chemical composition (low abundances of heavy elements), a stellar model has been constructed which is built on the assumption of negligible heavy-element content. This assumption implies that the opacity is caused mainly by free-free transitions and electron scattering and that the energy production is given by the proton-proton reaction. It is found that the configuration falls in the region of the H-R diagram where the subdwarfs are located. Causes of deviation of the stellar model from actual subdwarf stars are briefly discussed.

I. INTRODUCTION

Recent work by Miss Nancy G. Roman[1] presents strong evidence in favor of the existence of a homogeneous group of high-velocity stars, which in several respects show striking deviations from the normal main-sequence stars. Within a sphere, with radius of 100 parsecs, centered in the sun, seventeen objects have so far been found, and it is expected that this figure will not change very appreciably. The stars HD 19445 and 140283, studied earlier in high dispersion by Chamberlain and Aller (1951), are probably the best-known individuals of the group. The last star is illustrated in the Yerkes spectral atlas (Morgan *et al.* 1943). The existence of this type of stars was first noticed by Adams and Joy (1922, 1935), who termed them "intermediate white dwarfs," thus suggesting their location between the main sequence and the white dwarfs.

The data pertinent to the group members can be summarized as follows: The concentration toward the galactic plane is small, the rotational velocities round the galactic center are low. In both respects the stars resemble the globular clusters. The perigalactic distances and the very elongated galactic orbits, computed by Miss Roman under assumptions similar to those of M. Schwarzschild (1952) in related work on high-velocity stars, indicate clearly that the group members belong to the population II objects of the galactic bulge.

The spectroscopic evidence, though not unique, leads to the suggestion that these stars are similar to the main-sequence stars in the middle of the F spectral class. This is inferred from the strength of the *H* lines and from the behavior of the Balmer jump. These conclusions are in very good agreement with the theoretical predictions made by Chamberlain and Aller, who showed that the spectra of the two stars studied could be explained in terms of the properties of atmospheres that have temperatures appropriate to F-type stars. Their work also shows that while some metals have abnormally low abundances, the stars are not deficient in hydrogen.

Miss Roman's photoelectric color measurements of the group of seventeen stars mentioned show that the $U-B$ colors are around -0.2 mag., as compared to 0.0 mag. for main-sequence F stars (Johnson and Morgan 1953). This corresponds to a similar ultraviolet excess found by Morgan, Harris, and Johnson (1953) for subdwarfs. The ultraviolet excess of the F-type subdwarfs, as compared to main-sequence F stars, is presumably due to the relative weakness of the absorption-line spectrum in the ultraviolet. When this effect is taken into account, it is found that the photoelectric color indices are

[1] The author is much indebted to Miss Roman for permission to read her paper in manuscript.

compatible with the effective temperatures derived by Chamberlain and Aller (I owe this remark to Dr. Strömgren).

The scantiness of the data necessarily makes the determination of the absolute magnitude uncertain. From two, not entirely independent, computations Miss Roman suggests that the stars are probably located about $1\frac{1}{2}$ mag. below the main sequence, comparing dwarfs and subdwarfs of equal International color index.

The group isolated, therefore, seems to form a very pure sample of subdwarfs, characterized by small content of heavy elements. Consequently, it would be of considerable interest to try to explain the location of these stars in the H-R diagram with respect to the main sequence, in terms of deviations in chemical composition from that of the main-sequence stars. Following this suggestion by B. Strömgren (1952), which is also substantiated by the results of Chamberlain and Aller, a stellar model has been constructed which is based on the assumption that the abundances of heavy elements are negligible, namely, $Z = 0$. Even though this condition is not exactly encountered in nature, the configuration discussed here represents a limiting case toward which stars which are poor in heavy elements approach.

The condition $Z = 0$ has the following implications for the opacity and energy production: Through the absence of heavy elements, the opacity takes a value corresponding to free electron scattering and hydrogen and helium free-free transitions. The absorption by neutral hydrogen and helium is neglected. Its influence will be of importance only in the outermost low-temperature layers of the stellar interior (see below). The energy production is due to the proton-proton reaction. We shall assume further that the star is in radiative equilibrium and that the radiation pressure can be neglected. The molecular weight μ is assumed to be constant. The differential equations governing the internal structure of a gaseous, spherically symmetrical star in radiative equilibrium are the following (cf. Chandrasekhar 1939):

$$\frac{dP}{dr} = -\frac{GM(r)}{r^2}\rho, \qquad \frac{d(T^4)}{dr} = -\frac{3}{ac}\kappa\rho\frac{L(r)}{4\pi r^2}, \tag{1}$$

$$\frac{dM(r)}{dr} = 4\pi r^2\rho, \quad \text{and} \quad \frac{dL(r)}{dr} = 4\pi r^2\rho\epsilon(r). \tag{2}$$

Standard notations have been used throughout.

II. OPACITY

We shall now derive an expression for the opacity $\kappa(T, \rho)$ as a function of temperature and density. In discussions of stellar models with nonnegligible heavy-element content, Kramers' law of opacity, $\kappa \sim \rho T^{-3.5}$, or its modified form, $\kappa \sim \tau^{-1}\rho T^{-3.5}$, τ being the guillotine factor which is also a function of temperature and density, have proved good representations for the opacity. In the present case an interpolation formula of similar structure holds for the range of temperature and density covered.

We shall take the coefficient of opacity κ to be defined by the Rosseland mean, namely, the weighted harmonic mean of the mass-absorption coefficient κ_ν, taken over all frequencies ν. Here κ_ν consists of two parts, the frequency-dependent part, κ_ν, due to hydrogen and helium free-free transitions, and the free electron-scattering component, κ_{sc}, which is independent of frequency.

In forming the mean value, Rosseland has shown that the coefficient κ_ν should be corrected for influence of the induced emission; hence κ_ν contributes an amount $\kappa_\nu[1 - \exp(-h\nu/kT)]$. For the electron scattering, however, no such correction should be applied, as has been pointed out by Rudkjøbing (1947). Hence

$$\kappa_\nu' = \kappa_\nu(1 - e^{-x}) + \kappa_{sc}, \tag{3}$$

where

$$x = \frac{h\nu}{kT}. \tag{4}$$

Using standard notations (cf. Chandrasekhar 1939), the absorption coefficient κ_ν due to atoms of atomic weight A and number Z and caused by free-free transitions, is given by

$$\kappa_\nu = \frac{D_{ff}}{x^3}\, g(x)\,, \tag{5}$$

where

$$D_{ff} = \frac{Z^2}{AH}\,\frac{16\pi^2}{3\sqrt{3}}\,\frac{e^6 h^2}{c\,(2\pi m_e)^{3/2}}\,\frac{N_e}{(kT)^{3.5}} \tag{6}$$

and

$$N_e = \frac{\rho\,(1+X)}{2H}. \tag{7}$$

The contributions due to electron scattering are given by the expression

$$\kappa_{sc} = \kappa_0(1+X) \qquad (\kappa_0 = 0.2)\,. \tag{8}$$

Because $Z^2/A = 1$ for both hydrogen and helium, we can write

$$D_{ff} = 7.302 \times 10^{24}\,(1+X)\,\rho T^{-3.5}\,. \tag{9}$$

Inserting equations (5) and (8) in equation (3), we get, from the definition of the Rosseland mean,

$$\frac{1}{\kappa} = \frac{15}{4\pi^4\,(1+X)} \int_0^\infty \frac{\vartheta(x)}{\phi(x;\,\rho,T)}\,dx\,, \tag{10}$$

where the functions $\vartheta(x)$ and $\phi(x;\,\rho,T)$ are defined as follows:

$$\vartheta(x) = \frac{x^4 e^{-x}}{(1-e^{-x})^2}, \qquad \phi(x;\,\rho,T) = D_{ff}\,g(x)\,\frac{1-e^{-x}}{x^3} + \kappa_0\,. \tag{11}$$

For the Gaunt factor $g(x)$ the following approximate expression has been used:

$$g(x) = \frac{\sqrt{3}}{\pi}\,\ln\left[\frac{(0.76+x)^{1/2}+0.87}{(0.76+x)^{1/2}-0.87}\right], \tag{12}$$

which was first derived by Kulsrud,[2] who has computed the Gaunt factor for transitions of an electron under the conditions prevailing in the interior of a hydrogen star.

The opacity is therefore given as an integral which contains, as a parameter, the temperature and density only in the combination $\rho T^{-3.5}$. We shall compute the integral for certain values of this quantity which are likely to be encountered in the interior of the star. The range of variation of $\rho T^{-3.5}$ to be expected for a star of solar mass was derived from the solar model computed by P. Naur (Strömgren 1953). This model, being built on the proton-proton reaction and with opacity arising from absorption by heavy elements, free-free transitions, and electron scattering, is the most recent one available; it should be quite satisfactory for our purpose. The quantity $\log(\rho T^{-3.5})$, computed for values of temperature and density at points between the center of the model and 0.82 of the radius, ranges between -22.98 and -22.46. The results of the calculation of the

[2] The author is much indebted to Mr. Kulsrud for communicating these results in advance of publication.

opacity, based on the equation (10), are given in Table 1 for arguments not only within this range but also for such outside the limits.

The slope of the relation log κ versus log $(\rho T^{-3.5})$ ranges from 0.42 near the center to 0.58 in the outer regions. Adopting their average value, 0.5, which gives a sufficiently good approximation over the entire region of $\rho T^{-3.5}$ considered, the following interpolation formula for the opacity is valid:

$$\kappa = \tilde{\kappa}(1 + X)\rho^{0.5}T^{-1.75} . \tag{13}$$

Forming the product $\kappa(1 + X)^{-1}\rho^{-0.5}T^{1.75}$, we adopt, as its average value over the range -23.00 to -22.40, log $\tilde{\kappa} = 11.202$.

TABLE 1

VALUES OF THE LOGARITHM OF THE OPACITY

log $(\rho T^{-3.5})$	log $[\kappa(1+X)^{-1}]$	log $\tilde{\kappa}$	log $(\rho T^{-3.5})$	log $[\kappa(1+X)^{-1}]$	log $\tilde{\kappa}$
−24+0.40	−0.490	11.310	−23+0.30	−0.155	11.195
−24+ .60	− .435	11.265	−23+ .40	− .102	11.198
−24+ .80	− .378	11.232	−23+ .50	− .046	11.204
			−23+ .60	+ .013	11.213
−23+ .00	− .293	11.207			
−23+ .10	− .250	11.200	−23+ .80	+ .041	11.241
−23+0.20	−0.204	11.196	−22+0.00	+0.281	11.281

For the energy-production process the following law is assumed:

$$\epsilon(r) = \epsilon_0(X)\rho T^4 , \tag{14}$$

where the coefficient $\epsilon_0(X)$ has the value

$$\epsilon_0(X) = X^2 10^{-29} . \tag{15}$$

The foregoing formulae are taken from the most recent discussion of the proton-proton process by Salpeter (1952).

III. INTEGRATION OF DIFFERENTIAL EQUATIONS

We shall now turn to the numerical integration of the differential equations (1) and (2). The boundary conditions to be satisfied are the following:

$$a)\ M(r) = L(r) = 0 \qquad \text{for } r = 0 \tag{16}$$

and

$$b)\ T \to 0,\ \rho \to 0 \quad \text{simultaneously at the surface} . \tag{17}$$

Clearly, we must also require that $M(r) = M$ and $L(r) = L$ at the surface. Following Rosseland (1932), we shall change to the nondimensional variables τ, σ, ψ, λ, and x, defined as follows:

$$T = T_c\tau , \qquad \rho = \rho_c\sigma , \qquad M(r) = M_0\psi , \qquad L(r) = L_0\lambda , \qquad \text{and} \qquad r = r_0 x . \tag{18}$$

The boundary conditions (16) and (17) are now as follows:

$$a)\ x = 0 : \tau = \sigma = 1 , \qquad \psi = \lambda = 0 ; \tag{19}$$

$$b)\ x = x_0 : \tau \to 0 , \qquad \sigma \to 0 \text{ simultaneously} ; \qquad \psi = \psi_0 , \qquad \lambda = \lambda_0 . \tag{20}$$

For $x = x_0$ we also have the relations

$$M = M_0\psi_0\,, \qquad L = L_0\lambda_0\,, \qquad \text{and} \qquad R = r_0x_0\,. \tag{21}$$

Inserting equation (18) in equations (1) and (2), we obtain this new set of equations:

$$\frac{d(\sigma\tau)}{dx} = -\varpi\frac{\psi\sigma}{x^2}\,, \qquad \frac{d\tau}{dx} = -\frac{\lambda\sigma^{1.5}}{x^2\tau^{4.75}}\,, \tag{22}$$

$$\frac{d\psi}{dx} = x^2\sigma\,, \qquad \text{and} \qquad \frac{d\lambda}{dx} = x^2\sigma^2\tau^4\,, \tag{23}$$

where the conditions

$$\frac{\mu GH}{k}\frac{M_0}{r_0}\frac{1}{T_c} = \varpi\,, \qquad \frac{3\bar{\kappa}}{16\pi ac}\frac{L_0\rho_c^{1.5}}{T_c^{5.75}} = r_0\,, \tag{24}$$

$$4\pi r_0^3\rho_c = M_0\,, \qquad \text{and} \qquad 4\pi r_0^3\rho_c^2T_c^4 = L_0 \tag{25}$$

have been imposed upon the parameters.

Through numerical integrations of the system of equations (22) and (23) subject to conditions (19) and (20), we shall derive the eigen-value for which the surface conditions $\tau \to 0$ and $\sigma \to 0$, simultaneously, are satisfied. Hence we shall obtain a value of the radius of the star, x_0, the corresponding values of mass and luminosity, ψ_0 and λ_0, and the distributions of relative temperature, density, mass, and luminosity. This solution, being derived for one set of the parameters, can be transformed to any other set by means of homology transformations.

After finding the appropriate values x_0, ψ_0, λ_0, and ϖ_0, the quantities r_0, M_0, and L_0, given by equation (21), are inserted in equations (24) and (25). Solving for T_c and ρ_c, we get the following relations:

$$T_c = \frac{x_0}{\psi_0}\frac{1}{\varpi_0}\frac{M_\odot}{R_\odot}\frac{\mu GH}{k}\frac{M}{R}\,, \tag{26}$$

$$\rho_c = \frac{1}{4\pi}\frac{x_0^3M_\odot}{\psi_0R_\odot^3}\frac{M}{R^3}\,, \tag{27}$$

$$L = c_1\frac{1}{1+X}R^{-0.25}M^{4.25}\mu^{5.75}\,, \tag{28}$$

and

$$L = c_2X^2R^{-7}M^6\mu^4\,, \tag{29}$$

where M, L, and R are expressed in solar units. Formula (28) is the mass-luminosity relation and (29) the equation for energy generation. The constants c_1 and c_2 are the following:

$$c_1 = \frac{128\pi^{5/2}ac}{3}\left(\frac{GH}{k}\right)^{5.75}\frac{M_\odot^{4.25}x_0^{0.25}\lambda_0}{L_\odot R_\odot^{0.25}\psi_0^{4.25}\varpi_0^{5.75}}\frac{1}{\bar{\kappa}}\,, \tag{30}$$

and

$$c_2 = \frac{1}{4\pi}\left(\frac{GH}{k}\right)^4\frac{M_\odot^6x_0^7\lambda_0}{L_\odot R_\odot^7\psi_0^6\varpi_0^4}\,. \tag{31}$$

The integrations are commenced by means of power series development in τ, σ, $3\psi x^{-3}$, $3\lambda x^{-3}$, and are continued by standard methods. The well-known instability of the solution makes it profitable to replace the variable σ, from $x = 1.5$, by the new variable θ, defined as follows (Gardiner 1951*a*):

$$\theta = \sigma\tau^{-19/6}. \tag{32}$$

The condition $\tau \to 0$, $\sigma \to 0$ simultaneously at the boundary becomes $\tau \to 0$, $\theta \to \theta_0$ constant, for the following reasons: In the outer region close to the surface, we have $\psi' = \lambda' = 0$, or $\psi = \psi_0$, $\lambda = \lambda_0$; and we can therefore integrate the first two of the equations (22) exactly. Thus the equations

$$\sigma = \left(\frac{6}{25}\,\varpi_0\frac{\psi_0}{\lambda_0}\right)^{2/3}\tau^{19/6}, \qquad \tau = \frac{6}{25}\,\varpi_0\psi_0\left(\frac{1}{x}-\frac{1}{x_0}\right), \tag{33}$$

are obtained; from the first it follows that

$$\sigma\tau^{-19/6} = \theta_0 = \left(\frac{6}{25}\,\varpi_0\frac{\psi_0}{\lambda_0}\right)^{2/3}. \tag{34}$$

Equation (34) determines the constant θ_0. The system of equations (22)–(23) takes the form

$$\frac{d\theta}{dx} = \frac{25}{6x^2}\frac{\theta}{\tau}\left[\lambda\theta^{3/2} - \frac{6}{25}\,\varpi\psi\right], \qquad \frac{d\tau}{dx} = -\frac{\lambda\theta^{3/2}}{x^2}, \tag{35}$$

$$\frac{d\psi}{dx} = x^2\theta\tau^{19/6}, \qquad \text{and} \qquad \frac{d\lambda}{dx} = x^2\theta^2\tau^{31/3}. \tag{36}$$

This set has been used up to $x = 4.0$. It is, of course, not necessary to repeat the complete integration from the start for all ϖ values used. After a few approximate values

TABLE 2

DISTRIBUTION OF TEMPERATURE, DENSITY, MASS, AND LUMINOSITY

x/x_0	T/T_c	ρ/ρ_c	ψ/ψ_0	λ/λ_0
0.000	1.000	1.000	0.000	0.000
0.103	0.923	0.889	0.032	0.220
0.205	0.740	0.608	0.207	0.766
0.308	0.543	0.310	0.490	0.973
0.396	0.403	0.141	0.711	0.998
0.498	0.278	0.048	0.877	1.000
0.601	0.189	0.014	0.958	1.000
0.704	0.118	0.003	0.989	1.000
0.806	0.068	0.000$_5$	0.998	1.000
0.900	0.031	0.000	1.000	1.000
1.000	0.000	0.000	1.000	1.000

have been found on either side of the required value, an improved ϖ can, in fact, be easily interpolated.

The outward integrations pertaining to equations (35)–(36) give with sufficient accuracy the eigen-value ϖ_0 and the final λ_0. In order to obtain ψ_0 and the temperature, density, and mass distributions, it is necessary to perform integrations from the surface

inward. For given x_0 and ψ_0 the temperature just below the surface is computed from the second of equations (33), and hence σ and θ can be obtained. The outward integrations provide a sufficiently good estimate of the constant θ_0, which can be used for obtaining a good starting value for ψ_0 and hence for σ for the inward integrations. For this purpose the following system of equations was used (Strömgren 1932):

$$\frac{d \log \tau}{dt} = \lambda_0 (\xi - \xi_0) \frac{\sigma^{1.5}}{\tau^{5.75}}, \qquad \frac{d \log \sigma}{dt} = \varpi_0 \frac{\xi - \xi_0}{\tau} \psi - \frac{d \log \tau}{dt}, \tag{37}$$

and

$$\frac{d\psi}{dt} = -\frac{1}{\log e} \frac{\xi - \xi_0}{\xi^4} \sigma, \tag{38}$$

where

$$t = \log (\xi - \xi_0), \qquad \xi = x^{-1}, \qquad \xi_0 = x_0^{-1}. \tag{39}$$

In the regions considered we have $\lambda' = 0$.

The final results from the combined integrations where the outward and inward integrations are fitted together are presented in Table 2. From this solution we have

$$\varpi_0 = 2.412387, \qquad x_0 = 6.82, \qquad \psi_0 = 3.323, \qquad \lambda_0 = 0.37643.$$

IV. RELATIONS BETWEEN MASS, RADIUS, LUMINOSITY, EFFECTIVE TEMPERATURE, AND CHEMICAL COMPOSITION

From the mass-luminosity relation (28) and the equation of energy generation (29) we can derive expressions for luminosity and radius, L and R, as functions of the chemical composition and mass, μ and M. Further, we have

$$L = 4\pi\sigma R^2 T_e^4, \tag{40}$$

where σ is Stefan's constant. In solar units equation (40) becomes

$$L = c_3 R^2 T_e^4, \qquad c_3 = 4\pi\sigma \frac{R_\odot^2}{L_\odot}. \tag{41}$$

The following three relations result from the solution of equations (28), (29), and (41):

$$L = C_1 f_1(X) M^{113/27}, \qquad R = C_2 f_2(X) M^{7/27}, \qquad L = C_3 f_3(X) T_e^{452/99}. \tag{42}$$

The functions $f_1(X), f_2(X), f_3(X)$ are defined as follows:

$$f_1(X) = \frac{1}{(1+X)} \frac{1}{\{X^2(1+X)\}^{1/27}} \mu^{157/27}, \tag{43}$$

$$f_2(X) = \{X^2(1+X)\}^{4/27} \mu^{-4/27}, \tag{44}$$

$$f_3(X) = (1+X)^{14/99} \{X^2(1+X)\}^{34/99} \mu^{-140/99} \tag{45}$$

and the constants C_1, C_2, and C_3 are

$$C_1 = c_1 \left(\frac{c_1}{c_2}\right)^{1/27}, \qquad C_2 = \left(\frac{c_2}{c_1}\right)^{4/27}, \qquad \text{and} \qquad C = c_{13} \left(\frac{c_2}{c_1}\right)^{34/99} \left(\frac{c_3}{c_1}\right)^{113/99}. \tag{46}$$

In Table 3 are listed the logarithms of the values of the functions f_1, f_2, and f_3 computed for various values of the hydrogen content X. Adopting the luminosity $L = 1L_\odot$, the mass, radius, and effective temperature are computed for the three values of the hydrogen content $X = 0.6, 0.75, 0.9$, and listed in Table 4.

V. CHECKS OF ASSUMPTIONS

Two remarks which are of importance when judging the results should be made. The first concerns the validity of the basic assumption that radiative equilibrium obtains throughout the star. Applying the criterion that $(n+1)_{\text{rad}} = d \log (\sigma\tau)/d \log \tau < 2.5$ for convective instability, we find that convection sets in at a point corresponding to

TABLE 3

VALUES OF LOGARITHMS OF FUNCTIONS $f_1(X)$, $f_2(X)$, AND $f_3(X)$ FOR VARIOUS HYDROGEN CONTENTS

X	$\log f_1(X)$	$\log f_2(X)$	$\log f_3(X)$	X	$\log f_1(X)$	$\log f_2(X)$	$\log f_3(X)$
0.1	+0.3685	−0.3050	−0.7488	0.7	−1.4533	+0.0430	+0.3034
.2	−0.0304	− .1952	− .4417	0.75	−1.5642	+ .0580	+ .3534
.3	−0.3771	− .1247	− .2315	0.8	−1.6712	+ .0722	+ .4010
.4	−0.6854	− .0713	− .0655	0.9	−1.8737	+ .0984	+ .4899
.5	−0.9645	− .0274	+ .0742	1.0	−2.0623	+0.1224	+0.5716
0.6	−1.2188	+0.0100	+0.1955				

$$\log C_1 = 1.8902\,, \qquad \log C_2 = -0.1842\,, \qquad \log C_3 = -18+0.1445$$

TABLE 4

PHYSICAL PARAMETERS FOR THREE DIFFERENT HYDROGEN CONTENTS

X	M	R	T_e	T_c	ρ_c
0.6	0.691	0.609	7380	14.9×10^6	137
.75	.836	.714	6810	13.6×10^6	103
0.9	0.991	0.819	6360	12.7×10^6	81

about 7 per cent of the radius. Thus the convective core contains about 1 per cent of the mass, and approximately 9 per cent of the total luminosity is generated inside it. If one compares the temperature, density, and mass values for this central core computed under the assumption of radiative equilibrium, one finds that they are, within three-figure accuracy, entirely the same as the values derived for the zone under the assumption of convective equilibrium. This is also to be expected, because the polytropic index $n+1$ at the center of the model is equal to the eigen-value ϖ_0, which is less than 4 per cent lower than the limit 2.5. Therefore, we conclude that the presence of the small convective core has no significant influence on the structure of the outer zone, which is in radiative equilibrium.

The second remark concerns the validity of the interpolation formula (13) giving the opacity, when the calculations are extended toward larger masses. Application to much smaller masses is not likely to be considered. From the work of D. Osterbrock (1953) on dwarf stars it seems clear that in this case the stars are built on another model, consisting of a central core in radiative equilibrium surrounded by an extended convective core.

We shall estimate how much an increase in mass by a factor of 2 affects the results.

For a hydrogen content equal to 0.75, this corresponds to stars of mass about $1.7M_\odot$ (see Table 4), which certainly marks an upper limit on our estimate.

As $T_e \sim MR^{-1}$ and $\rho_c \sim MR^{-3}$, we have $\rho_c T_c^{-3.5} \sim T_c^{-0.5} M^{-2}$. An increase in M by a factor of 2 will roughly reduce the argument $\rho T^{-3.5}$ by a factor of 4, and the corresponding change in log $(\rho T^{-3.5})$ is 0.6 in the direction of a smaller argument. From Table 1 we find that, for the argument -23.60, the deviation in $\bar{\kappa}$ from constancy amounts to less than 30 per cent. An increase in $\bar{\kappa}$ implies a decrease in c_1. It follows from equation (42) that a change in c_1 results in a change in log T_e given by $\Delta \log T_e \approx 1/10\, \Delta \log c_1$.

Therefore, even if we alter $\bar{\kappa}$ by as much as 30 per cent, this figure referring to the largest deviation of the individual $\bar{\kappa}$ from the average value, we find that T_e is changed by only 3 per cent. The same change in c_1 will affect the quantities M and R by roughly 7 and 5 per cent, respectively. If we consider a change of mass from the original $0.84M_\odot$ to $1.3M_\odot$, corresponding to a factor of about 1.5, the resulting effect on temperature, mass, and radius will only be 1, 3, and 2 per cent approximately. Similarly, it is found that the deviations will be small for smaller masses down to about $0.5M_\odot$. The conclusion deduced will therefore be valid for a rather wide range of mass values—in fact, probably for the whole range for which the model considered is of interest. Large masses may not exist for the population II stars because of the effects of evolution; and for small masses the influence of the outer convective zone may strongly influence the stellar model (cf. Osterbrock 1953).

VI. LOCATION IN HERTZSPRUNG-RUSSELL DIAGRAM

In Figure 1 we have plotted log T_e from Table 4. The effective temperature scale is that given by Keenan and Morgan (1951); bolometric corrections are those of Kuiper (1938). The location of the model star is below the main sequence, displaced toward higher effective temperature; that is, the star has a lower luminosity for the same effective temperature. The temperatures correspond to the spectral classes F0–F6. This region in the H-R diagram is that where the population II subdwarfs of the F type studied by Miss Roman have been located. It is quite likely that the main sequences of globular clusters also pass through this region.

VII. CAUSES OF DEVIATIONS OF STELLAR MODEL FROM ACTUAL STAR

The results obtained refer to a stellar model which is constructed under certain assumptions, specified earlier. We shall briefly discuss the following sources of deviations of the actual star from the model considered: (*a*) the influence of the bound-free transitions of hydrogen and helium in the outer layers, (*b*) degeneracy in the central regions, and (*c*) variation of the molecular weight with distance from the center of the star.

In computing the opacity we have considered only the effect of absorption arising from the free-free transitions and electron scattering. For the outermost low-temperature layers of the stellar interior, the contribution to the opacity by neutral hydrogen and helium will become increasingly important. We shall estimate the opacity κ caused by neutral hydrogen only and compare this to the opacity due to free-free transitions and electron scattering in a pure hydrogen gas κ, as derived from equation (13). We utilize a formula provided by Miss Gardiner (1951*b*, eqs. [4], [5]) which we write as follows:

$$\log \bar{\kappa} = 28.37 + \log (\rho T^{-3.5}) - \log T \qquad (\log T > 5)\,. \tag{47}$$

The extra factor T^{-1} in the bound-free contributions to the opacity occurs because the absorption in the Lyman continuum has a factor $2I_H/kT$, as compared to the free-free absorption coefficient, where I_H is the ionization potential of hydrogen.

The results from calculations for three points corresponding to 0.6, 0.7, and 0.8 of the radius are contained in Table 5. For the first two arguments the effect of the neutral

hydrogen absorption, though increasing rapidly, is small compared to that of the free-free transitions and electron scattering. It is not likely that the inclusion of the neutral hydrogen and helium absorption will strongly influence the constitution of the stellar model and hence cause large deviations from the actual star.

The condition for the setting-in of nonrelativistic degeneracy is the following (cf. Strömgren 1936):

$$\left(\frac{K_1 H}{k}\right)^{3/2} \frac{1}{\mu} \frac{\rho}{T^{3/2}} > 1 \qquad (K_1 = 9.87 \times 10^{12}) \ . \tag{48}$$

The left-hand quantity, calculated for the central conditions appropriate to the mass values 0.84, 0.5, 0.3$M_\odot$ ($X = 0.75$), becomes 0.16, 0.26, and 0.45, respectively. Even for such small masses as three-tenths of a solar mass, which is well outside the range of mass values considered, we are far from the limit of degeneracy.

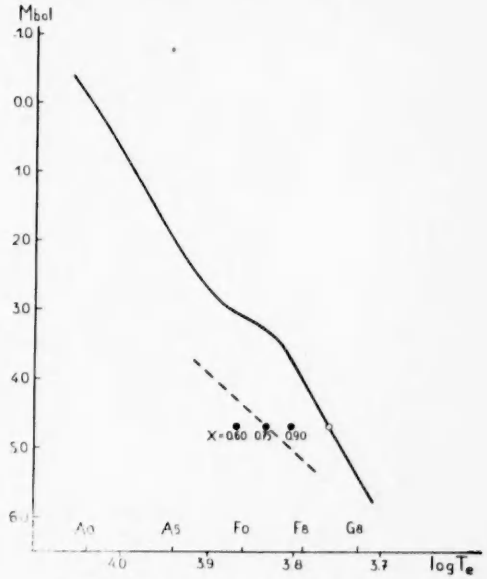

FIG. 1.—Solid curve refers to the main sequence in the M_{bol}, log T_e plane; the location of the sun is denoted by ⊙. Points refer to log T_e from Table 4 calculated for $L = 1 L_\odot$, and the numbers to the corresponding hydrogen contents. Dotted line represents the log L, log T_e relation, based on equation (42).

TABLE 5

COMPARISON OF OPACITY DUE TO NEUTRAL HYDROGEN, $\bar{\kappa}$, AND OPACITY DUE TO FREE-FREE TRANSITIONS AND ELECTRON SCATTERING, κ, $X = 1$

x/x_0	log $\bar{\kappa}$	log κ	x/x_0	log $\bar{\kappa}$	log κ	x/x_0	log $\bar{\kappa}$	log κ
0.6	−0.28	0.41	0.7	−0.04	0.41	0.8	0.31	0.51

When considering the third cause of deviation between the actual star and the model, we know that, for stars of mass of the size of the sun and smaller, the energy production is largely due to the proton-proton reaction. This is true also in case of nonnegligible heavy-element content. Mixing of the elements is negligible in these stars outside possibly existing small convective cores. The molecular weight will be highest in the center of the star and decrease outward. We shall have a continuous decrease of the hydrogen content in the central region, thus increasing the molecular weight. Following the way outlined by Strömgren (1952), one can take this effect into account; in doing so, we shall be able to study the evolutionary changes of the model. This will be attempted in a later paper.

The author is much indebted to Dr. Bengt Strömgren for helpful discussions and for his critical reading of the manuscript. He is grateful for the hospitality extended to him during the stay at the Yerkes Observatory when this work was carried out. Financial support from the Swedish Natural Science Research Council and from the Royal Physiographic Society in Lund is gratefully acknowledged.

REFERENCES

Adams, W. S., and Joy, A. H. 1922, *Ap. J.*, **56**, 242.
Adams, W. S.; Joy, A. H.; Humason, M. L.; and Brayton, A. M. 1935, *Ap. J.*, **81**, 187.
Chamberlain, J. W., and Aller, L. H. 1951, *Ap. J.*, **114**, 52.
Chandrasekhar, S. 1939, *An Introduction to the Study of Stellar Structure* (Chicago: University of Chicago Press).
Gardiner, J. G. 1951*a*, *M.N.*, **111**, 94.
———. 1951*b*, *ibid.*, p. 102.
Johnson, H. L., and Morgan, W. W. 1953, *Ap. J.*, **113**, 313.
Keenan, P. C., and Morgan, W. W. 1951, "Classification of Stellar Spectra," in *Astrophysics*, ed. J. A. Hynek, chap. 1, p. 12.
Kuiper, G. P. 1938, *Ap. J.*, **88**, 446.
Kulsrud, R. M. 1954, *Ap. J.*, **119**, 386.
Morgan, W. W.; Harris, D. L.; and Johnson, H. L. 1953, *Ap. J.*, **118**, 92.
Morgan, W. W.; Keenan, P. C.; and Kellman, E. 1943, *An Atlas of Stellar Spectra* (Chicago: University of Chicago Press).
Osterbrock, D. E. 1953, *Ap. J.*, **118**, 529.
Roman, N. G. 1954, *A.J.* (in press).
Rosseland, S. 1932, *Zs. f. Ap.*, **4**, 255.
Rudkjøbing, M. 1947, *Pub. Medd. Københavns Obs.*, No. 145.
Salpeter, E. E. 1952, *Phys. Rev.*, **88**, 547.
Schwarzschild, M. 1952, *A.J.*, **57**, 57.
Strömgren, B. 1932, *Zs. f. Ap.*, **2**, 345.
———. 1936, *Handb. d. Ap.*, **7**, 121.
———. 1952, *A.J.*, **57**, 65.
———. 1953, "The Sun as a Star," in *The Sun*, ed. Gerard P. Kuiper (Chicago: University of Chicago Press), chap. 2, p. 36.

APSIDAL MOTION AND RADIUS OF GYRATION OF SOLAR MODELS*

I. EPSTEIN AND L. MOTZ
Rutherfurd Observatory, Columbia University
Received March 22, 1954

ABSTRACT

The apsidal motion and radius of gyration are determined for the solar model recently calculated by Epstein and Motz. The effective polytropic index as determined from the apsidal motion for this model is 3.30. If the logarithm of the apsidal-motion constant is plotted against the logarithm of the radius of gyration, the point for this model is found to lie very close to the straight line for polytropes and other main-sequence models.

I. INTRODUCTION

Recent investigations (Epstein and Motz 1953, 1954) into the internal constitution of the sun have demonstrated that proton-proton solar models are extremely sensitive to the relative abundances of hydrogen and the metals. Because of this, it is necessary to use an opacity formula that is consistent with the chemical abundances and range of parameters in the solar interior. In what follows we calculate the apsidal-motion constant and the radius of gyration for such a solar model, using the data given by Epstein (1951).

II. RADIUS OF GYRATION AND APSIDAL MOTION

Previous calculations (Motz 1952) have shown that a linear relationship exists between the logarithm of the apsidal-motion constant and the logarithm of the radius of gyration for simple polytropes and for two-zone main-sequence stellar models for which a convective-core solution can be found with zero mass and luminosity discrepancy between the core and the envelope.

Applying the formulae and equations developed by Motz (1952), we find the following values for the apsidal motion constant k and the radius-of-gyration constant $(H/R)^2$ (these symbols are defined by Motz 1952):

$$k = 0.007285 , \qquad \left(\frac{H}{R}\right)^2 = 0.062229 .$$

From the value of k given here, we can determine the effective polytropic index by comparing with the apsidal-motion constants for complete polytropes. This gives the value

$$N_{\text{eff}} = 3.30 ,$$

which is smaller than the value found by Keller (1948) from an analysis of the observational data of actual binaries. The binaries studied by Keller, however, are all of spectral class F0 or earlier, and for these stars the carbon cycle, rather than the proton-proton reaction, is operative. Since one may expect to find a different effective polytropic index for stars governed by the carbon cycle from that for stars governed by the proton-proton reaction, this discrepancy is not unexpected.

In Figure 1 we have plotted $-\log k$ against $-\log (H/R)$ for six complete polytropes (n = 1, 1.5, 2, 3, 3.5, and 4) and for five different solar models. The Schwarzschild R.M. (1946) model and the Keller (1948) pure O model are convective-core carbon-cycle

* This work was supported in part by a contract with the Office of Naval Research, Nonr-266(19).

models with the abundance of heavy atoms assumed to be that of the Russell mixture and that of pure oxygen, respectively.

The proton-proton model I is that calculated by Epstein (1951), using the Bethe-Critchfield formula for the energy generation as corrected by Aller (1950) and the opacity tables computed by Mrs. M. H. Harrison (1948). The proton-proton model II is that

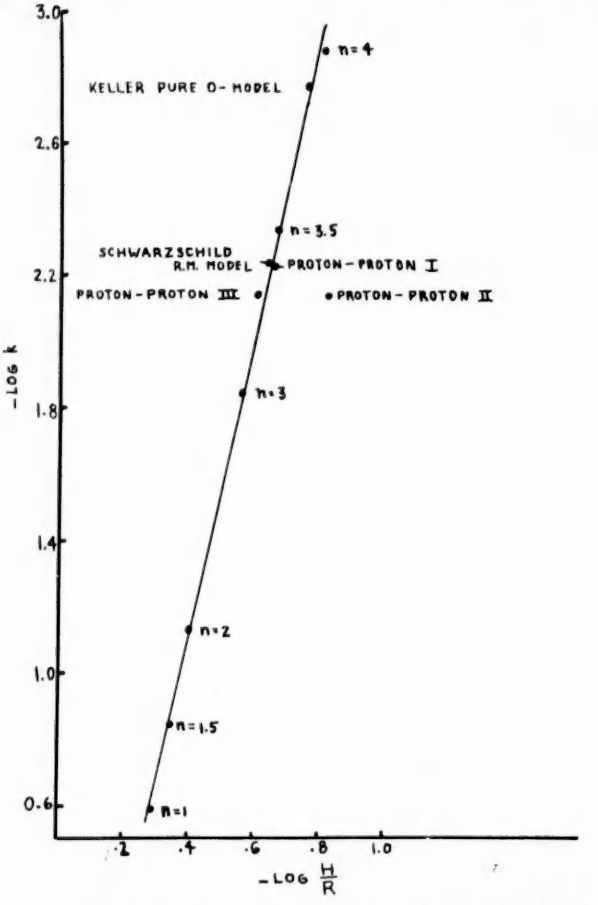

FIG. 1.—Plot of $-\log K$ versus $-\log (H/R)$ for various stellar models

calculated by Epstein and Motz (1953). In this model the coefficient of the energy-generation law for the proton-proton reaction is that found by Frieman and Motz (1953) and by E. E. Salpeter (1952). The opacity formula was again obtained from the tables calculated by Mrs. Harrison. This model gave much too large a percentage of hydrogen (99.8) and a zero helium content with a discrepancy of one part in a thousand for the mass and luminosity fit between the convective core and the radiative envelope.

The proton-proton model III described by Epstein and Motz (1954) was calculated with the same energy-generation formula as that used in model II, but with an improved opacity formula which included the contribution of the hydrogen free-free transitions. We see that for this latest model the plotted point falls very close to the straight line for polytropes.

We wish to thank Mr. Richard Rosen for performing the numerical integrations in this paper.

REFERENCES

Aller, L. H. 1950, *Ap. J.*, **111**, 173.
Epstein, I. 1951, *Ap. J.*, **114**, 438.
Epstein, I. and Motz, L. 1953, *Ap. J.*, **117**, 311.
———. 1954, *ibid.*, **120**, 156.
Harrison, M. H. 1948, *Ap. J.*, **108**, 310.
Keller, G. 1948, *Ap. J.*, **108**, 347.
Motz, L. 1952, *Ap. J.*, **115**, 562.
———. 1953, *ibid.*, **118**, 147.
Motz, L. and Frieman, E., 1953, *Phys. Rev.*, **89**, 648.
Salpeter, E. E. 1952, *Phys. Rev.*, **88**, 549.
Schwarzschild, M. 1946, *Ap. J.*, **104**, 203.

ON THE GRAVITATIONAL STABILITY IN A ROTATING ISOTHERMAL MEDIUM

WALTER FRICKE*
Yerkes Observatory
Received April 2, 1954

ABSTRACT

The wave propagation of a disturbance in a rotating isothermal medium, which is stratified in plane-parallel layers symmetrical to a central plane with maximum density, is studied. The conditions for gravitational instability are deduced.

I. INTRODUCTION

Chandrasekhar (1954) has recently shown that Jeans's criterion for gravitational instability in an infinite homogeneous medium is unaffected by Coriolis force. This paper deals with the propagation of a perturbation in a rotating isothermal medium. The medium is supposed to be stratified in plane-parallel layers symmetrical to a central plane, where the density ρ is a maximum. The problem of gravitational stability in the analogous nonrotational case was solved by P. Ledoux (1951).

II. THE EQUATIONS OF THE PROBLEM

Suppose the medium is rotating with an angular velocity $\mathbf{\Omega}$. In the case of an adiabatic perturbation of the equilibrium state, the fluctuations of density ($\delta\rho$), pressure (δp), and gravitational potential (δV) are governed by the following equations:

$$\frac{\partial \boldsymbol{u}}{\partial t} - 2\boldsymbol{u} \times \mathbf{\Omega} = -\frac{1}{\rho}\operatorname{grad}\,\delta p + \frac{\delta\rho}{\rho}\operatorname{grad}\,p + \operatorname{grad}\,\delta V\,, \tag{1}$$

$$\frac{\partial}{\partial t}\,\delta\rho = -\operatorname{div}(\rho\boldsymbol{u})\,, \tag{2}$$

$$\delta p = \gamma\frac{p}{\rho}\,\delta\rho + \delta r\left(\gamma\frac{p}{\rho}\operatorname{grad}\,\rho - \operatorname{grad}\,p\right), \tag{3}$$

$$\nabla^2\delta V = -4\pi G\delta\rho\,. \tag{4}$$

For an isothermal variation of an isothermal state, equation (3) reduces to

$$\delta p = a^2\delta\rho \qquad \text{with} \qquad a^2 = \frac{p}{\rho} = \text{Const}\,. \tag{5}$$

Furthermore,

$$-\frac{1}{\rho}\operatorname{grad}\,\delta p + \frac{\delta\rho}{\rho^2}\operatorname{grad}\,p = -a^2\operatorname{grad}\frac{\delta\rho}{\rho}\,. \tag{6}$$

If the co-ordinate system is oriented so that the xy-plane denotes the central plane and the density is supposed to be a function of z only, then the equation of continuity (2) becomes

$$-\frac{\partial}{\partial t}\,\delta\rho = \rho\operatorname{div}\boldsymbol{u} + w\frac{d\rho}{dz}\,, \tag{7}$$

where w is the velocity component in the z-direction. Choosing the z-axis as the axis of rotation and denoting the frequency of the perturbation by ω, so that

$$\frac{\partial}{\partial t} = i\omega\,, \tag{8}$$

* Guest investigator from the Hamburg Observatory, Germany. The research reported in this paper was made possible by a grant of the Deutsche Forschungsgemeinschaft, Germany.

we can write the equations of the problem as follows:

$$\omega^2 \delta \mathbf{r} + 2i\omega \begin{pmatrix} \Omega \delta y \\ -\Omega \delta x \\ 0 \end{pmatrix} = \operatorname{grad} (\theta - \delta V), \tag{9}$$

$$\theta = -a^2 \left(\operatorname{div} \delta \mathbf{r} + \delta z \frac{d\rho}{\rho dz} \right), \tag{10}$$

$$\nabla^2 \delta V = -\frac{4\pi G \rho}{a^2} \theta, \tag{11}$$

where we have introduced the abbreviation

$$\theta = a^2 \frac{\delta \rho}{\rho}. \tag{12}$$

Equations (9)–(11) determine the quantities δx, δy, δz, θ, and δV, which describe the fluctuation. These equations can be reduced to two for θ and δV as follows: After differentiating equations (9) by x, y, and z, respectively, we obtain, by summation,

$$\omega^2 \operatorname{div} \delta \mathbf{r} + 2i\omega\Omega \left(\frac{\partial \delta y}{\partial x} - \frac{\partial \delta x}{\partial y} \right) = \nabla^2 (\theta - \delta V). \tag{13}$$

Using the integrability condition,

$$2\omega^2 \Omega \operatorname{div} \delta \mathbf{r} + i\omega^3 \left(\frac{\partial \delta y}{\partial x} - \frac{\partial \delta x}{\partial y} \right) = 2\Omega \frac{\partial^2}{\partial z^2} (\theta - \delta V), \tag{14}$$

to eliminate

$$\frac{\partial \delta y}{\partial x} - \frac{\partial \delta x}{\partial y}$$

and taking into account the equation of continuity to substitute for div $\delta \mathbf{r}$, we obtain

$$(\omega^2 - 4\Omega^2) \left(\frac{\omega^2}{a^2} \theta + \frac{d\rho}{\rho dz} \frac{\partial}{\partial z} [\theta - \delta V] \right) + \omega^2 \nabla^2 (\theta - \delta V) = 4\Omega^2 \frac{\partial^2}{\partial z^2} (\theta - \delta V). \tag{15}$$

This equation, together with equation (11), determines the fluctuations θ and δV.

For solutions which respresent a plane wave in the x-direction (and similarly in the y-direction), we have

$$\theta = \theta_1 (z) e^{i(\omega t + kx)}, \qquad \delta V = \delta V_1 (z) e^{i(\omega t + kx)}, \tag{16}$$

and

$$\nabla^2 = \frac{\partial^2}{\partial z^2} - k^2, \tag{17}$$

where k denotes the wave number $k = 2\pi/\lambda$.

III. THE DENSITY IN THE EQUILIBRIUM STATE

The density function $\rho = \rho(z)$ follows from the condition of hydrostatic equilibrium,

$$\frac{1}{\rho} \frac{dp}{dz} = \frac{dV}{dz}, \tag{18}$$

the assumption of an isothermal state,

$$\frac{p}{\rho} = a^2, \tag{19}$$

and Poisson's equation,

$$\nabla^2 V = -4\pi G\rho\,. \tag{20}$$

Following Ledoux's (1951) procedure, we introduce μ as a new variable instead of z by

$$\mu = \frac{1}{M}\int_0^z \rho(z)\,dz\,, \qquad M = \int_0^\infty \rho(z)\,dz\,, \tag{21}$$

and obtain, for the density function,

$$\rho = \rho_0(1-\mu^2)\,, \tag{22}$$

where

$$\rho_0 = \frac{2\pi G M^2}{a^2} \tag{23}$$

is the density in the xy-plane.

IV. SOLUTIONS OF THE PROBLEM

A solution of equations (11) and (15) can be given for a wave propagation, in which

$$\frac{\partial}{\partial z}\,\delta V \ll \frac{\partial}{\partial z}\,\theta\,. \tag{24}$$

Further, it will be shown that

$$\frac{\partial}{\partial z}\,\delta V = \frac{\partial}{\partial z}\,\theta \tag{25}$$

corresponds to a stable mode of wave propagation. The extreme case that all derivatives of δV are large compared with the corresponding derivatives of θ means that practically no density variations occur and that we are dealing with deformations of the system. This case is of no interest in our present connection. Under condition (24) it follows from equations (11), (15), and (17) that

$$(\omega^2 - 4\Omega^2)\left(\frac{d^2\theta_1}{dz^2} + \frac{d\rho}{\rho dz}\frac{d\theta_1}{dz}\right) + \omega^2\left(\frac{\omega^2 - 4\Omega^2}{a^2} + \frac{4\pi G\rho}{a^2} - k^2\right)\theta_1 = 0\,. \tag{26}$$

Substituting for the density in accordance with equation (22) and introducing μ instead of z as independent variable, we can rewrite equation (26) in the form

$$(1-\mu^2)^2\frac{d^2\theta_1}{d\mu^2} - 4\mu(1-\mu^2)\frac{d\theta_1}{d\mu} + \frac{\omega^2}{\omega^2 - 4\Omega^2}\left[2(1-\mu^2) + (\omega^2 - 4\Omega^2 - k^2a^2)\frac{M^2}{\rho_0^2 a^2}\right]\theta_1 = 0\,. \tag{27}$$

Now

$$\theta_1 = \theta_0(1-\mu^2)^a \tag{28}$$

is the solution of equation (27), which is finite over the whole interval $-1 \le \mu \le +1$, provided that a and ω satisfy the conditions

$$2a^2 + 3a - \frac{\omega^2}{\omega^2 - 4\Omega^2} = 0\,, \tag{29}$$

$$\frac{\omega^2}{\omega^2 - 4\Omega^2}\left[2 + (\omega^2 - 4\Omega^2 - k^2a^2)\frac{M^2}{\rho_0^2 a^2}\right] = 2a\,, \tag{30}$$

and a is positive. The condition $a > 0$ is fulfilled for

$$a = -\frac{3}{4} + \frac{1}{2}\sqrt{\left(\frac{9}{4} + 2\,\frac{\omega^2}{\omega^2 - 4\Omega^2}\right)}, \tag{31}$$

whenever

$$\frac{\omega^2}{\omega^2 - 4\Omega^2} > 0\,, \tag{32}$$

i.e., for all

$$\omega^2 < 0\,, \qquad \omega^2 > 4\Omega^2\,. \tag{33}$$

From equations (29) and (30) it follows that

$$\omega^2 = k^2 a^2 + 4\Omega^2 - \frac{2a+2}{2a+3}\,4\pi G\rho_0\,. \tag{34}$$

Since

$$0 \leq a \leq \frac{\sqrt{17} - 3}{4} \tag{35}$$

for

$$\omega^2 \leq 0$$

instability exists whenever

$$k^2 a^2 < \frac{1 + \sqrt{17}}{3 + \sqrt{17}}\,4\pi G\rho_0 - 4\Omega^2\,. \tag{36}$$

This result differs only slightly from that obtained by Chandrasekhar (1954) for an infinite medium of uniform density ρ. In Chandrasekhar's case the condition of instability for waves propagated perpendicular to the axis of rotation is

$$k^2 c^2 < 4\pi G\rho - 4\Omega^2\,, \tag{37}$$

where c denotes the velocity of sound. Finally, it can be shown that the case of equation (25),

$$\frac{\partial}{\partial z}\,\delta V = \frac{\partial}{\partial z}\,\theta \qquad \text{or} \qquad \delta z = 0 \qquad \text{for} \qquad \omega^2 \neq 0 \tag{38}$$

corresponds to the stable mode,

$$\omega^2 = 4\Omega^2\,. \tag{39}$$

Under condition (38), equation (15) reduces to

$$\frac{\omega^2 - 4\Omega^2}{a^2}\,\theta = k^2(\theta - \delta V) \tag{40}$$

and we obtain the solution

$$\theta_1(z) = \text{Const.}, \qquad \omega^2 = 4\Omega^2\,. \tag{41}$$

I wish to express my deep-felt gratitude to Dr. S. Chandrasekhar for encouraging this investigation and for many valuable discussions on stability questions. Furthermore I am indebted to the University of Chicago for generous hospitality.

REFERENCES

Chandrasekhar, S. 1954, *Ap. J.*, **119**, 7.
———. 1954, *Vistas in Astronomy* (London: Pergamon Press).
Ledoux, P. 1951, *Ann. d'ap.*, **14**, 438.

THE EXCITATION OF HYDROGEN IN AURORAE*

JOSEPH W. CHAMBERLAIN
Yerkes Observatory
Received February 26, 1954

ABSTRACT

The Balmer emission produced when protons penetrate the atmosphere during an aurora is investigated by the method of statistical equilibrium. The *Hα* luminosity versus height is computed for several incident proton energies and is compared with computations for the luminosity distribution in other emissions. It is found that each incident proton should produce a total of about 50 quanta of *Hα*, which leads to a rough estimate for the proton flux of about 6×10^7 cm^{-1} sec^{-2} during the arc stage of a moderately strong aurora. The Balmer decrement is computed, and the theoretical *Hα* profile for an arc in the magnetic zenith is compared with Meinel's observed profile. This comparison suggests that the incident protons undergo considerable scattering, which produces a rather large effect on the observed profile and the luminosity distribution.

I. INTRODUCTION

The penetration of aurora-producing particles into the ionosphere and the resulting distribution of emission with height have been discussed in several papers, principally by the Norwegian workers, since about 1910 (cf. Harang 1951). Usually electrons were assumed to be the primary particles, although positively charged ions were occasionally treated. Recently Bates and Griffing (1953*a*) called attention to the fact that much of the earlier work was based on false assumptions, and they have computed luminosity-curves for aurorae produced by protons. They assumed that the luminosity is proportional to the ionization rate of the air, and they based their calculations on experimentally determined range-energy relations and Bragg-curves.

A detailed examination, however, of the excitation of auroral hydrogen has not previously been made. Meinel's (1951) observation of Doppler-shifted *Hα* in an arc at the magnetic zenith leaves little doubt that protons penetrate the atmosphere during at least the quiet-arc stage of an aurora. Observers have not detected hydrogen emission in the ray structures, which often follow the arcs in the development of a typical auroral storm.

In this paper I wish to examine the various processes tending to excite auroral hydrogen. A quantitative treatment of this problem not only can give information on the expected luminosity distribution for hydrogen emission but may also provide an indication of the absolute number of Balmer transitions resulting from unit flux of protons. Moreover, the Balmer decrement and the expected *Hα* line profile may be computed and compared with relevant observations. In view of the fact that there are some uncertainties in the cross-sections, particularly at low energies, and in the model atmosphere adopted in this paper, the results must accordingly be considered as provisional and preliminary. Future improvements in these data, however, will probably not have large effects on the computations presented here.

II. SOLUTION OF THE EQUATIONS FOR STATISTICAL EQUILIBRIUM

To determine the populations of the various hydrogen levels, and hence the amount of Balmer emission, we shall adopt the statistical-equilibrium approach, which has been used by several authors in discussing hydrogen excitation in gaseous nebulae and stellar atmospheres. Here we may safely neglect excitation resulting from captures of, or inelastic collisions with, free electrons. The calculations show that, by the time the protons

* The research reported in this paper was supported in part by the Geophysics Research Directorate of the Air Force Cambridge Research Center under Contract AF 19(122)-480.

have been slowed down to velocities where the cross-sections for capture of free electrons become appreciable, virtually all hydrogen ionization has already ceased, and no protons are available. This fact and the relatively low electron densities encountered make the effect of free electrons completely negligible.

The first fundamental equation expresses the fact that the number of atoms per cubic centimeter per second entering an excited state by (*a*) captures of bound electrons from oxygen and nitrogen atoms and molecules, (*b*) cascading from all higher levels, and (*c*) inelastic collisions from the ground state must equal the number leaving by spontaneous emission. Collisions involving excited hydrogen atoms should be negligible at the higher altitudes, except in the case of the metastable 2s configuration. In the absence of the required cross-sections, it is not possible to take an accurate account of this metastability, but neglecting it should not produce any great error in our results for the Balmer lines. Thus for any level with $n > 2$, when all the incident particles are traveling at the same velocity, v, at some height x,

$$N_p N_a \sigma_{\kappa n} v + \sum_{n''=n+1}^{\infty} N_{n''} A_{n''n} + N_1 N_a \sigma_{1n} v = N_n \sum_{n'=1}^{n-1} A_{nn'} . \tag{1}$$

Here N_a denotes the number density of atmospheric atoms, N_p is the proton density, and N_n is the density of hydrogen atoms with principal quantum number n. Also, $A_{nn'}$ represents the Einstein coefficients of spontaneous emission, which have been calculated by Menzel and Pekeris (1936). The cross-section per atom for capture into the nth Bohr orbit for protons in air is $\sigma_{\kappa n}$, and the excitation cross-section for hydrogen in air is σ_{1n}. We assume throughout that the total number of neutral hydrogen atoms is essentially the number in the ground configuration, N_1.

Let us write the fraction of neutral hydrogen atoms in level n as $f_n = N_n/N_1$ and define

$$\eta_n = \frac{N_p}{N_1} \sigma_{\kappa n} v + \sigma_{1n} v . \tag{2}$$

Furthermore, let

$$a_n = \sum_{n'=1}^{n-1} A_{nn'} .$$

Then equation (1) becomes

$$\sum_{n''=n+1}^{\infty} f_{n''} A_{n''n} + N_a \eta_n = f_n a_n . \tag{3}$$

This equation represents an infinite number of simultaneous equations in an infinite number of unknowns. A series solution may be obtained rather simply, however, by the method of successive approximations or by the more complex, but more rigorous, matrix method discussed by Menzel and Baker (1937). The solution to equation (3) is

$$f_n = \frac{N_a}{a_n} \left\{ \eta_n + \sum_{i=n+1}^{\infty} \frac{\eta_i A_{in}}{a_i} + \sum_{j=n+1}^{\infty} \left(\sum_{i=j+1}^{\infty} \frac{\eta_i A_{ij}}{a_i} \right) \frac{A_{jn}}{a_j} + \cdots \right\} . \tag{4}$$

Fortunately, for purposes of obtaining numerical solutions, the summations in equation (4) converge rather rapidly. The numerical values depend on the ratio N_p/N_1, which

may be obtained from the equation expressing the condition of ionization equilibrium for hydrogen: At a given height,

$$\sum_{n'=1}^{\infty} N_p N_a \sigma_{\kappa n'} v = N_1 N_a \sigma_{1\kappa} v . \tag{5}$$

Although it is not obvious that ionization equilibrium should exist in the atmosphere, measurements made by Bartels (1930) indicate that equilibrium *will* be obtained over a path length that is very short compared with the scale height in auroral regions or with the vertical thickness of an auroral arc.

It is convenient to express the hydrogen density and Balmer radiation in terms of the proton flux, $\tilde{\delta}$, penetrating the atmosphere. We obtain from equation (5), for a constant flux,

$$\frac{N_1}{\tilde{\delta}} = \frac{\sum_{n'=1}^{\infty} \sigma_{\kappa n'}}{v\left(\sum_{n'=1}^{\infty} \sigma_{\kappa n'} + \sigma_{1\kappa}\right)} . \tag{6}$$

III. APPLICATION TO THE IONOSPHERE

The procedure for applying equations (4) and (6) to the aurora has been to calculate the excitation and rate of Balmer emission (per cubic centimeter per unit proton flux per unit atmospheric density) as functions of the velocity only. Then these calculations were fitted to a model atmosphere by assuming various initial velocities for protons traveling in straight paths and entering the atmosphere at the observer's zenith. First, let us examine the data chosen for the former calculations.

Bates and Griffing (1953*b*) have computed by the Born approximation the excitation, σ_{1n}, and ionization, $\sigma_{1\kappa}$, cross-sections for neutral hydrogen in hydrogen gas. No experimental excitation cross-sections are available, but the computed values of $\sigma_{1\kappa}$ are smaller than Ribe's (1951) measurements, over the energy range important in the aurora, by a factor of slightly less than 2. Bates and Griffing have suggested reasons for these small discrepancies. On the other hand, experimental ionization cross-sections for hydrogen in *air*, determined by Kanner (1951) with apparatus and techniques nearly identical to those used by Ribe, are considerably larger than Ribe's hydrogen-in-hydrogen cross-sections. Altogether, an increase of a factor of 5 was applied to Bates and Griffing's values of $\sigma_{1\kappa}$ and σ_{1n} to make them suitable for the auroral problem.

Capture cross-sections, $\sigma_{\kappa n}$, for protons in atomic hydrogen have recently been computed by Bates and Dalgarno (1953) for $n \leq 4$. These computations agree very well with Ribe's (1951) experimental capture cross-sections for proton energies greater than about 30 keV. Again, however, Kanner's (1951) measurements for protons in air indicate that we should revise the computed values upward by a factor of 2. Moreover, the computed cross-sections for capture into the 1s configuration become extremely large at low velocities because of resonance between the energy levels of the initial and final hydrogen atoms. Since this complication does not exist for protons in H_2 or in air,[1] the cross-section $\sigma_{\kappa 1}$ for energies less than 30 keV has been taken from experimental determinations in H_2 (Massey and Burhop 1952). In all cases the capture cross-sections per atom in air were

[1] Dr. Bates (private communication) has pointed out, however, that proton collisions with *O* I would also exhibit the resonance phenomenon for 1s captures, inasmuch as *H* and *O* I have nearly identical ionization potentials. Fortunately, by the time the velocities are low enough for the resonance effect to be appreciable, over 85 per cent of the hydrogen is already neutral, and it may be seen from equation (6) that an increase in $\sigma_{\kappa 1}$ would have little effect, even in the higher aurorae where *O* I is relatively plentiful.

taken to be twice the corresponding cross-sections in hydrogen. For values of n higher than those explicitly discussed by Bates and his associates, the capture and excitation cross-sections have been extrapolated.

For these computations I have adopted Kallman's (1953) model atmosphere, which assumes that oxygen is partially dissociated between 80 and 120 km and completely dissociated above 120 km. This atmosphere was reduced to conditions of S.T.P., and the proton velocities at each height were then found from recent range-energy measurements

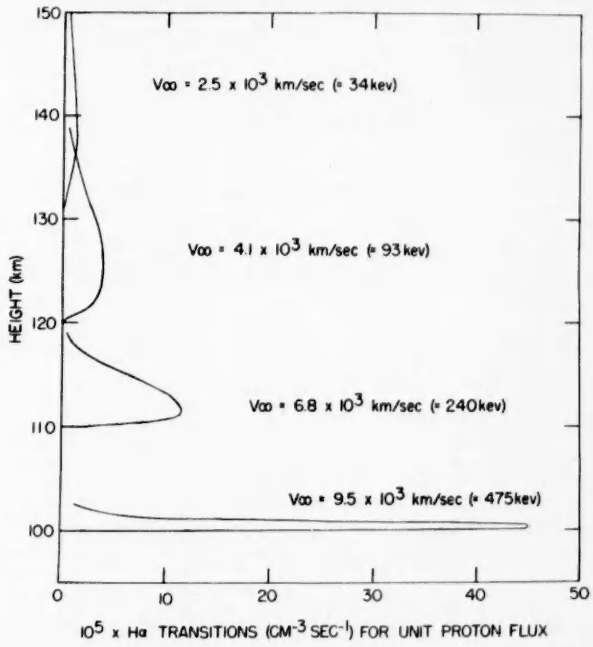

FIG. 1.—Luminosity distribution in $H\alpha$ for several velocities of the incident protons. The protons are assumed to enter the atmosphere from the zenith and to travel in rectilinear paths. An arc at the 90-km level would be produced by protons entering at 14.6×10^3 km/sec (1100 kev). It would have a maximum intensity of 240, in the units of the figure, and a half-width of 0.2 km.

(Cork, Jones, and Jorgensen 1953; Reynolds, Dunbar, Wenzel, and Whaling 1953; Jesse and Sadauskis 1950).

In Figure 1 are presented the $H\alpha$ luminosity-curves computed for several incident energies. In Figure 2 the $H\alpha$ luminosity for an arc at the 110-km layer is compared with a similar curve for emission resulting from atmospheric ionization (Bates and Griffing 1953*a*). At auroral latitudes the observer's magnetic zenith is close enough to his geocentric zenith that relatively little correction need be applied to the computed curves. For an auroral arc with its lower edge at the same height as a curve in Figure 1, the effect would be to narrow the arc by the factor $\cos z$, where z is the zenith distance of the proton radiant. The total amount of emission would be unchanged.

The decrease in $H\alpha$ emission per cubic centimeter at higher altitudes is just compensated by the increased vertical extent of the arc. Hence the total emission in $H\alpha$ and the

net Balmer decrement are independent of the height of the aurora or the energy of the incident protons, so long as they exceed a certain minimum energy (about 90 keV). The Balmer decrement should vary somewhat through the arc, as shown in Figure 2.

The entire arc produces approximately 50 $H\alpha$ quanta per proton. This value at first seems rather high in view of the fact that less than one capture out of 20 produces an $H\alpha$ transition (Bates and Dalgarno 1953). Part of this apparent discrepancy arises from the fact that some $H\alpha$ is excited from the ground state by inelastic collisions. The most important factor, however, is collisional ionization of a hydrogen atom following a capture. Each proton will undergo about 700 captures and reionizations in its flight through the

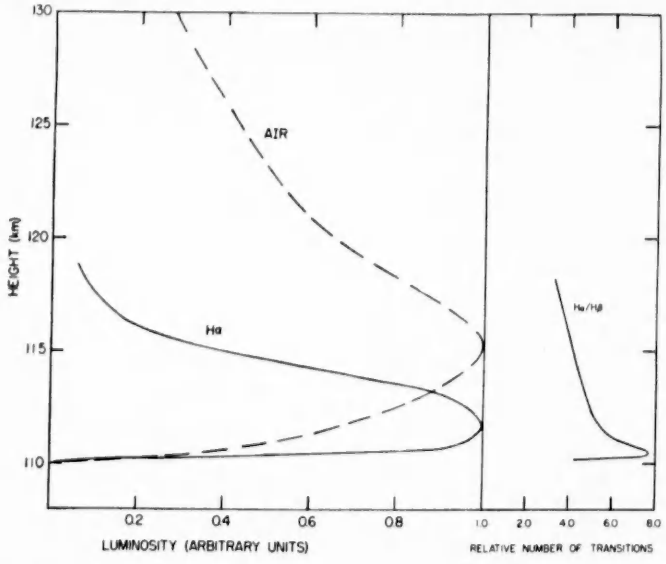

FIG. 2.—Comparison of computed luminosity distribution for $H\alpha$ and for emissions arising from ionization of air (Bates and Griffing 1953*a*). The two curves were computed with similar model atmospheres for protons with sufficient energy to penetrate to the 110-km level. The maximum intensity of each curve has arbitrarily been set equal to unity. The curve on the right side of the figure gives the variation of the relative number of transitions in $H\alpha$ and $H\beta$ over an arc.

ionosphere. The rate of hydrogen ionizations at any height is nearly proportional to the $H\alpha$ luminosity-curve, except that the number of ionizations drops off more rapidly below the peak. In other words, captures are the dominant factor in producing radiation in the upper part of the arc; near the peak, captures and collisional excitation are about equal; on the bottom edge, collisional excitation rules.

IV. DISCUSSION

The present investigation has indicated the following points regarding hydrogen in an auroral arc:

1. *Luminosity-curve.*—As shown in Figure 1, an arc viewed on the magnetic horizon in the light of $H\alpha$ should be rather sharp if its lower edge is below 110 km or so and if at each height all the protons have the same velocity. The luminosity resulting from atmospheric ionization produced by protons should be somewhat broader, according to the calculations

of Bates and Griffing (1953*a*). The latter point seems to have been confirmed by Meinel (1952), who made spectra of an arc with a 30° field-of-view focused on the spectrograph slit. His plates showed the arc to have a considerably narrower vertical extent in *Hα* than in other emissions. Bates and Griffing (1953*a*) have already mentioned that, since the observed luminosity-curves seem to be much broader than the computed curves, we should at least consider the possibility that there is a significant dispersion in the velocities of the incident protons. It should be pointed out, however, that scattering of the incident protons would also tend to broaden the luminosity-curves (see paragraph 4 below).

2. *Proton flux.*—Each incident proton results in about 50 quanta of *Hα*, regardless of the height of the aurora, if the initial proton velocities exceed about 4000 km/sec (= 90 keV). No accurate measurements of the *Hα* intensity have been made as yet, but C. Y. Fan (private communication) estimated for one moderately brilliant arc that *Hα* was of the order of one-tenth as strong as λ 5577 [*O* I]. If we assume that λ 5577 was 100 times

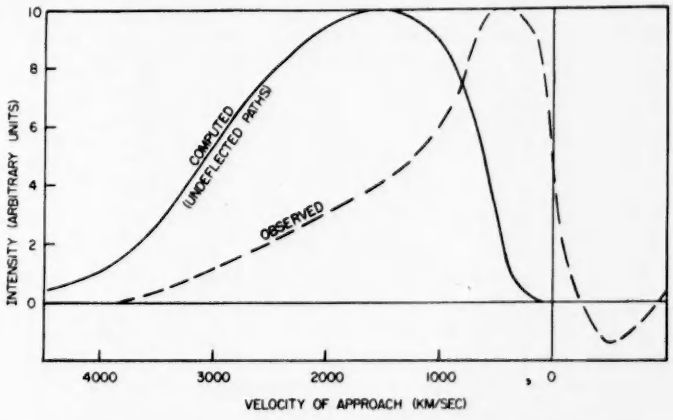

FIG. 3.—Comparison of computed *Hα* profile for an arc in the magnetic zenith with Meinel's (1951) observed profile. Scattering of the incident particles has not been considered in the computed curve.

the intensity of the airglow green line for an observer seeing this aurora in his zenith, we obtain an *Hα* emission of about 3×10^9 quanta/cm²-column sec and a flux of 6×10^7 protons/cm² sec. Such aurorae would have an international brightness coefficient between II and III, according to Seaton's (1953) calibration. Reliable intensity measurements might be more easily obtained from *Hβ*, which is less affected by neighboring emissions than is *Hα*.

3. *Balmer decrement.*—The computed relative number of Balmer transitions over an entire auroral arc is *Hα*: *Hβ*: *Hγ* = 4.5 : 1.00 : 0.29. This leads to a Balmer decrement, for the integrated light of an arc, of $I_\alpha : I_\beta : I_\gamma = 3.34 : 1.00 : 0.33$. Observed values of the decrement have not yet been published. Careful measurements of the decrement might disclose variations with height, as shown in Figure 2, if proton scattering should turn out to be unimportant. At any rate, the *Hβ* and *Hγ* luminosity-curves would not be greatly different from that for *Hα*.

4. *Hα profile.*—The intensity profile observed when the line of sight is in the direction of the proton radiant is also independent of the height of the aurora, if the energy of the incident protons exceeds about 90 keV. The computed profile is compared in Figure 3 with Meinel's (1951) Doppler-shifted profile obtained for a brilliant arc in the magnetic

zenith. The agreement is rather poor, and this discrepancy may give a clue to the true particle trajectories. In the theory we have neglected scattering of the incident protons and any departures from rectilinear paths produced by the magnetic field.

There are still very many uncertainties in the theoretical trajectories for charged particles entering the atmosphere. Departures from the assumed rectilinear paths in only one direction would shift the maximum of the profile toward smaller radial velocities. Moreover, a dispersion in the incident directions of the protons would broaden the observed arc, but the total amount of emission for a low-lying arc would not be changed.

The fact that $H\alpha$ is broadened (but not shifted) on the magnetic horizon also suggests that deviations from the simple paths treated here are quite important. The arcs and zenith profile produced when the incident protons possess a dispersion in directions will be treated in a later paper.

I am greatly indebted to Dr. C. Y. Fan for a number of discussions on this problem and for supplying much helpful information on the empirical determinations of cross-sections.

REFERENCES

Bartels, H. 1930, *Ann. Phys.*, **6**, 957.
Bates, D. R., and Dalgarno, A. 1953, *Proc. Phys. Soc.*, *A*, **66**, 972.
Bates, D. R., and Griffing, G. 1953*a*, *J. Atm. Terr. Phys.*, **3**, 212.
———. 1953*b*, *Proc. Phys. Soc.*, *A*, **66**, 961.
Cook, C. J.; Jones, E., Jr.; and Jorgensen, T., Jr. 1953, *Phys. Rev.*, **91**, 1417.
Harang, L. 1946, *Geofys. Pub.*, Vol. **16**, No. 13.
———. 1951, *The Aurorae* (New York: John Wiley & Sons, Inc.), chap. vii.
Jesse, W. P., and Sadauskis, J. 1950, *Phys. Rev.*, **78**, 1.
Kallman, H. K. 1953, *J. Geophys. Res.*, **58**, 209.
Kanner, H. 1951, *Phys. Rev.*, **84**, 1211.
Massey, H. S. W., and Burhop, E. H. S. 1952, *Electronic and Ionic Impact Phenomena* (Oxford: Clarendon Press), p. 526.
Meinel, A. B. 1951, *Ap. J.*, **113**, 50.
———. 1952, *Mem. Soc. R. Sci. Liége*, **12**, 203.
Menzel, D. H., and Baker, J. G. 1937, *Ap. J.*, **86**, 70.
Menzel, D. H., and Pekeris, C. L. 1936, *M.N.*, **96**, 77.
Reynolds, H. K.; Dunbar, D. N. F.; Wenzel, W. A.; and Whaling, W. 1953, *Phys. Rev.*, **92**, 742.
Ribe, F. L. 1951, *Phys. Rev.*, **83**, 1217.
Seaton, M. J. 1953, *J. Atm. Terr. Phys.*, **4**, 285.

NOTES

POLARIZATION OF THE CLUSTER M29*

The brighter members of the galactic cluster M29 in Cygnus have been observed for interstellar polarization. The available observations are recorded in Table 1. The first column gives the number of each star assigned by Zug (1933). The polarization in magnitudes is given in the second. The position angle of the plane of vibration in equatorial and galactic co-ordinates is given in the third and fourth columns, respectively. The last column contains the visual intersetllar absorption kindly supplied by Harris (1954).

TABLE 1

Zug No.	p	θ	θ'	a_v	Zug No.	p	θ	θ'	a_v
1	0.039	100.9	154.0	3.54	8	0.020	72.8	125.9	3.15
3	.034	75.1	128.2	3.60	13	.023	73.4	126.5	3.06
4	.026	89.9	142.9	3.30	15	.030	88.7	141.8	3.33
6	.035	66.6	119.7	(3.78)	16	0.012	63.4	116.5	2.91
7	0.021	61.1	114.2	3.27					

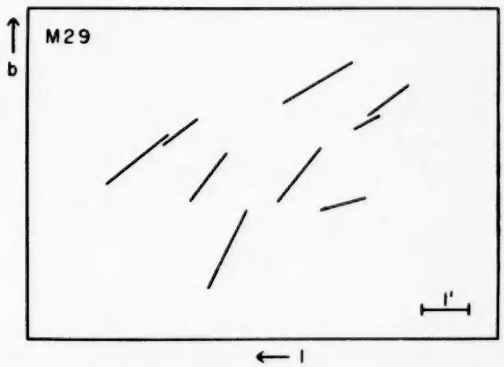

FIG. 1.—Polarization of nine stars in M29

The polarization data are plotted in Figure 1. It is apparent from this figure that neither the amount of polarization nor the plane of vibration is nonvariant for the cluster members. The differences in the plane of vibration show a correlation with position of the individual stars within the cluster. The members to the left of the figure have a plane of vibration in the mean about 20° larger than those on the right. A more striking correlation exists between the amount of polarization and the interstellar absorption. This is shown in Figure 2. The slope of the interpolation line is 0.037, which is approximately half the accepted maximum for polarization per magnitude of absorption, or about equal to the mean in the direction of Cas-Per where the polarization per unit of absorption is at

* *Contributions from the McDonald Observatory, University of Texas*, No. 240.

a maximum. The diagram also shows that 2.6 mag. of absorption are not contributing any observable polarization.

The polarization observations give added support to the conclusion by Harris (1954) that the cluster members exhibit an irregular obscuration. If the assumption is made that the irregular obscuration occurs within the cluster, it follows that the magnetic lines of force are not parallel within the cluster, which has a minimum dimension of 5

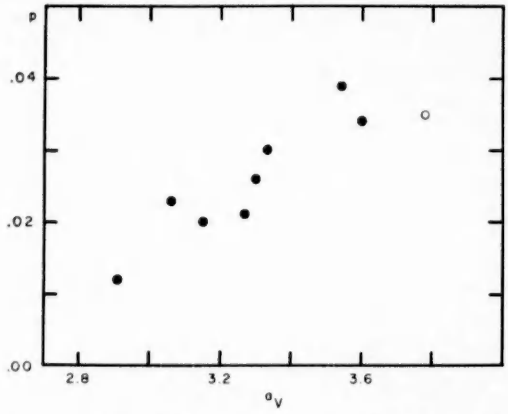

FIG. 2.—Polarization versus absorption for nine members of M29. The open circle refers to star No. 6, for which the absorption is well determined.

parsecs. It does not follow, however, that the curvature is as great as that suggested by Figure 1, since the direction of the lines of force are seen in projection. This factor is especially significant in Cygnus, where it is believed that the line of sight is nearly parallel to the magnetic lines of force. The density of the dust within the cluster is nearly 10^3 that of the mean for the Galaxy.

W. A. HILTNER

YERKES AND MCDONALD OBSERVATORIES
April 14, 1954

REFERENCES

Harris, D. L. 1954, private communication.

Zug, R. S. 1933, *Lick Obs. Bull.*, **16**, 135.

GALACTIC ABSORPTION OF RADIO WAVES

Absorption of 21-cm wave-length radio waves by material in isolated regions in the sky has been discovered in the course of our work, using a 21-cm receiver in the 50-foot radio telescope. Our program is to study several selected regions in the sky and determine the spectrum with the hydrogen line equipment, the angular dimension of the region, and the relative brightness of the region in the continuous background. The regions of all the known strong radio sources were investigated, as were the regions of the bright hydrogen emission nebulae. The receiver uses two channels, one approximately 1.5 Mc wide, which is normally used as a comparison channel, and a second channel, 55 kc wide,

which is tuned to the hydrogen radiation whose frequency in the absence of Doppler shift is 1420.405 Mc. These two channels are separated by 3.25 Mc.

In the experiments reported here a measurement was made of the hydrogen line radiation by observing the difference between the broad and narrow channels, and, in addition, the background signal was simultaneously measured in the broad channel alone. The broad channel corresponds to a conventional radiometer when used in this way.

Many sources were identified at 21-cm wave length, and some new ones were discovered. This part of the work will be reported elsewhere. At the position of the radio sources the intensity and spectrum of the neutral hydrogen emission were measured. The

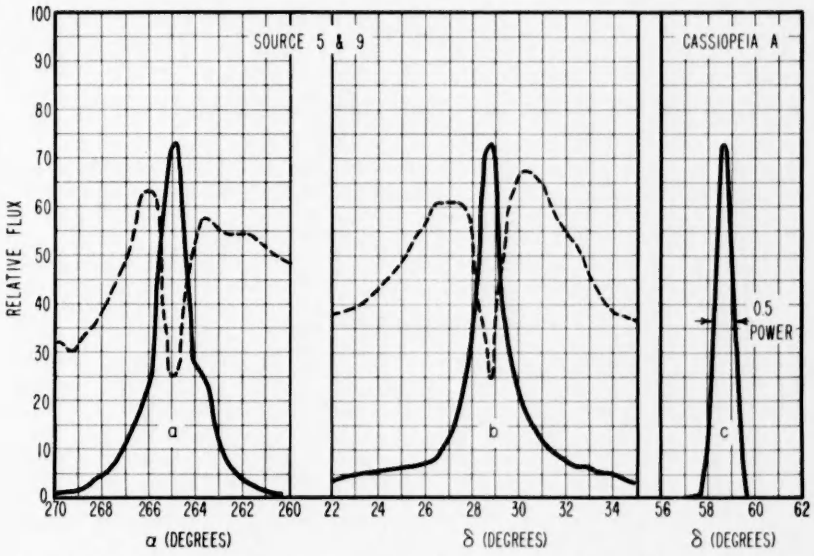

FIG. 1.—Angular sweeps through source, showing background radiation (*solid curve*) and neutral hydrogen radiation (*dotted curve*), and a sweep through Cassiopeia A for comparison.

receiver was then tuned to a peak in the hydrogen spectrum, and the antenna swept in hour angle or declination through the position of the source. In several cases there is clear evidence of absorption of the neutral hydrogen radiation in the direction of the region identified as the radio source. In general, the radio source is an ionized region, whereas the line radiation must come from a neutral hydrogen cloud. The two outstanding cases of absorption are those connected with the Crab Nebula and with a region very near the galactic center identified as NRL No. 5 (Haddock, Mayer, and Sloanaker 1954). The position of source No. 5 is R.A. 17^h43^m, and Dec. S. $28°45'$. Figure 1, *a* and *b*, shows the variation in intensity in temperature units of the neutral hydrogen radiation (*dotted curve*) and the background radiation (*full curve*) as the antenna is swept in hour angle and declination through the position of the star. The intensity of the neutral hydrogen radiation is reduced to somewhat less than half as the antenna passes through the position of the source. Similar curves, but none with so great an absorption, have been taken of several other sources. Figure 1, *c*, is a drift-curve of the radio source in Cassiopeia shown for comparison. A comparison of the two curves shows that source No. 5 has a

diameter of about $\frac{1}{2}°$ and that it is superposed on a second, much wider, source, No. 9. Since the beam width of the antenna is about 1° and the absorption from the $\frac{1}{2}°$ source about 50 per cent, then the source must be quite opaque, if most of the neutral hydrogen cloud is behind the source.

A search of star charts and photographic atlases of this region shows no clearly defined unusual object. The position of source No. 5 is in a bright star cloud in Sagittarius. While its position is near that of an emission nebula No. 12 in the list published by Sharpless (1953), owing to the peculiar radio spectrum it is interesting to speculate that the narrow hot peak in the background emission corresponds to the dense core of the nucleus of our Galaxy, where there may be little hydrogen; that the broader peak in the background is due to radiation from either a less dense region surrounding the nucleus and elongated in the plane of the Galaxy or the beginning of a spiral arm which is directed toward the sun. The neutral hydrogen which is absorbed may come from hydrogen clouds beyond the nucleus. There is little Doppler shift in the hydrogen line radiation, and from existing models of the Galaxy it is thus impossible to infer distance. This effect is being studied in detail and a more complete paper will be submitted shortly for publication.

The writers are grateful to Mrs. N. Hepburn for assistance in preparing the graphs. The possibility of absorption of 21-cm radiation by the four major radio stars was discussed in a private communication from Mr. George Field.

JOHN P. HAGEN
EDWARD F. MCCLAIN

NAVAL RESEARCH LABORATORY
WASHINGTON, D.C.

REFERENCES

Haddock, F. T.; Mayer, C. H.; and Sloanaker, R. M. 1954, *Ap. J.*, **119**, 456.
Sharpless, S. A. 1953, *Ap. J.*, **118**, 362.

THE LOCATION OF CEPHEIDS WITH RESPECT TO THE SPIRAL ARMS IN THE ANTICENTER REGION OF THE MILKY WAY

The revision of the zero point of the absolute magnitudes of the classical cepheids has provided a new basis for a rediscussion of the distribution of these objects in the Milky Way. The present note contains the summarized results of a study of this problem; a detailed discussion will be given elsewhere.

The material used comprises all cepheids (47) in the longitude interval $80° < l < 175°$ listed by Joy (1937), with the exception of SW Tau, at $b = -28°$, which has been excluded.

In determining the distance modulus $m - M$, the apparent magnitude has been taken from the *General Catalogue of Variable Stars* and Supplements 1–4 (Kukarkin and Parenago 1948, 1949–1952). It has been combined with the absolute magnitude computed from the period-luminosity relation,

$$M = -1.60 - 1.74 \log P .$$

In this expression the correction to the zero point, as suggested by work done by Baade (1952), Blaauw (1953), Mineur (1952), Stebbins (1953), Shapley (1953), and Thackeray and Wesselink (1953), has been applied.

The problem of correcting the modulus for the influence of absorption has been treated as follows: In cases where a sufficient number of B stars exists in the environment of the cepheids, the absorption has been derived, utilizing the colors of B stars measured by

Stebbins, Huffer, and Whitford (1940) combined with the appropriate normal colors as given by Morgan, Harris, and Johnson (1953). The distances for the B stars are either listed by Morgan, Whitford, and Code (1953) for stars in associations or have been derived from the MK standards. In some cases distances for OB stars have been used. For reducing the color excess to absorption, the factors 6.1, visual (Morgan, Harris, and Johnson 1953), and 8.4, photographic (Harris 1953) have been used. In a number of cases the foregoing way of determining the absorption has been supplemented by the results from the star counts (Baker and Nantkes 1944, 1948; Heeschen 1951; Kiefer and Baker 1941; Bok, Olmsted, and Boutelle 1949; McCuskey 1949*a*, *b*, 1952). On a few occasions

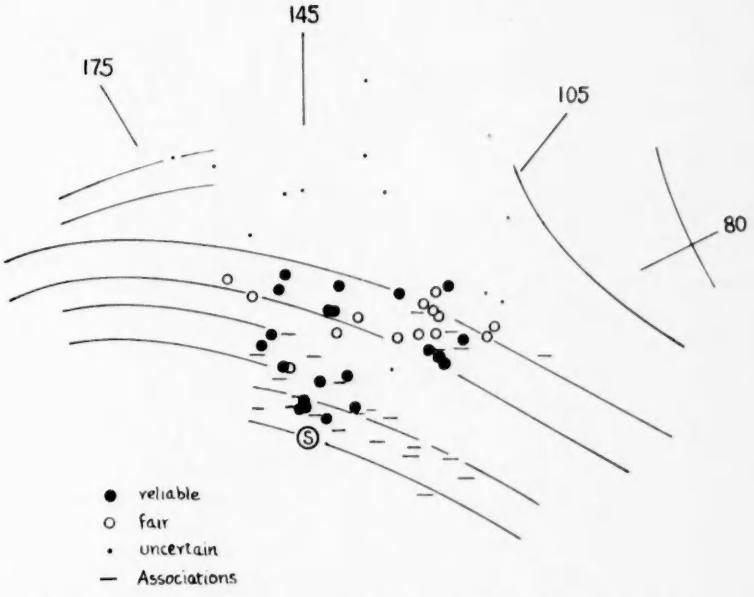

FIG. 1.—Location of Cepheids between galactic longitudes 80° and 175°. The sun is at *S;* the distance between the two arms in the direction of longitude 105° is around 2 kpc.

the direct color determinations by Eggen (1951) and Dziewulski, Iwanowska, and collaborators (1946) have served the same purpose.

In the longitude inerval 80°–105° (Cassiopeia) the number of B stars at distances larger than 2 kpc generally appears sufficient for basing the determination of the absorption on this type of stars. In a number of cases it has been desirable to obtain additional information concerning the distribution of the absorbing matter near the cepheid; for this purpose star counts by Baker and Nantkes (1944, 1948) and Heeschen (1951) have been employed. For one cepheid in this interval (SU Cas, distance 0.35 kpc) the determination of the absorption was based on star counts only.

For the longitude interval 105°–175°, B stars have also been used for the determination of the absorption. However, the scantiness of this material in the interval has made it necessary to utilize star counts to a considerable extent.

The results of the calculations are shown in Figure 1, where also the location of the

associations according to Morgan, Whitford, and Code (1953) are plotted. The orientation of the spiral arms is according to the radio astronomical work carried out by Oort, van de Hulst, and Muller (see, e.g., Waldmeier 1953). It appears from the figure that the connection between the cepheids and the spiral arms is real, even if the scatter in some regions is rather large. In order to arrive at a more definite picture of the situation, we shall need improved magnitudes and color excesses of the cepheids.

The author wishes to acknowledge her gratitude to Professor K. Lundmark for the facilities afforded her at the Lund Observatory.

INGRID TORGÅRD

LUND OBSERVATORY
April 20, 1954

REFERENCES

Baade, W. 1952, *I.A.U., Rome Meeting, Commission 28.*
Baker, R. H. and Nantkes, E. 1944, *Ap. J.*, **99**, 125.
———. 1948, *ibid.*, **107**, 113.
Blaauw, A. 1953, Private communication.
Bok, B. J.; Olmsted, M.; and Boutelle, B. D. 1949, *Ap. J.*, **110**, 21.
Dziewulski, W.; Iwanowska, W.; Dziewulska, A.; and Mackiewicz, M. 1946, *Torun. Bull.*, No. 1.
Eggen, O. J. 1951, *Ap. J.*, **113**, 367.
Harris, D. L. 1953, Private communication.
Heeschen, D. S. 1951, *Ap. J.*, **114**, 132.
Joy, A. H. 1937, *Ap. J.*, **86**, 363.
Kiefer, L., and Baker, R. H. 1941, *Ap. J.*, **94**, 482.
Kukarkin, B. V., and Parenago, P. P. 1948, *General Catalogue of Variable Stars.*
———. 1949–1952, Supplements 1–4.
McCuskey, S. W. 1949*a*, *Ap. J.*, **109**, 139.
———. 1949*b*, *ibid.*, p. 414.
———. 1952, *ibid.*, **115**, 479.
Mineur, H. 1952, *C.R.* **235**, 1607.
Morgan, W. W.; Harris, D. L.; and Johnson, H. L. 1953, *Ap. J.*, **118**, 92.
Morgan, W. W.; Whitford, A. E.; and Code, A. D. 1953, *Ap. J.*, **118**, 318.
Shapley, H. 1953, *Proc. Nat. Acad. Sci.*, **39**, 349.
Stebbins, J. 1953, *Pub. A.S.P.*, **65**, 118.
Stebbins, J.; Huffer, C. M.; and Whitford, A. E. 1940, *Ap. J.*, **91**, 20.
Thackeray, A. D., and Wesselink, A. J. 1953, *Nature*, **171**, 693.
Waldmeier, M. 1953, *Vierteljahrschr. d. Nat. forsch. Gesellsch.* in Zürich, Heft 4.

ABSTRACTS OF ASTROPHYSICAL JOURNAL SUPPLEMENT SERIES

Supplement No. 5, Volume I, pages 121–146, September, 1954

ON NUCLEAR REACTIONS OCCURRING IN VERY HOT STARS I. THE SYNTHESIS OF ELEMENTS FROM CARBON TO NICKEL

F. HOYLE*
MOUNT WILSON AND PALOMAR OBSERVATORIES
CARNEGIE INSTITUTION OF WASHINGTON
CALIFORNIA INSTITUTE OF TECHNOLOGY

The present paper aims to show that the abundances of the chemical elements over the portion of the periodic table from carbon to nickel are consistent with the view that the elements originate at the high temperatures that probably occur in the interiors of certain types of stars. The argument takes its most definite form in the discussion of the synthesis of elements below sodium, where it seems that the abundances are in fairly close accord with the known properties of the various nuclei. For sodium and heavier elements sufficiently precise nuclear data are not available, and hence the argument becomes more qualitative than quantitative. Nevertheless, the general nature of the agreement between calculation and observation for these latter nuclei makes the discussion of them worth presenting.

The early parts of the paper are concerned with the relation to cosmogony of the theory of the origin of the elements.

* Normally at St. John's College, Cambridge.

Supplement No. 6, Volume I, pages 147–174, September, 1954

ON THE DISSIPATION OF GAS AND VOLATILIZED ELEMENTS FROM PROTOPLANETS

HAROLD C. UREY
INSTITUTE FOR NUCLEAR STUDIES, UNIVERSITY OF CHICAGO

The past studies of the writer and others relating to the fractionation of elements during the formation of the planets and the model previously presented by the writer are reviewed in this paper, and these studies are extended to the possible fractionation of the less volatile elements. The essential facts are as follows:

1. The permanent gases, hydrogen, and the inert gases, have been lost almost completely, and the low-temperature volatiles—water, nitrogen as NH_3, and carbon as methane—have been lost to a great extent, though not completely, from the terrestrial planets,

2. A fractionation of iron and silicates has occurred in varying degrees in the formation of the terrestrial planets,

3. The abundances of the elements less volatile than mercury as observed in the meteorites indicate that no systematic separation of the more volatile from the less volatile elements has occurred,

4. Iron exists in the meteorites and earth in oxidized states, e.g., *FeS* and *FeO* and iron silicates; in the reduced state as metallic iron, whereas at low temperatures only oxidized iron as *FeS* and *FeO* and its silicates are stable thermodynamically; and at high temperatures, e.g., above the melting point of metallic iron, only the metallic iron should be stable in the presence of cosmic mixtures of hydrogen, water, and hydrogen sulphide.

From this evidence it is concluded that the course of events during the formation of the solar system as previously proposed by the writer must be essentially correct. In order that the abundances of the elements in the meteorites and earth shall not show systematically markedly lower values for the more volatile elements, as compared to the less volatile elements, it is necessary that the material of these bodies must have accumulated from solid dust particles at low temperatures and that this material was never heated to high temperatures, e.g., the melting point of iron, in finely divided form. Yet, because massive metallic iron exists in the meteorites and in the terrestrial planets, such high temperatures must have existed for some time. It is argued that the time of this high-temperature stage was not long, for otherwise evaporation of the solid objects or volatilization of the more volatile constituents from them would have occurred. In particular, mercury, arsenic, cadmium, and zinc are very volatile as compared to silicon, magnesium, calcium, and aluminum in their thermodynamically most stable compounds. Even the latter elements have markedly different volatilities.

These facts and deductions show that the earth could not have condensed from a high-temperature gaseous cloud. If no silicate fraction were volatilized and lost in the process, the volatiles would have been concentrated at the surface, that is, the part which condensed last; this does not seem to be the case. On the other hand, if a substantial preferential volatilization of the silicates had occurred in such a process in order to account for the varying densities of the planets, then the more volatile elements should have been lost to a high degree; and this certainly is not the case.

It is concluded that substantial objects some hundreds of kilometers in radius, such as the asteroids and the Imbrian planetesimal which fell on the moon, and indeed, the moon itself, probably accumulated at low temperatures, retaining the volatiles, including water, ammonia, and carbon-hydrogen-nitrogen, etc., compounds. These were subsequently heated above the melting points of silicates and iron. The large masses of hydrogen, helium, and other gases were lost to a high degree, and then the terrestrial planets accumulated from these solid objects. Silicates were lost preferentially to metallic iron during these processes and in varying degrees from the different terrestrial protoplanets.

Three different possible sources for the high-temperature stage are discussed.

1. The chemical data would be most readily explained, if at an appropriate stage in the development of the planetary system the sun had existed as a star of high luminosity, $\sim 10^4 L_\odot$, for a brief period of time. During this time the planetesimals would have been melted superficially, iron partially reduced, silicates partially volatilized, and all gases and dust would have been driven from the solar system by light-pressure from the sun.

2. Adiabatic compression of gases in their own gravitational field would not be satisfactory for the asteroids, if the massive iron of the meteorites was produced in these bodies and if each asteroid had its own protoplanetary gas mass, since high temperatures could not be produced in small objects. High temperatures could be expected in the case of the terrestrial protoplanets, but its is not clear that dust could escape and that extensive removal of the more volatile elements would not occur. This source of heat does not seem satisfactory, but the process must have been most complicated, and analysis of the actual situation may be inadequate.

3. The large solid objects may have been present in a presolar gaseous mass which was partially captured by the sun. In this case an unsymmetrical collision between the sun and such a mass should have resulted in a partial separation of the gas and solid objects.

Silicate dust and small objects could have been lost with the gases, thus providing a mechanism for the loss of silicates and hence accounting for the variable densities of the planets. This process would provide for high temperatures, the loss of silicates, and the very complicated structures of the chondritic meteorites. The process may be related to that necessary for the formation of the Algol binaries, as discussed by Struve. However, no mechanism for the collection of large objects in the gas cloud is proposed.

Supplement No. 7, Volume I, October, 1954

CATALOGUE AND BIBLIOGRAPHY OF EMISSION-LINE STARS OF TYPES LATER THAN B

WILLIAM P. BIDELMAN
LICK OBSERVATORY
UNIVERSITY OF CALIFORNIA

This work is similar in form to Merrill and Burwell's well-known *Catalogue and Bibliography* of bright-line stars of early type. The catalogue lists 1113 middle- and late-type stars whose spectra show bright hydrogen lines and an additional 426 stars whose spectra show emission lines of ionized calcium. An attempt has been made to group similar objects together to the extent that present data allows. The contents of the various tables comprising the catalogue are as follows:

No. of Table	Type of Object Included	No. of Stars
	Part I. Hydrogen Emission Stars	
1	Variables of the *o* Ceti Class	685
2	Long-Period Variables of Small Range, Semiregular, and Irregular Variables of Types M, S, and C	109
3	Variables of Unknown Type of Variation	16
4	Intrinsic Variables of Types F, G, and K	49
5	Stars with Combination Spectra	23
6	Variables of the U Geminorum Type	9
7	Emission-Line Stars Associated with Nebulosity	74
8	M-Type Dwarf Stars with Hydrogen Emission	67
9	Binaries with Hydrogen Emission	35
10	Binaries of the VV Cephei Type	8
11	Miscellaneous Emission-Line Stars	39
	Part II. *Ca* II Emission Stars	
12	Spectroscopic Binaries with *Ca* II Emission	72
13	Giant, Subgiant, and Supergiant Stars with *Ca* II Emission	116
14	Dwarf Stars with *Ca* II Emission	222
15	Cepheid Variables with *Ca* II Emission	16

The catalogue is intended to be complete for all published data up to August 1, 1953, but a considerable amount of previously unpublished material is included in remarks concerning the objects. The only late-type emission stars not included in the catalogue are the large number of recently discovered bright *Hα* stars found in nebulous regions which have not yet been studied on slit spectrograms. The bibliography gives references to all spectroscopic observations of the stars included which have bright hydrogen lines, but only references pertaining specifically to observations of the emission lines in the case of the *Ca* II emission stars. In all, 903 references are listed.

It is hoped that this catalogue and bibliography will provide a convenient summary of present knowledge of the objects included and will encourage further research on emission-line stars of this type.

ANNOUNCING

THE ASTROPHYSICAL JOURNAL SUPPLEMENT SERIES

These *Supplements* are intended to provide a medium for the publication of extensive investigations, such as wave-length lists of stars of special interest, photometric data, results of numerical integrations pertaining to stellar interiors, model stellar atmosphere calculations, and theoretical investigations not immediately related to astronomical problems.

Supplement No. 7

"Catalogue and Bibliography of Emission-Line Stars of Types Later than B." WILLIAM P. BIDELMAN

This catalogue enumerates the known middle- and late-type emission-line stars and provides a comprehensive bibliography of the spectroscopic observations of these objects. The total number of stars included is 1540, of which 1114 have spectra showing bright hydrogen lines while the remaining stars show bright lines of ionized calcium. A considerable amount of previously unpublished data is included in the notes.

(Ready October, 1954. Price $4.50)

An abstract of each supplement will be published in THE ASTROPHYSICAL JOURNAL. The Supplements will appear irregularly and may be purchased separately or by subscription. Each volume of Supplements will consist of approximately 500 pages.

Subscriptions

$8.00 per volume

Canada, $8.75. Foreign, $9.50.

To members of the American Astronomical Society, $6.00 per volume.

Orders now accepted.

THE UNIVERSITY OF CHICAGO PRESS

5750 ELLIS AVENUE CHICAGO 37, ILLINOIS

THE OBSERVATORY

FOUNDED 1877

* * *

A Magazine presenting current developments in Astronomy by means of Articles, Correspondence, Notes on discoveries and Reviews of important astronomical books. The papers read at the Meetings (Astronomical & Geophysical) of the Royal Astronomical Society and the discussions which follow are also fully reported.

* * *

Annual subscription for 6 issues, post free, £1 (U.S.A. and Canada, $3.00) should be sent to

The Editors, ROYAL GREENWICH OBSERVATORY

Herstmonceux Castle, Hailsham, Sussex, England

COMPANION VOLUMES

ASTROPHYSICS

THE ATMOSPHERES OF THE SUN AND STARS

LAWRENCE H. ALLER, *University of Michigan*

THOROUGH COVERAGE of present-day knowledge concerning the atmospheres of the sun and stars and solar-terrestrial relationships. Provides a short introduction to astronomy and a review of relevant physics. Treats all major astrophysical principles—atomic structure and spectra, gas laws and velocity distribution, ionization, excitation, etc.—and applies them to the radiation of the sun and stars, to their continuous and dark-line spectra, to solar phenomena, and to solar-terrestrial relationships. Each principle is applied to a definite numerical problem concerned with the interpretation of stars and nebulae. *116 ills., 44 tables, 412 pages.* **$12**

"Hard to overemphasize the importance of this book . . . presents the subject of stellar atmospheres as it is known and accepted today."

—Publications of the Astronomical Society of the Pacific

CONTENTS: Survey of Basic Data—Atomic and Molecular Spectra—Gas Laws and Equations of State, Turbulence—Excitation, Ionization, and Dissociation—Emission and Absorption of Radiation—Radiation of Stars—Continuous Spectra of Sun and Stars—The Fraunhofer Spectrum—Solar Phenomena

ASTROPHYSICS

NUCLEAR TRANSFORMATIONS, STELLAR INTERIORS, AND NEBULAE

also by **LAWRENCE H. ALLER**

JUST PUBLISHED. A comprehensive study of thermal nuclear reactions, the interiors of stars, pulsating variable stars, and the interstellar medium. Covers fundamentals and major modern developments in the field. Emphasis is placed on the methods and procedures by which results are obtained. The book treats of the properties of matter at high temperatures, stellar energy generation, internal constitution of stars, stellar evolution and the origin of the elements, novae and supernovae, gaseous nebulae, with particular attention to discoveries achieved by radio astronomy. Illustrated with numerous diagrams and photographs, many reproduced here for the first time. *52 ills., 16 tables, 291 pages.* **$12**

CONTENTS: Stellar Interiors and Nuclear Transformations—Model Stars—The Cepheids and Long-Period Variables—Stars with Extended Envelopes, Novae, and Supernovae—The Planetary Nebulae—The Interstellar Medium

Order through your bookstore or from:

THE RONALD PRESS COMPANY · 15 E. 26th St., N.Y. 10